České vysoké učení technické v Praze
Fakulta strojní

Collagen in bone tissue regeneration: Focusing on the mechanical and structural constraints

Tomáš Suchý

Habilitační práce 2020

Anotační list (Annotation)

Název: Kolagen v regeneraci kostní tkáně: zaměření na mechanická a strukturní omezení

Title: Collagen in bone tissue regeneration: Focusing on the mechanical and structural constraints

Autor (Author): Ing. Tomáš Suchý, Ph.D.

Druh publikace (Kind of publication): Habilitační práce (Habilitation thesis)

Obor habilitace (Branch): Aplikovaná mechanika (Applied mechanics)

Univerzita (University): České vysoké učení technické v Praze (Czech Technical University in Prague)

Fakulta (Faculty): Fakulta strojní (Faculty of Mechanical Engineering)

Ústav (Department): Ústav mechaniky, biomechaniky a mechatroniky 12105 (Department of Mechanics, Biomechanics and Mechatronics)

Rok (Year): 2020

Počet stran (Number of pages): 151

Počet obrázků (Number of figures): 91

Počet tabulek (Number of tables): 4

Anotace: Tato práce si klade za cíl, popsat vliv různých podmínek zpracování mikro a nanostrukturovaných kolagenových materiálů, určených pro regeneraci kostní tkáně, na jejich mechanické a strukturní vlastnosti. První část se zabývá nalezením vhodných podmínek síťování a vhodným složením kolagenových mikrostrukturovaných kompozitů, se zaměřením na obsah kolagenu, a na jejich výsledné mechanické vlastnosti, vnitřní strukturu a porozitu v suchém i hydratovaném stavu. Druhá část se zabývá hodnocením podmínek zpracování a síťováním nanostrukturovaných elektrostaticky zvlákněných kolagenových materiálů s ohledem na jejich mechanické vlastnosti a zachování přirozené struktury kolagenu. Třetí část představuje vývoj implantátu opatřeného kolagenovou nanostrukturovanou kompozitní vrstvou, která má za cíl snížit riziko vzniku zánětu za současného zvýšení míry oseointegace.

Annotation: This study demonstrates the effect of various processing conditions on the mechanical, structural and utility characteristics of collagen materials to be used for bone tissue regeneration purposes in both the microstructured and nanostructured forms. The first part presents the effective cross-linking conditions and composition of collagen microstructured composites, focusing on the collagen content and their final characteristics such as mechanical properties, internal structure and porosity in both the dry and hydrated states. The second part presents an assessment of the effective processing and cross-linking conditions of nanostructured electrospun collagen with respect to its mechanical and structural properties and the preservation of the native structure of the collagen. The third part presents the development of a biodegradable nanostructured electrospun composite layer for the treatment of implant-associated infections and improvements with respect to the rate of osseointegration.

Shrnutí
Kolagen, jedinečný přírodní polymer s komplexní hierarchickou strukturou a mimořádnými vlastnostmi, je potenciálně využitelný pro konstrukci materiálů pro regeneraci kostní tkáně. Aplikace jeho laboratorně připravené formy je však omezena z důvodů horších mechanických vlastností, vysoké míry nasákavosti ve vodném prostředí, nízkou strukturní stabilitou a nízkou úrovní odolnosti vůči enzymatické degradaci. Tato omezení vznikají vinou komplexních procesů přípravy, které je nutné použít jak pro jeho izolaci z nativních tkání, tak pro následné zpracování do požadovaných materiálových aplikací. Při zpracování kolagenu do mikro- nebo nano-strukturovaných forem je proto velmi důležité zachovat rovnováhu mezi úspěšným zpracováním a zachováním jeho jedinečných vlastností bez výrazné denaturace.

Experimentální výsledky této práce ukazují, že mechanické a strukturní vlastnosti mikrostrukturovaných kolagenových materiálů lze optimalizovat pomocí chemického síťování a tvorbou kompozitních materiálů, ve kterých je kolagenová matrice vyztužena vlákny nebo částicemi. Bylo ukázáno, že výběr vhodného síťovacího systému je klíčovým faktorem. Přestože je zvýšení stability kolagenu po zesítění provázeno změnou mechanických vlastností, tyto změny není možné hodnotit izolovaně, bez ohledu na související ovlivnění sekundární struktury kolagenu a celkové ovlivnění strukturních vlastností daných materiálů. Mimo to práce ukazuje, že změny v mechanických, chemických a strukturních vlastnostech kolagenu musí být ideálně hodnoceny spíše v hydratovaných stavech, které lépe simulují prostředí, pro které jsou tyto materiály navrženy. Bylo ukázáno, že vhodný výběr podmínek pro simulaci tělního prostředí je dalším důležitým a často opomíjeným faktorem, stejně tak volba vhodných metod pro jejich charakterizaci.

Elektrostatické zvlákňování kolagenu do submikronových vláken a nanovláken představuje další perspektivní přístup pro jeho aplikaci v regeneraci kostní tkáně. Stále není zcela zřejmé, do jaké míry celý proces elektrostatického zvlákňování ovlivní přirozenou strukturu kolagenu. Tato práce dokládá, že k částečnému porušení této struktury skutečně na určité úrovni dochází, zejména pak v souvislosti se způsobem přípravy kolagenového roztoku pro zvlákňování. Současně je ale doloženo, že tyto negativní změny lze minimalizovat vytvářením nových chemických vazeb mezi molekulami kolagenu. Práce ukazuje, že volba vhodných parametrů rozpouštění a zvlákňování, stejně tak volba vhodných podmínek síťování, může výrazně přispět k zachování přirozené struktury elektrostaticky zvlákněného kolagenu i jeho morfologie. Vliv těchto parametrů byl demonstrován zlepšením mechanických vlastností a jejich stability v simulovaných tělních podmínkách. Práce dále kriticky hodnotí variabilitu elektrostaticky zvlákněného kolagenu, kterou dokumentuje pomocí hodnocení mechanických vlastností a sekundární struktury kolagenu.

Poslední část práce se věnuje perspektivám v aplikaci kolagenových materiálů představením vývoje povrchových vrstev ortopedických implantátů pro použití v případech známého zánětu nebo jako preventivní postup při primoimplantaci do potenciálně infekčního prostředí. V této části jsou ukázány výhody a omezení různých způsobů jak samostatné, tak kombinované aplikace antibiotik prostřednictvím kolagenových vrstev s různým obsahem hydroxyapatitu. Výsledky ukazují, že tyto kompozitní vrstvy s antibiotiky, elektrostaticky zvlákněné přímo na povrch tištěných titanových implantátů, vykazují dostatečnou míru antimikrobiální aktivity, nejsou cytotoxické a navíc zvyšují míru osteointegrace, jak je v práci demonstrováno na dvou experimentálních *in vivo* zvířecích modelech. Obě antimikrobiální a osteoindukční funkce vyvinutých elektrostaticky zvlákněných vrstev mohou snížit počet revizních operací a prodloužit životnost kostních implantátů.

Klíčová slova: *kolagen; síťování; elektrostatické zvlákňování; mikrostruktura; nanovlákna; mechanické vlastnosti; kostní regenerace; antibiotika; protetické infekce*

Summary
Collagen, a unique natural polymer with a complex hierarchical structure and outstanding properties, constitutes a potential candidate for the construction of materials for use in the field of bone tissue regeneration. With respect to the limitations imposed by the complex processes applied in the processing of collagen from native tissue to the intended form, its application is limited due to its poor mechanical properties, high swelling rate in aqueous environments, low structural stability and low level of resistivity to enzymatic degradation. It is important that the balance be maintained between the successful processing of collagen into microstructured and nanostructured constructs and the preservation of its unique structure without some degree of denaturation.

The experiments presented demonstrated that the mechanical and structural properties of microstructured collagen materials can be improved by chemical cross-linking and by creating composite materials in which the collagen matrix is reinforced by fibres or particles. It was demonstrated that the suitable selection of the cross-linking system is a key factor. It was also shown that the enhancement of collagen stability following cross-linking is demonstrated by an improvement in the mechanical properties; however, such changes cannot be evaluated separately without the evaluation of other effects, e.g. on the secondary structure of the collagen and the overall structural properties of collagen materials. Moreover, it was shown that changes in the mechanical, chemical and structural properties of collagen must be evaluated in the hydrated state, which simulates the environment for which such materials are designed, rather than in the dry state. It was documented that for the simulation of the body environment, it is important to establish the most suitable conditions. Moreover, as with the evaluation of the structural parameters, it is important to select a suitable method for the characterisation of the material.

The electrospinning of collagen to submicron fibres or nanofibers represents a further promising approach to its application for bone tissue regeneration purposes. It is still unclear whether the electrospinning process as a whole influences the native structure of collagen. It has been demonstrated that the partial disturbance of its structure at some level following collagen dissolution and electrospinning can be improved via the creation of new additional chemical bonds between the collagen molecules. It has been shown that the suitable selection of the solution and processing parameters as well as that of the cross-linking system is able to preserve the native collagen structure and morphology. The effects of cross-linking were demonstrated via the improvement of the mechanical properties and their stability under simulated body conditions. Moreover, it was shown that electrospun collagen evinces variability at some level in terms of its mechanical properties and in its secondary structure, and that the extent of variability should be taken into account in the medical application design process.

Finally, the study considered a further potential application for collagen-based materials via the introduction of the development of a collagen coating for orthopaedic implants to be used particularly in the case of known prosthetic joint infections or as a preventative procedure regarding primary joint replacement at a potentially infected site. The study demonstrated the benefits and limitations of the single and combined application of antibiotics in collagen electrospun layers with differing amounts of hydroxyapatite. The study revealed that collagen electrospun layers that exhibit sufficient antimicrobial activity are not directly toxic for human cells. Moreover, it was demonstrated that collagen/hydroxyapatite layers directly electrospun on the surface of 3D printed titanium implants and impregnated with vancomycin have the potential to prevent infection while effectively improving the rate of osseointegration. Both the antimicrobial and osteoinductive functions of electrospun collagen/hydroxyapatite/vancomycin layers help to reduce the revision rate and enhance the long-term success of bone implants.

Keywords: *collagen; cross-linking; electrospinning; microstructure; nanofibers; mechanical properties; bone regeneration; antibiotics; implant-associated infection*

Acknowledgement

First and foremost, the author would like to express his thanks to his wife Tereza and his children Bára and Johanka for their endless patience and understanding while compiling the study.

He also expresses his cordial thanks to his colleagues and friends Zbyněk Sucharda, Monika Šupová, Radek Sedláček, Lukáš Horný, Marek Pokorný, Petr Mikeš and Lucie Vištejnová who very kindly devoted their time to help put together the jigsaw of often serendipitous and unexpected results attained through working with collagen. Finally, special thanks go to Darren Ireland for the language revision of the English manuscript.

This study has been partially supported by the following institutions:

Ministry of Health of the Czech Republic under project No. NV 15-25813A

Technology Agency of the Czech Republic under project No. TA04010330

The author gratefully acknowledge the financial support provided for his work by the long-term conceptual development research organisation under project no. RVO: 67985891 of the Institute of Rock Structure and Mechanics, Academy of Sciences of the Czech Republic.

Contents

List of symbols

α	[-]	parameter modulating the strain-stiffening response
AECD	[μm]	area-equivalent circle diameter
BICD	[μm]	biggest inner circle diameter
CP	[%]	closed porosity
C		right Cauchy-Green strain tensor
D	[%]	mass loss
Δl	[mm]	elongation
ΔP	[Pa]	pressure drop throughout the sample thickness
ε	[-]	engineering strain
E_{sw}	[%]	swelling ratio
$E_{\sigma 20\text{-}\sigma 70}$	[MPa]	elastic gradient
F	[N]	force
F		deformation gradient tensor
I_1		first principal invariant of the right Cauchy-Green strain tensor
K_0	[m^2]	mean permeability
$\lambda_1, \lambda_2, \lambda_3$	[-]	principal stretches
l_0	[mm]	initial length
μ	[kPa]	stress-like material parameter corresponding to the infinitesimal shear modulus
MD	[μm]	major diameter of the analysed pore
MT	[μm]	mean thickness
n	[-]	number of samples
OP	[%]	open porosity
p	[kPa]	Lagrangean multiplier
P	[%]	porosity
P		first Piola-Kirchhoff stress tensor
Q	[$\mu L.min^{-1}$]	flow rate
R^2	[-]	coefficient of determination
RNB	[%]	ratio of new bone volume
σ	[MPa]	stress
σ_{pl}	[MPa]	plateau stress
σ_{ps}	[MPa]	compressive proof strength

S	[mm^2]	cross sectional area
ϑ	[Pa.s]	fluid viscosity
t	[mm]	mean scaffold thickness
W	[kPa]	strain energy density function
W_a	[$MJ.m^{-3}$]	energy absorption
W_e	[%]	energy absorption efficiency
W_{sw}	[g]	weight of the swollen sample
W_t	[g]	dried weight of the sample after degradation
W_0	[g]	initial dried weight
$\boldsymbol{x}$		position vector in the deformed state
$\boldsymbol{X}$		position vector of a material particle in the reference configuration

List of acronyms

α MEM	Minimum Essential Medium Eagle
Arg	arginine
bCaP	bioapatite (calcium phosphate nanoparticles isolated from bovine bone)
CG	standard antibiotic discs with gentamicin
COL	collagen
COLHA	collagen/hydroxyapatite electrospun layers
COLHA+V	collagen/hydroxyapatite electrospun layers impregnated by vancomycin
CP	titanium printed samples
CV	standard antibiotic discs with vancomycin
DMEM	Dulbecco's Modified Eagle Medium
ECM	extracellular matrix
EDC	1-ethyl-3-(3-dimethylaminopropyl)-1-carbodiimide hydrochloride
EDS	energy dispersive spectroscopy
EDTA	ethylenediaminetetraacetic acid
EI0	collagen electrospun layers impregnated with vancomycin
EI15	collagen electrospun layers with 15 wt% of hydroxyapatite impregnated with vancomycin
EI5	collagen electrospun layers with 5 wt% of hydroxyapatite impregnated with vancomycin
ES+P	collagen electrospun with polyethylene oxide
ES-P	collagen electrospun without polyethylene oxide
EtOH	ethanol
FBS	foetal bovine serum
FTIR	Fourier transform infrared spectroscopy
G	gentamicin
HA	hydroxyapatite
HFIP	hexafluoro-2-propanol
HPLC	high performance liquid chromatography
HYA	sodium hyaluronate
Hyl	hydroxylysine
IQR	interquartile range
LYO	lyophilised collagen
Lys	lysine

MIC	minimum inhibitory concentration
micro-CT	micro-computed tomography
MRSA	methiciline-resistant *Staphylococcus aureus*
N	needle spinning
NC	non-cross-linked collagen
NHS	N-hydroxysuccinimide
NL	needleless spinning
P	3D printed titanium
PBS	phosphate buffer saline
PDLLA	poly DL-lactide
PEO	polyethylene oxide
PMMA	polymethylmethacrylate
PS	polystyrene
S	titanium plasma sprayed
SBF	simulated body fluid
SD	sample standard deviation
SEM	scanning electron microscopy
TNBS	2,4,6-trinitrobenzenesulphonic acid
UV-VIS	ultraviolet-visible spectrophotometry
V	vancomycin
VG	vancomycin and gentamicin
VOI	volume of interest
VRSA	vancomycin resistant *Staphylococcus aureus*

Introduction

The increasing demand for artificial bone tissue replacements has led to changes in the fundamental properties of biomaterials. Over the past five decades, biomaterials undergone an evolution from inert and biocompatible materials to bioresorbable, bioactive and biomimetic materials. Materials intended for bone tissue regeneration are required to allow for the functioning of repair mechanisms by providing a temporary porous scaffold that, in turn, provides mechanical support for cells up to the time that the tissue has regenerated and remodelled itself naturally. The scaffold should also provide the appropriate structural, chemical and biological cues for the promotion of normal cellular behaviour and functioning. One of a number of potential candidates for the construction of such materials is collagen – the most abundant protein present in mammals and a unique natural polymer with complex hierarchical structure and outstanding properties. Collagen type I constitutes most of the organic part of bones, critically influences their mechanical properties and is fundamentally involved in bone tissue remodelling. However, the application of collagen in terms of bone tissue regeneration is limited due to its poor mechanical properties, high swelling rate in the aqueous environment, low structural stability and low level of resistivity to enzymatic degradation. These limitations are due to the complex processes applied for collagen processing from native tissues to the various intended forms and, moreover, by the variability of the source tissue depending on the animal species, type of tissue, age and history. Thus, it is difficult to maintain a balance between the successful processing of collagen into regenerating constructs with suitable mechanical and structural properties and the preservation of its unique structure without some degree of denaturation.

State of the Art

Over the past thirty years, tissue engineering and regenerative medicine have become rapidly developing biomedical fields. They maintain a stable position in the development of materials for the treatment of various tissues such as bone, tendons, cartilage, nerves and many others. In the case of bone tissue, these approaches aim to provide for the safe and predictable treatment of bone defects resulting from a range of conditions (e.g. trauma, tumour, inflammation) as well as for bone tissue regeneration and healing [1]. The advances in the field have been of a multidisciplinary nature - both disciplines (tissue engineering and regenerative medicine) utilize methods and principles adopted from various fields such as chemistry, material and mechanical engineering, biology and others. Such combinations allow for the creation of materials that provide very close approximations to the native bone structure, material composition and physio-chemical properties, all of which result in effective bone regeneration and repair.

The traditional (and successful) materials used for decades for the treatment of bone tissue include metals, ceramics and polymers. However, these materials generally fail to respect the composite nature, nano-architecture and mechanical properties of natural bone tissue. Each of these material types are characterized by specific advantages. Metallic materials (titanium, titanium alloys, stainless steel, chromium and cobalt alloys, etc.) are mechanically resistant, ceramic material resembles the

inorganic component of the bone tissue and synthetic polymers mimic the organic component of the natural extracellular matrix (ECM). However, metallic materials are usually too rigid (i.e., their elastic modulus differs by orders of magnitude from that of natural bone) which may lead to damage to, and the aseptic loosening of, adjacent bone or cartilage. In addition, metallic materials have the potential to release cytotoxic or immunogenic ions. High rigidity coupled with their brittle nature and relatively low resistance to fatigue failure and fracture are characteristic of ceramic materials such as oxide ceramics, tricalcium phosphate, hydroxyapatite and calcium silicate. The use of synthetic polymers is limited by their very low rigidity and/or their low thermal and solvent resistance, e.g. during sterilization. From a further perspective, metallic materials, except for magnesium alloys, can be described as neither bioactive nor bioresorbable materials [2] while, conversely, ceramics and polymers are either bioactive or bioresorbable [2].

The advantages of artificial materials can be enhanced and their drawbacks minimized by constructing composite materials with a suitable combination and suitable spatial arrangement of the various components. In other words, no single-phase material is able to provide all the essential features of bone and/or other calcified tissues. There is, therefore, a pressing need to engineer multi-phase biomaterials with structural, chemical and mechanical properties and the biological performance that provide for the mimicking of native tissue. The ideal combination of a ductile polymer matrix with brittle, hard and bioactive reinforcement offers many advantages for biomedical application. Particular attention has been devoted to polymer-polymer composites, i.e. materials in which both the matrix and its reinforcement are made of synthetic polymers. At least to a certain degree, these composites are able to mimic the architecture of natural bone, in which the amorphous organic component of the ECM is reinforced by collagen fibres. The generation of composite materials can be described as both bioactive and bioresorbable [2].

Microstructured collagen materials for bone tissue regeneration

With increasing demand for artificial replacements, the need has arisen for constant innovation in the field of biomaterials. In this respect, tissue-engineered composites make up the so-called “last generation” of biomaterials [2]. Tissue engineering offers the potential for the regeneration and replacement of damaged tissue employing a combination of scaffolds, biochemical/physical stimuli, and cells. In general, ideal bone replacement materials should be biodegradable, with non-toxic degradation products, supportive in terms of cell attachment, and re-modellable by local cells [3]. Current engineered materials do not provide the functionality associated with living biological tissues [4]. Moreover, allografts (transplants from a donor) may provoke an immune response, and autografts (transplants from elsewhere on the patient) are often associated with donor site morbidity [5]. Thus, artificial scaffolds are increasingly being considered as new ideal materials for bone tissue regeneration. The scaffold should provide the appropriate chemical, biological and mechanical cues required to promote normal cellular behaviour and functioning, and thus provide assistance for the early repair of defected tissue. Ideally, the scaffold should be able to perform its intended function, including the appropriate degradation profile, without eliciting any undesirable local or systemic effects in the host over the long term [6]. These effects may be influenced by inflammation processes,

microvascular changes, osteoblast and osteoclast responses, fibrous encapsulation and protein absorption [7].

Biological materials are multicomponent, i.e. they consist of tissues that contain cells surrounded by ECM materials. Hybrid tissue engineering approaches are, therefore, also required to be multicomponent, i.e. based on a combination of biomaterial scaffolds (for the replacement of the natural ECM) with living cells and bioactive factors [4]. Although this strategy has become well established in over 30 years of tissue engineering literature, it does not yet enjoy widespread clinical application [4]. Porous scaffolds seeded with autologous progenitor cells, e.g. extracted from bone marrow, may be capable of addressing some of the main issues associated with the current use of autogenic and allogenic bone grafts [8]. Tissue formation and ingrowth within the scaffold is influenced by a large number of parameters. The design of the ideal scaffold must respect a number of parameters, e.g. permeability features, the degree of pore interconnectivity [9,10], pore size and porosity, elasticity, stiffness, stability, surface topography, degradation rate etc. [11–13].

One of a number of methods employed for the preparation of optimal bone replacement materials consists of the imitation of real bone composition and structure. Such composite materials combine the advantages of natural and synthetic biodegradable polymers and bioactive inorganic components [3]. Collagen-based materials are being widely studied as potential tissue engineering materials due to the positive effect of collagen on a large number of cell types, its lattice-like organisation ability and for reasons of biocompatibility [14]. Various combinations of natural and synthetic compounds have already been designed, indeed scaffolds made of collagen and calcium phosphate combined with polylactide, polycaprolactone fibres, polyetheretherketone, glycosaminoglycans, various growth factors and nanodiamonds have already been extensively reported [15–20]. Moreover, the application of specific processes such as lyophilisation, electrospinning, electro-spraying and cross-linking, etc. is critical for the enhancement of scaffold stability [11,21,22]. However, the application of collagen in terms of tissue engineering is limited due to its poor mechanical properties, high swelling rate in aqueous environments, low structural stability and low level of resistivity to the enzymatic degradation of its untreated form [23]. Consequently, collagen-based materials exhibit relatively low structural stability, which may well constitute an important limiting factor in terms of cell seeding [5]. It is of particular importance to gain a thorough understanding of the degradation process, specifically of more rapid internal degradation and degradation-induced morphological, compositional and mechanical changes. Thus, changes in the mechanical, chemical and structural properties during degradation need to be evaluated. The ideal scaffold should enable cell infiltration and colonization so as to allow cell-material interactions and the fundamental ECM remodelling process that contributes to both the maintenance of tissue structure and function, and appropriate tissue regeneration and recovery. Tissue remodelling constitutes a key factor in terms of bone tissue regeneration since dysfunctional bone tissue remodelling results in osteoporosis or osteosclerosis [24].

Nanostructured collagen materials for bone tissue regeneration

In addition to the processing of collagen to microstructured scaffolds, the processing of collagen to submicron fibres or nanofibres represents a further promising approach to its application for bone

tissue regeneration purposes. Nanofibrous forms of collagen have been studied extensively with respect to their use in medicine in hard tissue orthopaedic applications through soft tissue applications in cardiology, surgery, dermatology, urology and other fields in the form of bioprosthetic implants, vascular grafts, burn and wound/skin dressings and nerve regeneration and plastic surgery applications [25–34]. In addition, collagen is also being studied as an effective antibiotic delivery matrix for the prevention and treatment of post-operative wound infection and the infection of implanted endoprostheses [35–37].

Electrospinning is seen as possessing great potential in terms of the development of nano-structured biomedical materials. Unlike synthetic polymers, the reproducibility of biopolymer spinning is generally problematic, one of the main reasons being the variability of the source tissue depending on the animal species, type of tissue, age and history. A further important aspect consists of the isolation/processing procedure [38]. Moreover, it remains unclear whether the electrospinning process itself influences the native structure of collagen. In addition, in order to ensure the success of the electrospinning process, natural collagen must be well dissolved, which involves a partial disturbance of its structure at a certain level. Because of the complexity of these processes, it is difficult to maintain a balance between the successful processing of collagen and the preservation of its structure without denaturation. Electrospun collagen fibres exhibit poor mechanical properties in comparison to those of its native form and they present a higher rate of sensitivity to elevated temperatures, poor water stability and uncontrollable enzymatic degradation [39,40] which may limit their use in a number of applications.

Electrospun collagen must be stabilized to a sufficient degree so as to improve the mechanical properties of the fibres, attain stability in aqueous environments, reduce the enzymatic sensitivity and increase the denaturation temperature. Electrospun collagen can be stabilized by creating new additional chemical bonds between the collagen molecules. Unlike the cross-linking of porous collagen scaffolds prepared via lyophilisation, the cross-linking of electrospun forms is more complicated due to their high surface-area-to-volume ratios, and the preservation of nanostructured morphology is complicated. While the electrospun collagen morphology can be preserved by means of the optimization of the cross-linking conditions, it is difficult to maintain the balance between a successful rate of cross-linking and the preservation of its morphology without the occurrence of significant changes in its sub-micron or nanofibrous structure.

In some cases of bone tissue regeneration, especially in the treatment of implant-associated infections, the ideal approach consists of the simultaneous repair of large-size bone defects and the inhibition of related infections. The most critical element of contemporary implant technology and design consists not of the bulk material from which an implant is produced, but rather its surface, which is required to provide an interface that is suitable for the purposes of post-implantation integration between the bone and the replacement. Inflammatory reactions to both local and systemic infection represent the greatest threat to successful osseointegration and may lead to the formation of a bacterial biofilm which creates a barrier to the binding of the implant. This process may, in turn, result in the loosening and thus suboptimal functioning of the implant and even an indication towards re-implantation. The

use of an osteoconductive biomaterial with antibiotic and growth factor release capabilities as well as osteogenesis-matched degradation properties would present the ideal solution [41].

Several strategies are applied aimed at ensuring physical, chemical and mechanical cohesion between implants and bone. At the same time, such bioactive layers serve as local carriers of antibiotics, the gradual release of which serves for the prevention of osteomyelitis. Ceramic materials, synthetic and natural polymers and their combinations provide for clinically-applied or experimentally-developed biodegradable local carriers of antibiotics [37,42–51]. The local application of antibiotics is generally preferred since it enables the introduction of higher dosages; moreover, the short transport path and minimal levels of antibiotic fluctuation in the blood stream also represent significant advantages. Thus, antibiotics administered in this way also act in the avascular zones without increasing systemic toxicity. On the other hand, one of the drawbacks of local carriers of antibiotics concerns the inhibition of osseointegration [52]. Thus, both antimicrobial activity and osseoconductivity must be combined in the one implant. Due to its unique properties and potential to imitate the organic part of real bone composition and structure, collagen offers significant potential for the creation of a coating for orthopaedic implants in the form of a nanofibrous layer which exerts a strong local anti-infection effect and, simultaneously, does not lead to a decrease in the rate of osseointegration necessary for the suitable fixation of the implant.

Objectives of the thesis

The overall objective of this thesis is to demonstrate the effect of various processing conditions on the mechanical, structural and utility characteristics of collagen materials intended for use in bone tissue regeneration in both the microstructured and nanostructured forms. The thesis is divided into three parts with respect to the fulfilment of three main objectives. The ***first objective*** of the thesis was to determine effective cross-linking conditions and the composition of collagen microstructured composites, focusing on the content of collagen and its final characteristics such as mechanical properties, internal structure and porosity in both the dry and hydrated states. The ***second objective*** of the thesis was to evaluate the processing and cross-linking conditions of nanostructured electrospun collagen with respect to its mechanical and structural properties and the preservation its native structure. The ***third objective*** of the thesis was to develop a biodegradable nanostructured electrospun composite layer for the treatment of implant-associated infections and the prevention of infection during the joint replacement procedure.

Arrangement of the thesis

The study is divided into three main chapters and three appendices. The first two chapters summarize the author's experience with concern to the processing of collagen and the investigation of its mechanical and structural properties following its processing into two main material forms - porous microstructured scaffolds and nanofibres. The final chapter highlights the various perspectives of the development of collagen-based materials and summarizes the development of an orthopaedic implant with a strong local anti-infection effect and with an improved rate of osseointegration. Each chapter is composed of the author's previous work, some of which has been published in international journals and part of which consists of selected results attained with students under his supervision and selected parts of a grant project in which the author was the main investigator. Each chapter also contains a brief introduction to collagen processing according to its intended form prepared by means of two different technologies, i.e. lyophilisation and electrospinning. These introductions are composed of substantially shortened parts of a review paper published by Šárka Rýglová, Martin Braun and Tomáš Suchý in *Macromolecular Materials and Engineering* in 2017[1]. In all the chapters the author addresses the most crucial issues inherent in the understanding of collagen as a variable material of natural origin with regard to its mechanical and structural aspects.

The first chapter addresses the development of microstructured collagen composite constructs for bone regeneration purposes. This chapter focuses on the determination of effective cross-linking conditions and the composition of collagen composite scaffolds with regard to their mechanical and structural properties that render them suitable for seeding with mesenchymal stem cells and further biological evaluation under *in vivo* conditions. This chapter also addresses differences in the mechanical behaviour of such highly porous and hydrophilic structures in the dry and hydrated states. The author also reflects on a number of frequently neglected issues associated with the *in vitro* simulation of the human body environment and the selection of a suitable approach for the determination of the structural parameters of scaffolds. The chapter is composed of selected results obtained by the author and published by him and his co-authors in *Biomedical Materials* in 2015[2] and in the *Journal of Materials Science: Materials in Medicine* in 2018[3]. It also contains selected results obtained in two diploma theses and two PhD theses which were supervised by the author.

The second chapter addresses problematic issues related to the electrospinning of collagen. The author focuses particularly on the processing and post-processing of electrospun collagen with respect to its mechanical and structural properties, and addresses problematic issues related to the isolation, handling, electrospinning and cross-linking of collagen with regard to the preservation of its native character. The author also reflects on the behaviour of electrospun collagen in the simulated human body environment and the degree of variability in the mechanical and structural properties of electrospun collagen. The chapter includes the author's unpublished results from experiments that dealt with electrospinning and the cross-linking of collagen and selected results published by him and his co-authors in the *European Journal of Pharmaceutical Sciences* in 2017[4]. It also contains selected results provided in two diploma theses which were supervised by the author.

The ***third chapter*** addresses the potential for the future development of collagen-based materials and introduces the development of a collagen composite electrospun nanostructured layer for the

enhancement of the survival rate of implants, the objective of which was to develop an osteo-inductive resorbable layer that allows for the controlled elution of antibiotics to be used as a bone/implant bioactive interface particularly in the case of prosthetic joint infections, or as a preventative procedure with respect to primary joint replacement at a potentially infected site. The first part addresses the modification of electrospun collagen by means of hydroxyapatite nanoparticles and the evaluation of its influence on the mechanical properties, structural stability and adhesion of the electrospun layers on model implant surfaces. The second part concerns an evaluation of antibiotic release kinetics and the antimicrobial activity of such layers. The final part of the chapter describes a biological evaluation performed under *in vitro* and *in vivo* conditions as an essential element of the development of a successful medical device. The chapter is composed of selected results published by the author and his co-authors in the *Journal of Pharmaceutical Sciences* in 2016[5], in the *European Journal of Pharmaceutical Sciences* in 2017[4] and in the *European Journal of Pharmaceutics and Biopharmaceutics* in 2019[6]. It also contains yet unpublished results from an *in vivo* biological evaluation which formed the final stage of a project supported by the Technology Agency of the Czech Republic in which the author was the main investigator, and selected results provided in two bachelor theses which were supervised by the author.

The first two appendices provide supporting information and consist of detailed descriptions of the materials (***Appendix A***) and methods (***Appendix B***) employed in particular experiments and which are not described directly in the main text. ***Appendix C*** briefly summarizes the range of statistical methods applied in this thesis.

Full bibliographical records:

[1] Š. Rýglová, M. Braun, T. Suchý, Collagen and its Modifications - Crucial Aspects with Concern to its Processing and Analysis, Macromolecular Materials and Engineering 302 (2017) 1600460.

[2] T. Suchý, M. Šupová, P. Sauerová, M. Verdánová, Z. Sucharda, Š. Rýglová, M. Žaloudková, R. Sedláček, M. Hubálek-Kalbáčová, The effects of different cross-linking conditions on collagen-based nanocomposite scaffolds-an in vitro evaluation using mesenchymal stem cells, Biomedical Materials 10 (2015) 65008.

[3] T. Suchý, M. Šupová, M. Bartoš, R. Sedláček, M. Piola, M. Soncini, G.B. Fiore, P. Sauerová, M. Hubálek-Kalbáčová, Dry versus hydrated collagen scaffolds: are dry states representative of hydrated states?, Journal of Materials Science: Materials in Medicine 29 (2018) 20.

[4] T. Suchý, M. Šupová, E. Klapková, V. Adámková, J. Závora, M. Žaloudková, Š. Rýglová, R. Ballay, F. Denk, M. Pokorný, P. Sauerová, M. Hubálek-Kalbáčová, L. Horný, J. Veselý, T. Voňavková, R. Průša, The release kinetics, antimicrobial activity and cytocompatibility of differently prepared collagen/hydroxyapatite/vancomycin layers: Microstructure vs. nanostructure., European Journal of Pharmaceutical Sciences 100 (2017) 219–229.

[5] T. Suchý, M. Šupová, E. Klapková, L. Horný, Š. Rýglová, M. Žaloudková, M. Braun, Z. Sucharda, R. Ballay, J. Veselý, H. Chlup, F. Denk, The sustainable release of vancomycin and its degradation products from nanostructured collagen/hydroxyapatite composite layers., Journal of Pharmaceutical Sciences 105 (2016) 1288–1294.

[6] T. Suchý, M. Šupová, P. Sauerová, M. Hubálek-Kalbáčová, E. Klapková, M. Pokorný, L. Horný, J. Závora, R. Ballay, F. Denk, M. Sojka, L. Vištejnová, Evaluation of collagen/hydroxyapatite electrospun layers loaded with vancomycin, gentamicin and their combination: Comparison of release kinetics, antimicrobial activity and cytocompatibility, European Journal of Pharmaceutics and Biopharmaceutics 140 (2019) 50-59.

Chapter I

Microstructured collagen materials for bone tissue regeneration

I.1 Motivation

Bone substitutes generated via the tissue engineering approach enable the functioning of repair mechanisms by providing a temporary porous scaffold that, in turn, provides mechanical support for cells up to the time that the tissue has regenerated and remodelled itself naturally. These scaffolds can be seeded with specific cells and coated with signalling molecules in order to maximise both tissue growth and the rate of degradation. Optimal bone replacement materials imitate real bone composition and structure. Such composite materials combine the advantages of natural and synthetic biodegradable polymers, such as collagen and bioactive inorganic components. However, collagen-based scaffolds exhibit relatively poor mechanical properties. The study presented in this thesis resulted in the design and construction of a new composite material, the composition of which combines the advantages of a natural collagen matrix, biodegradable polylactide electrospun nano-fibres or submicron fibres, sodium hyaluronate and natural calcium phosphate nano-particles (bioapatite).

The combination of the nanofibre material, its extensive specific surface and fibre orientation provide for cell adhesion regulation, proliferation, movement, differentiation and cell behaviour in general [53–55]. Conversely, since their surfaces are hydrophobic, polylactide polymers display an insufficient degree of cell adhesion - an adverse effect which might be diminished via the incorporation of basic salts within the polymer. Moreover, the addition of calcium phosphate could serve to both buffer the associated degradation products [56] and to provide effective support for the adhesion, growth, and osteogenic differentiation of human osteoblast-like cells [57]. Indeed, polylactide materials are often applied as bonding agents for bioceramics and decalcified bone grafts as well as carriers for factors supporting the growth of bone tissue. In a similar way to collagen, these materials can also be combined with calcium phosphates for bone tissue engineering purposes. A further analogy to the amorphous component of the bone extracellular matrix, applicable in the field of bone tissue engineering, consists of hyaluronic acid, i.e. unbranched high molecular-weight glycosaminoglycan which is widely distributed within the connective tissues of the human body and is also active in the mineralisation process. In addition, hyaluronic acid is employed extensively in biomedical applications such as wound healing and tissue engineering scaffolds, the treatment of arthritis and as an implant material component [57,58].

Collagen-based scaffolds are being widely studied as potential tissue engineering materials due to the positive effect of collagen on a large number of cell types, its lattice-like organisation ability and for reasons of biocompatibility [14]. However, the application of collagen in terms of tissue engineering is limited due to its poor mechanical properties, high swelling rate in aqueous environments, low structural stability and low level of resistivity to the enzymatic degradation of its untreated form [23]. Therefore, a large part of the research work focused on improving the physico-chemical properties of collagen so as to enhance its applicability in terms of tissue engineering. Thus, cross-linking methods

e.g. physical cross-linking and chemical cross-linking are being developed aimed at both improving the material's mechanical properties and at slowing down the biodegradation rate of collagen-based biomaterials. Generally, biocomposites contain several heterogeneous components which may potentially react with a cross-linking agent as well as collagen component reacts. The use of a cross-linking reagent is specific for an existing composite system and, therefore, the testing and comparison of individual cross-linking agents are necessary for each case. Following the preparation and characterisation of biomaterials, the biological *in vitro* evaluation thereof is necessary as is the verification of the handling of the biomaterial under cell cultivation conditions, its cytotoxicity and its interactions with cells. Subsequently, the *in vivo* assessment of the proven biomaterial can be conducted. Such steps are fundamental in terms of the application of any biomaterial at the clinical practice level.

Other crucial features of scaffolds intended for bone-tissue engineering applications consist of the topological characteristics of the 3D structure: scaffold porosity, pore size, interconnectivity and tortuosity. From a fluidic point of view, the effect of all these parameters can be summarised in the scaffold permeability, which could be tailored by properly tuning the scaffold topology. In the case of collagen-based composites, the pore size and porosity features might be controlled in the final collagen concentration [59] and the freezing rate [60] foregoing the lyophilisation process. In addition, hydraulic permeability affects nutrient/oxygen diffusion and the waste removal within the scaffold and, more importantly, plays a crucial role in promoting or inhibiting cell proliferation and differentiation and cell migration that eventually conditions the tissue regeneration process. Collagen scaffolds have been characterised in various ways in both the dry and wet (hydrated) states; naturally they are always hydrated *in vivo*. It is known that collagen, as well as other natural polymers, such as gelatine or chitosan, are hydrophilic as a result of their polar groups and, thus, the resulting scaffolds are subject to swelling [61]. A larger swelling index may be ascribed to higher porosity and greater average pore size, which facilitate the penetration of water into the scaffolds [62]. Significant differences in the swelling index can also be ascribed to various degrees of cross-linking [63]. A greater collagen concentration in the precursor slurry causes an increase in both pore wall closure and the thickness of the pore walls which, together, lead to greater volume swelling on hydration. Conversely, the penetration of water into a scaffold may cause the swelling of the hydrophilic parts of the scaffold and, consequently, a decrease in porosity in the hydrated state [64] and, in some cases, even the closure of the pores [65]. Increasing pore wall closure has been found to determine the time-dependent nature of the hydrated scaffold response, with a decrease in permeability [66].

The hydrated state may also strongly affect the mechanical properties of scaffolds [67]. It is known that the Young's modulus of 3D scaffolds depends upon the relative density of the sponge, the elastic modulus of the struts (the solid material from which scaffolds are formed) and a constant related to pore geometry. Gorczyca et al. [63] proved that when scaffolds were in the swollen state, the pores filled with water, and that pore size contributed more to mechanical strength than did the effect of the crosslinking reaction. Davidenko et al. [68] detected a significant decrease in the Young's modulus of collagen-based scaffolds (~65%) following 10 days of incubation in water. Xingang et al. [69] found that scaffolds based on hydrophilic materials, such as collagen and chitosan, exhibited significantly decreased mechanical strength than did scaffolds based on relatively hydrophobic materials such as

poly(L-lactide-co-glycolide). A decrease in stiffness was observed following hydration by Varley et al. [70], probably caused by the weakening of hydrogen bonds within the molecular structure of the collagen, as illustrated by the Young's modulus values obtained (∼5-10 kPa for the dry and ∼0.5-1 kPa for the hydrated forms). Kane et al. [71] determined a compressive modulus of up to ∼1 MPa following the hydroxyapatite reinforcement of collagen scaffolds which were prepared by means of compression moulding with paraffin microspheres employed as the porogen. Moreover, the compressive modulus was found to be at least one order of magnitude greater than for comparable freeze-dried scaffolds.
In comparison to dry scaffolds, a major decrease in stress and significantly extended stress–strain curve plateau zones were registered with respect to the hydrated samples [62,72]. The swollen scaffolds exhibited reduced compressive strength while the ability to respond to compressive deformation increased, which led to significant differences in the stress–strain curves compared to those of the dry scaffolds. Jose et al. [73] studied the effect of material composition on the final properties of the scaffold. They proved that varying the collagen concentration, while keeping all the other parameters constant, resulted in an increase in the amount of absorbed water in the scaffolds and, thereby, increased the hydrophilicity of poly (lactide-co-glycolide) scaffolds. Uniaxial tensile testing revealed a decrease in modulus with increasing collagen content. It is evident that the content of hydrophilic components in the composite comprises a further key factor that influences the final properties of scaffolds [68,74–77]. The hydrated state much better approximates to the *in vivo* situation. However, the measurement of composite properties in this state, such as porosity and mechanical properties, is frequently neglected [76,78–82] and often not determined at all [83].

The ***first part*** of this chapter presents a study, the aim of which was to determine effective cross-linking conditions for collagen composite scaffolds with regard to the mechanical and structural properties suitable for seeding by mesenchymal stem cells and following biological evaluation. With this aim in view, it was necessary to investigate scaffolds that were cross-linked in various ways and commonly described in the literature as relatively standard collagen cross-linking methods, and to compare their influence on the mechanical and structural properties in the dry state, as well as the swelling ratio and mass loss of the cross-linked scaffolds. The ***second part*** of the chapter concerns follow-up research aimed at describing the influence of eight differing scaffold material compositions focusing on the collagen content and their final properties such as mechanical properties, internal structure and porosity in both the dry and hydrated states. It was anticipated that the differences in the physical properties following hydration would represent a significant limiting factor for the seeding, growth and differentiation of mesenchymal stem cells and the overall applicability of such hydrophilic materials.

I.2 The effects of different cross-linking conditions

I.2.1 Composition of scaffolds

Composite scaffolds based on a collagen matrix (50.5 wt%, isolated from freshwater fish skin of *Cyprinus Carpio*, Třeboň fishery, Czech Republic, COL), poly DL-lactide nanofibres (47 wt%, PDLLA), calcium phosphate nanoparticles isolated from bovine bone (2 wt%, bCaP) and 0.5 wt% of sodium hyaluronate powder (HYA) were prepared from an aqueous collagen dispersion (5 wt%) by lyophilisation (freezing temperature -70 °C). The detailed preparation of scaffolds is described in *Appendix A.1*.

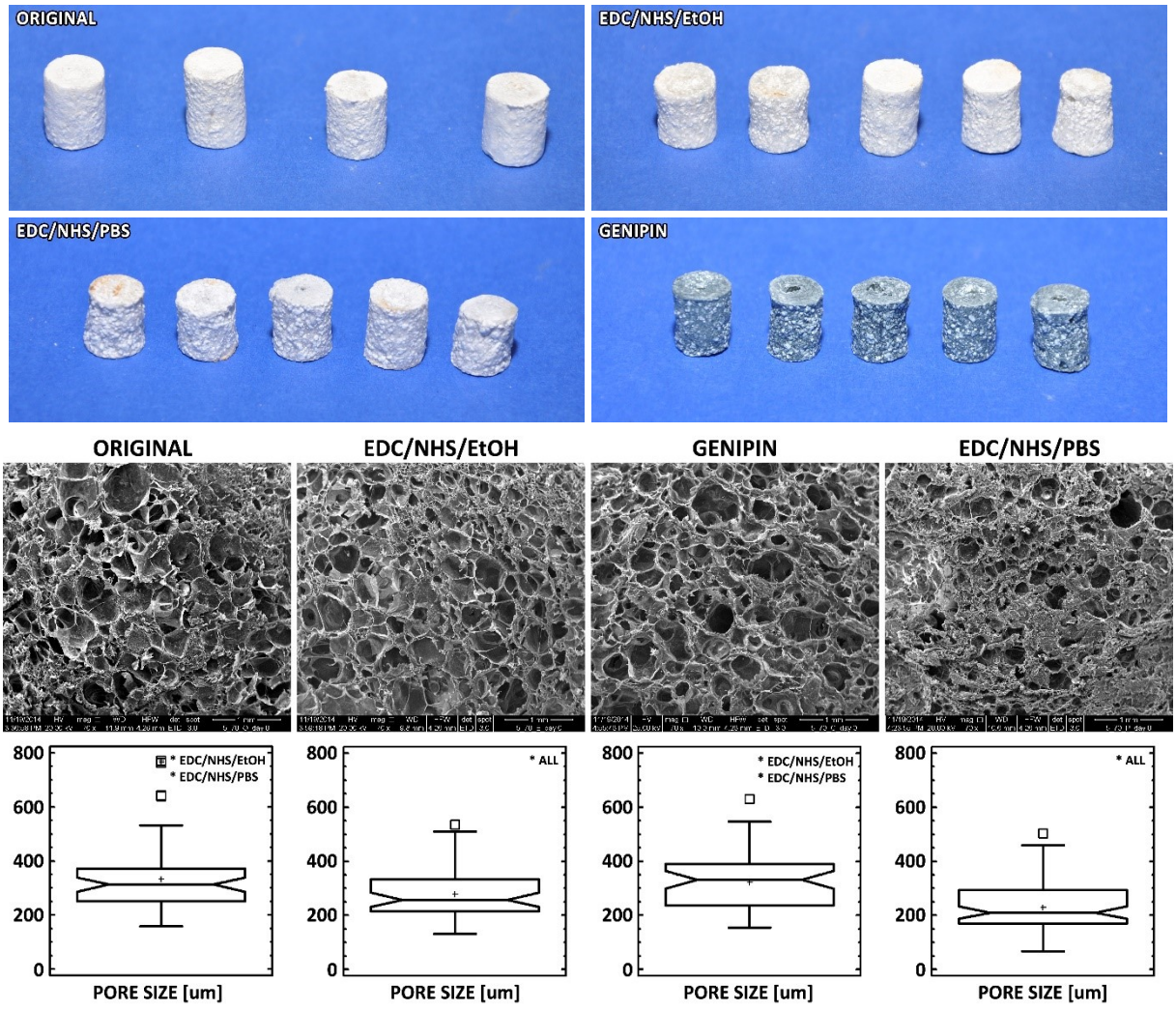

Fig. 1 Representative images of scaffolds (above) and SEM images of scaffold cross-sections (middle) prior to cross-linking (ORIGINAL) and following chemical cross-linking employing chemical agents. Box plots of pore size before and after cross-linking, * denotes statistically significant differences (Mann-Whitney, *0.05, n=130*).

I.2.2 Cross-linking conditions

Chemical cross-linking of collagen can be attained via *i*) covalent amine/imine linkage, mainly with the ε-amino group of lysine residue (e.g., glutaraldehyde, isocyanate crosslinking); *ii*) the carboxyl group in collagen (in the first phase reaction) (e.g., 1-ethyl-3-(3-dimethylaminopropyl)-1-carbodiimide

hydrochloride (EDC) cross-linking); *iii*) the H-bond between the polyphenolic OH group and different amino acids (e.g., genipin crosslinking) or *iv*) metal-protein complex formation (e.g., chromium crosslinking) [35]. In this study, the collagen part of the scaffolds was cross-linked employing three different chemical treatments. The first group of samples (EDC/NHS/EtOH) was cross-linked with an ethanol solution containing EDC and N-hydroxysuccinimide (NHS). The second group (EDC/NHS/PBS) was cross-linked by means of a phosphate buffer saline (PBS) solution containing EDC/NHS. The third group (GENIPIN) was cross-linked using a PBS containing genipin. Structural parameters and images of samples are shown in Figure 1. The theoretical concentration of particular chemical cross-linking agents was calculated based on the determined amino acid composition of collagen. The cross-linking procedure is in detail described in *Appendix A.2*.

Covalent crosslinking using EDC and NHS is a commonly employed method (e.g. [59,84–86]). The reaction is based on the formation of an amidic bond from lysine or hydroxylysine NH_2 and C=O from glutamic or aspartic acid [87]. EDC is not included in the new crosslink bond (thus so-called the zero-length cross-link) but is simply transformed into water-soluble urea-derivatives. EDC is known as a low cytotoxic cross-linker since it is not itself incorporated into the cross-linked structure. Combination of EDC/NHS, where the NHS acts as a competitor, slows crosslinking, by competing with EDC in the reaction, thus adding additional reaction step (Figure 2). Furthermore, it inhibits the hydrolysis and reduces formation of by-products and intermediates (N-acylurea and O-acylurea derivates) [87]. The rate of crosslinking can be controlled via the concentration of the EDC and EDC/NHS ratio. Evidently the reaction also depends on water content in the environment and alcohol vapors (which accelerate dissolution) [35].

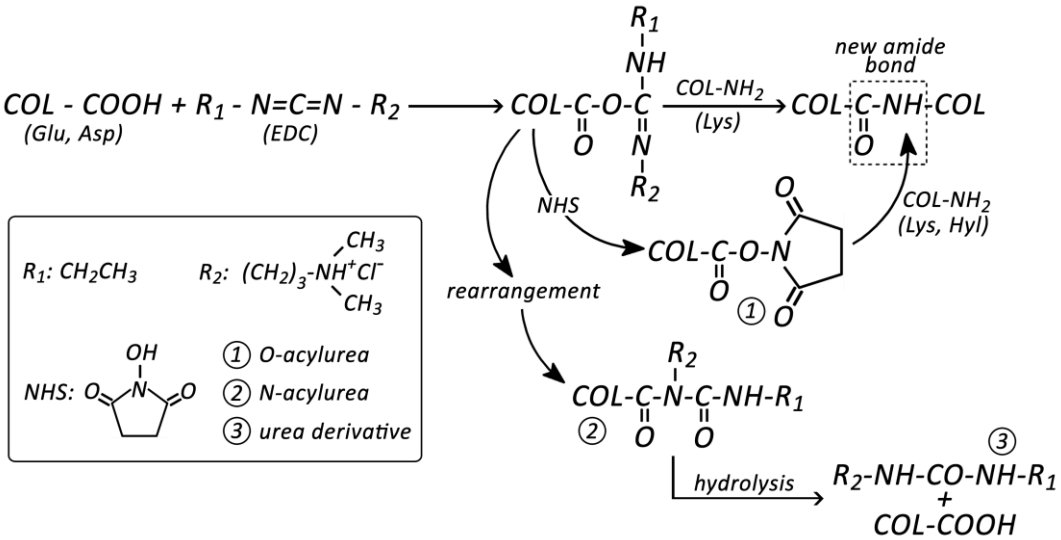

Fig. 2 A representative crosslinking scheme of collagen either with EDC or in combination with NHS in order to modify amount of intermediates and side-by products.

Genipin is a natural nontoxic, biocompatible cross-linker [85,86,88]. It consists of an iridoid derivative (aglycone of geniposide) isolated/extracted from fruits of *Gardenia jasminoides*. Although the cross-linking mechanism of genipin is not completely understood, there are already several proposals of the reaction mechanism (e.g. [87,89,90]). It is known that genipin reacts with the free NH_2 groups of lysine,

hydroxylysine and arginine in collagen forming a dark blue color and a monomeric/oligomeric bridge (Figure 3). It is supposed that the mechanism consists of a nucleophilic attack of the primary amine on the C3 carbon atom of genipin followed by the opening of the dihydropyran ring. Attack by the secondary amine group results in an aldehyde group. Subsequently, it is believed to dimerize radically so as to form inter/intramolecular crosslinks with collagens [91].

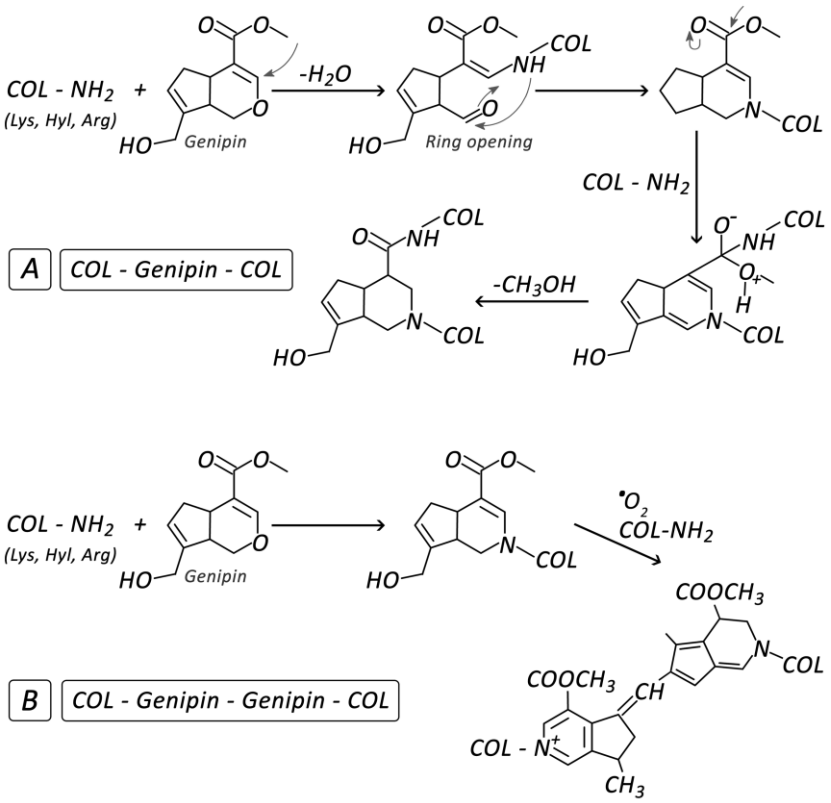

Fig. 3 Two basic schemes of proposed mechanism of crosslinking of collagen with genipin; scheme *A* results in one genipin molecule between two collagen reaction sites, while scheme *B* results in dimerization of genipin molecule between two collagen reaction sites.

I.2.3 Mechanical properties

In general, the behaviour of porous materials under deformation is somewhat different from the behaviour of common compact materials and the testing methods for standard non-porous materials or materials with low porosity cannot be easily adopted. In order to describe the mechanical behaviour of the scaffolds prior to cross-linking and following the application of different cross-linking conditions, compression tests were performed by means of the adaptation of the ISO 13314 standard which refers to the mechanical testing of porous and cellular metals. The mechanical properties of the scaffolds were measured on dry samples before and after cross-linking. The stress-strain curves obtained were used to determine the mechanical properties as follows: Plateau stress (σ_{pl}) was defined as the arithmetical mean of the stresses between 20% and 30% compressive strain. The elastic gradient ($E_{\sigma 20\text{-}\sigma 70}$) was calculated as the gradient of the elastic straight lines determined by elastic loading and unloading between stresses of 70% and 20% of the σ_{pl}. Compressive proof strength (σ_{ps}) was determined as compressive stress at a plastic compressive strain of 1.0%. Energy absorption (W_a) was calculated as the area under the stress-strain curve up to 50% strain. Finally, energy absorption

efficiency (W_e) was calculated as energy absorption divided by the product of the maximum compressive stress within the strain range and the magnitude of the strain range. Plateau stress and elastic gradient represent the closest concepts to that of yield stress and Young's modulus respectively which are employed for solid materials [92]. In order to simplify the comparison of our results and the results of other studies, we assumed that plateau stress represents compression strength and that elastic gradient represents the modulus of elasticity under compression [92–94]. More details are described in *Appendix B.1*.

The mechanical properties of the scaffolds obtained in the study are provided in Table 1. The successful effect of cross-linking could be expected in the improvement of mechanical properties. Both the compressive strength (represented by plateau stress and compressive proof strength) and elastic modulus (represented by the elastic gradient) increased following the application of all the cross-linking conditions. The statistically significant (Mann-Whitney, *0.05*) highest compressive strength and elastic modulus values were evinced by samples cross-linked with genipin. As for a comparison of the three cross-linking conditions applied, the lowest increase in mechanical properties (Mann-Whitney, *0.05*) was evinced by the EDC/NHS/EtOH samples. The improvement in resistance to deformation of the scaffolds following cross-linking is illustrated by an increase in calculated energy absorption. Here again, the highest values (Mann-Whitney, *0.05*) were obtained for samples cross-linked with genipin. The same values (Mann-Whitney, *0.05*) of calculated energy absorption efficiency illustrate the similar character of the stress-strain curves of all the tested materials. This indicates minimal changes in the inner structure of the scaffolds following cross-linking.

Table 1. Summary of the mechanical properties of the composite scaffolds measured via the performance of compression tests. Both mean and standard deviation are presented. The sign "*" denotes statistically significant differences in comparison with the non-cross-linked (original) samples (Mann-Whitney, *0.05*, *n=5*).

		σ_{pl} [MPa]	$E_{\sigma 20\text{-}\sigma 70}$ [MPa]	σ_{ps} [MPa]	W_a [MJm^{-3}]	W_e [%]
ORIGINAL	**mean**	**0.51**	**11.20**	**0.50**	**0.26**	**61.0**
	SD	*0.10*	*4.01*	*0.02*	*0.03*	*2.9*
EDC/NHS/ETOH	**mean**	**0.86***	**24.70***	**0.67***	**0.42***	**61.8**
	SD	*0.26*	*9.97*	*0.09*	*0.13*	*2.6*
GENIPIN	**mean**	**1.98***	**57.30***	**1.50***	**0.91***	**62.1**
	SD	*0.32*	*7.21*	*0.10*	*0.11*	*3.4*
EDC/NHS/PBS	**mean**	**1.01***	**29.9***	**0.83***	**0.50***	**60.0**
	SD	*0.17*	*5.08*	*0.08*	*0.06*	*2.7*

I.2.4 Collagen secondary structure

The FTIR (Fourier transform infrared spectroscopy, for details please see *Appendix B.2*) spectra (Fig. 4, Table 2) of non-cross-linked (original) and cross-linked composite scaffolds contain bands typical for collagen such as N–H stretching at ~3 303 cm^{-1} for amide A and C–H stretching at ~3 080 cm^{-1} for amide B. Generally, amide I bands (~1 650 cm^{-1}) originate from C=O stretching vibrations coupled with N–H bending vibration. Amide II bands (~1 548 cm^{-1}) arise from N–H bending vibrations coupled with C–N stretching vibrations. The observed spectra bands consist of PDLLA as well as bands of PDLLA shared with collagen (Fig. 4).

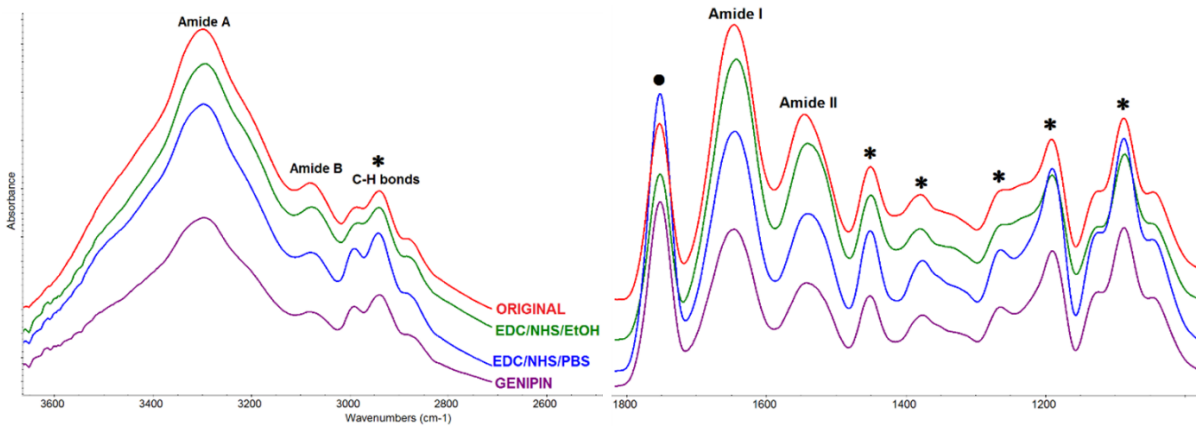

Fig 4. The FTIR spectra of non-cross-linked and cross-linked composite scaffolds. ● = PDLLA bands, ∗ = collagen and PDLLA shared bands.

Table 2. The area containing amide bands and their positions within the FTIR spectra of collagen before and after chemical cross-linking (*n=5*).

Amidic band	Amide A		Amide B		Amide I		Amide II	
	Peak position	Area	Peak position	Area	Peak position	Area	Peak position	Area
ORIGINAL	3298	10.40	3081	0.20	1646	4.51	1545	1.86
EDC/NHS/EtOH	3294	9.90	3077	0.19	1643	4.71	1541	2.06
GENIPIN	3297	5.90	3081	0.09	1645	2.48	1542	1.14
EDC/NHS/PBS	3297	9.50	3079	0.15	1645	3.87	1541	1.68

Following chemical cross-linking the position of the FTIR bands remained practically unchanged which may suggest that the secondary structure of collagen was not destroyed (Table 2). However, individual spectra differ in terms of the integral absorbance of amidic bands. As can clearly be seen in Fig. 4 and Table 2, those scaffolds cross-linked with EDC/NHS/EtOH, with EDC/NHS/PBS and with genipin embody smaller areas of amide A and amide B as compared to non-cross-linked scaffolds. The amide A and OH bands (from water bonded to collagen) are located within the same range (3 700-3 100 cm^{-1}) of the FTIR spectrum. The reduced integral absorbance is caused by the loss of water bonded to collagen during the cross-linking reaction. The same trend was observed by Sionkowska et al. [95]. It can be expected that the intensity of the amide I and amide II bands will increase with the level of polymer cross-linking due to the increasing strength of C=O and N-H vibrations in the new covalent bonds [96]. However, this cannot be taken as a certainty; according to Wang et al. [97], due to the transformation of $–NH_2$ into N-H groups in cross-linked collagen, the intensity of the amide II band may decrease since the intensity of the $–NH_2$ band is stronger than that of N-H. It was observed by Chaubaroux et al. [98] that during rinsing following the cross-linking procedure some of the non-cross-linked collagen elements in the sample were washed away. Consequently, there is a lower number of C=O vibrations and thus a smaller amide I peak area. It would also appear that the presence of PDLLA does not negatively influence the cross-linking of collagen; however, PDLLA was found to share bands with collagen (Fig. 4). A region from 1 410 to 1 500 cm^{-1} which demonstrates the formation of conjugated alkene and which confirms cross-linking by genipin is overlapped by a PDLLA band and, consequently, it is difficult to assess the effectiveness of cross-linking in genipin cross-linked scaffolds. It can, however, be confirmed that scaffolds cross-linked with EDC/NHS/EtOH show similar integral

absorbencies of amidic bands as non-cross-linked scaffolds. On the basis of FTIR analysis, the application of EDC/NHS/PBS and genipin cross-linkers appears to be the most effective in this respect.

I.2.5 Degradation

The rate of cross-linking can be also assessed by means of testing the degradation of scaffolds under *in vitro* conditions, i.e. by determination of mass loss and the swelling ratio. The experiment aimed to simulate the conditions of *in vitro* biological test - the samples were immersed in a fully supplemented cultivation medium (α MEM, Life Technologies, USA) at 37 °C and a 5 % CO_2 atmosphere for 8 days (for details please see *Appendix B.3*). The degradation experiment aimed both to verify changes to the physical and structural properties of cross-linked scaffolds during *in vitro* cellular cultivation and to provide support for the findings of the determination of cross-linking rate. Due to the extensive disintegration of the non-cross-linked (original) samples under degradation test conditions, it was not possible to use them as control samples. The mass losses of cross-linked scaffolds are summarised in Fig. 5. Accelerated mass loss was observed in the case of the EDC/NHS/EtOH cross-linked sample (23-29%); the mass loss of this sample increased markedly as early as on the first day of the experiment and continued to increase up to day 8 (up to a further 5%). In contrast, in the case of cross-linking with EDC/NHS/PBS and genipin, the mass loss did not change significantly from day 1 to day 8. The accelerated mass loss in the case of the EDC/NHS/EtOH cross-linked samples may indicate an insufficient rate of collagen matrix cross-linking.

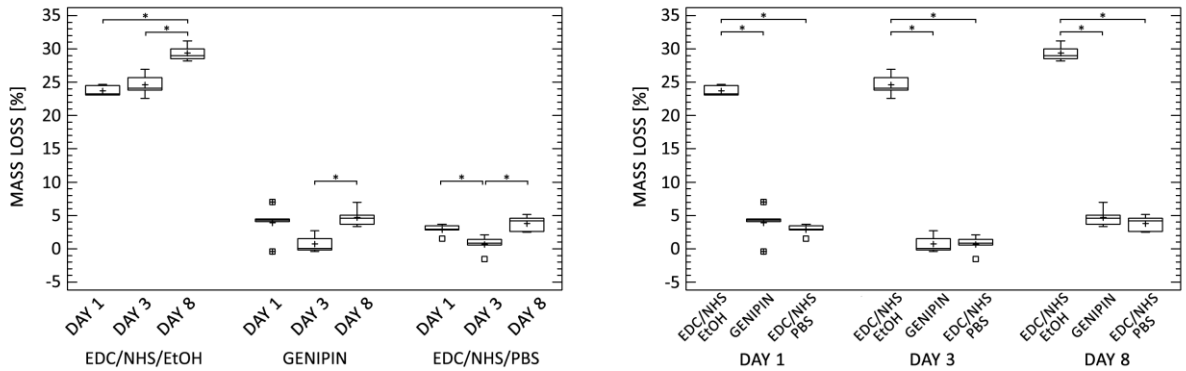

Fig. 5. The mass loss of cross-linked scaffolds. The sign "*" denotes statistically significant differences (Mann-Whitney, *0.05*, *n=5*).

The swelling ratio is summarised in Fig. 6. On the first day those scaffolds cross-linked with EDC/NHS/EtOH show the highest swelling ratio rate (548%); conversely, those scaffolds cross-linked with genipin show the lowest rate (407%). The swelling ratio of scaffolds cross-linked with EDC/NHS/PBS was found to be somewhere between that of the afore-mentioned two scaffolds. However, the swelling ratio of EDC/NHS/EtOH samples remained unchanged over the 8-day incubation period. Fig. 6 (left) shows the data variance between swelling ratios, especially in the case of day 8. The assessed swelling ratio values may have been influenced by the degradation processes occurring within each sample. The accelerated mass loss of the EDC/NHS/EtOH samples influenced the high rate of variability of the swelling ratio data due to the gradual disintegration of the samples. Interestingly, the mass loss of the EDC/NHS/PBS and genipin cross-linked samples were found not to be statistically

significantly different over time; however, a differing trend was observed in terms of the swelling ratio from day 8.

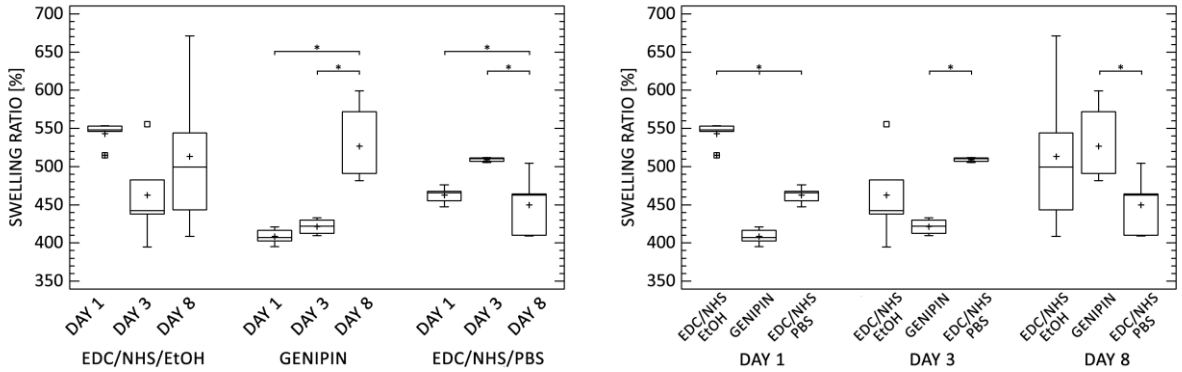

Fig. 6. The swelling ratios of cross-linked scaffolds. The sign "*" denotes statistically significant differences (Mann-Whitney, *0.05*, *n=5*).

Mass loss and swelling ratio provide effective indices for the evaluation of the scaffold cross-linking rate. The highest mass losses were related to samples cross-linked with EDC/NHS/EtOH: weight loss occurred immediately following 24 hours of immersion. Assuming that the collagen part of the scaffold (50.5 wt%) is the only component susceptible to rapid degradation within such a short time period, then the mass loss of the collagen part of the EDC/NHS/EtOH would be equal to half of its complete amount within the scaffold (up to 29%). This behaviour, as well as the considerable variance in the swelling ratios after the third and eighth days of incubation, indicates the lowest stability level of the collagen part and thus the whole of the scaffold structure. It is possible to hypothesise that the structural stability of the scaffold is related to the degree of cross-linking [99]. In contrast to the scaffolds cross-linked in an ethanol solution, the mass loss of samples cross-linked with EDC/NHS/PBS and genipin show the same low level of mass defects, i.e. the highest stability levels and, most probably, the highest degree of cross-linking. Nevertheless, their structural stability evaluated in terms of swelling behaviour evinces a different tendency following the early stages of incubation. In both cases the swelling ratios on day 1 and day 3 are equal, however, 8 days subsequent to incubation the swelling ratio of the genipin cross-linked samples increased; conversely, the swelling ratio of the EDC/NHS/PBS cross-linked samples decreased. The decrease in swelling ratio was not reflected in mass loss which might have indicated the disintegration of the internal structure.

I.2.6 Concluding remarks

It was shown that the effectiveness of cross-linking via different methods, as studied here, varies considerably. It should be observed that the differences occurred primarily between the different solutions. There was a clear difference between the behaviour of composite scaffolds cross-linked by the EDC/NHS system in the aqueous solution and pure ethanol. The differences in the mechanical behaviour, degradation profile and secondary structure of the collagen clearly illustrate the role of the water content in the cross-linking reaction. In addition to the cross-linker concentration, the temperature and time of the reaction and the water or moisture content must be taken into account in order to achieve a successful reaction. This effect can be illustrated on an example of genipin cross-linking by means of a simple experiment. The successful cross-linking of collagen via genipin is

accompanied by the formation of a dark blue colour, which is a side effect of the reaction of genipin with the free NH_2 groups of lysine, hydroxylysine and arginine in the collagen. Figure 7 illustrates the role of water content in the genipin cross-linking reaction. While the scaffolds in the genipin ethanol solutions with higher amounts of water evinced a typical blue colour, the scaffolds immersed in solutions with low amounts of water did not evince any sign of a cross-linking reaction.

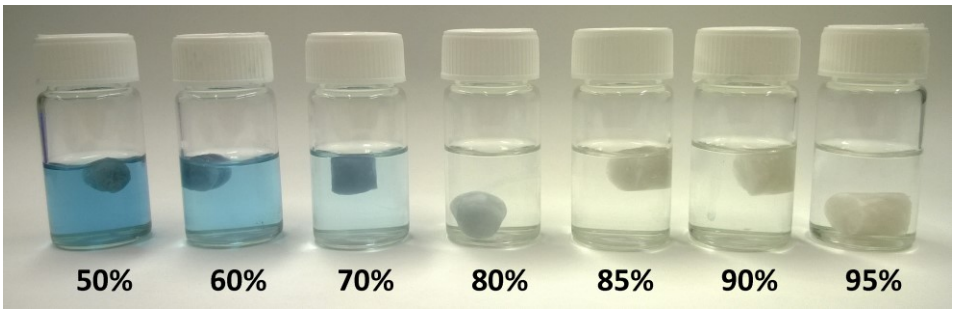

Fig. 7. A simple experiment proving the role of water in the collagen cross-linking reaction. All the scaffolds have been immersed in ethanol with different weight amounts of water (5-50 wt%). The time of the reaction as well as the genipin concentration and temperature were maintained at the same level for all the samples.

Since the secondary structure of collagen can be damaged by its processing, collagen materials as prepared prior to additional cross-linking may be prone to dissolution in aqueous solutions. From this point of view, the application of ethanol-based cross-linking systems would be advantageous in terms of the preservation of the inner structure of the prepared samples, particularly for highly porous scaffolds. It is then necessary to strike a compromise between the amount of water as the reaction catalyser and ethanol. In the case of low aqueous contents, the reaction can be improved by means of prolonged times or an increase in temperature. The effect of increased temperature is illustrated by the FTIR spectra (Fig. 8) of non-cross-linked collagen (original) and collagen cross-linked by genipin in 100% ethanol at room temperature (RT) or at 37°C.

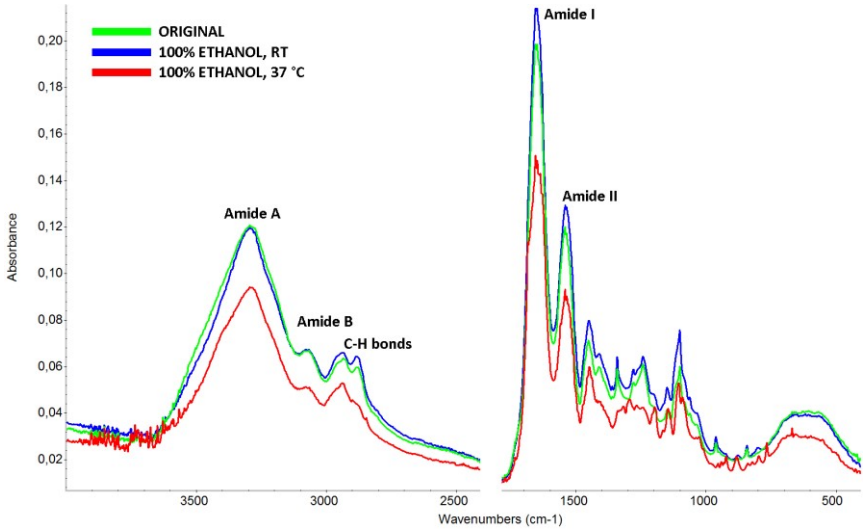

Fig. 8 The FTIR spectra of non-cross-linked collagen (original) and collagen cross-linked by genipin in 100% ethanol at room temperature (RT) or at 37°C.

The reduced integral absorbance of the amide A and OH bands of collagen cross-linked at 37°C are the result of the loss of the water that bonded to the collagen during the cross-linking reaction. The cross-linking reaction was accompanied by a decrease in the intensity of the band at ~2900 cm^{-1} (related to the C-H bonds of the CH_2 groups in the collagen and genipin) caused by the participation of CH_2 groups in cross-linking, e.g. in the dimerization of genipin.

The effect of a prolonged reaction time was illustrated by a simple experiment depicted in Fig. 9. The collagen samples were kept in 100% ethanol with three different genipin to collagen weight concentrations (1:1, 2.5:1 and 5:1) at room temperature for up to 108 days. The typical dark blue colour that accompanied the genipin cross-linking reaction, which is visible for all the concentrations, suggests that cross-linking can be attained even under such conditions.

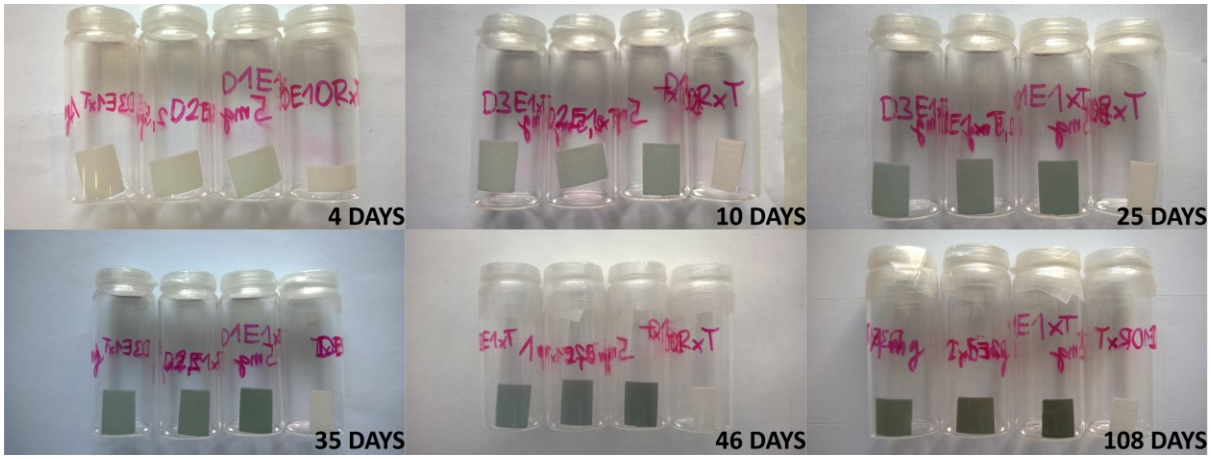

Fig. 9 The genipin cross-linking reaction in collagen samples kept in 100% ethanol with three different genipin to collagen weight concentrations (from left in each photograph: 1:1, 2.5:1 and 5:1) at room temperature for up to 108 days. The sample container on right in each photograph contains a collagen sample immersed in 100% ethanol without genipin (control sample).

It is clear that in many cases the methods described herein represent a compromise between the degree of disruption/modification of the structure of collagen and the maximum conservation of the inner structure, desired mechanical and degradation properties. A further very important issue concerns the preservation of the biological functions of the collagen biomaterial. Therefore, in this study, the biological evaluation under *in vitro* conditions was performed by means of the cultivation of human mesenchymal stem cells in the cross-linked scaffold infusions (i.e. the degradation products of the individual scaffolds) in order to check for the release of cytotoxic agents from the individual scaffolds into the cultivation medium. The next step involved the seeding of the cells directly on the infused scaffolds and cultivation for 2 and 7 days, whereupon the number of adhered cells on the scaffolds was determined. Examples of the fluorescence images of the cells is provided in Figure 10. The *in vitro* cell tests are described in detail in a paper by the author [3]. Briefly, based on *in vitro* testing, the genipin cross-linked scaffold was selected as having provided the best results and it was strongly recommended for further advanced in vitro (3D cultivation) and *in vivo* testing. However, with regard to the very high price of genipin and the low stability of all three types of tested scaffolds during 3D cell cultivation under dynamic conditions, a further improvement in scaffold stability was necessary.

Hence, several tests were performed aimed at the optimization of cross-linking conditions, and a novel cross-linking system based on EDC/NHS and 95 wt% ethanol was proposed and verified. In addition, it was necessary to improve the composition of the scaffolds. The aim of the work described in the next chapter was to describe the influence of eight differing scaffold material compositions focusing on the collagen content and their final properties such as internal structure, porosity and mechanical properties in both the dry and hydrated states. It was anticipated that the differences in the physical properties following hydration would represent a significant limiting factor for the seeding, growth and differentiation of mesenchymal stem cells and the overall applicability of such hydrophilic materials.

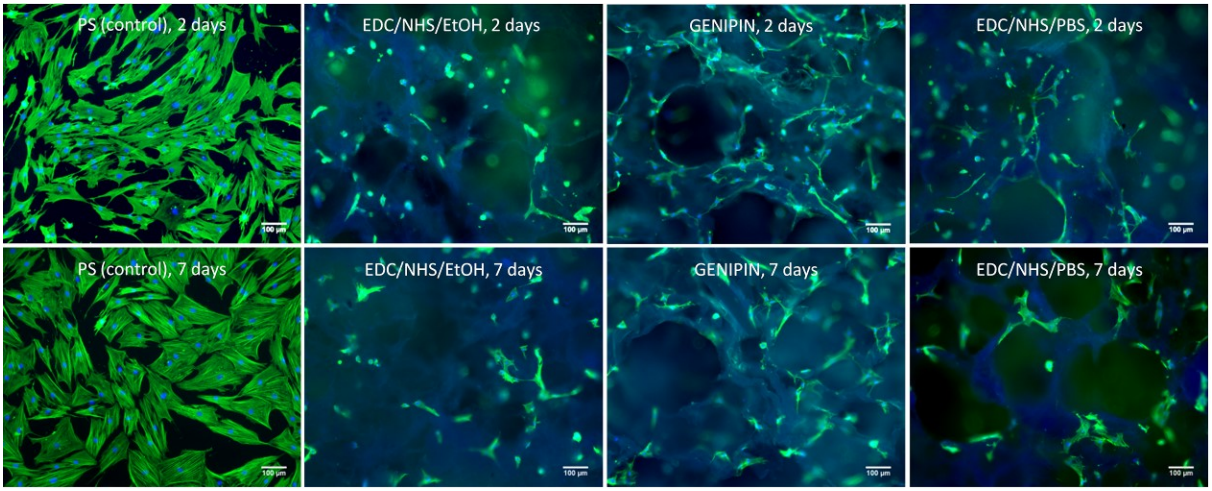

Fig. 10 Fluorescence images of human mesenchymal stem cells cultivated on the control polystyrene (PS) and the tested scaffolds cross-linked with EDC/NHS/EtOH, genipin and EDC/NHS/PBS for 2 d (upper line) and 7 d (lower line). Actin filaments representing cell morphology are stained in green, the cell nuclei in blue.

I.3 The effects of different scaffold compositions in the dry and hydrated states

I.3.1 Composition of the scaffolds

Composite scaffolds as described in *Chapter I.2* were prepared in 8 material variations with different amounts of each component, i.e. collagen matrix (COL), poly DL-lactide sub-micron fibres (PDLLA), bioapatite (bCaP) and sodium hyaluronate powder (HYA) employing the procedure described in detail in *Appendix A.1*. The composition of the scaffolds is provided in Figure 11. The collagen part of the scaffolds was cross-linked by EDC/NHS at a weight ratio of 4:1 in a 95 wt% ethanol solution.

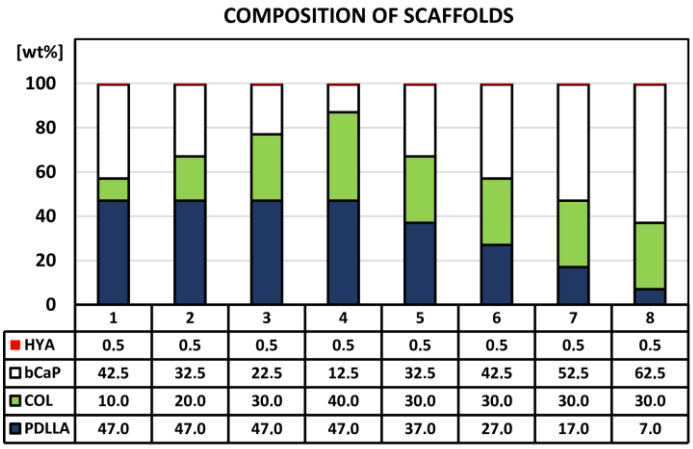

	1	2	3	4	5	6	7	8
HYA	0.5	0.5	0.5	0.5	0.5	0.5	0.5	0.5
bCaP	42.5	32.5	22.5	12.5	32.5	42.5	52.5	62.5
COL	10.0	20.0	30.0	40.0	30.0	30.0	30.0	30.0
PDLLA	47.0	47.0	47.0	47.0	37.0	27.0	17.0	7.0

Fig. 11 Composition of the scaffolds in relation to the dry basis.

I.3.2 Mechanical properties

In order to describe the mechanical behaviour of the scaffolds in the dry and hydrated states, compression tests were performed again by means of the adaptation of the ISO 13314 standard (in details described in *Appendix B.1*). The mechanical properties of the scaffolds were measured on both dry samples and samples hydrated in α MEM medium (Life Technologies, USA) for 24 and 48 h. Six cylindrical samples with a diameter of 6.2 mm and a length of 8.5 mm were tested in each group (i.e., a sample length to diameter ratio of ~1:4). The mechanical properties of the scaffolds in the dry and hydrated states obtained in the study are provided in Figures 12-14.

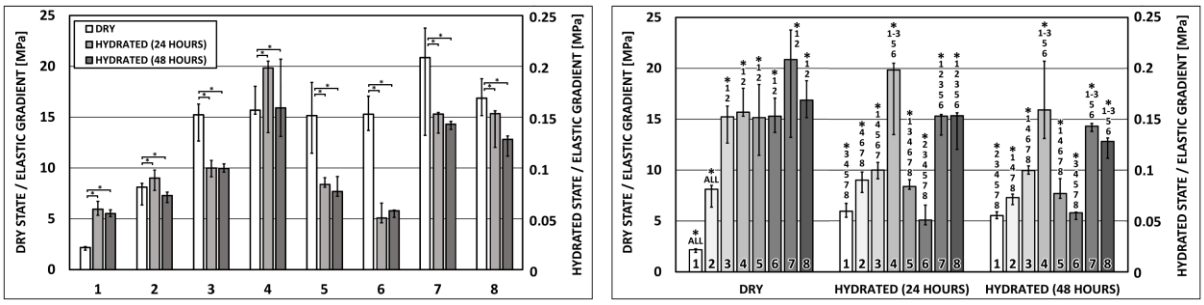

Fig. 12 Elastic gradient (elastic modulus) of the scaffolds in the dry and hydrated (24 and 48 h) states (median, IQR). Note that opposite axes have different scales. * denotes statistically significant differences (Mann–Whitney, *0.05*, *n=6*) between different states (left) and different samples (right).

The mechanical properties of composite scaffolds were influenced by their composition, namely the weight or volume fraction of particular components. In our case, it appears that the collagen matrix played an essential role in terms of mechanical behaviour in both the dry and hydrated states. In the dry state, the low amount of collagen (10–20 wt%) reduced the degree of stiffness (represented by the elastic gradient) to ~2–7 MPa and compressive strength (represented by plateau stress) to ~0.1 - 0.3 MPa. 30 - 40 wt% of collagen appeared to represent a sufficient amount so as to provide for the appropriate bonding of all the components of the scaffolds. This was represented by the stable level of stiffness (15 MPa) and compressive strength (0.5 MPa) of samples 3–8; the differing weight fractions of PDLLA and bCaP did not exert a statistically significant effect on the mechanical properties (Figs. 12, 13).

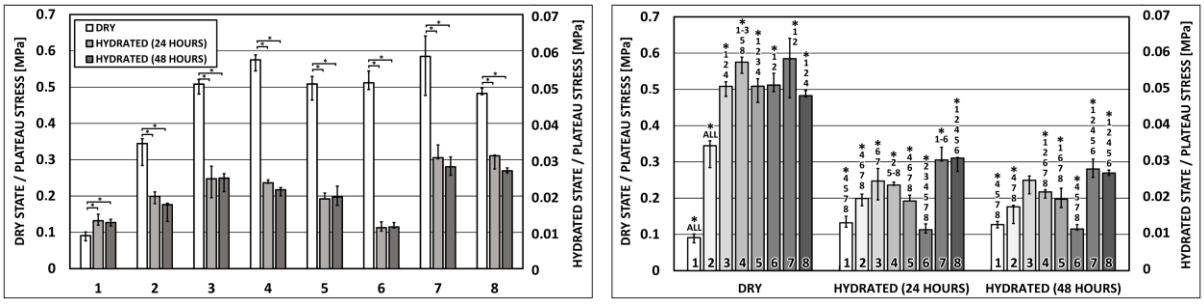

Fig. 13 Plateau stress (compressive strength) of the scaffolds in the dry and hydrated (24 and 48 h) states (median, IQR). Note that opposite axes have different scales. * denotes statistically significant differences (Mann–Whitney, *0.05*, *n=6*) between different states (left) and different samples (right).

The elastic modulus of all eight samples decreased immediately following hydration (Fig. 12). This statistically significant drop was represented by an up to 100 times lower degree of stiffness. A further 24 h of hydration was found to exert no significant effect on stiffness. A similar trend was evinced by the compressive strength of all the samples following hydration (Fig. 13). The plateau stress of all the samples decreased up to 10 times following 24 h and remained stable after a further 24 h. In contrast to previous findings, energy absorption efficiency (Fig. 14) decreased only up to 20% following hydration. This parameter represents the ability of the material to effectively absorb deformation energy. A comparison of energy absorption efficiency in the dry and hydrated states indicated relatively low changes in the inner structure of the scaffolds following hydration.

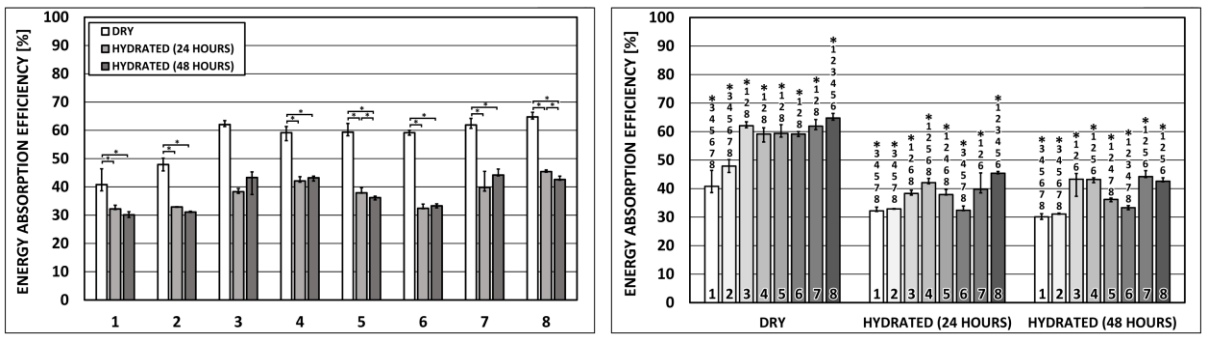

Fig. 14 Energy absorption efficiency of the scaffolds in the dry and hydrated (24 and 48 h) states (median, IQR). * denotes statistically significant differences (Mann–Whitney, *0.05*, *n=6*) between different states (left) and different samples (right).

I.3.3 Scaffold characterisation in the dry and hydrated states

The investigation of mechanical properties was further accompanied by analysis of the effect of hydration on scaffolds structural parameters. The morphology of the scaffolds was investigated by means of micro-CT analysis in both the dry (Fig. 12) and hydrated states. The main structural parameters consisted of open porosity volume (percent), closed porosity volume (percent) and pore size which was assessed in 3D based on the structure thickness distribution determined via the sphere-fitting algorithm. Detailed description of micro-CT procedures and contrasting of samples are described in *Appendix B.4*.

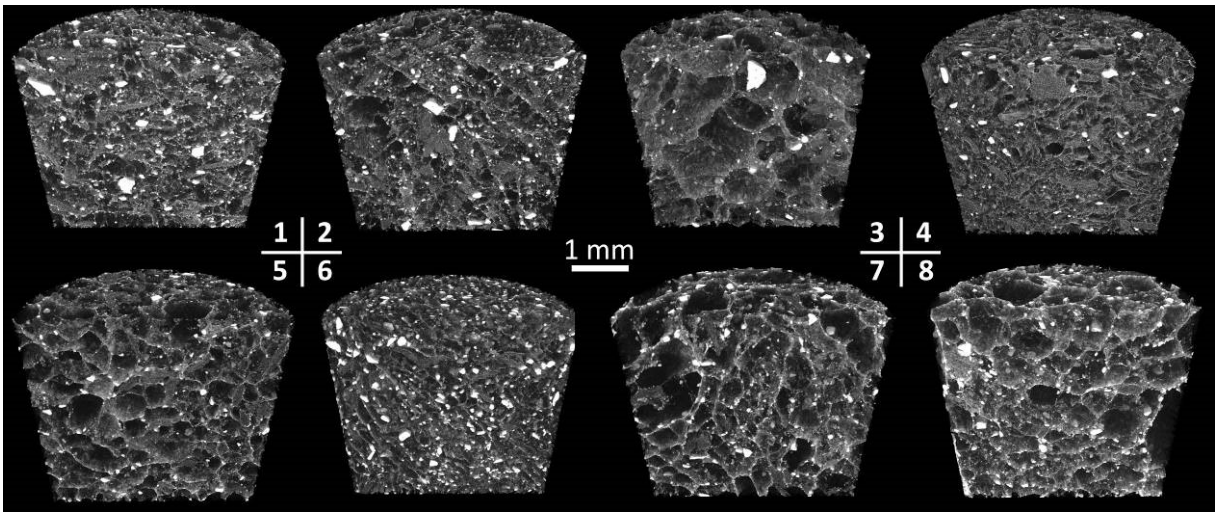

Fig. 12 Micro-CT visualisation of the 8 types of scaffolds in the dry state. Scale bar 1 mm.

The morphology parameters obtained by means of micro-CT analysis are presented in Figure 13. Pore size in the dry state varied for each type of scaffold, with concern to which the respective types can be divided into 3 groups with similar values: low-pore size (scaffolds 1, 2, 4 and 6), medium pore size (scaffolds 5, 7 and 8) and large pore size (scaffold 3).

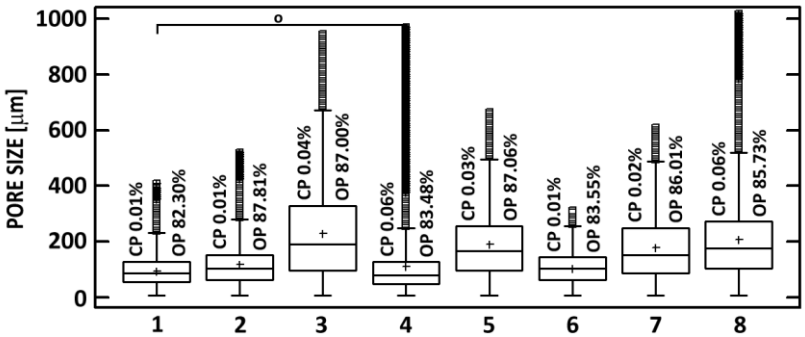

Fig. 13 Pore size, closed porosity (CP) and open porosity (OP) of the composite scaffolds in the dry state measured employing micro-CT 3D analysis. All the values exhibited statistically significant differences except those values designated by the symbol "o" (Mann–Whitney, *0.05*, *n=3*).

Open porosity values (OP = volume of the open pores/total VOI volume) ranged from 82.3 to 87.81%. Open pores were defined as spaces within the scaffold structure which displayed a connection with the space outside the object. All the scaffold types provided a high degree of open porosity. Closed

porosity values (CP = volume of closed pores/scaffold volume + the volume of closed pores) ranged from 0.01 to 0.06%. Scaffold volume was taken to mean the volume of scaffold material without the pores. Closed pores were defined as spaces completely surrounded by the scaffold structure with no connection in 3D with the surface of the scaffold. All the specimens exhibited a very low degree of closed porosity, thus suggesting a high degree of interconnected pores.

In order to provide for the illustration of the influence of hydration on the inner structure, the porosity of selected samples with different compositions (scaffolds 3, 6 and 8) was measured by means of micro-CT 3D analysis. Three types of scaffold were subjected to analysis during hydration in deionised water (Fig. 14).

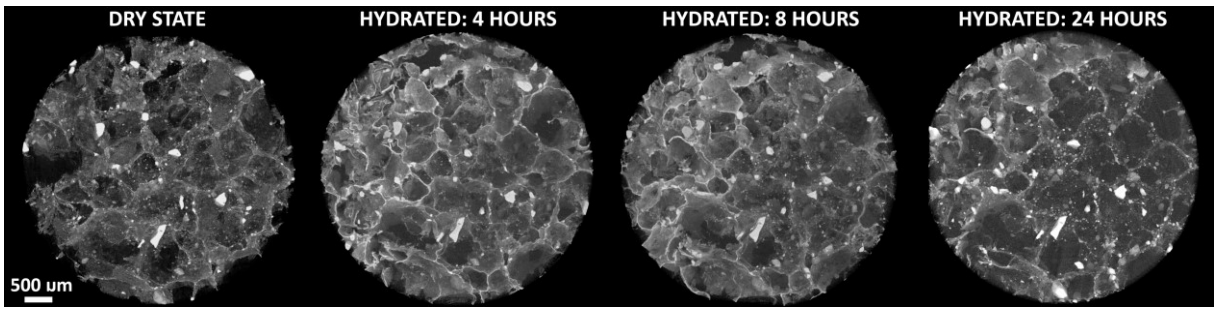

Fig. 14 3D visualisations of sections of scaffold specimen in the same position (type 3) in the dry state and at different time intervals following initial hydration. The inner structures of the scaffolds are visible including the pore walls, pore spaces and bCaP particles (higher X-ray density). Increased scaffold structure thickness can be observed as a result of hydration with an X-ray contrast agent, probably due to collagen swelling. Scale bar 500 µm.

One specimen was chosen from each group of scaffolds (based on differing pore size as mentioned above as group with low, medium and large-pore size) (Fig. 15). Analysis was performed in the same way as in the dry state. The time intervals were 0 (dry state), 4, 8 and 24 hours following initial hydration. An initial reduction in open porosity (4 hours) to below the dry state value was followed by a slight increase in this parameter with respect to all the specimens. Closed porosity initially slightly increased (4 hours) with concern to all the specimens, following which a reduction was observed concerning specimens 3 and 8. Specimen 6 maintained the increased level of closed porosity.

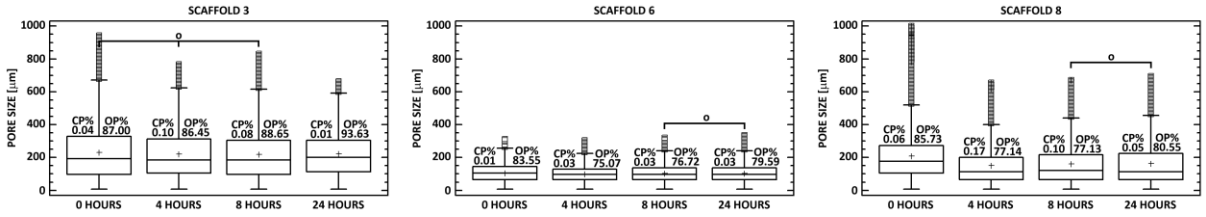

Fig. 15 The pore size, closed porosity (CP) and open porosity (OP) [%] of the composite scaffolds in the dry state and hydrated for 4, 8 and 24 h measured by means of micro-CT 3D analysis. All the values exhibit statistically significant differences except those values designated by the symbol "o" (Mann-Whitney, *0.05*, *n=3*).

In order to determine the effect of hydration on the inner structure, permeability of scaffolds within the 24 hours was measured (for details please see *Appendix B.5*). The permeability of 71 scaffolds was tested (from *n=6* to *n=11* specimens for each of the eight scaffold types) and three measurements were performed for each scaffold immediately following a hydration period of 5min (K_0), and after 4 (K_4), 8 (K_8) and 24 (K_{24}) hours. The overall K_0 mean permeability was found to be in the range 2×10^{-13} (type 4) and 8.5×10^{-13}m^2 (types 1 and 7). Permeability measurements over time revealed the stable behaviour of the scaffolds irrespective of scaffold type with no significant differences. Notably, scaffold type 2 exhibited a pronounced increase in the permeability value after 4 hours (Fig. 16, left). The statistical comparison of the 8 types of scaffold revealed a number of significant differences (Fig. 16, right); importantly, scaffold type 1 exhibited very high-permeability values (especially after 24 hours) which differed significantly from the other scaffold type values (Fig. 16, right).

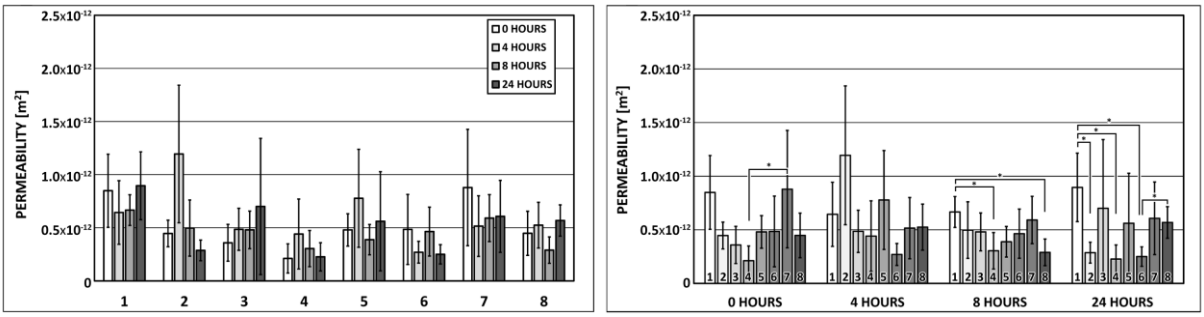

Fig. 16 Permeability after 5 min hydration (0 h) and after 4, 8 and 24 h (arithmetical mean, standard deviation). * denotes statistically significant differences (Mann-Whitney, *0.05*, *n=6-11*) between different periods (left) and different samples (right).

The effects of scaffolds exposition in α MEM medium (37 °C, 5% CO_2 atmosphere) was also evaluated by means of the determination of mass loss and swelling ratio. The evaluation of degradation test is in details described in *Appendix B.3*. The *in vitro* degradation rates of 8 scaffold material compositions in α MEM medium expressed as mass loss and swelling ratios are summarised in Figs. 17 and 18. Negative values of degradation (Fig. 17) indicate a weight increase.

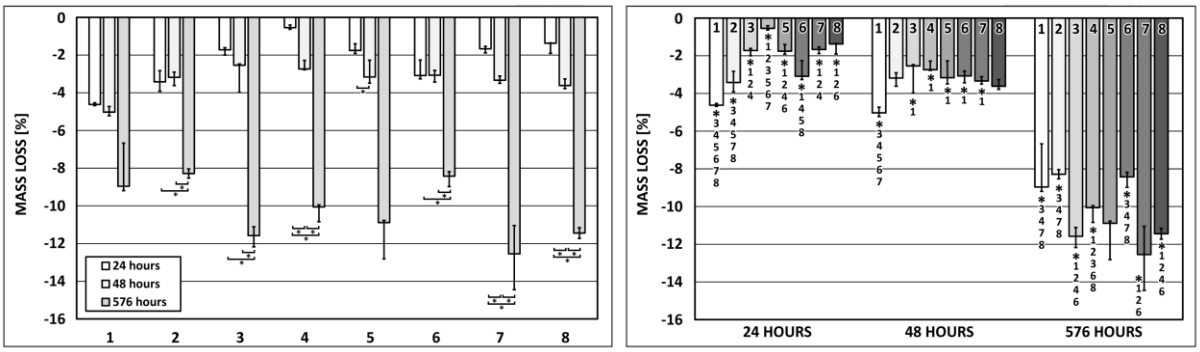

Fig. 17 The mass loss of the scaffolds following 24, 48 and 576 (24 days) hours of immersion in α MEM. * denotes statistically significant differences (Mann-Whitney, *0.05*, *n=3*) between different states (left) and different samples (right).

As can be seen from Fig. 17, the increment size increased over time. The swelling ratio of scaffolds 1 and 6 remained almost unchanged over the 24-day incubation period. All the other scaffolds exhibited an increment in the swelling ratio, which increased according to the period of incubation. This phenomenon was most apparent with respect to scaffolds 7 and 8.

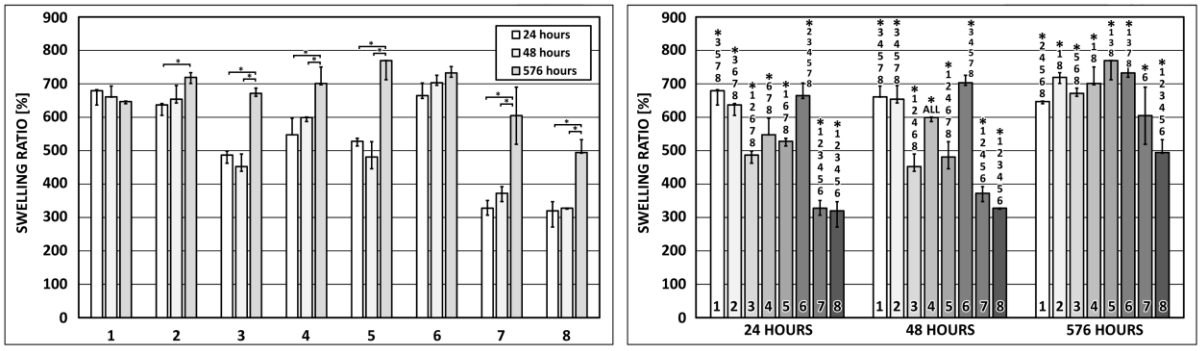

Fig. 18 The swelling ratios of the scaffolds following 24, 48 and 576 (24 days) hours of immersion in α MEM. * denotes statistically significant differences (Mann–Whitney, *0.05*, *n=3*) between different states (left) and different samples (right).

I.3.4 Scaffold characterisation after enzymatic degradation

Moreover, the degradation of scaffolds was also carried out in enzymatic environment (collagenase Clostridium histolyticum) aiming at simulation of activity of bone cells (for detailed procedure please see *Appendix B.6* and *B.3* for test evaluation). The mass loss of individual material compositions after 1 hour of collagenase treatment and their comparison with non-cross-linked collagen (NC) is summarised in Fig. 19, left. Degradation was expressed as wt% loss of the composite and this was recalculated to wt% loss of collagen in the scaffold. Statistically significant differences are evident with respect to scaffolds 1, 2 and the sample NC. Scaffolds 3–8 exhibited a composite loss of up to 1.5 wt% and a collagen loss of ∼4 wt%. Scaffold 1 achieved an almost 8 wt% composite loss and a significant 78 wt% collagen loss.

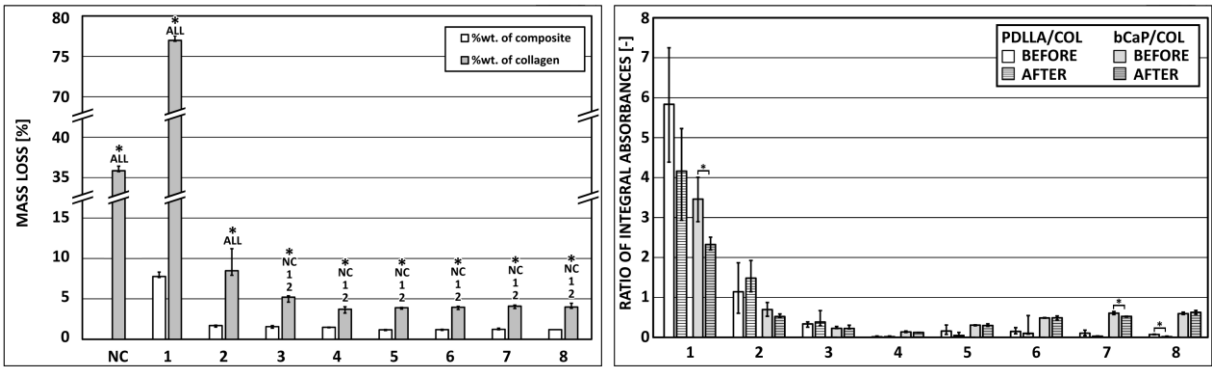

Fig. 19 Left: the mass loss of the scaffolds after 1 hour of collagenase treatment and their comparison with non-cross-linked collagen (NC). * denotes statistically significant differences (Mann-Whitney, *0.05*) between the wt% collagen medians. Right: comparison of the ratio of integral absorbances PDLLA/COL and bCaP/COL of the original scaffolds and then following 1 h of collagenase treatment. * denotes statistically significant differences (Mann-Whitney, *0.05*, *n=4*) between the medians prior to and following collagenase degradation.

FTIR spectroscopy was employed in order to clarify these somewhat anomalous results. Changes in the integral absorbances of individual scaffold components (PDLLA, COL and bCaP) were determined before and after 1 hour of collagenase treatment (Fig. 19, right). For details please see *Appendix B.2*. It was anticipated that these ratios would explain the changes in the composition of the composite following degradation. The strong band ~1750 cm^{-1} belonging to PDLLA, the amide I band (~1650 cm^{-1}) typical for collagen and the ν_4 PO_4 domain (510–660 cm^{-1}) related to apatites were used for the calculation of the ratios of the integral absorbances of individual scaffold components (PDLLA/COL and bCaP/COL). The strongest band ~1030 cm^{-1} belonging to the apatites was not used for calculation purposes due to a partial overlap with the shoulder of the PDLLA band. The medians of the integral absorbance of PDLLA and bCaP (Fig. 19, right) related to COL remained the same or decreased following degradation. Statistically significant differences were most apparent with respect to scaffolds 1 and 7 in the case of the bCaP/COL ratio and scaffold 8 in the case of the PDLLA/COL ratio.

I.3.5 Concluding remarks

Scaffold permeability, combining the topological properties of the 3D structure (such as scaffold porosity, pore size, interconnectivity and tortuosity), plays an important role in determining overall scaffold performance in terms of fluid mass transport (i.e. nutrients and oxygen), waste removal and cell penetration to the core of the scaffold [10]. Hence, defining the optimal scaffold permeability range provides a challenge in terms of the potential use of such scaffolds in tissue engineering applications. The permeability of the 8 types of scaffold presented in this study (order of magnitude of 10^{-13} m^2) is comparable to that reported in literature for collagen-based scaffolds [70,100,101] and falls between the permeability values obtained for trabecular (range from 10^{-10} to 10^{-9} m^2 [102]) and cortical bone (10^{-17} m^2 [103]). The scaffold composition and permeability data indicated that both collagen and apatite content contributed slightly towards determining scaffold permeability at time 0. Briefly, i.e. during the time that the collagen content inversely affected scaffold permeability, apatite content directly influenced the hydraulic behaviour of the scaffolds (Fig. 11 and Fig. 16, right panel). The temporal evolution of scaffold permeability was also investigated up to 24 hours, the results revealing the stable behaviour of all 8 scaffold types. These results are in agreement with the morphological measurement results (pore size, open porosity and closed porosity) obtained via micro-CT (Fig. 13 and Fig. 9). Importantly, this morphological data revealed that scaffold hydration does not affect open porosity, thus guaranteeing stable permeability behaviour over time.

With respect to the swelling and permeability data at 24 hours, an opposite relationship between the swelling ratio (Fig. 18, right panel) and the permeability measurement results (Fig. 16, right panel) was observed. High swelling ratio values corresponded to lower permeability values (i.e. types 2, 4 and 6) and *vice versa* (i.e. types 3, 5, 7 and 8). In addition, type 1 exhibited higher swelling ratio values and high permeability; however, these values were not statistically significant.

The weight increase observed during degradation in α MEM (Fig. 17) can be explained by means of the adsorption of various components (proteins, saccharides, vitamins and salts) contained in the α MEM medium. The weight increments increased with incubation time, which was also observed with concern to swelling (Fig. 18); however, after 576 hours the composites differed from each other less than they did after just 24 and 48 hours of incubation. The smallest swelling values were exhibited by

samples 7 and 8, which contained over 50 wt% of bCaP. Degradation occurred (albeit not particularly apparent) simultaneously to adsorption. The mass loss values of all the scaffolds varied only in terms of units of % and, therefore, it is not possible to state explicit conclusions in this respect.

Conversely, collagenase degradation exhibited the highest rate of collagen degradation with respect to scaffold 1. Scaffolds 3-8 exhibited a difference between the degradation of the composite and that of the collagen of up to 4%, while for scaffold 2 this difference was 7% and for scaffold 1 as much as 70%. These discrepancies can be explained by the low content of collagen acting as a binder holding the scaffolds together. The integral absorbance of PDLLA and bCaP (Fig. 19) related to COL remained the same or decreased following degradation, although these components were not attacked by collagenase. It follows that these components are released from the scaffold. The lower degree of scaffold consistency allows for the enhanced accessibility of collagenase to the collagen and hence the easier degradation thereof. These changes were most evident with respect to scaffolds 1 and 2 which had the lowest collagen content.

Collagen-like peptides tend to adopt the polyproline II helix and have *trans* isomers of their peptide bonds with dihedral angles ($\psi \approx 150^\circ$, $\phi \approx -75^\circ$). *Trans* configuration for the peptide bond is favoured over the *cis* form by 1.3 kcal/mol. The potential energy of the system is a function of the dihedral angle. Gautieri et al. [104] performed the Ramachandran analysis of a fully equilibrated full-atomistic collagen microfibril system in both hydrated (wet) and dehydrated (dry) conditions. They proved that hydrated collagen microfibril lies within a region of the diagram ($\psi \approx 150^\circ$, $\phi \approx -75^\circ$) characteristic of the polyproline II chain and thus of collagen-like peptides. However, an analysis of the dehydrated collagen microfibril system revealed a broader range of dihedral angles indicating a certain level of molecular unfolding. Dehydrated microfibrils exhibit higher dihedral energy than they do in the hydrated state. This suggests that in the dehydrated microfibril the deformation mechanism initially involves primarily the straightening of the collagen molecules and not the stretching of the molecules. Conversely, the hydrated state allows collagen molecules to adopt conformations with maximal entropy, and the system exhibits a low level of dihedral (potential) energy. However, the mechanical properties are highly scale dependent. A direct numerical comparison suggests differences in Young's modulus of from several GPa for a single molecule to a few hundred MPa for collagen microfibrils, representing a striking change in the mechanical properties at different hierarchical levels [104]. The system studied herein was much more complicated since the collagen was chemically cross-linked. The presence of covalent inter-molecular cross-links increased adhesion at the ends of each molecule [105]. In addition, the system had a high porosity level and elastic deformation occurred primarily via the bending of slender structural elements, such as the cell walls. This allowed for significant deflections under low applied loads – i.e. the generation of low levels of stiffness – and this makes up the basis of many types of (highly compliant) fibre network materials [70].

Due to the possible future application of scaffolds, it is suggested that the results also be considered with respect to the cell perspective. The results indicate that the combination of materials, the ratio of material components, fibre organisation into higher structural units and specific environmental conditions determine the surface area, porosity, swelling and degradation of the composite. All of them are capable of fundamentally determining cell adhesion as well as overall function [54,55]. The

results revealed that bCaP had no significant effect on the mechanical properties of the scaffolds tested. Thus, from the cell perspective, scaffolds with a higher bCaP content may be more preferable. However, the results also showed that the mechanical properties of the scaffolds were directly influenced by the presence of collagen. The results confirmed the previously observed dependency between collagen and the mechanical properties of the scaffolds and revealed the opposite proportionality between collagen content and the stiffness of the material. Therefore, scaffolds with a collagen content in the scaffold of around 30-40% would appear to be more appropriate in terms of predicted cell adhesion. If we take this result together with the afore-mentioned potential biological benefits of bCaP, it can be assumed that the optimum mechanical properties in terms of cell application will be provided by scaffolds with a higher bCaP content and a collagen content of around 30-40%. That said, a more specific determination of the best ratios of both components in the scaffold can be provided only by means of a biological evaluation. The results revealed the elastic deformation of the tested scaffolds, which indicated a low degree of stiffness. In general, material stiffness determines the generation of cell traction forces and, subsequently, affects changes in cell morphology and movement and cell differentiation [13,106,107]. With respect to bone tissue engineering, scaffolds with the highest levels of rigidity (lowest elasticity) are recommended with concern to cell osteo-differentiation.

The results also revealed variability with respect to other factors which may crucially impact cell behaviour - swelling, porosity and pore-size [108]. The observed general elevation of the swelling rate following hydration may be significantly affected by the scaffold environment, thus by the presence of a cultivation medium (specifically α MEM supplemented with foetal bovine serum (FBS)). Moreover, water binding by medium proteins (originating in FBS), in connection with other scaffold components (which differed with respect to all the scaffolds tested), may have resulted in differences in the swelling rate of the tested scaffolds [109,110]. Therefore, the optimal scaffolds for cell application would appear to be those that change only slightly during the first 24 hours of incubation (scaffolds 1 and 6) or those scaffolds with the lowest swelling ratio (scaffolds 7 and 8). From the viewpoint of permeability, which is directly related to swelling (as the results indicate) and which is important with respect to cell nourishment and penetration, those scaffolds displaying higher permeability would appear to be more suitable (i.e. scaffolds 3, 5, 7 and 8).

Swelling is also closely related to pore size and porosity. From the perspective of biomaterial engineering and the development of artificial extracellular matrices, we determined no clear results concerning the ideal pore size and porosity of cells [111,112]. The variable results suggest, therefore, the importance of the context of the entire scaffold. The scaffold porosity results predicted a degree of porosity of 85% and a high degree of interconnected pores, both of which are important factors in terms of cell nutrition and cell migration. When compared to native bone, the scaffolds are close to cortical bone with respect to pore size (porosity 3–12%, pore-size 100–200 μm); however, the degree of porosity indicates a closer approximation to trabecular bone (a high porosity of around 50–90%, pore size diameters of up to 1 mm) [113,114]. Thus, from the perspective of the native state of bone, the scaffolds have the potential to provide an artificial bone matrix. In addition, the aim of the scaffold is to allow cells to adhere within the structure of the scaffold and to remain in this position for subsequent proliferation and differentiation.

The pore size, permeability and mechanical properties of tissue engineering scaffolds influence migration and cell growth in the context of cell seeding and further cultivation. Permeability connects the structural properties of the 3D structure and affects the hydration of the scaffold. Moreover, depending on the composition of the material, the hydration of such highly porous structures may further influence mechanical behaviour and porosity due to swelling. This mechanism is particularly obvious in the case of scaffolds prepared based on the use of hydrophilic materials, such as collagen, gelatine and chitosan as natural polymers. This study evaluated both the mechanical and structural properties of scaffolds in the dry and hydrated states. Hydration, simulating the conditions of cell seeding and cultivation up to 48 and 576 hours, was found to exert a minor effect on the morphological parameters, such as pore size, open porosity, and on the permeability. The mass loss of individual scaffolds was detected only following the application of targeted enzymatic treatment by means of collagenase, with no indication of degradation in the cultivation media. Conversely, hydration had a major statistically significant effect on the mechanical behaviour of all the tested scaffolds with no effect according to the amount of collagen. The elastic modulus and compressive strength of all the scaffolds with 10–40 %wt of collagen decreased by ~95%. Despite a small change in the structural properties, this decrease confirms the importance of analysing scaffolds in the hydrated rather than the dry state since the former more precisely simulates the real environment for which such materials are designed. The measurement of scaffolds in the dry state is, however, useful with respect to the basic characterisation of the selection of preparation methods and chemical treatment; however, it is important that real conditions not be neglected, especially with concern to hydrophilic polymers.

I.4 Notes on the use of different approaches to the evaluation of bone tissue engineering scaffolds

I.4.1 The effects of various simulated body fluids

The previous part of the thesis drew the reader's attention to the importance of analysing scaffolds in the hydrated state due to its more precisely simulating the real environment for which such materials are designed. In this final section, the author would like to point out the main pitfall regarding the selection of the simulated body environment. In the course of the development of biomaterials, it is not always possible to perform *in vivo* animal experiments, especially in the early stages that deal with the determination of the processing parameters and the optimization of the mechanical and structural parameters, evaluation of possible toxicity, etc. The application of experimental animal models is strictly controlled by ethical rules and, most often, is employed only in the final part of the biomaterial development process. Thus, the *in vitro* simulation of the body environment represents a useful approach in the overall experimental process. When designing such experiments, the researcher must answer a number of questions: What kind of simulated body fluid or medium to use? What test conditions to apply? What kind of information is required? Is it possible to interpolate the experimental *in vitro* results to real *in vivo* conditions or processes? Is it possible to verify them?

In the previous paragraphs, the author employed the cell cultivation medium for simulating *in vitro* biological evaluation conditions by means of mesenchymal stem cells. Hence, the same medium and conditions, e.g. temperature and atmosphere, were applied. The results consisted of the prediction of the mechanical and structural behaviour during the *in vitro* test. Such information is beneficial in terms of the interpretation of cell behaviour since changes in both the mechanical and structural properties of scaffolds may exert an important influence in this respect. Similarly, the application of collagenase or other enzymes may, to a certain extent, simulate cell activity. The importance of the proper selection of the *in vitro* simulated body conditions can be illustrated with an experiment in which the effects of three different media, commonly published in the literature, on the mechanical and structural properties of collagen scaffolds were compared. This work formed part of a diploma thesis that was co-supervised by the author and that was nominated by the Zvoníček Foundation for the awarding of the Dean of the Faculty of Mechanical Engineering of the Czech Technical University in Prague prize for the most outstanding diploma thesis.

The study involved the preparation of collagen scaffolds based on collagen type I (VUP Medical, Czech Republic) from a 5 wt% aqueous dispersion employing the procedure described in detail in *Appendix A.1*. The scaffolds were cross-linked by EDC/NHS at a weight ratio of 4:1 in 95 wt% ethanol solution (*Appendix A.3*). Three different media were used for the simulation of *in vivo* conditions. The first medium was a simulated body fluid (SBF) as proposed by Tadashi Kokubo and Hiroaki Takadama [115]. SBF was originally proposed for the *in vitro* determination of bone-bonding ability as a replacement for, particularly, the *in vivo* biological evaluation of ceramic-based materials. SBF simulates the ion concentration of the inorganic part of human blood plasma and is commonly suggested in the literature as the medium used for the determination of the degradation profiles of various (not only ceramic) materials. SBF enjoys wide popularity in scientific papers; the original research paper by Kokubo and Takadama [115] contains over 4,500 citations (Web of Science Core Collection, Jan 13th

2020). With respect to the comparison of the influence of SBF, human blood plasma (3 donors of different blood groups, sex and age) supplemented with antibiotics (penicillin and streptomycin) was used as the second medium. Phosphate buffer saline (PBS) was selected as the final medium. PBS is one of the most commonly used media in degradation experiments due to its availability, simplicity and physiological pH. In all three cases, the samples were incubated at 37°C in a 5% CO_2 atmosphere, thus simulating inner body conditions, for up to 14 days. The mechanical and structural effects of each medium was determined (for a detailed description of the method, please see *Appendices B.1* and *B.3*). Images obtained via scanning electron microscopy of the collagen scaffolds prior to and after degradation are shown in Figures 20-22.

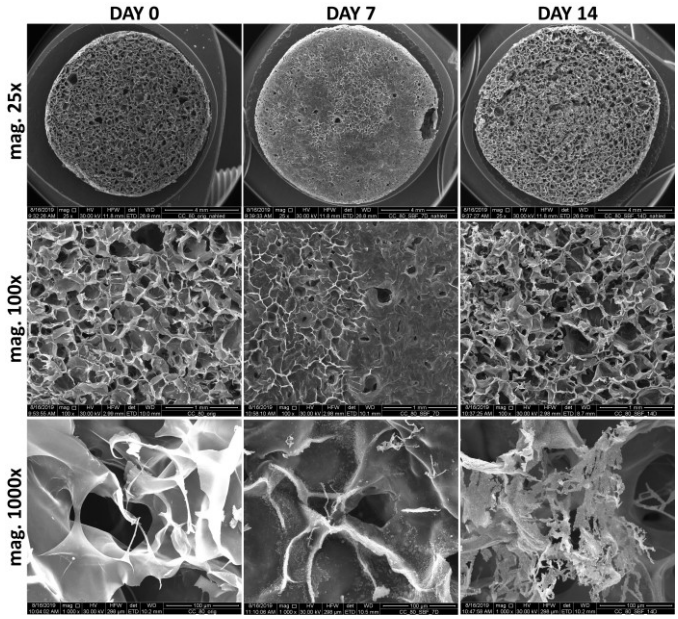

Fig. 20 SEM images of the original collagen scaffolds and those immersed in simulated body fluid (SBF) for 7 and 14 days.

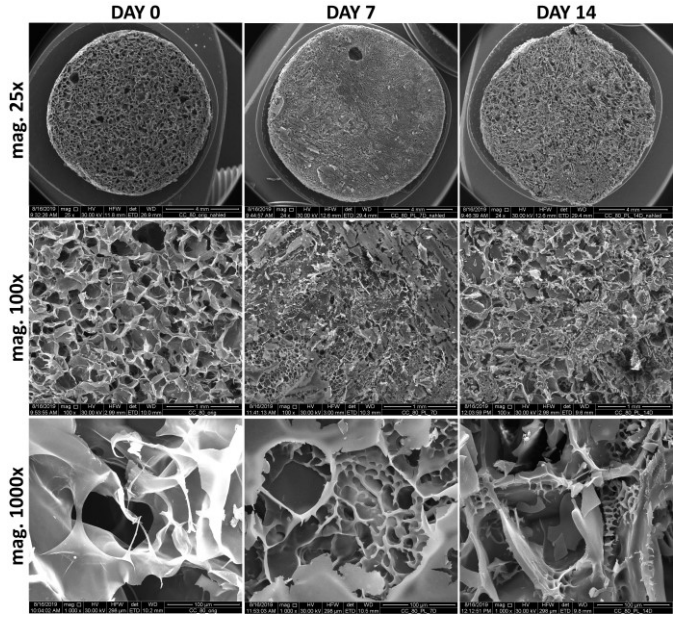

Fig. 21 SEM images of the original collagen scaffolds and those immersed in human blood plasma for 7 and 14 days.

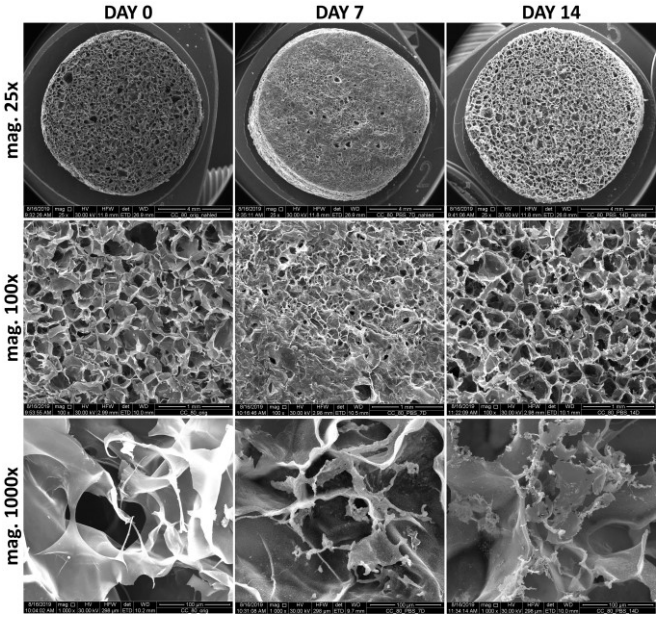

Fig. 22 SEM images of the original collagen scaffolds and those immersed in PBS for 7 and 14 days.

Although each of the three media used in this study simulated the same human body environment, the behaviour of the collagen scaffolds differed significantly. The differences in the behaviour of the collagen samples is illustrated in Figures 23-25. The principal differences can be observed in the case of the human blood plasma and SBF, which simulated its inorganic part ion concentration. Although the mechanical behaviour of the scaffolds remained comparable within the first 7 days, 14 days following immersion in the SBF, all the samples had completely degraded with regard both to the elastic gradient and plateau stress. Surprisingly, the vigorous loss of mechanical stability was not accompanied by a measurable mass loss. The scaffolds immersed in SBF evinced only a slight increment in weight, while the samples immersed in plasma evinced an approx. 80% increment in weight. This illustrates the problematic nature of the determination of the degradation profile of such highly porous and hydrophilic materials. The increases in weight can be explained by the precipitation of salts from the SBF and by the adsorption of various components (proteins, saccharides and vitamins) of the blood plasma following exposure. These processes are illustrated in the form of SEM micrographs in Figure 26. Although the SBF simulated the blood plasma ion concentration, the ionic species the concentrated solution altered the collagen solubility and influenced its mechanical properties. With respect to both the mechanical properties and the degradation processes, the results obtained were mutually inconsistent. It can be hypothesised that the individual application of SBF would lead to the conclusion that collagen scaffolds degrade in the human body within the first 14 days and that this process is accompanied by a total loss of their mechanical stability. Conversely, the individual application of human blood plasma would lead to conclusion that collagen scaffolds do not degrade in the human body within the first 14 days and that their mechanical properties remain stable without remarkable changes. The application of PBS offers a relatively easier interpretation of results. The reduction in the mechanical stability observable via a drop decrease in both the elastic gradient and the plateau stress within the first 7 days and its maintaining at the same level over the next 7 days was accompanied by a gradual mass loss. It can be hypothesised that the individual application of PBS would lead to the conclusion that collagen scaffolds degrade in the human body gradually and that this process is accompanied by a drop loss in their mechanical stability within the first seven days, in which case a

further decrease is not anticipated. The influence of PBS in terms of the simulated body environment is, thus, very difficult to compare to the situation observed in the cases of SBF and blood plasma.

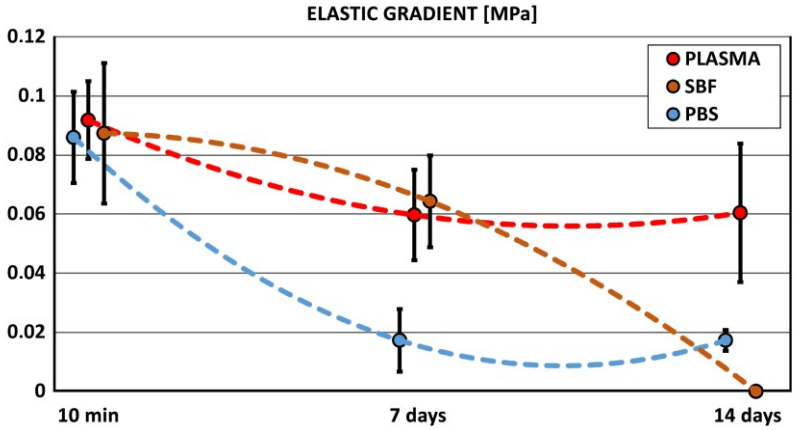

Fig. 23 Elastic gradient (elastic modulus) of the collagen scaffolds immersed in SBF, human blood plasma and PBS for 10 minutes, 7 and 14 days (*n=10*). The trend lines were added so as to highlight the evaluation of the elastic gradient.

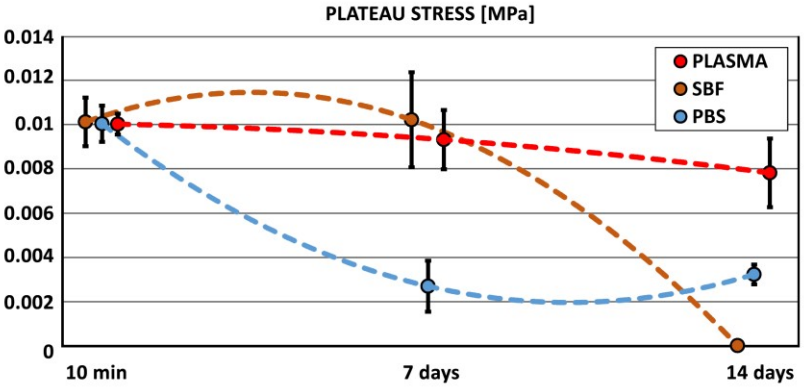

Fig. 24 Plateau stress (compressive strength) of the collagen scaffolds immersed in SBF, human blood plasma and PBS for 10 minutes, 7 and 14 days (*n=10*). The trend lines were added to highlight the evaluation of the compressive strength.

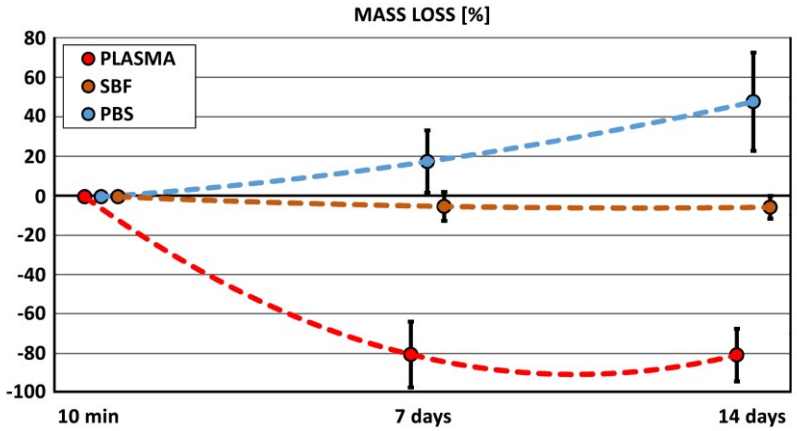

Fig. 25 The mass loss of the scaffolds immersed in SBF, human blood plasma and PBS for 10 minutes, 7 and 14 days (*n=10*). The trend lines were added to highlight the evaluation of the mass loss.

The results point to the need for a reliable *in vitro* model for the prediction of *in vivo* scaffold degradation as well as the need for the option to correlate the *in vitro* to *in vivo* situation. The interpretation and interpolation of such results to the real situation can be misleading. The advantage of *in vitro* laboratory experiments is that they avoid the conducting of animal experiments, while a further important role lies in the biomaterial development process, namely for the comparison of process parameters, etc. Nevertheless, the simplification of their results and interpolation to the *in vivo* situation should be avoided in the case of a lack of supporting data from the characterization of degradation processes as conducted, ideally, via several different methods.

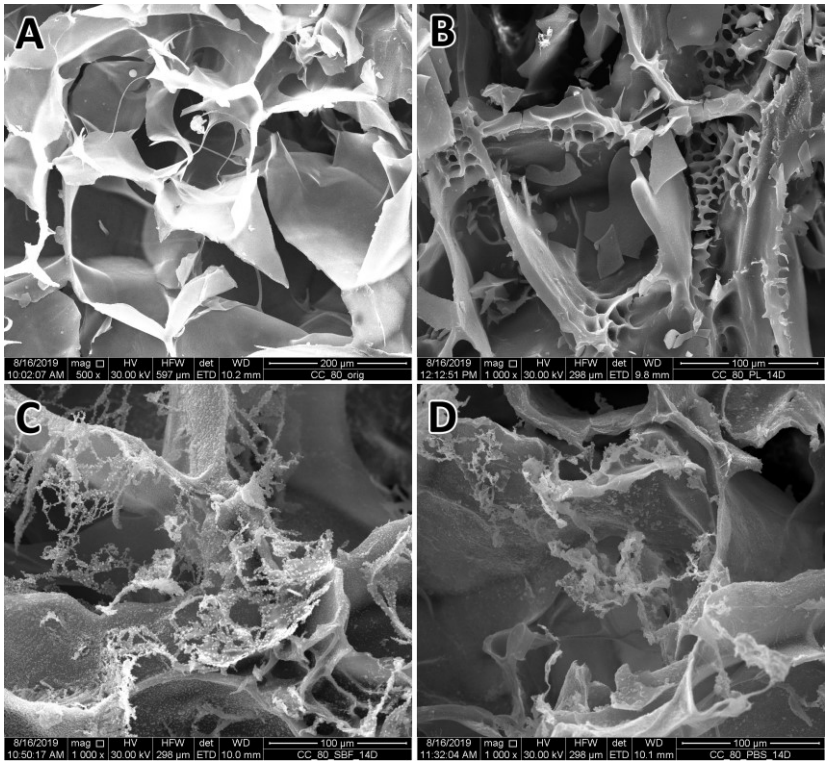

Fig. 26 Representative SEM images (mag. 1,000x) of the inner structure of collagen scaffolds prior to experimentation (A) and exposed for 14 days in human blood plasma (B), SBF (C) and PBS (D). The detailed images reveal the adsorption of various components of the blood plasma (e.g. proteins, saccharides, vitamins, etc.) (B) and salt precipitates (C and D) after exposure in selected media.

I.4.2 Different approaches to determine the structural parameters

In addition to the importance of the evaluation of bone engineering scaffolds in states that simulate the real environment for which such materials are designed, and the suitable selection of the experimental *in vitro* conditions, the selection of a suitable approach for the determination of the scaffold structural parameters represents a further important issue in the evaluation process.

Porosity represents a further crucial scaffold parameter in terms of cell ingrowth, cell growth and migration, and scaffold colonization. Scaffold porosity is determined by closed and open pores of varying size, shape, spatial distribution and mutual interconnection. Open porosity, particularly, exerts a substantial influence on scaffold–tissue interaction, cell migration, vascularization, mechanical

properties, diffusion and fluid permeability. Pores usually consist of interconnected channels rather than isolated homogeneous void spheres, which presents a major challenge with respect to pore analysis, particularly with concern to pore size. Indeed, the situation is considerably more complicated than it may at first seem as determined by 2D specimen sections showing isolated pores with circular or elliptical shapes; thus, it is advisable that pores should be evaluated with respect to their 3-dimensional structure. Various approaches exist for the determination of scaffold porosity (e.g. gravimetry, liquid displacement and mercury intrusion, image analysis in a number of 2D sections, etc.). Their application is inappropriate for collagen-based scaffolds, namely because of the alteration of the structure via liquid intrusion or orientation-dependent analysis in the case of the 2D analysis of the 3D structure, the alteration of the specimens via sectioning or measurement in a vacuum, etc.

Finally, the author would like to briefly point out the main pitfall regarding the use of different approaches to determine the pore sizes of tissue engineering scaffolds. This work formed part of a doctoral thesis, which was co-supervised by the author, and which was published by Martin Bartoš and Tomáš Suchý and co-authors in *BioMedical Engineering OnLine* in 2018 [116] and substantially in *Ceramics-Silikáty* in 2018 [117]. Selected results of the micro-CT evaluation of porous materials were also published in *Microscopy Research & Technique* in 2017 [118] and *Annals of Anatomy* in 2018 [119]. Finally, the characterization of the structural as well as the mechanical properties of collagen scaffolds formed an important part of a doctoral thesis which was co-supervised by the author, and which was published by Pavla Sauerová and Tomáš Suchý and co-authors in *Molecular Biology Reports* in 2019 [5].

In this study, composite scaffolds were prepared based on a collagen matrix, poly DL-lactide sub-micron fibres, bioapatite and sodium hyaluronate powder employing the procedure described in detail in *Appendix A.1*. The collagen part of the composite scaffolds was cross-linked using a PBS at two different temperatures, i.e. room temperature, ~20°C (RT) and 37°C (37). Three different concentrations of genipin were used - maximum (MAX), medium (MID), minimum (MIN) of genipin, i.e. MAX (0.67 g of genipin/1 g of collagen), MID (0.053 g/1 g) and MIN (0.026 g/1 g) (Fig. 27). The MID concentration was determined as a theoretical concentration sufficient for collagen cross-linking based on the determination of the amino acid concentration in the collagen.

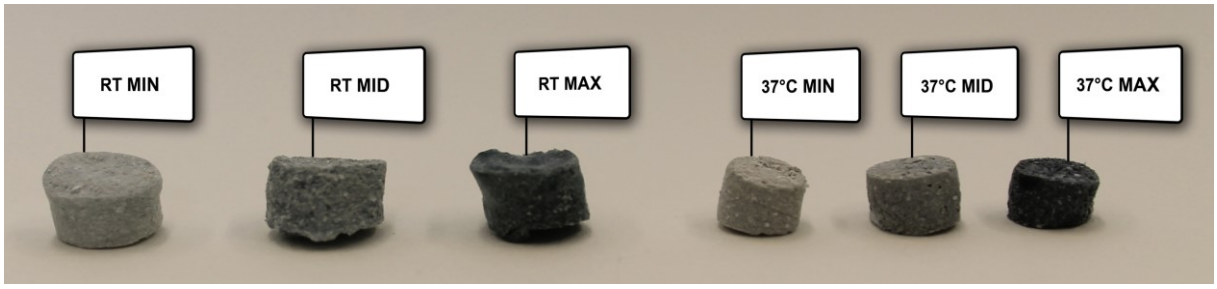

Fig. 27 Photograph of the collagen composite scaffolds analysed in the study aimed at the evaluation of different approaches to determining the structural parameters.

The micro-CT analysis (for details please see *Appendix B.7*) of the pore sizes in the whole of the specimen was performed in 3D using a sphere-fitting algorithm. 2D sections of the scaffolds (transverse

plane perpendicular to the axis of the cylindrically-shaped specimens; 5 sections) were evaluated for pore size values employing the following parameters: major diameter (MD, major diameter of the analysed pore), mean thickness (MT, based on a circle-fitting algorithm similar to the sphere-fitting procedure), biggest inner circle diameter (BICD, diameter of the biggest circle that fitted the analysed pore) and the area-equivalent circle diameter (AECD, the diameter of a circle of an area equivalent to the area of the analysed pore). The same specimens which were analysed via micro-CT were characterized by means of SEM. The scaffolds were cut into 2 mm thick discs (perpendicular to the long axis of the cylinder) prior to the SEM analysis. The pore size dimensions were measured by means of ImageJ software (Rasband, W.S., ImageJ, US National Institutes of Health, Bethesda, Maryland, USA, http://image j.nih.gov/ij/, 1997–2015). The manual mode of the ImageJ analyser was used for the measurement of the average diameter of the pores. At least 40 pores were assessed in each of five SEM micrographs (mag. 100×) for each scaffold type. Randomly selected pores were analysed for both the long and short pore axis.

The pore sizes of all the scaffolds evaluated by means of 6 different parameters evinced significant differences between their values. The median pore size values ranged from 20 µm (MT) to 490 µm (AECD). The mean median values for each method were (in descending order): AECD (378.6 µm), SEM (235.6 µm), 3D (78.4 µm), MD (75.3 µm), BICD (31.9 µm), and MT (27.9 µm). The interquartile range was (in descending order): AECD, SEM, MD, 3D, BICD and MT. The differences between the methods and parameters were statistically significant ($p \leq 0.05$) with the exceptions presented in Fig. 28.

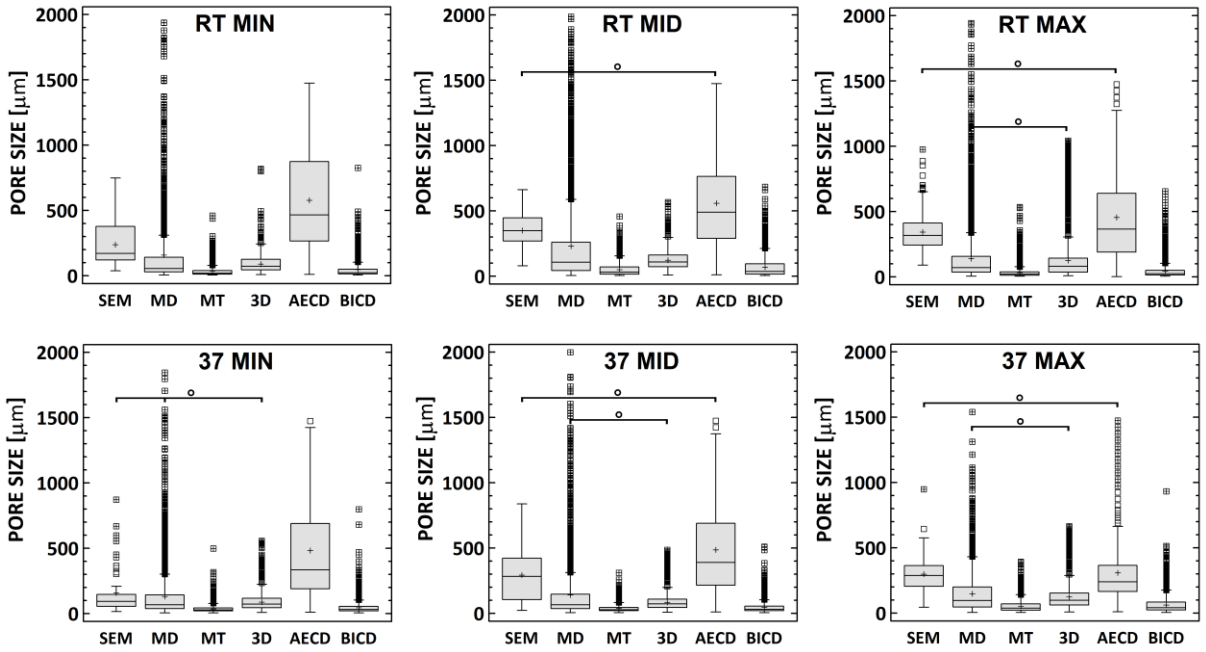

Fig. 28 An example of the differences between the various approaches to determining porosity. The determined pore size values differ significantly with respect to the selected approaches. All the values exhibit statistically significant differences except those values designated by the symbol “o” (Kruskal-Wallis, Bonferroni procedure, *0.05*, *n=3*).

Since the exact pore size value is unknown, all the values present some level of uncertainty. Hence, a comparison of the different methods based on their accuracy in terms of structural characterization

was not possible. The pore size results differed significantly between the parameters, with median values ranging from 20 to 490 µm. The SEM values were approximately three times higher than the micro-CT 3D values. Semi-quantitative assessment based on superiority to the other methods/parameters was finally employed in the study. The evaluated qualities were: non-destructivity, time efficacy, orientation independent direct 3D analysis, whole specimen evaluation, high resolution, irregular pore assessment, low image processing bias and widespread use. Non-destructivity is a major advantage of micro-CT; time efficacy is a benefit of micro-CT, especially of the 2D parameters; direct 3D analysis and whole specimen analysis are benefits of micro-CT 3D analysis (while whole specimen evaluation by means of micro-CT 2D analysis is possible, the results require an enormous amount of further data processing); high resolution is a major advantage of SEM; the evaluation of irregularly shaped pores is, in principle, beneficial using parameters based on the averaging of the fitted spheres/circles (3D, MT); the potential for the determination of the importance of the influence of image processing bias (e.g. binarization) is generally considered a major disadvantage of micro-CT analysis; to date, the widespread use of SEM remains superior to that of micro-CT. A detailed discussion of all the approaches can be found in a paper by Bartoš, Suchý and Foltán [116].

Chapter II

Nanostructured collagen materials for bone tissue regeneration

II.1 Motivation

The processing of collagen to submicron fibres or nanofibres represents a further promising approach to its application in medicine. The nanofibrous forms of collagen types I, II, III, and IV [25–27] have been studied extensively for use in medicine from hard tissue orthopaedic applications through soft tissue applications in cardiology, surgery, dermatology, urology and other fields in the form of bioprosthetic implants, vascular grafts, burn and wound/skin dressings and nerve regeneration and plastic surgery applications [27–34]. In addition, collagen is also used as a drug carrier [35]. In some cases of bone tissue regeneration, especially in the treatment of implant-associated infections, the ideal approach consists of the simultaneous repair of large-size bone defects and the inhibition of related infections. The use of an osteoconductive biomaterial with antibiotic and growth factor release capabilities as well as osteogenesis-matched degradation properties would provide an ideal solution [41].

Electrospinning, a promising processing technique that utilises electrical forces to produce ultrafine polymeric fibres from polymer solutions is seen as having great potential in terms of the development of nano-structured biomedical materials. The resulting electrospun fibres have been successfully investigated with respect to their use as matrices containing antibiotics [120], sandwich structures for the repair of infected wounds [121–123] and the electrospun local carriers of antibiotics [124,125]. Ying- Chao Chou et al. [126] have used electrospinning for the preparation of an artificial periosteum that incorporates biodegradable drug-embedded nanofibres so as to provide an adequate level of drug release capacity as well as biodegradable stents for the mimicking of the mechanical properties of the periosteum in connection with the management of open fractures. A further promising technique concerning the bioactive modification of the surface of titanium implants consists of electromechanically-assisted deposition by means of which collagenous or chitosan interfaces can be created [127–131]. The technology and conditions concerning composite preparation are of particular importance since they are able to significantly affect the final nano/microstructure of the composite and, consequently, the antibiotic release profile. Collagen offers great potential with regard to the creation of a coating for orthopaedic implants in the form of nanofibrous layers which exert a strong local anti-infection effect and, simultaneously, do not lead to a decrease in the rate of osseointegration necessary for the suitable fixation of the implant. Moreover, its submicron- or nanofibrous forms are particularly efficient drug delivery agents due to their high surface-area-to-volume ratios, high porosities and 3D open porous structures [132].

Unlike synthetic polymers, the reproducibility of the spinning of biopolymers is usually problematic due to the level of variability in the various properties that depends not only on the source and isolation/processing procedures applied, but also on the exact technique used [38]. It is still unclear whether the electrospinning process influences the native structure of collagen. Natural collagen, in order to be electro-spinnable, must be well dissolved so that its structure is disturbed at some level.

These processes are complex and it is difficult to maintain the balance between the successful processing of collagen and the preservation of its structure without denaturation. Solvent systems are capable of breaking down most of the hydrogen bonds within the adjacent collagen molecules; on the other hand, certain inter/intra molecular bonds within the collagen must be maintained so as to stabilize its triple helix. Electrospun collagen fibres exhibit poor mechanical properties compared to those of its native form, they exhibit sensitivity to elevated temperatures and poor water stability [39,40]. They also exhibit uncontrollable enzymatic degradation. All these issues limit the use of electrospun collagen in various applications.

Electrospun collagen must be stabilized to a sufficient degree so as to attain stability in aqueous environments, reduce enzymatic sensitivity, improve the mechanical properties of the fibres and increase the denaturation temperature. Electrospun collagen can be stabilized by creating new additional chemical bonds between the collagen molecules. Unlike the cross-linking of porous collagen scaffolds prepared via lyophilisation, the cross-linking of electrospun forms is more complicated due to their high surface-area-to-volume ratios and, moreover, the preservation of the nanostructured morphology is complicated. While the electrospun collagen morphology can be preserved via the optimization of the cross-linking conditions, it is complicated to maintain the balance between the successful rate of cross-linking and the preservation of its morphology without significant changes occurring in its sub-micron or nanofibrous structure.

The ***first part*** of this chapter briefly addresses various problematic issues related to the electrospinning of collagen. The ***second part*** focuses on the cross-linking of electrospun collagen with regard to its morphology, mechanical properties and the preservation of its native character. The ***third part*** of the chapter concerns the mechanical properties and variability of electrospun collagen in its hydrated states.

II.2 Electrospinning of collagen

As mentioned above, electrospinning offers many unique advantages such as a high surface volume ratio, adjustable porosity and the flexibility that allows spinning to various shapes and sizes. While electrospinning is not particularly demanding in terms of its installation, its complexity lies in the management of the molecular setting, processing and the technical parameters that lead to the production of fibres with the desired properties [133]. The spinning of natural and water-soluble polymers is difficult and is more complicated than the spinning of synthetic polymers. Natural polymers are difficult to electrospin due to their high molecular weight, viscosity, rigid chain conformation, etc. Unlike synthetic polymers, the reproducibility of the spinning of biopolymers is usually problematic since a number of variability properties exist that depend not only on the source and isolation/processing procedures, but also on the exact technique used [38]. The non-formation of fibres, electrospraying and the consequent formation of beads sometimes occurs instead of the formation of regular fibres due to physicochemical properties of the solution. Biopolymers such as collagen must, therefore, be well dissolved. The electrospinning process is influenced by several parameters such as the applied voltage, feeding rate, type of collector and emitter, emitter-to-collector distance, humidity, temperature etc. In addition to the processing parameters, the solution parameters also play an essential role in the process. The overall process and properties of elspun fibres are influenced primarily by the solvent system, solution concentration, surface tension, molecular weight, viscosity and conductivity. The following paragraphs address the optimization of the suitable parameters for collagen electrospinning.

II.2.1 Electrospinning conditions - solution

Collagen is an ampholytic polypeptide and its solubility depends on the pH of the solvent system. So-called green solvents based on ionic liquids are currently applied for the dispersion of poorly soluble natural biomass.

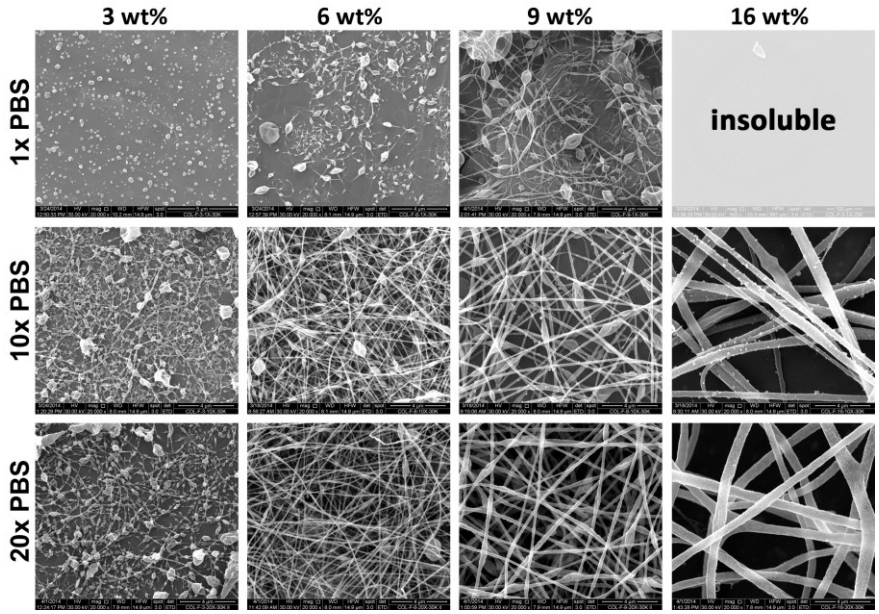

Fig. 29 An example of materials electrospun from collagen PBS/ethanol solutions with different collagen concentrations (3, 6, 9 and 16 wt%) and different concentrations of PBS. The SEM images illustrate the variability of the final product (mag. 20,000x, the bar represents 4 μm).

Fig. 29 illustrates the optimization of the electrospinning solution. Here, the collagen type I (fish skin, for details of extraction please see *Appendix A.1*) was dissolved in 1x, 10x and 20x concentrated PBS. The solution was further supplemented with ethanol (PBS/ethanol 1/1 v/v). Further process conditions were kept the same (voltage of 30 kV, distance, feeding rate, etc.). The addition of hydrophobic ethanol reduced the tension on the interfacial solvent-collagen and thereby increased the solubility of the collagen and eased the evaporation of the solution within the electrospinning process. The higher the ionic concentration of the solution, the easier is collagen solubilisation. The higher salt concentration in the PBS enabled the preparation of highly concentrated collagen solutions (16 wt%). The effect of PBS concentration on collagen solubilisation exerts a subsequent impact on the solution's spin ability. An optimized solution enables the preparation of fibres with minimum defects (e.g. beads, drops), while poorly solubilised collagen is difficult to spin into fibres. The differences in the properties of the solution were further demonstrated by the different fibre diameters of the electrospun layers (Fig. 30).

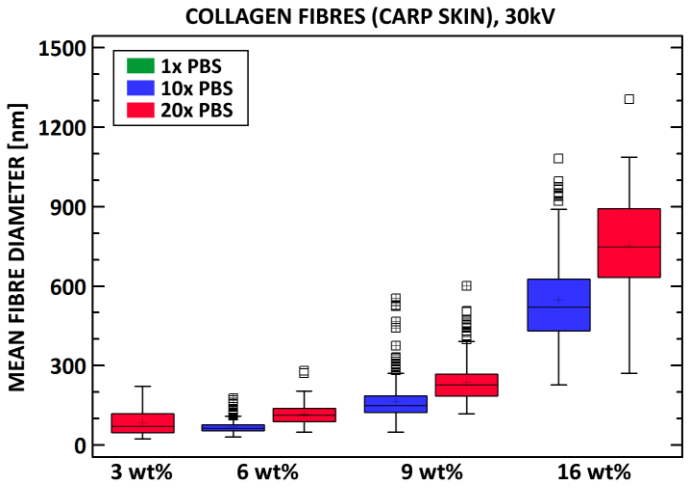

Fig. 30 Fibre diameters of electrospun layers prepared from different concentrations of PBS/ethanol solutions from a previous experiment (*n=250*). In the case of 1x PBS, no fibres were obtained.

Unlike the solution parameters, the processing parameters are not so important in terms of the dimensions of electrospun fibres. For example, the applied voltage or distance between the emitter and collector are more important for the production rate, the presence of defects and the joining of particular fibres or bundles as a result of the insufficient evaporation of the solvent. This process is also affected by the solution parameters, e.g. by the higher affinity of the solvent in the case of acids, namely acetic acid. However, most often, the properties of final elspun mats are influenced by the interplay of various processing and solution parameters, and the results obtained for a particular solution cannot easily be generalized for other solutions. This is illustrated by a simple experiment with the electrospinning of a collagen (type I, calf skin, VUP Medical, Czech Republic) PBS/ethanol solution. Here again, the PBS was used in three different concentrations (1x, 10x and 20x) with the addition of ethanol (1/1 v/v). In this experiment, different voltages (15 - 55 kV) were applied, while the other spinning parameters were kept the same. The SEM images in Figure 31 illustrate the similar structure and dimensions of fibres obtained under different voltages (a 16 wt% collagen solution of 1xPBS/ethanol).

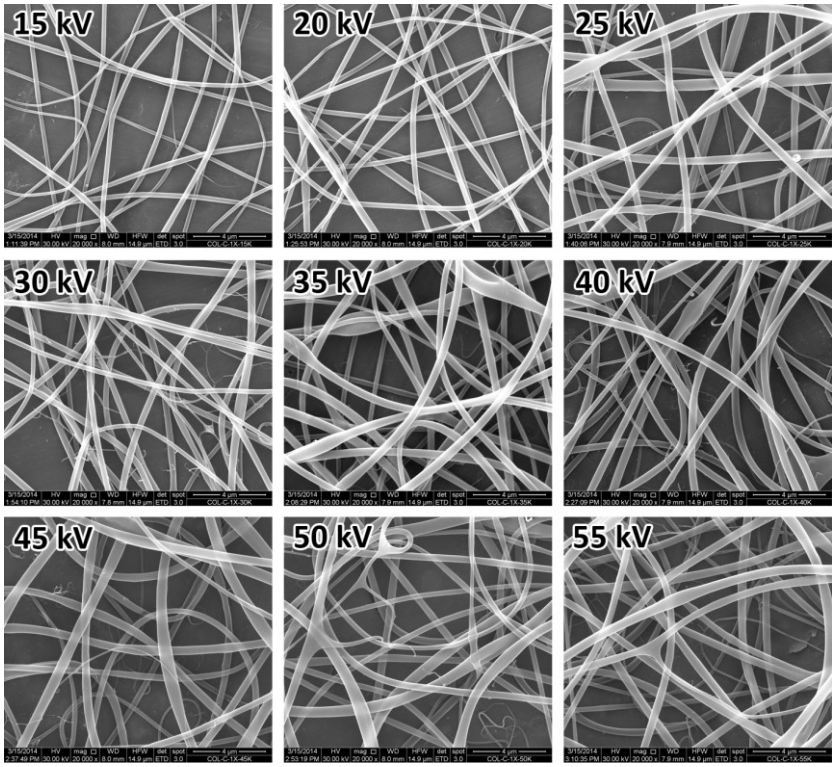

Fig. 31 Fibres obtained via the electrospinning of a 16 wt% collagen 1xPBS/ethanol solution under different applied voltages (15-55 kV). Mag. 20,000x, the bar represents 4 μm.

Figure 32 summarizes the quantification of the fibre diameters and the electrical conductivity of particular solutions that differed in terms of the concentration of PBS. Unlike the effect of the applied voltage, the influence of conductivity on the fibre diameter seems to be insignificant, which is in contradiction with commonly published data, and which illustrates the variability of the process. For example Tan et al. found the electrical conductivity to be a significant parameter in terms of the morphology of electrospun nanofibres [134].

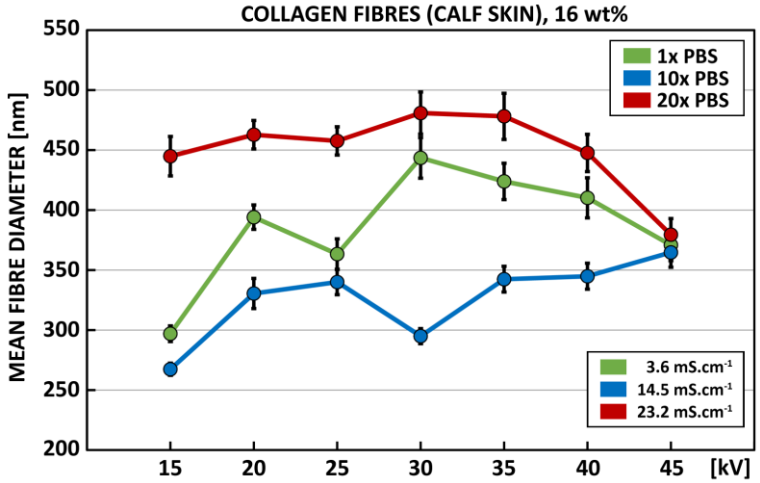

Fig. 32 Mean diameter of fibres (*n=150*) electrospun from a 16 wt% collagen PBS/ethanol solution (calf skin) with different concentrations of PBS (1x, 10x and 20x). The electrical conductivity of the solutions differs in accordance with the PBS concentration; nevertheless, its influence on the fibre diameter is ambivalent.

The variability of collagen electrospinning can also be illustrated via the comparison of Figures 29 and 31. Unlike the solution based on collagen isolated from calf skin, the solution based on collagen isolated from fish skin could not be electrospun under the same process and solution parameters. The variability of collagen most probably makes up the most important and most difficult to control parameter of the electrospinning process. It is expected that the chemical and physical properties of collagen type I isolated form different animal species (mammal, fish, bird etc.) or sources (e.g. skin, scale, foot etc.) may differ. The main differences lie in the amino acid composition and molecular weight, both of which influence the dissolution of the collagen and the electrospinning process. Unfortunately, the physio-chemical properties of collagen also differ slightly in isolates from the same animal species and the same source. Such differences are influenced by further parameters, namely age, gender and the physical condition of the animals. Unfortunately, it is not possible to determine any significant parameter or parameters that facilitate the process of the preparation of spinnable collagen solutions and each collagen isolate has to be optimized to a certain extent repeatedly.

However, the problem of the spinnability of natural polymers can be overcome via the addition of auxiliary polymers, e.g. polyethylene oxide (PEO) in the case of collagen, that functionalize the reactive groups on the surface, or via the use of a co-solvent [38]. In all probability, these added polymers will lead to the weakening of over-strong inter/intra chain interactions and thus to a reduction in the viscosity of the solution. The effect of PEO on the spinnability of collagen is illustrated in Fig. 33. The addition of PEO to the collagen solution eases the electrospinning process. The optimal amount of PEO, in this case, was estimated in the range 6-10 wt% to collagen. PEO is a non-toxic polymer, one of the advantages of which is its solubility. PEO does not bond to collagen and it can be simply washed out of the layers after electrospinning.

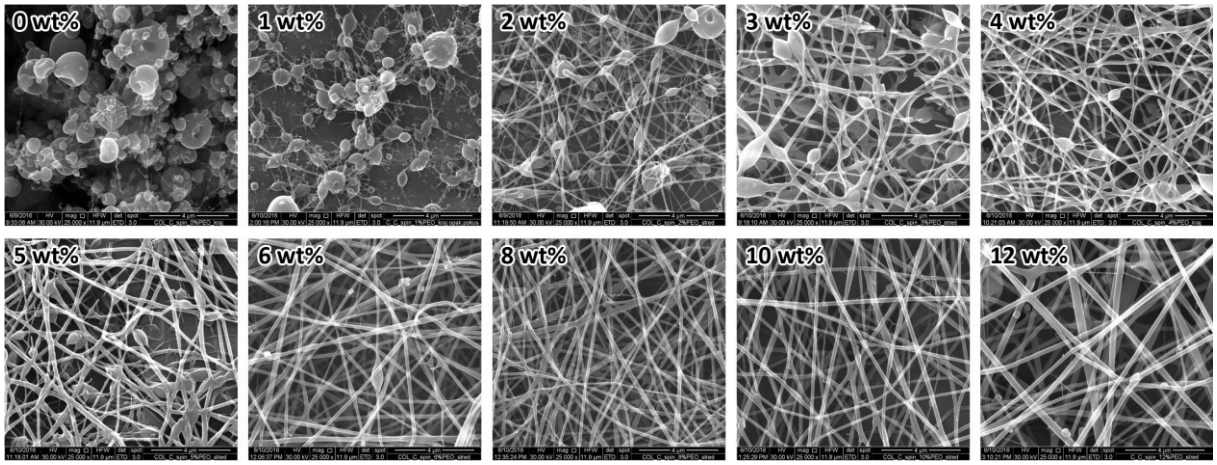

Fig. 33 SEM images of layers electrospun from collagen (type I, calf skin) 8 wt% PBS/ethanol solution supplemented with different amounts of PEO (molecular weight 900,000) to collagen. Mag. 25,000x, the bar represents 4 μm.

II.2.2 Electrospinning conditions - comparison of spinning methods

It is still unclear whether the electrospinning process as a whole, mainly due to the application of different solvent systems, influences the native structure of collagen. For example, frequently

referenced fluorinated alcohols, e.g. hexafluoro-2-propanol (HFIP), not only denature the native structure but also lower the denaturation temperature of the proteins. The loss of the native biological and physio-chemical properties of collagen during electrospinning from fluoroalcohol solutions has been well depicted by Zeugolis et al. [135] by posing the question of whether the electro-spinning of pure collagen nano-fibres is not just an expensive way to make gelatin. Unfortunately, this question can be generalized to the majority of collagen solution systems. Natural collagen, in order to be electrospinnable, must be well dissolved so that its structure is disturbed at some level. The effect of solvents on the native structure of the collagen and secondary structure after spinning from different solvent systems - HFIP, trifluoroacetic acid, PBS/ethanol or acetic acid/ethanol systems has been studied previously [136]. Finally, it was concluded that while collagen completely unfolds in fluorinated solvents, it is partially refolded during the electrostatic spinning process (even up to 42%). In contrast, the folded structure was found to be partially preserved in acetic acid/ethanol. Nevertheless, the secondary structure was similar in all the electrospun collagen samples and was independent of the type of solvent used [137].

Unlike electrospinning, other spinning methods can be used to process collagen into the submicron-fibrous and nanofibrous forms. A comparison of the influence of the most commonly used spinning methods on the secondary structure of collagen is described later in the paper. Since, in addition to electrospinning, the centrifugal force spinning process appears to present a further promising method for the spinning of collagen solutions, the needle and needleless centrifugal spinning technology and the electrospinning technology were compared. Moreover, the effect of the process parameters and collagen solution conditions on the final form of the material was analysed. Submicron- and nanofibrous materials were prepared based on collagen (type I, calf skin, VUP Medical, Czech Republic). Fibrous mats were prepared employing the spinning of 4, 6, 8, 12 and 16 wt% collagen solutions in PBS/etahnol with (ES+P) and without (ES-P) the addition of 8 wt% PEO (to collagen). Electrospun mats were prepared using a high voltage level of 45 kV (4SPIN, Contipro, Czech Republic). Two methods were employed for the centrifugal force spinning of collagen solutions with 8 wt% PEO, i.e. needle (N) and needleless (NL) spinning using laboratory-made equipment (TU Liberec, Czech Republic) and two different circumferential velocities were applied, namely 15 (N15 and NL15) – 35 $m.s^{-1}$ (N35 and NL35). The layers thus prepared were characterized by means of scanning electron microscopy and FTIR (for the FTIR details please see *Appendix B.2*).

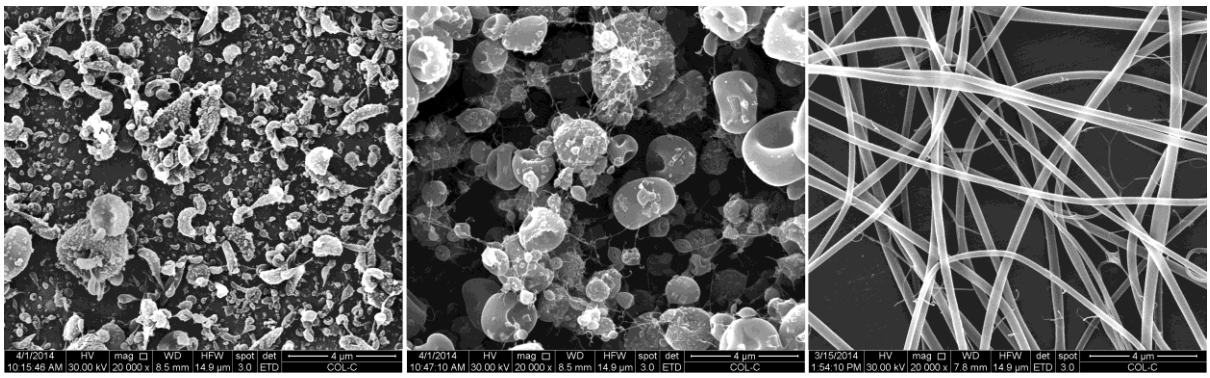

Fig. 34 Representative SEM images of samples electrospun from collagen solutions (without PEO) with concentrations of (from left) 4, 8 and 16 wt% (mag. 20,000x, the bar represents 4 μm).

Figures 34 and 35 provide representative SEM images of collagen electrospun from solutions with different concentrations. In the case of solutions with no PEO, fibres were formed only from a solution with a concentration of 16 wt% (Fig. 34). Following the addition of PEO, fibres were formed from collagen solutions with a lower concentration of 8 wt% (Fig. 35).

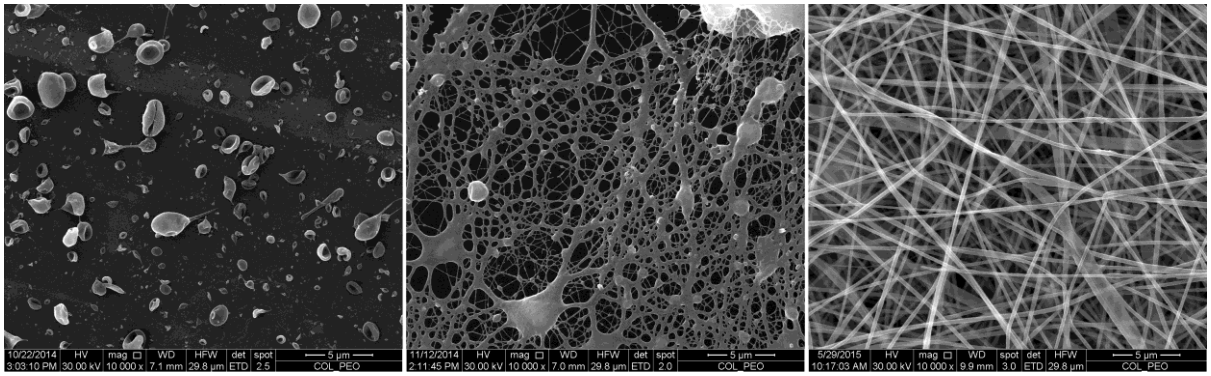

Fig. 35 Representative SEM images of samples electrospun from collagen solutions (with PEO) with concentrations of (from left) 4, 6 and 8 wt% (mag. 10,000x, the bar represents 5 μm).

In the case of needle and needleless centrifugal force spinning, the production process was optimized by means of changing both the concentration of the collagen solution and the circumferential velocities. Fibres were formed from collagen solutions with concentrations of higher than 12 wt% following the application of both methods (see Fig. 36). Nevertheless, the main complication issuing from the centrifugal force spinning of the solutions consisted of the rate of production; consequently, only the 12 and 16 wt% collagen solution samples spun at velocities of 15 $m.s^{-1}$ and 35 $m.s^{-1}$ were subjected to further analysis.

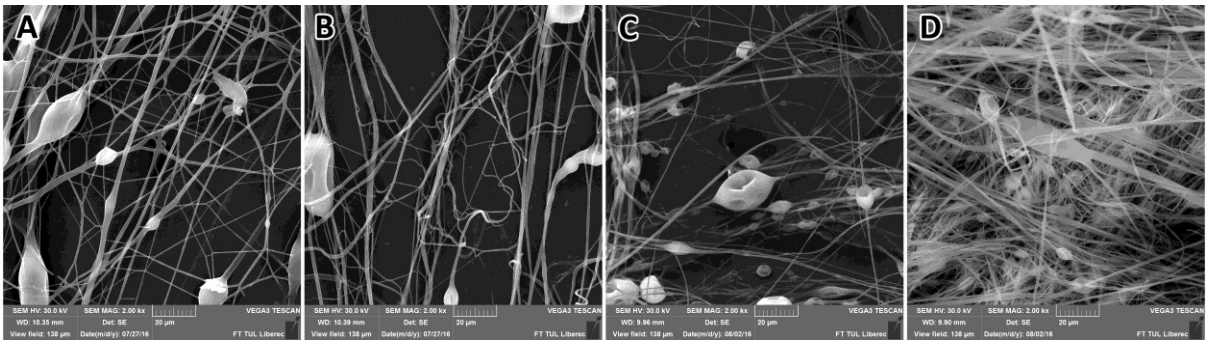

Fig. 36 Representative SEM images of samples prepared employing the needleless (A, B) and needle (C, D) centrifugal force spinning of the collagen solutions (with PEO) with a concentration of 12 wt% and circumferential velocities of 15 $m.s^{-1}$ (A, C) and 35 $m.s^{-1}$ (B, D) (mag. 2,000x, the bar represents 20 μm).

The amide I region of the native collagen spectrum (∼1650 cm^{-1}) could be deconvolved into three distinct bands with maxima at ∼1660, ∼1640 and ∼1630 cm^{-1} (see *Appendix B.2*). Following denaturation, the bands did not shift appreciably in terms of position; however, the relative intensities of the 1660 and 1630 cm^{-1} bands shifted from >1 to <1, in other words, the component positioned at

around 1630 cm^{-1} increased and the component positioned at around 1660 cm^{-1} decreased in intensity. The ~1660 cm^{-1} band was assigned to the triple helix with contributions from the α-helix and β-turns [138], while the ~1630 cm^{-1} band was assigned to imide residues (and partly to the β-sheet) [139]. The quantitative band-fitting analysis of the amide I area (expressed as a ratio of the areas of the 1660 and 1630 bands) of the materials prepared using different spinning technologies and their comparison with lyophillized collagen is summarised in Fig. 37. Lyophilised collagen (LYO) demonstrated the highest 1660/1630 ratio value and demonstrated statistically significant differences compared to the materials prepared using other spinning technologies, which suggests that LYO contained a high proportion of the component related to the triple helical structure. The NL35 material embodied no further statistically significant differences compared to the materials prepared by means of electrospinning; it contained the lowest proportion of the component related to the triple helical structure (~1660 cm^{-1}) and the highest area contributed by the 1630 component related to the denaturated state. The other materials were mutually comparable.

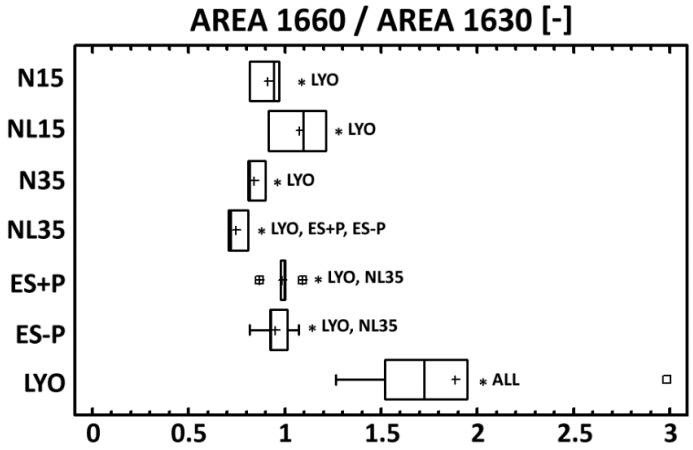

Fig. 37 Comparison of the ratio of the integral absorbances of materials prepared using different spinning technologies. N15 and N35 – needle centrifugal spinning with a concentration of 12 wt% and circumferential velocities of 15 $m.s^{-1}$ and 35 $m.s^{-1}$; NL15 and NL35 – needleless centrifugal spinning with a concentration of 12 wt% and circumferential velocities of 15 $m.s^{-1}$ and 35 $m.s^{-1}$; ES+P and ES-P – electrospun from collagen solutions with a collagen concentration of 16 wt% (with and without PEO) and their comparison with lyophillized collagen (LYO), i.e. original collagen prior to its dissolution. * denotes statistically significant differences (Mann-Whitney, *0.05*, *n=10*).

Fig. 38 provides examples of the deconvoluted ATR-FTIR spectra of the LYO and NL35 materials. The spectra also contained other components corresponding to other structural states. The component at ~1615 cm^{-1} is related to gelatin, the band at ~1650 cm^{-1} corresponds to random coils and the component at ~1690 cm^{-1} can be attributed to helices of aggregated collagen-like peptide [139]. As is apparent from Fig. 38, the LYO material contains a proportionally large area related to the triple helical structure (~1660 cm^{-1}) compared to the other structural states (~1615 cm^{-1}, ~1650 cm^{-1} and ~1690 cm^{-1}) whereas the NL35 sample exhibits the opposite behaviour. The further processing of lyophillized collagen (dissolution and spinning) was found to lead to spectral changes in the amide I region which corresponded to changes in the secondary structure of the collagen.

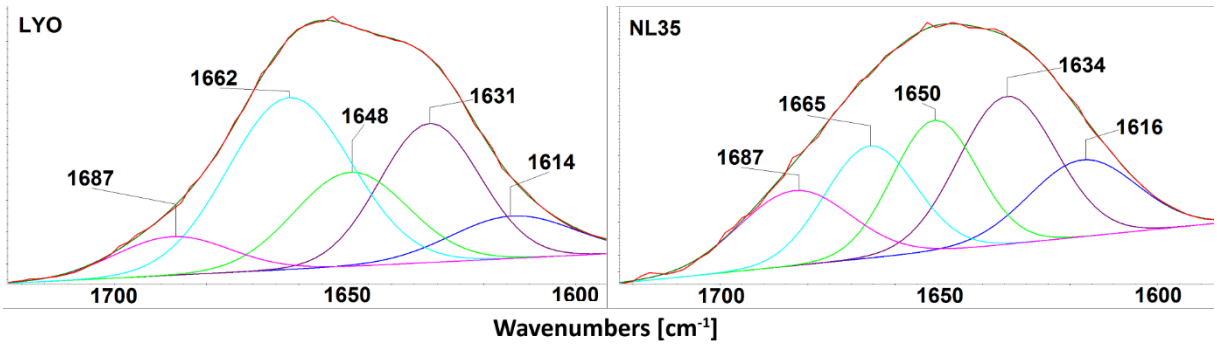

Fig. 38 Comparison of the deconvoluted ATR-FTIR spectra of lyophilized collagen (LYO) and the NL35 material.

The processes concerning both the isolation of collagen to its dissolution and from solution to the artificially-produced fibrous form are complex. Solvent systems are capable of breaking down most of the hydrogen bonds within the adjacent collagen molecules; on the other hand, certain inter/intra molecular bonds within the collagen must be maintained so as to stabilize its triple helix. It is clear therefore that it is difficult to maintain the balance between the successful processing of collagen and the preservation of its structure without denaturation. These results indicate that centrifugal force spinning and electrospinning lead to the preparation of collagen fibres with very similar properties but that, in general, spinning processes (or the preparation of collagen solutions) influence the structure of the collagen, which was illustrated by the occurrence of spectral changes corresponding to changes in the structure of the collagen. The denaturation rate of collagen and the potential for the improvement of the partially damaged native structure of collagen (e.g. by cross-linking) remain to be specified.

II.3 Cross-linking of electrospun collagen

II.3.1 Cross-linking of electrospun collagen - morphology

Whereas native collagen tissue possesses unique physio-chemical properties, they may be lost, to some extent, subsequent to electrospinning in which case the material is even soluble in pure water due to the loss of the quaternary structure. Electrospun collagen fibers exhibit poor tensile strength, i.e. much lower than that of the native form and are sensitive to humidity (poor water stability, swelling in solutions) and to elevated temperatures [39,40]; they also exhibit uncontrollable enzymatic degradation, all of which may limit the use of collagen in various applications. Moreover, native cross-linking is not secured *in vitro*. Therefore, such collagen must be cross-linked to a sufficient degree so as to attain stability in solutions, reduce enzymatic sensitivity and increase the mechanical strength of the fibers and the denaturation temperature. In addition, cross-linking allows for a reduction in the antigenicity of collagen and sometimes decreases its calcification [140].

In the case of electrospun collagen forms, it is necessary to preserve the sub-micron or nanofibrous structure. Unlike the cross-linking of porous collagen scaffolds prepared via lyophilisation, the cross-linking of electrospun forms is more complicated due to their high surface-area-to-volume ratios, and the preservation of the nanostructured morphology is relatively complicated. Figure 39 illustrates the loss of the nanofibrous structure of layers electrospun (4SPIN, Contipro, Czech Republic) from an 8 wt% collagen (type I, fish skin) PBS/ethanol solution with 8 wt% PEO (to collagen) after exposure to a cross-linking ethanol solution with genipin (2.5/4 w/w to collagen).

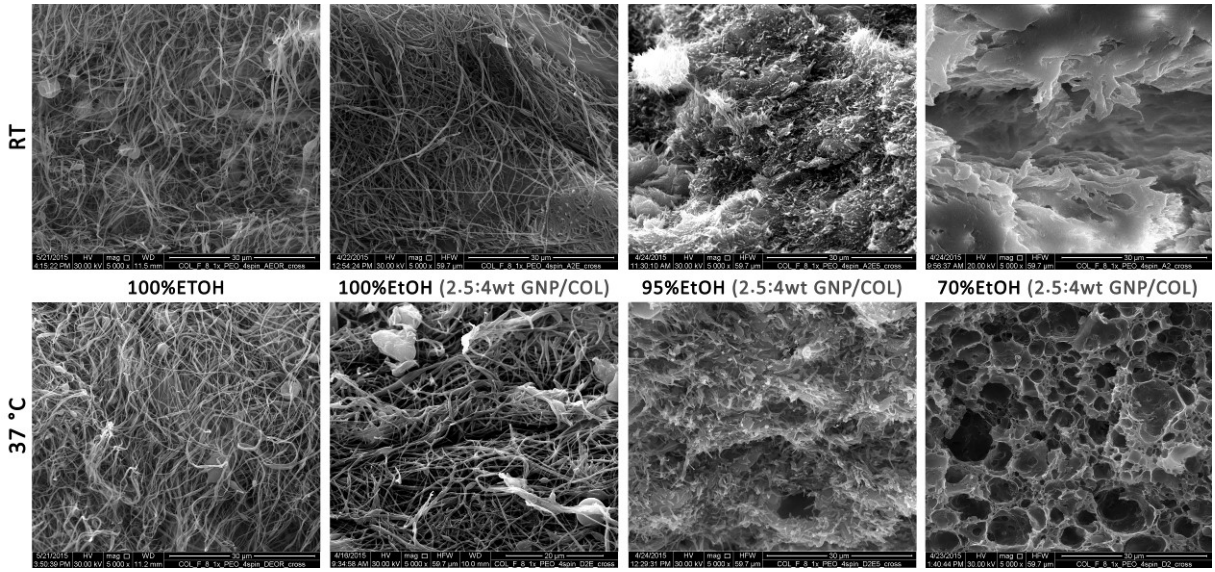

Fig. 39 SEM images of layers electrospun from an 8 wt% collagen (type I, fish skin) PBS/ethanol solution with 8 wt% PEO (to collagen) after exposure to a cross-linking ethanol (100%, 95% and 70%) solution with genipin (2.5/4 w/w to collagen). Mag. 5,000x, the bar represents 30 μm.

Unlike the preservation of the nanofibrous structure in pure ethanol and pure ethanol with genipin, the structure is not preserved following the addition of 30 wt% of water as the reaction catalyser. In the case of 70% ethanol, this phenomenon occurs under both room temperature and a temperature

of 37°C, which acts to accelerate the cross-linking reaction. In the case of 95% ethanol, the nanofibrous structure is preserved when higher temperatures are applied.

Similarly, the application of EDC/NHS in a 70% ethanol solution does not preserve the nanofibrous collagen (type I, fish skin) structure, even under a temperature of 37°C. The role of water is illustrated in Figure 40. Unlike 70% ethanol, 100% ethanol preserves the nanofibrous structure. However, the success rate of this procedure remains not only in the preservation of the inner structure, but also (mainly) in the successful cross-linking reaction.

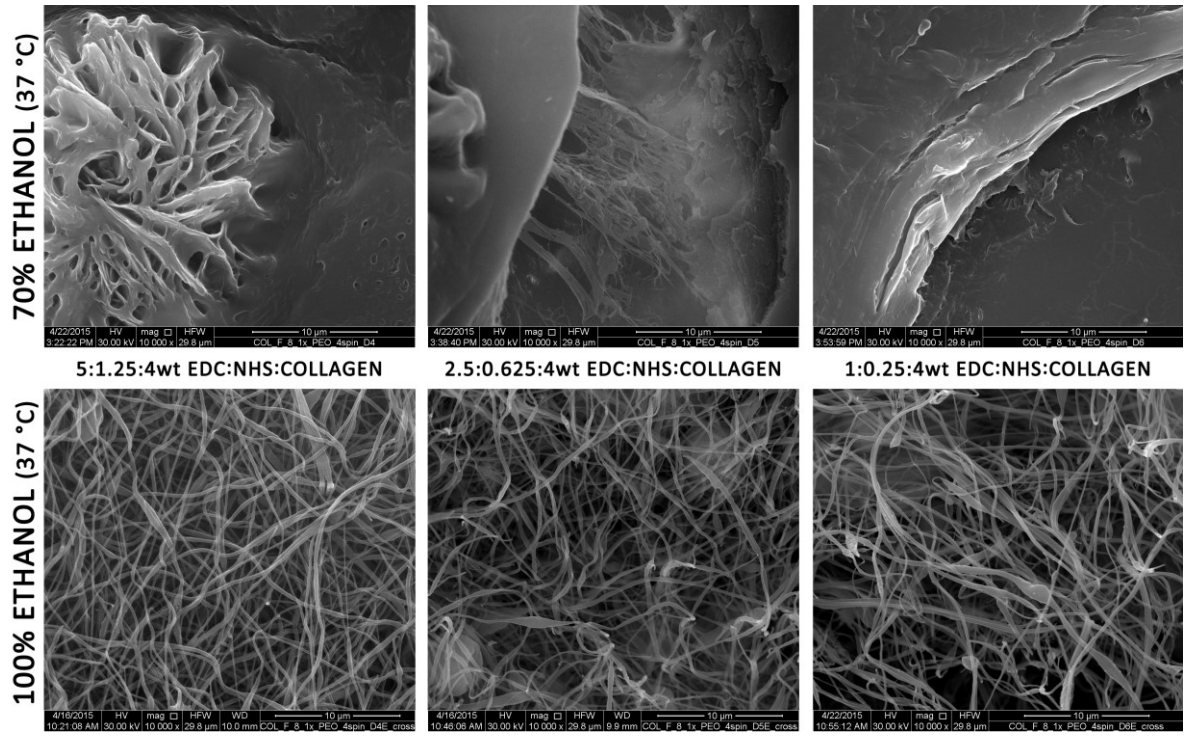

Fig. 40 SEM images of layers electrospun from an 8 wt% collagen (type I, fish skin) PBS/ethanol solution with 8 wt% PEO (to collagen) after exposure to cross-linking 70% and 100% ethanol solutions with EDC/NHS in three different concentrations. Mag. 10,000x, the bar represents 10 μm.

Unlike the non-preservation of the inner structure, the application of cross-linking agents in 70% ethanol leads to the successful cross-linking of collagen. All the collagen layers described above were cross-linked by genipin and EDC/NHS in three different concentrations to collagen (w/w: MAX = 5/8, MID = 2.5/8, MIN = 1/8; EDC/NHS 4/1), except for the lowest concentration of genipin under room temperature (Figure 41). The rate of cross-linking was determined by FTIR (data not shown). It points out the necessity to evaluate the rate of cross-linking comprehensively.

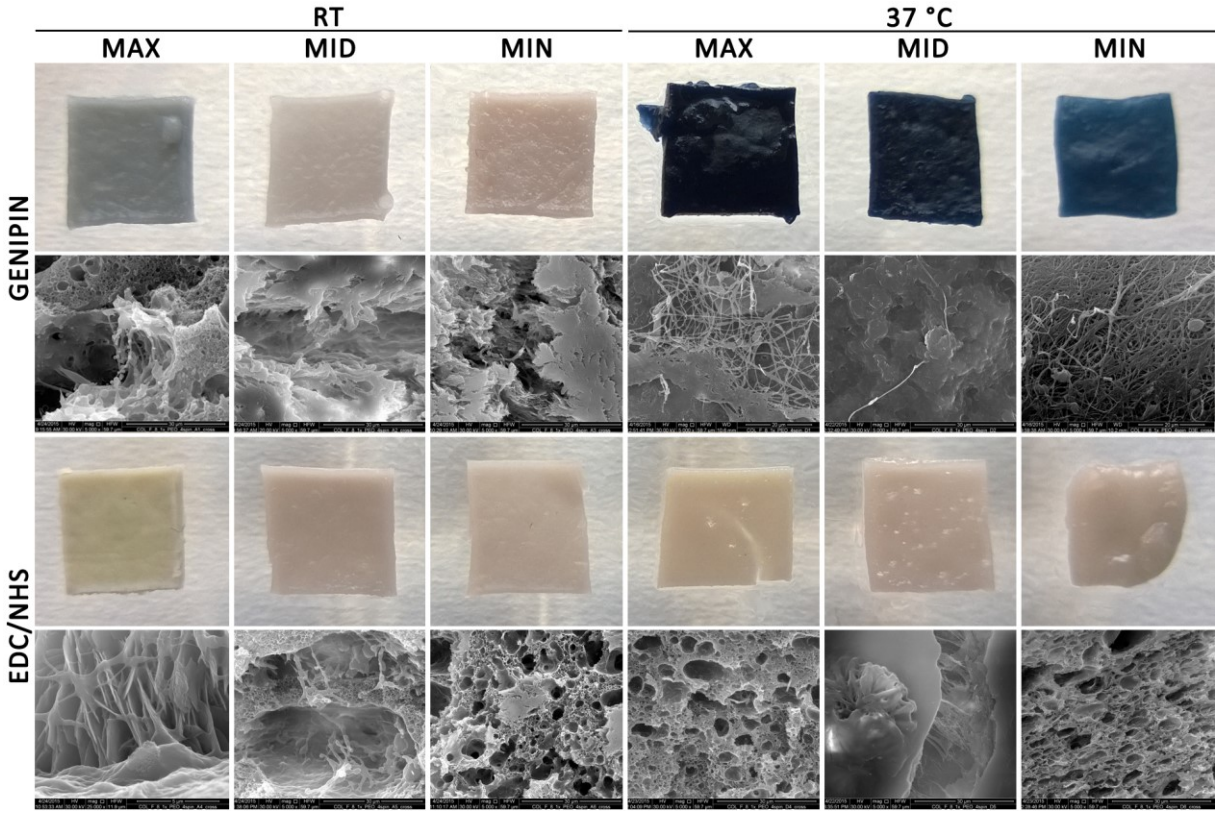

Fig. 41 Photographs and SEM images (mag. 5,000, bar 30 μm) of collagen layers (type I, fish skin) successfully cross-linked (except for genipin RT MIN) in a 70% ethanol solution with genipin or EDC/NHS in three different concentrations to collagen (w/w: MAX = 5/8, MID = 2.5/8, MIN = 1/8; EDC/NHS 4/1).

II.3.2 Cross-linking of electrospun collagen - mechanical properties

It can be expected that a successful cross-linking rate will be manifested by changes in the mechanical properties. Thus, the analysis of the mechanical properties provides another piece in the jigsaw of the characterization of collagen behaviour. The mechanical properties of collagen electrospun materials were evaluated by means of the uniaxial tensile testing of rectangular strips of the layers. During the test procedure the value of strain at failure (the maximum strain sustained by the material before breaking, where strain is defined as the ratio of the elongation of the sample to reference length), the ultimate tensile strength (the maximum nominal stress sustained by the material; nominal stress is defined as the ratio of applied force to the reference cross-section of a sample) and the modulus of elasticity (the slope of the tangent made to a stress-strain relationship on the initial linear part) were determined. Tensile tests were conducted using a Zwick/Roell multipurpose testing machine equipped with a built-in video extensometer. By using contrasting marks on the surface of samples, the video extensometer automatically determined the reference length and elongation of the samples. Tensile experiments were conducted at a constant clamp velocity of 0.1 $mm.s^{-1}$. The loading force was measured by a force transducer (±250 N). For a detailed description of the mechanical tests please see *Appendix B.8*.

The first mechanical property analysis described the effect of cross-linking with EDC/NHS and genipin dissolved in 95 wt% or 70 wt% ethanol (37°C) on the behaviour of materials electrospun from a

collagen (8 wt%, fish skin) PBS/ethanol solution with 8 wt% of PEO (to collagen). In this case, the initial Young's modulus and ultimate tensile strength were calculated (Fig. 42). Since the native structure of collagen was partially damaged and the prepared samples evinced poor water stability following electrospinning, the mechanical properties were evaluated in the dry state to enable a comparison with the non-cross-linked material (ORIGINAL).

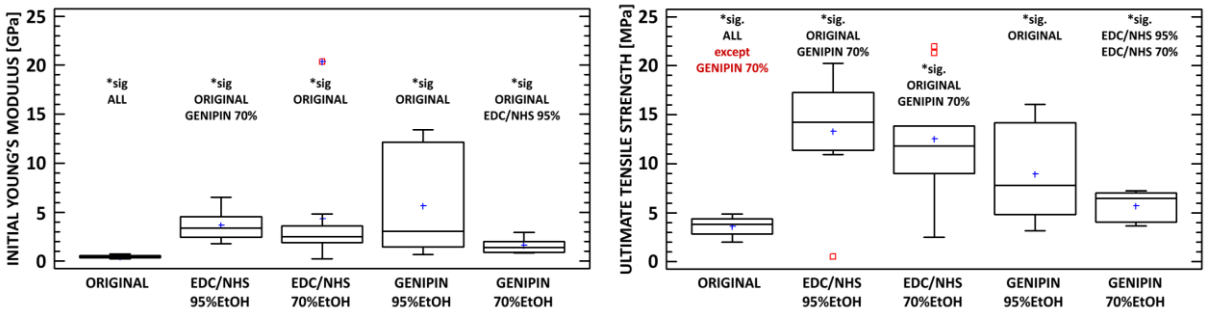

Fig. 42 Initial Young's modulus and ultimate tensile strength of the collagen electrospun layers before (ORIGINAL) and after cross-linking with EDC/NHS or genipin dissolved in 95 wt% or 70 wt% ethanol (EtOH) at 37°C. * denotes statistically significant differences (Mann-Whitney, *0.05*, *n=8*).

All the cross-linked samples evinced a statistically significant increase in both the initial Young's modulus and ultimate tensile strength. The changes in stiffness were represented by an approx. 790% (EDC/NHS/95%EtOH), 580% (EDC/NHS/70%EtOH), 720% (GENIPIN/95%EtOH) and 330% (GENIPIN/EtOH) increase in the Young's modulus compared to the non-cross-linked samples (ORIGINAL). The changes in the strength were represented by an approx. 370% (EDC/NHS/95%EtOH), 310% (EDC/NHS/70%EtOH), 210% (GENIPIN/95%EtOH) and 170% (GENIPIN/EtOH) increase in the Young's modulus compared to the non-cross-linked samples (ORIGINAL). A comparison of the 95% and 70% ethanol cross-linking solutions indicated no differences for either the EDC/NHS or genipin chemical agents. From this point of view, both ethanol solutions appear to be suitable for collagen cross-linking. However, it was also necessary to assess the impact of cross-linking via image analysis with regard to the preservation of the collagen nanofibrous structure.

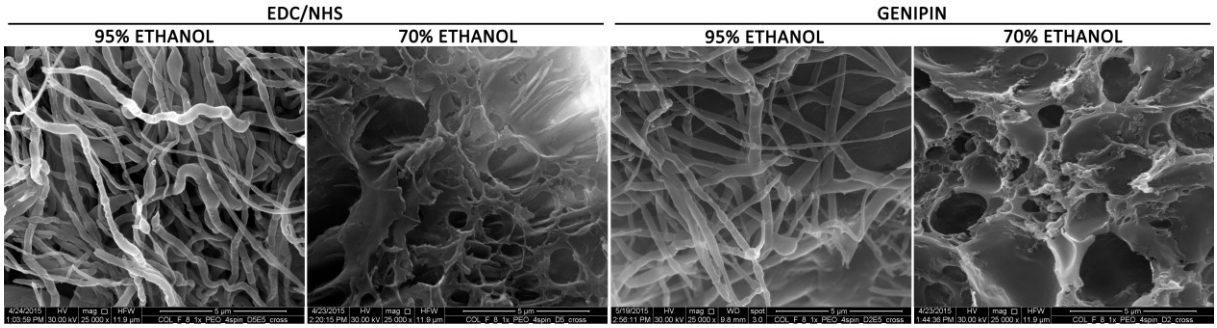

Fig. 43 SEM images of cross-linked collagen electrospun layers after cross-linking with EDC/NHS or genipin dissolved in 95 wt% or 70 wt% ethanol (37 °C). Mag. 25,000x, the bar represents 5 μm.

The image analysis revealed the significant impact of different ethanol concentrations on the collagen nanofibrous structure (Fig. 43). Unlike cross-linking with EDC/NHS and genipin in 95% ethanol that preserves the inner structure, the application of 70% ethanol led to the dissolution of the collagen

nanofibers. This finding represents a significant drawback concerning the application of 70% ethanol as the cross-linking procedure and indicates the necessity for the accompanying evaluation of the potential effects on the inner structure of the electrospun collagen material. The effect of different ethanol concentrations is also illustrated in Figure 44. Unlike the non-ability of the 70% ethanol solution with or without the EDC/NHS to preserve the nanofibrous collagen structure, 100% ethanol and 95% ethanol were both found to preserve the structure. Although collagen is cross-linked in 70% ethanol, the reaction is probably not fast enough to increase the water stability of the partially damaged electrospun collagen and thus prevent its dissolution.

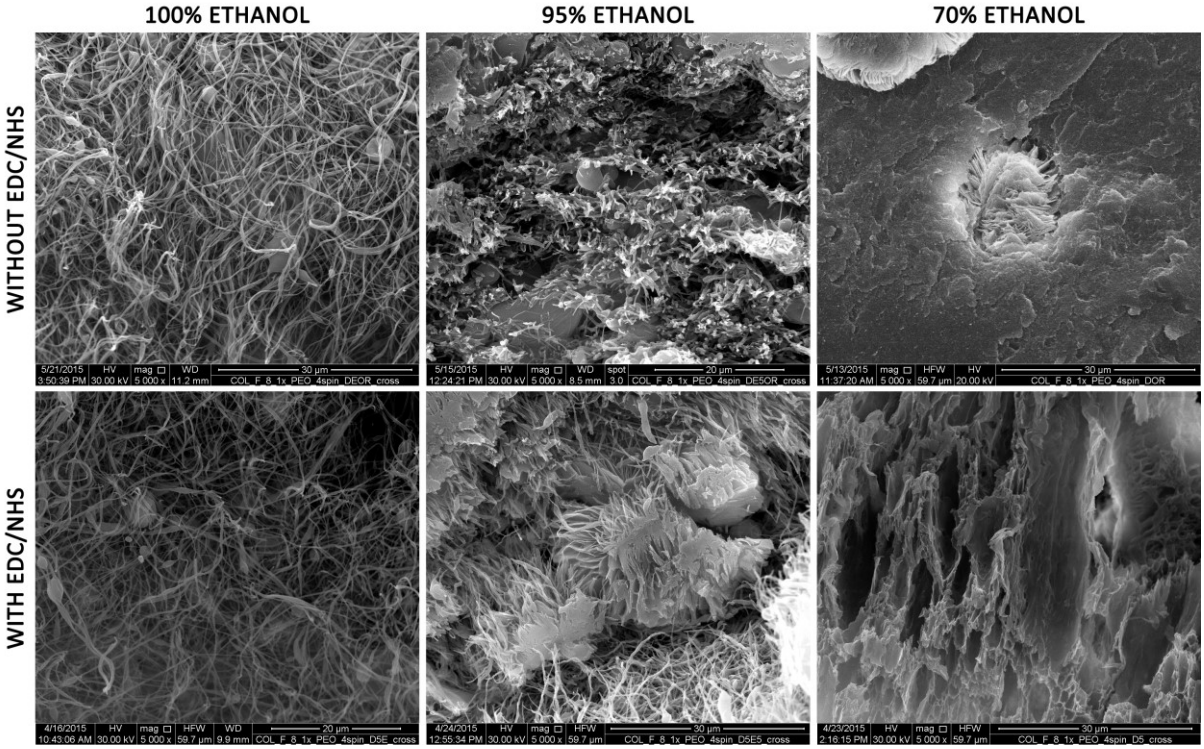

Fig. 44 SEM images of collagen electrospun layers after immersion in 100%, 95% and 70% ethanol with and without the EDC/NHS cross-linker at 37°C (mag. 5,000x).

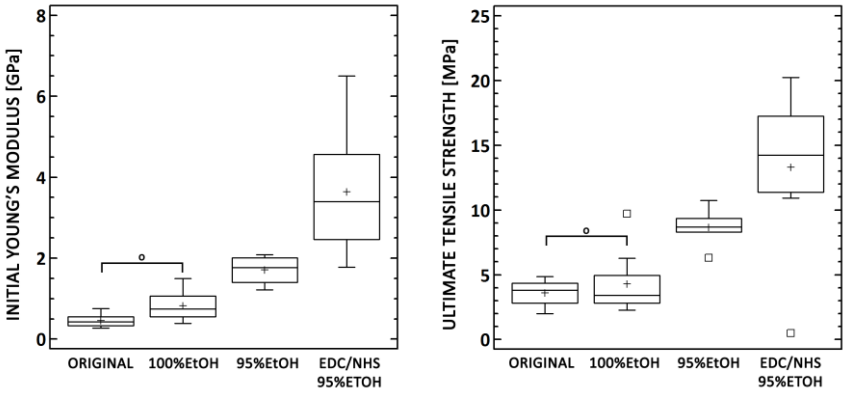

Fig. 45 Initial Young's modulus and ultimate tensile strength of the collagen electrospun layers before (ORIGINAL) and after immersion in 100% and 95% ethanol and 95% ethanol with EDC/NHS at 37°C. "o" denotes values without statistically significant differences (Mann-Whitney, *0.05*, *n=8*).

The analysis of the mechanical properties of electrospun collagen treated with 100% and 95% ethanol and a 95% ethanol solution with EDC/NHS revealed that the application of 95% ethanol exerts an impact on the increase in both stiffness and ultimate tensile strength (Fig. 45). Unlike treatment with pure ethanol, that does not exert a statistically significant impact on the evaluation of the mechanical properties, treatment with 95% ethanol was found to increases both the Young's modulus (up to 430%) and the ultimate tensile strength (230%) compared to the non-cross-linked samples. This may indicate changes in the inner structure of the electrospun samples. Such an improvement in the mechanical properties might be explained by the joining of particular fibres or their bundles as a result of the partial dissolution of partially-damaged electrospun collagen due to the presence of 5% of water in the ethanol. The formation of such joints would further affect the mechanical properties.

The chemical cross-linking reaction is influenced by several factors and conditions. In addition to other parameters, the rate of cross-linking can be controlled via the concentration and reaction time. In the experiment described hereinafter, nanofibrous layers electrospun from an 8 wt% collagen (type I, calf skin, VUP Medical, Czech Republic) PBS/ethanol solution with PEO (8 wt% to collagen) were cross-linked by EDC/NHS in 95% ethanol at a temperature of 37°C. Three different concentrations of EDC/NHS were applied, namely a theoretical concentration calculated based on the amino acid composition (assuming the formation of an amidic bond from lysine or hydroxylysine NH_2 and C=O from glutamic or aspartic acid) and half or double the theoretical concentration. Three different cross-linking periods were applied, namely 24, 72 and 168 hours. The effects of the cross-linker concentration and cross-linking period were evaluated by means of uniaxial tensile testing in the dry state (with a view to a comparison with non-cross-linked electrospun collagen).

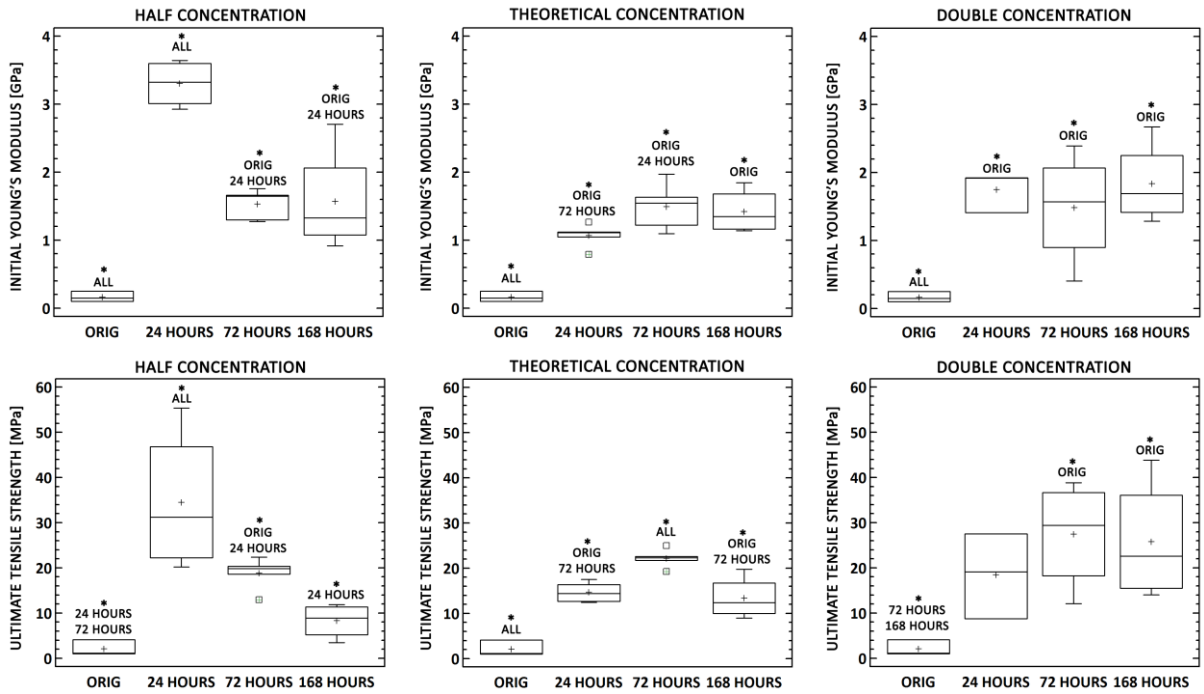

Fig. 46 Initial Young's modulus and ultimate tensile strength of the collagen electrospun layers before (ORIG) and after cross-linking with EDC/NHS in three different concentrations and for three periods in 95 wt% ethanol at 37°C. * denotes statistically significant differences (Mann-Whitney, *0.05*, *n=6*).

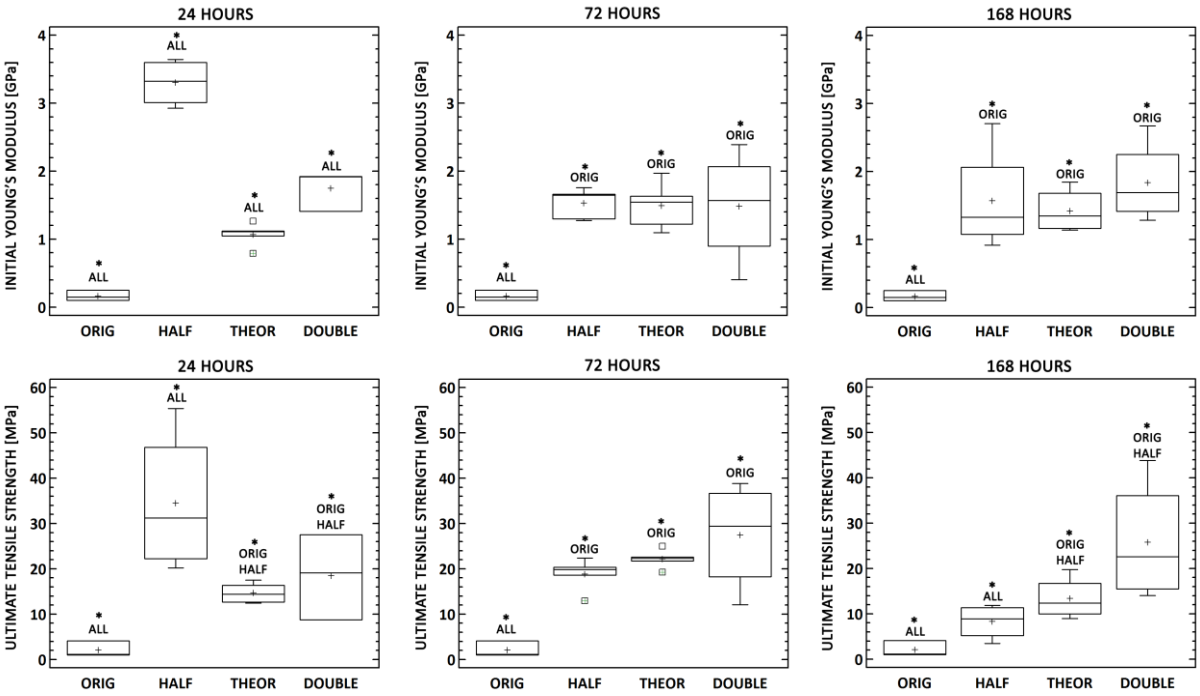

Fig. 47 Initial Young's modulus and ultimate tensile strength of the collagen electrospun layers before (ORIG) and after cross-linking with EDC/NHS in three different concentrations and for three periods in 95 wt% ethanol at 37°C. * denotes statistically significant differences (Mann-Whitney, *0.05*, *n=6*).

The mechanical properties determined (Fig. 46 and 47) suggested the statistically significant increase in the initial Young's modulus and ultimate tensile strength after the application of the selected cross-linking conditions. In contrast to the samples cross-linked with the half theoretical concentration, the samples cross-linked with the theoretical and double theoretical concentrations of EDC/NHS evinced a step increase in both stiffness and strength after 24 hours (Fig. 46). In general, the prolonged cross-linking time did not significantly affect the mechanical behaviour of the cross-linked samples. The application of the double theoretical concentration increased the variability of the assessed mechanical properties, which indicated possible structural inhomogeneity under such a high cross-linker concentration. Contrary to expectations, the collagen samples cross-linked for 24 hours at half the theoretical concentration evinced the highest Young's modulus values and ultimate tensile stiffness. However, this trend was not repeated after 72 and 168 hours of cross-linking. This was most probably caused by the coalescence of the fibres into a foil and a loss of porosity (see Fig. 48) in connection with the low concentration of EDC/NHS together with too short a time period for sufficient cross-linking. Such sample inhomogeneity also reflected higher data variance compared to the other samples measured in this period. Moreover, in general, the different EDC/NHS concentrations did not significantly affect the mechanical behaviour of the cross-linked samples. Based on the SEM image analysis of the cross-linked collagen sample cross-sections (Fig. 48), it can also be concluded that the half theoretical concentration did not fully preserve the nanofibrous and homogeneous structure. Similarly, the prolonged cross-linking time had a similar impact on the structure. Based on these results it can be concluded that the application of the theoretical concentration for 24 hours is suitable for a sufficient rate of collagen cross-linking and the preservation of the inner fibrous structure as opposed to prolonged times and higher concentrations.

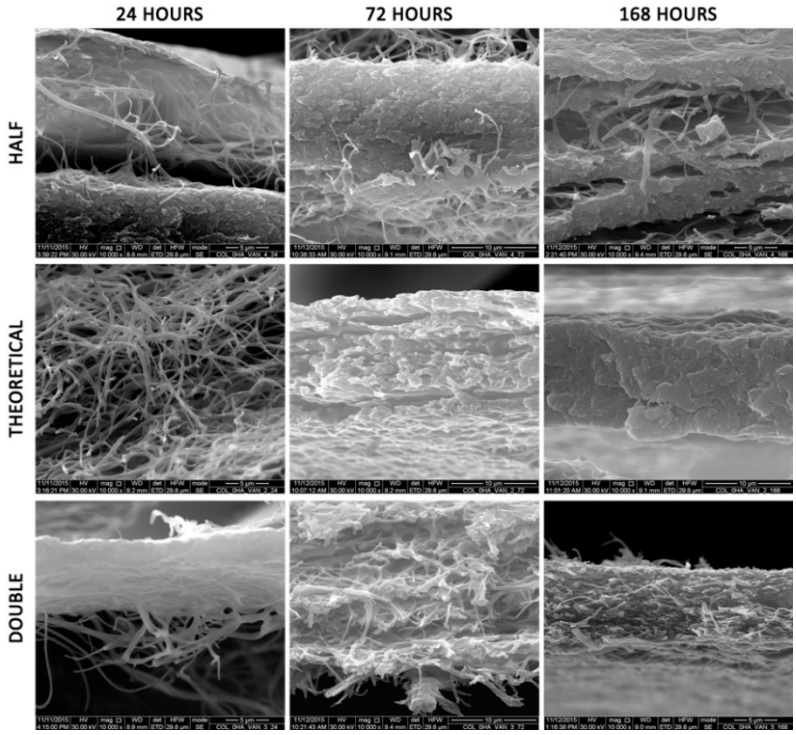

Fig. 48 SEM images of collagen (type I, calf skin) electrospun layers cross-linked with theoretical, half and double theoretical concentrations of EDC/NHS for 24, 72 and 168 hours (mag. 10,000x).

Moreover, the degradation test under physiological conditions was used to assess the stability of the collagenous layers (for analysis details please see *Appendix B.9*). UV-VIS spectrophotometry was used for the quantification of the free amino groups released during the degradation of the samples immersed in the PBS (37°C, pH 7.4). Figure 49 summarizes the degradation rates expressed as the free amino acid concentration. The release of amino acids from the collagen samples was caused by collagen dissolution; thus, the higher the concentrations assessed, the lower is the stability. In all the cases of the applied conditions, the stability of the electrospun collagen was enhanced by cross-linking as compared to the non-cross-linked electrospun collagen. The application of EDC/NHS in the theoretical and double theoretical concentrations for 24, 72 and 168 hours evinced similar effects on the stability of the electrospun fibres. Half the theoretical concentration of the cross-linker seems to be insufficient, which is in agreement with previous results. 10 days after immersion in the PBS, the stability of such cross-linked layers evinced similar degradation rates as non-cross-linked electrospun collagen.

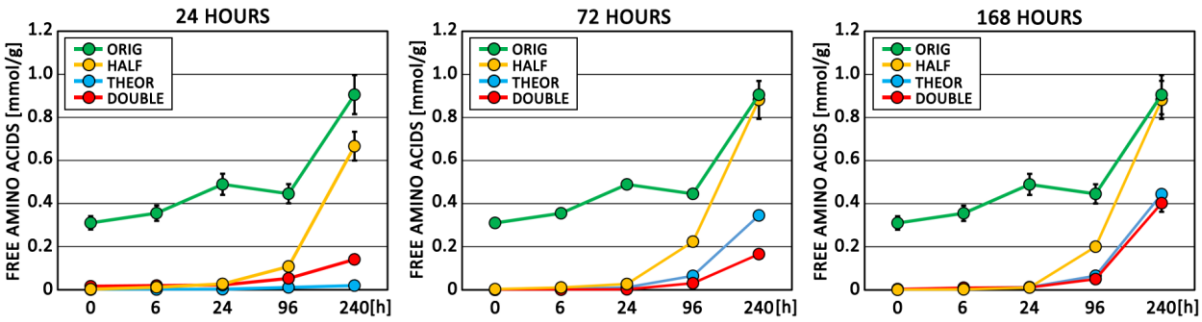

Fig. 49 The concentration of amino acids released from the electrospun collagen prior to and after cross-linking with 1x, ½x and 2x theoretical concentrations of EDC/NHS for 24, 72 and 168 hours (*n=3*).

II.4 Mechanical properties and variability in hydrated states

II.4.1 Mechanical properties under simulated body conditions

As mentioned in chapter I.3, hydration may strongly affect the mechanical properties of collagen materials [67]. The hydrated state also much better approximates to the *in vivo* situation. For a better approximation of electrospun collagen behaviour after implantation, mechanical properties under simulated body conditions were studied. In this experiment, the mechanical behaviour of collagen electrospun from 8 wt% PBS/EtOH solution with 8 wt% of PEO (to collagen), and cross-linked by 95% EDC/NHS solution (24 hours, 37°C) was determined under three different conditions. It was expected that the artificial materials following implantation would be surrounded not only by a specific environment, but also by hard and soft tissues cells, macrophages, enzymes, blood components etc. Thus, for a better *in vivo* approximation, electrospun collagen samples were exposed to Dulbecco's Modified Eagle Medium (DMEM) with and without dermal fibroblasts (iz_171017, Biomedical Centre, Medical Faculty in Pilsen, Charles University) or osteoblasts (human line SAOS-2) under a 5% CO_2 atmosphere at a temperature of 37°C. The cultivation conditions are described in detail in *Appendix B.10*.

Prior to mechanical testing, successful cell cultivation was verified by means of biological testing, namely via the assessment of the cell metabolic activity and fluorescence microscopy (for details please see *Appendix B.10*). Moreover, the mechanical tests were accompanied by the determination of structural changes in the collagen via FTIR and the SEM image analysis of the electrospun samples.

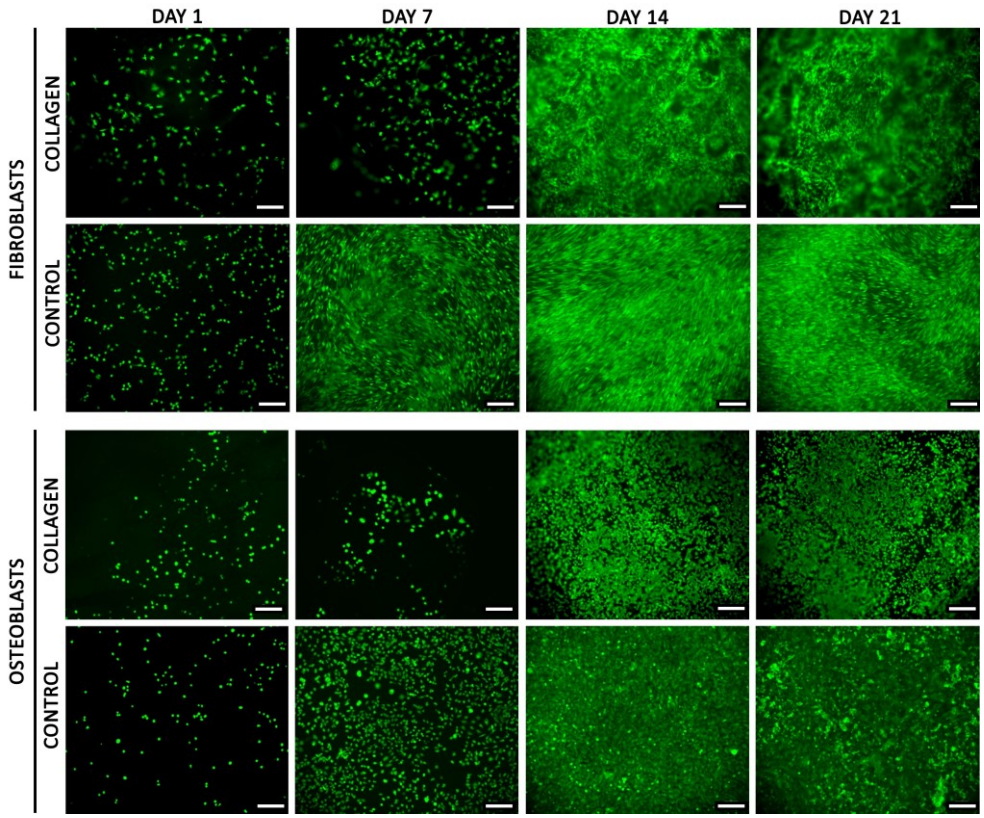

Fig. 50 Fluorescence images of dermal fibroblasts and osteoblasts cultivated on electrospun collagen and polystyrene (control) for 1, 7, 14 and 21 days. The cells were stained with calcein AM (bar 200 μm).

Figure 50 illustrates successful cell cultivation, which was the main requirement for the assessment of their activity with respect to the mechanical properties of electrospun collagen. Cell behaviour was also quantified by the determination of their metabolic activity, which was comparable to the metabolic activity of cells cultured on the standard control polystyrene material (control), data not shown.

The mechanical properties were measured by means of the uniaxial tensile test (*n=8*). Because of the viscoelastic behaviour of hydrated electrospun collagen, which also depends on previous deformation, it was necessary to load and relieve the sample several times before performing the inter-strength test. The estimation of the initial modulus of elasticity was made both for the first load cycle - from which the effect of cell activity on the surface layers of the material could be determined, and the last (fifth) load cycle from which the effect of cells on the inner structure of the material could be estimated (Fig. 51). Moreover, the ultimate tensile strength was calculated (Fig. 52). Measurements were carried out on a multi-axis test machine (Zwick/Roell, Germany) with U9B force sensors by HBM with a range of ±25N and ±250N equipped with a non-contact optical extensometer.

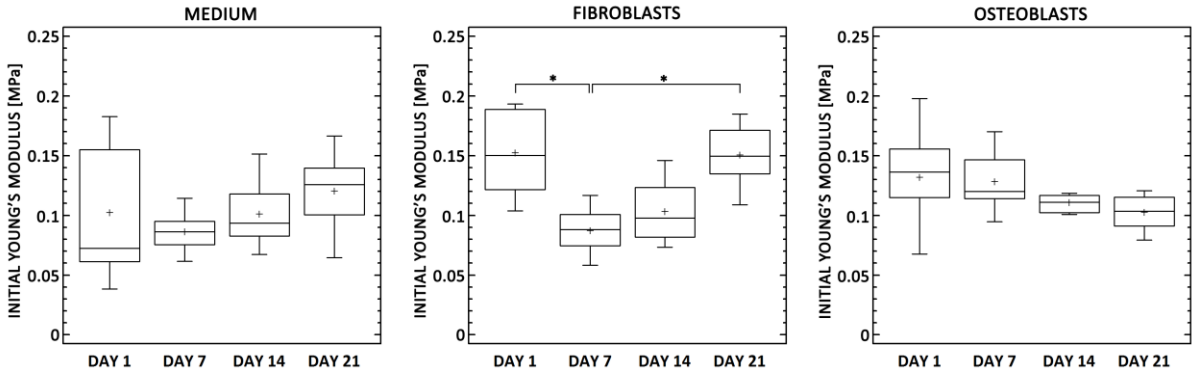

Fig. 51 Initial Young's modulus of the electrospun collagen layers exposed to DMEM without cells and with dermal fibroblasts or osteoblasts for 1, 7, 14 and 21 days. * denotes statistically significant differences (Kruskal-Wallis test, Bonferroni procedure, *0.05*, *n=8*).

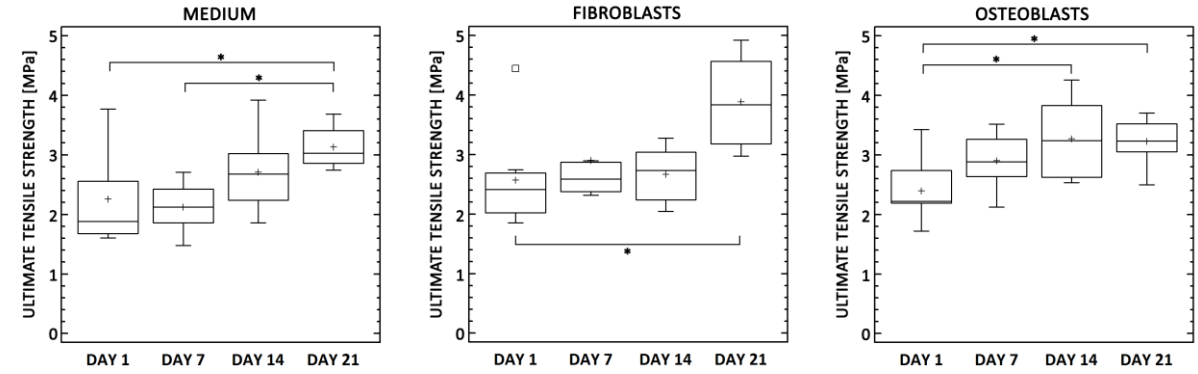

Fig. 52 Ultimate tensile strength of the electrospun collagen layers exposed to DMEM without cells and with dermal fibroblasts or osteoblasts for 1, 7, 14 and 21 days. * denotes statistically significant differences (Kruskal-Wallis test, Bonferroni procedure, *0.05*, *n=8*).

The initial modulus of elasticity of the collagen samples exposed to the cell-free medium remained at the same level after three weeks of testing. A partial statistically insignificant increase in modulus (up to 70% on the 21st day) was explained by the adsorption of DMEM protein components into the high-surface area of the nanostructured collagen (for an illustration see Fig. 53). Such adsorbed substances may increase the stiffness of samples by reinforcing their inner structures. A similar trend, but statistically significant, was evident in the case of ultimate tensile strength (up to 61% on the 21st day). Nevertheless, the results indicated the stability of collagen under simulated body conditions over a period of 3 weeks.

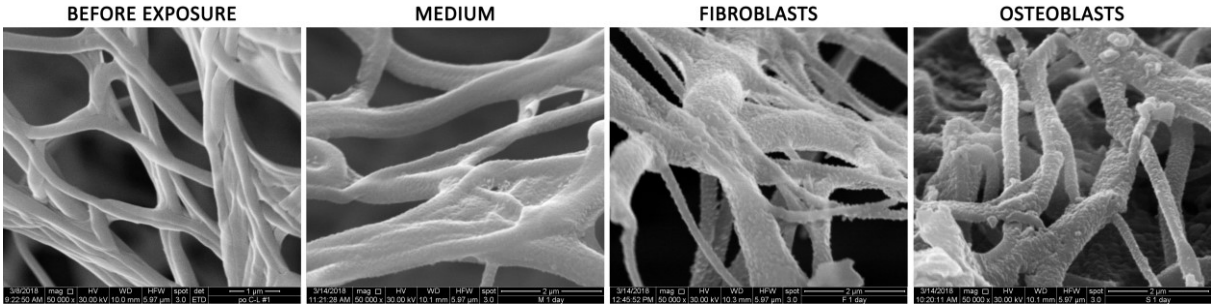

Fig. 53 SEM images of the electrospun collagen layers illustrating the adsorption of medium components into the inner structure immediately 1 day after exposure to the medium with or without cells (mag. 50,000x).

As mentioned above, the mechanical behaviour of collagen in the dry and hydrated states differs. Electrospun collagen samples prepared via the same procedure and tested in the dry state (for a comparison please see Fig. 46 - samples cross-linked by a theoretical EDC/NHS concentration for 24 hours) evinced a Young's modulus in the order of thousands of MPa, whereas hydrated electrospun collagen evinced a Young's modulus in the order of tenths of MPa. The influence of the activity of both fibroblasts and osteoblasts on the collagen samples determined from the fifth loading cycle was not significant. With the exception of the statistically significant drop in the Young's modulus on the 7th day (and an insignificant decrease on the 14th day) after cultivation with fibroblasts (40% decrease), no obvious further changes occurred. The activity of the osteoblasts was not demonstrated at all. In the case of ultimate tensile strength, a statistically significant increase was detected for the materials exposed for 21 days to media with both fibroblasts (up to 60%) and osteoblasts (up to 45%). This increase was probably influenced by the adsorption of DMEM components rather than by cell activity since a similar increase was recorded in the case of the samples exposed to the medium without cells (up to 61% on the 21st day).

The effect of cell activity on the mechanical properties of the electrospun collagen samples was determined from the first loading cycle. Due to the sample dimensions (thickness of approx. 300 μm) and relatively short duration of cultivation, cell activity was anticipated in the surface layers of the material. The effect of possible changes in the surface layers was expected to diminish after repeated loading. For this reason, the activity of the cells was evaluated via the effect on the initial Young's modulus determined from the first loading cycle (Fig. 54).

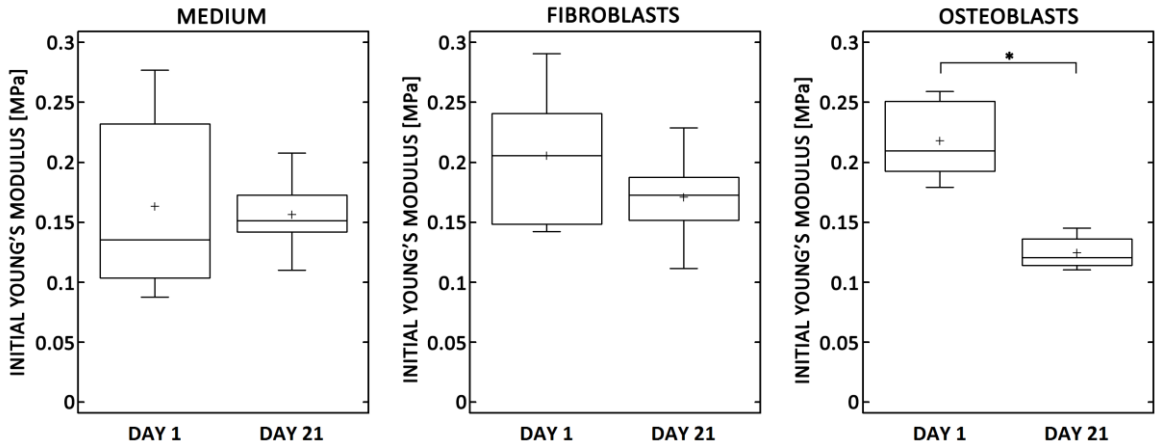

Fig. 54 Initial Young's modulus (in the first loading cycle) of the electrospun collagen layers exposed to DMEM cell culture medium without cells and with dermal fibroblasts or osteoblasts for 1 and 21 days. * denotes statistically significant differences (Kruskal-Wallis test, Bonferroni procedure, *0.05*, *n=10*).

The activity of the cells was demonstrated in the case of osteoblasts, the activity of which decreased the stiffness of the collagen samples. On the 21st day, the initial Young's modulus of the electrospun collagen samples decreased by 40%. In the case of the fibroblasts, a 17% decrease in the modulus was not statistically significant, while in the case of the samples immersed in the cell-free DMEM, the Young's modulus remained at the same level.

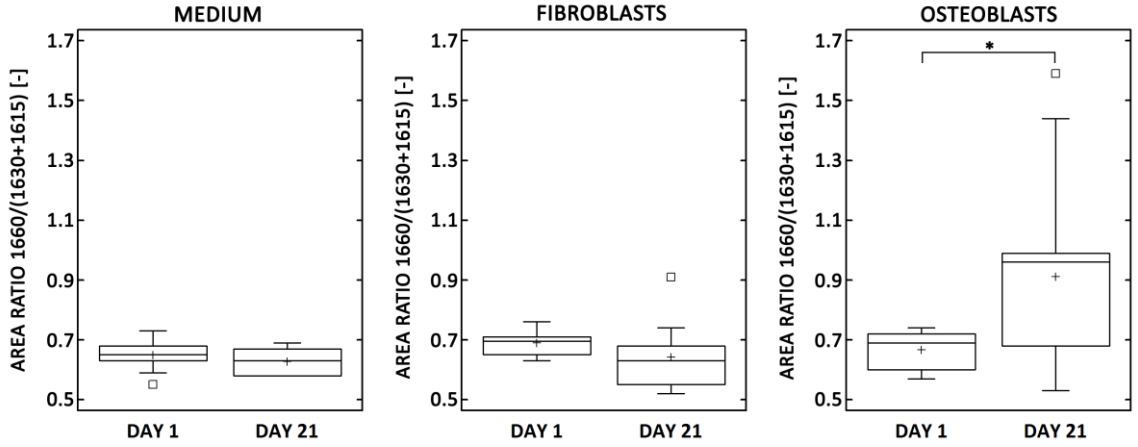

Fig. 55 Ratio of the helical and denatured collagen areas (1660/(1630+1615) of the electrospun collagen layers exposed to DMEM cell culture medium without cells and with dermal fibroblasts or osteoblasts for 1 and 21 days. * denotes statistically significant differences (Mann-Whitney, *0.05*, *n=10*).

Osteoblast activity was also proven by FTIR (Fig. 55). For details of the analysis please see *Appendix B.2*. The ratio of the helical part of the collagen (represented by band 1660 cm^{-1}) and the denatured collagen part (bands 1630 and 1615 cm^{-1}) revealed an increase in the helical structure of the collagen. This increase can be explained by the presence of osteoblasts, which are able to metabolise electrospun collagen and simultaneously produce their own collagen. The relatively high variance in the determined ratios may have been related to local inhomogeneities (surface areas with variable amounts of helical parts).

II.4.2 Variability of electrospun collagen

The last part of this section is devoted to a discussion of a further important issue associated with the electrospinning of collagen and its post-processing, i.e. the variability of the process itself. In general, one of the major limitations of the electrospinning of polymers is scatter in the dimensions of the obtained fibres, the variable surface density of the electrospun materials and inhomogeneity. Unlike synthetic polymers, the electrospinning of collagen is rather more complicated because of its natural character, the problematic nature of its dissolution, susceptibility to denaturation and the need for subsequent cross-linking. Each step of the preparation process introduces a certain rate of variability in the final properties. The structural variability of electrospun collagen subsequently affects its mechanical properties and other characteristics affected by the fibre dimensions (e.g. drug carriers, wound healing bandages, tissue engineering scaffolds, etc.), and thus poses a significant limitation in terms of its applicability. With regard to these limitations, attention must be devoted to control throughout the whole of the electrospun collagen preparation process and the verification of the reproducibility of this process. The variability of the properties of electrospun collagen is illustrated by the following experiment.

The experiment involved the characterisation of the mechanical behaviour of collagen electrospun from 8 wt% PBS/EtOH solution with 8 wt% of PEO (to collagen), and cross-linked by a 95% EDC/NHS solution (24 hours, 37°C). The preparation of the electrospun layers was repeated 15 times under the same processing conditions (45 kV, needle to collector distance 20 cm, feeding rate 80 $\mu L.min^{-1}$, temperature 24-26°C, relative humidity 23-26%, the flow of preheated air 25°C with a flow rate of 10 $L.min^{-1}$) and from the same collagen solution. A static collector (22 x 29 cm) was used. Similarly, the layers were cross-linked using the same procedure. The mechanical properties were evaluated by means of the uniaxial tensile testing of rectangular strips of the layers (approx. 40 x 10 mm). For the analysis, 5 layers were randomly selected. Prior to the mechanical testing, all the samples were fully hydrated in PBS. During the test procedure, 5 preloading cycles were carried out as preconditioning. The sixth loading sequence was used in the subsequent mathematical modelling. The engineering strain (ratio of the elongation of the sample to its reference length) and nominal stress (ratio of the applied force to the reference cross-section of the sample) was determined from the experimental recordings.

Concerning the evaluation of variability, a hyperelastic material description was adopted for the modelling of the fully nonlinear mechanical behaviour of the electrospun collagen in the hydrated state [141]. The hyperelastic material was characterised by the strain energy density function W. The Fung-Demiray exponential model [142], frequently used in soft tissue biomechanics, was employed. Its particular form is expressed by Eq. (1).

$$W = \frac{\mu}{2\alpha}\left(e^{\alpha(I_1-3)} - 1\right), \text{ where} \tag{1}$$

μ represents the stress-like material parameter corresponding to the infinitesimal shear modulus and α represents a dimensionless parameter modulating the strain-stiffening response. I_1 is the first principal invariant of the right Cauchy-Green strain tensor **C** which is obtained from $\mathbf{C} = \mathbf{F}^T\mathbf{F}$, where **F** is the deformation gradient tensor. The kinematics of the uniaxial tensile test was assumed to be

described by Eq. (2). Here $\boldsymbol{X}$ is the position vector of a material particle in the reference configuration and $\boldsymbol{x}$ is its position vector in the deformed state. In such a case, the deformation gradient $\mathbf{F} = \partial x/\partial X$ has the form $\mathbf{F} = diag[\lambda_1, \lambda_2, \lambda_3]$ and $I_1 = \lambda_1^2 + \lambda_2^2 + \lambda_3^2$.

$$x_1 = \lambda_1 X_1, \quad x_2 = \lambda_2 X_2, \quad x_3 = \lambda_3 X_3 \tag{2}$$

In hyperelastic materials, the strain energy density function W serves as a potential function for stress. In the case of the nominal (the first Piola-Kirchhoff) stress tensor $\mathbf{P}$, this is expressed in Eq. (3) which plays a role of the constitutive equation.

$$\mathbf{P} = \frac{\partial W}{\partial \mathbf{F}} - p\mathbf{F}^{-T} \tag{3}$$

In Eq. (3), the assumption of the incompressible behaviour of collagen was adopted, which means that p is the Lagrangean multiplier enforcing the incompressibility constraint and has to be determined from a force boundary condition. Combining (1), (2), (3), the incompressibility condition $\det(\mathbf{F}) = 1$, and the isotropy of the material, the final expression for the nominal stress sustained by the sample in uniaxial tension applied in direction 1 is obtained. It is expressed in (4). The relation between λ_1, used in (4), and the engineering strain ε_{11}, measured in the experiment, is given by $\lambda_1 = 1 + \varepsilon_{11}$.

$$P_1 = \mu\left(\lambda_1 - \frac{1}{\lambda_1^2}\right) e^{\alpha\left(\lambda_1^2 + \frac{2}{\lambda_1} - 3\right)} \tag{4}$$

Employing least square method, the parameters μ and α that characterised every tested sample were determined. Least square optimization was carried out in the Maple multipurpose computer algebra system (Maplesoft, Canada). The coefficient of determination R^2 was used to evaluate the quality of the regression model described in Eq. (4).

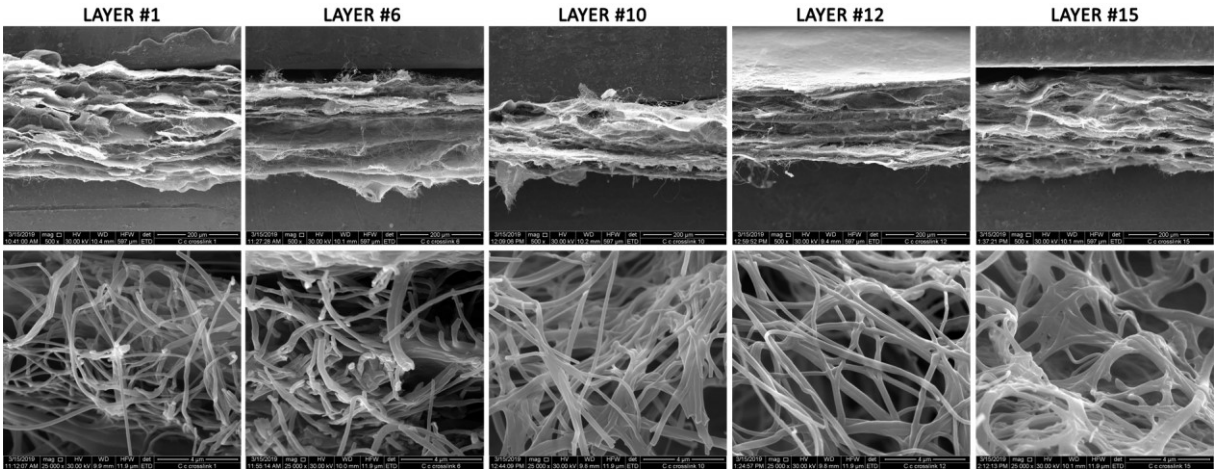

Fig. 56 Representative SEM images of five collagen electrospun layers randomly selected for the evaluation of variability (first line: mag. 500x, bar 200 μm; second line: mag. 25,000x, bar 4 μm).

Figure 56 summarizes representative images of the selected layers. The mean values (arithmetic mean in the case of the normally distributed data of parameter μ and the median in the case of the non-

normally distributed data of parameter α) of the material parameters estimated in the nonlinear regression analysis are presented in Table 3.

Table 3. Expected values of the material parameters and their variability. IQR denotes the interquartile range, SD denotes the sample standard deviation, *n* denotes the number of the tested samples.

layer	*n*	α [-]	IQR	μ [kPa]	SD
# 1	*7*	5.27	5.17 - 5.34	16.97	4.30
# 6	*8*	4.34	4.14 - 4.50	17.34	4.03
# 10	*8*	4.57	4.44 - 4.69	16.49	3.66
# 12	*5*	4.18	4.05 - 4.34	16.42	4.09
# 15	*4*	4.32	4.22 - 4.46	16.54	4.71

The cluster analysis was used to evaluate the variability of the obtained material characteristics (Fig. 57). The cluster analysis procedure is designed to group observations or variables into clusters based upon the similarities between them.

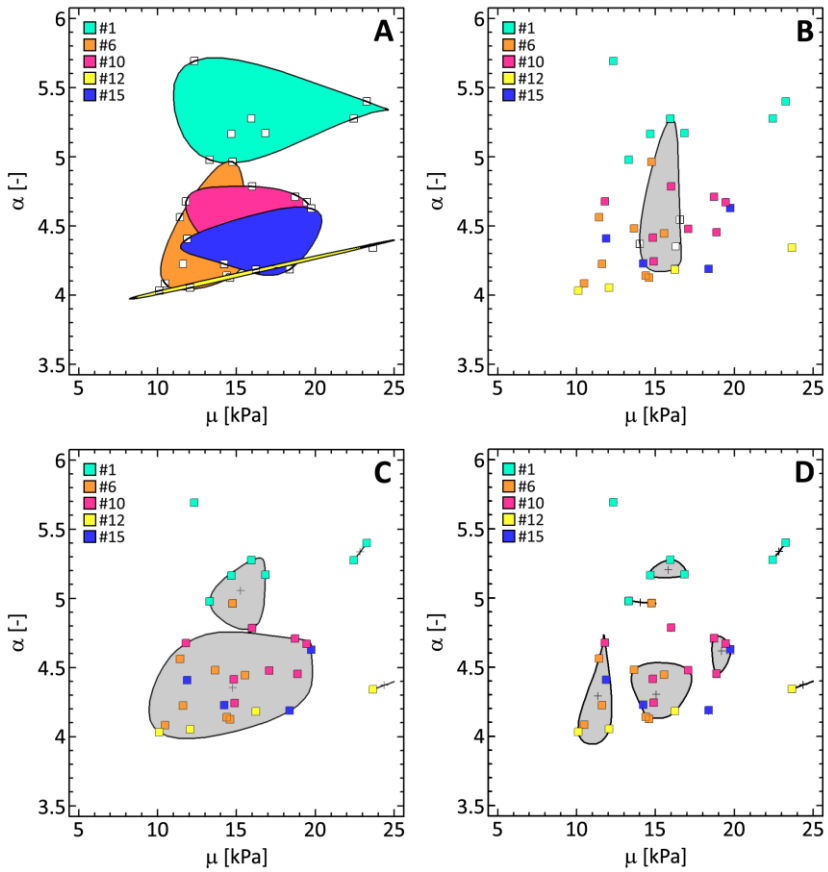

Fig. 57 2D cluster scatterplots showing clustering with respect to any of the variables of the stress-like material parameter μ and α. For comparative purposes, splines were used to connect the observations on the borders of each cluster, namely A: clusters represent the data sets of individual layers, B: the cluster represents the medians of each data set, the points represent particular determined parameters for each of the tested samples, C: the theoretical clustering assuming 5 clusters (i.e. 5 different layers), D: the clustering assuming 10 clusters as an optimum estimated by the elbow method.

The agglomerative method is based on placing each value in a separate cluster and then combining clusters based on their distance from each other, until the desired number of clusters is formed. In this case, the distance between two clusters, in the *p*-dimensional space of variables, was defined as the minimum distance between any member of one cluster and a member of the other (Nearest Neighbour Method). As the metric for measuring the distance between two items, represented by x and y, the square Euclidian distance was:

$$d(x,y) = \sum_{i=1}^{p}(x_i - y_i)^2 \tag{5}$$

The cluster scatterplot (Fig. 57) documents the variability of the determined parameters of the mechanical model describing the behaviour of five randomly selected electrospun collagen layers. Ideally, all the clusters would overlap each other (Fig. 57 A). In this case, at least one group (layer #1) seems to be different from the others since it has an empty intersection with all the other groups. Assuming that the parameter μ seems to fall into approximately the same range in all the groups, α is the only parameter which reflects the differences between the material groups in the model (4).

The analysis of the mechanical properties was accompanied by the FTIR analysis of the secondary structure of the collagen (for details of the analysis please see *Appendix B.2*). Firstly, the collagen layers were compared before and after cross-linking. From the point of view of the FTIR analysis, all the prepared layers were comparable prior to and after cross-linking. Bands ~1205, 1240, 1280 (amide III) and 1340 cm^{-1} proved the presence of a triple-helical structure, which was preserved after all the preparation steps. The amide I region of the spectrum of the collagen (~1650 cm^{-1}) could be deconvoluted (for an illustration see Fig. 58) into several distinct bands with maxima at ~1685-1690, 1660, 1630-1635 and 1610-1615 cm^{-1} [143].

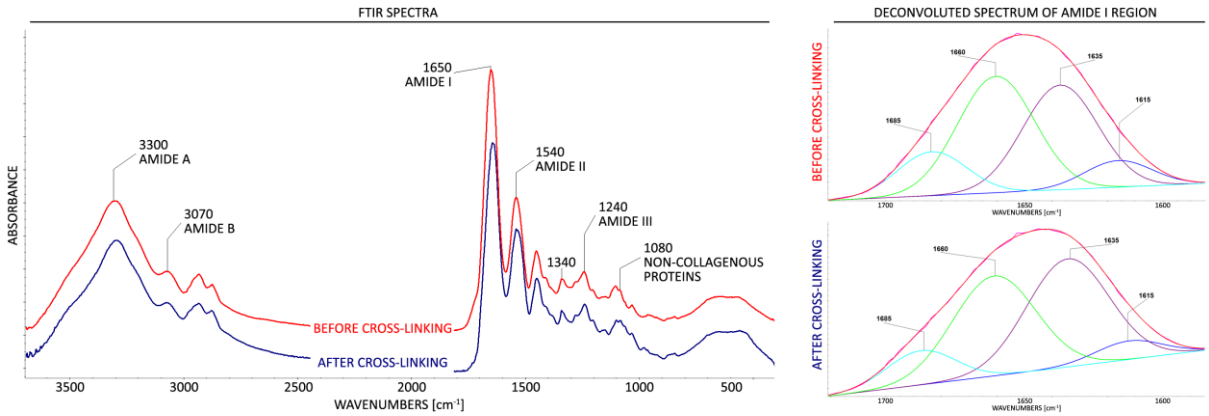

Fig. 58 An example of the FTIR spectra and deconvoluted spectra of the amide I region of the electrospun collagen prior to and after cross-linking.

Band ~1660 cm^{-1} was assigned to the triple helix, with a contribution from the α-helix [143], while band ~1630-1635 cm^{-1} was assigned to the aggregate β-sheet structure and the left-handed triple-helix in the denatured state [143]. The component at ~ 1610-1615 cm^{-1} was related to aromatic amino acids which may be more spectroscopically active in the case of the denatured state of collagen, such as gelatine [139]. The band at 1685-1690 cm^{-1} was attributed to the β-turn and antiparallel β-sheet

structure [143]. Upon denaturation, the bands did not shift appreciably in position, but the relative intensities of the 1660 and ~1635 cm^{-1} bands shifted from > 1 to < 1; in other words, the component found at around ~1635 cm^{-1} increased and the component found at around 1660 cm^{-1} decreased in intensity. A further spectral region consisted of the so-called carbohydrate region (960–1140 cm^{-1}) where sub-bands of non-collagenous proteins and carbohydrates were present [144]. Upon denaturation, the areas of the bands belonged to the increase in non-collagenous proteins. The changes in these parameters could be quantified and used for the comparison of each of the prepared layers.

Figure 59 compares five selected collagen electrospun layers after cross-linking. Briefly, the higher increase in the ratio of the area of amide A and that of amide I represents the presence of fewer crosslinks in the collagen, namely in the case of layer #10. Similarly, the ratio of the areas of the non-collagenous band and amide I proves the higher rate of collagen denaturation, namely in the case of layers #10, #12 and #15. The increase in the ratio of the area of band 1615 cm^{-1} is accompanied by the higher presence of gelatine, which is evinced by layers #12 and #15. The higher rate of collagen denaturation is also manifested via an increase in the ratio of areas 1630 cm^{-1} and 1690 cm^{-1}. In contrast, the increase in the ratio of the area of band 1660 cm^{-1} represents a lower rate of collagen denaturation, namely in the case of layers #1, #6 and #10.

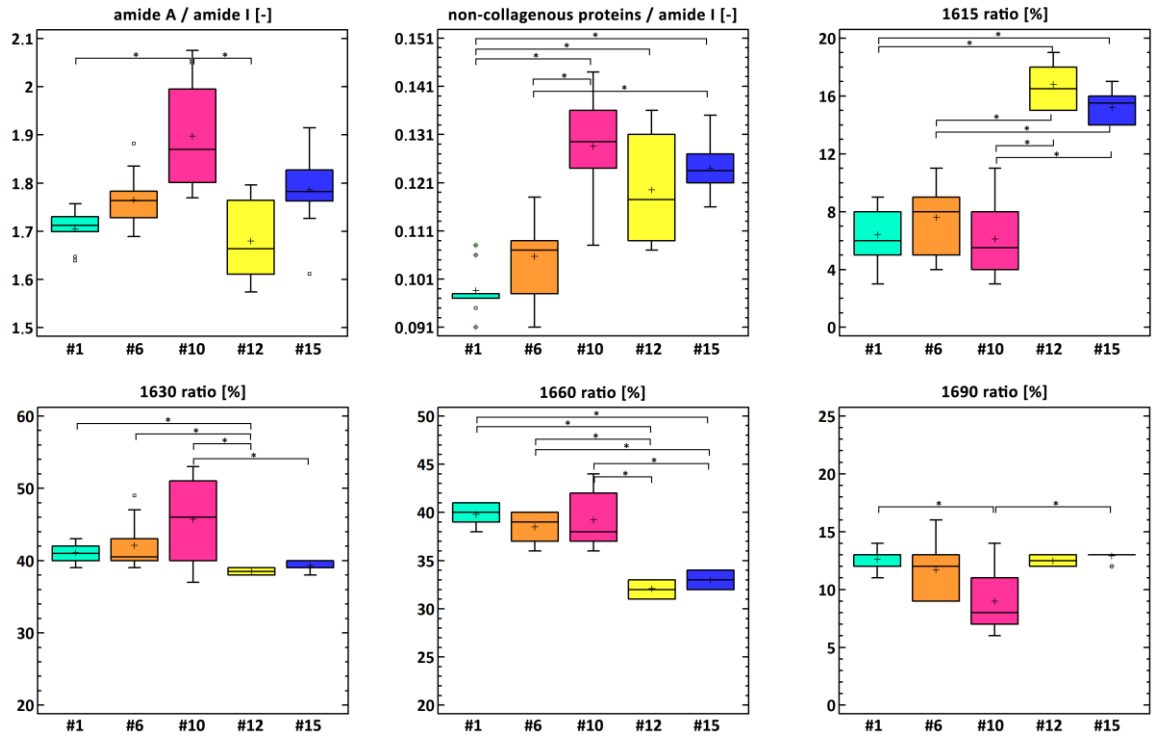

Fig. 59 Quantification of electrospun cross-linked collagen variability based on various FTIR parameters, namely the ratio of amide A and amide I areas, the ratio of the non-collagenous protein band and amide I areas, the areas of band 1615, 1630, 1660 and 1690. * denotes statistically significant differences (Kruskal-Wallis, Bonferroni procedure, *0.05*, *n=10*).

It should be noted that all the prepared layers evinced some rate of variability in the parameters studied herein. Similarly, the relatively higher variance of the assessed data (*n=10*) may indicate the

presence of local inhomogeneity. Based on the collected spectral characteristics, the collagen layers can be roughly divided into two groups. The first group consists of layers #1, #6 and #10, in which the helical part of the collagen decreases in favour of aggregated β-structures and the helical structure in denatured states. In addition to the achievement of the statistical significance of these findings, the quantified differences were somewhat insignificant from the point of view of the preservation of the secondary structure of the collagen. Nevertheless, they do indicate the variability of the electrospun collagen. The second group (#12 and #15) represents samples with a greater decrease in the helical structure in favour of the structural states characteristic of gelatine.

The analysis of the mechanical and structural properties of randomly-selected materials electrospun separately and cross-linked under the same conditions and the identical solution and process parameters demonstrate the variability of the preparation of nanofibrous collagen. The variability is influenced by several factors, the definition of which begins at the collagen isolation stage and continues through each of the processing stages. Unfortunately, no methodology that is able to simply control the properties of electrospun collagen is easily accessible and, most likely, is not available at all. In the case of collagen, the extent of variability should be taken into account in the of medical application design process, rather than attempting to improve methods for the control of its practically uncontrollable variability.

Chapter III

Development of a soft on hard matter implant

III.1 Motivation

The increasing number of primary joint replacement procedures has led to a corresponding increase in the need for endoprosthesis revision surgery due to the incidence of bacterial infections resulting either from contamination caused by microorganisms intrinsic to the patient or from external contamination initiated at the time of surgery. Thus, the need has arisen to develop novel strategies that are safe and easily implementable, and which reduce the risk of the reoccurrence of infection. The usual strategy is based on surgical revision involving the removal of the foreign material and supplementary antimicrobial therapy, in which case antibiotics must be administered at high dosages for an extended period of time [145]. One of the ways in which to increase the efficacy of therapy consists of the application of a local antibiotic delivery system [146–148]. The local delivery of antibiotics maximises target tissue concentration while minimising the risk of systemic toxicity. The most extensively studied and earliest commercially available device designed for the controlled release of antibiotics was developed in the 1970s according to Buchholz and Engelbrecht's [149] innovative idea of releasing antibiotics from polymethylmethacrylate (PMMA) bone cement. This device is still widely used; however, it enables only a small fraction of the loaded drug to diffuse through the polymer pores and provides an initial burst release of antibiotics with the larger part of the loaded antibiotic remaining within the cement. Since PMMA is not biodegradable, secondary surgery is subsequently necessary to remove the PMMA before new bone can regenerate. Thus, with a view to overcoming these disadvantages, various biodegradable devices made from both natural and synthetic polymers have been produced by means of various processes in recent years [150].

Over the past decade, researchers have developed biodegradable polymeric scaffolds [151–153], degradation beads [154], sheets [155] and membranes [121] for use in the treatment of bone infections. A further alternative method with respect to the treatment of osteomyelitis involves the use of a hydrogel structure that is easily administered (injectable) [156–158] and, moreover, is not particularly invasive. Antibiotic-loaded implant coatings provide a straightforward approach to the prevention of implant-associated infections [128,129,131,159,160]. This "soft matter on hard matter" method provides an immediate response to the threat of implant contamination and, moreover, does not require the use of any other carrier than the orthopaedic implant itself.

The loading of drugs can be conducted via the use of a number of different techniques, the most simple of which consists of the straightforward mixing of the polymer and antibiotics in the form of a dry powder [154] or solution [152,155,156,161,162]. Although all the approaches employed are generally successful in terms of providing for the long-lasting release of therapeutic antibiotic concentrations, drug loading is often conducted by means of the mixing of the drug with polymers sometimes dissolved in harsh solvents. A further method involves the soaking of the antibiotics by means of immersion in a drug-containing solution [158,163–169]. Electrospinning is seen as having great potential in terms of the development of nano-structured biomedical materials. The resulting electrospun fibres have been

successfully investigated with respect to their use as matrices containing antibiotics [120], sandwich structures for the repair of infected wounds [121–123] and the electrospun vancomycin-loaded coating for titanium implants [124,125]. The technology and conditions concerning composite preparation are of particular importance since they are able to significantly affect the final nano/microstructure of the composite and, consequently, the antibiotic release profile. Collagen offers significant potential for the creation of a coating for orthopaedic implants in the form of a nanofibrous local carrier of antibiotics. Moreover, its submicron- or nanofibrous forms provide particularly efficient drug delivery agents due to their high surface-area-to-volume ratios, high porosities and 3D open porous structures [132].

The previous chapters addressed the crucial issues important for the understanding of collagen as a variable material of natural origin with regard to its mechanical and structural aspects. In the last part of the thesis, the author highlights the various perspectives of the development of collagen-based materials and addresses the employment of the experience obtained of collagen processing in a specific medical application. Here, the author summarizes the development of a collagen coating for orthopaedic implants in the form of a nanofibrous layer, which exerts a strong local anti-infection effect with no indication of cytotoxic effects and, simultaneously, leads to an increase in the rate of osseointegration necessary for the suitable fixation of the implant. It is expected that such a layer will be used particularly in the case of known prosthetic joint infections or as a preventative procedure regarding primary joint replacement in a potentially infected site. The layer will provide a bone/implant (titanium alloy) bioactive interface, which will enhance the physiological healing process, will be capable of filling bone defects, and will act as a powerful antibacterial agent. The development of this layer had three main parts. ***In the first part***, the author addresses the modification of electrospun collagen by hydroxyapatite nanoparticles and the evaluation of its influence on the mechanical properties, structural stability and adhesion of the electrospun layers on model implant surfaces. ***The second part*** deals with an evaluation of the antibiotic release kinetics and antimicrobial activity of such layers. Since the biological evaluation makes up a crucial element of the development of successful medical devices, a biological evaluation performed under *in vitro* and *in vivo* conditions is described in ***the third part*** of this chapter.

III.2 Modification of collagen by hydroxyapatite - mechanical properties and stability

With regard to imitating the composition of bone tissue and improving the biological response, collagen electrospun layers were modified by hydroxyapatite (HA) nanoparticles. Three different layer compositions were analysed, the aim of which was to verify the potential effect of HA on the mechanical properties and structural stability. Moreover, regarding direct application on the surface of implants, an assessment was conducted of the adhesion of collagen electrospun layers to differently prepared and chemically treated titanium surfaces.

III.2.1 Mechanical properties of the collagen/hydroxyapatite electrospun layers

Nanostructured layers were prepared based on collagen (type I, calf skin, VUP Medical, Czech Republic) with 0 wt%, 5 wt% and 15 wt% of hydroxyapatite nanoparticles (avg. 150 nm, Sigma Aldrich, Germany). The layers were prepared via the electrospinning of an 8 wt% collagen PBS/ethanol solution modified by 8 wt% (to collagen) polyethylene oxide (M_v 900,000, Sigma Aldrich, Germany) with dispersed HA particles. Electrospun mats were prepared using a high voltage level of 45 kV and the feeding rate was set at 130 µl·min^{-1} (4SPIN, Contipro, Czech Republic). The production rate of the nanofibrous collagen mats was increased via the application of electroblowing; the flow rate of the preheated air (25°C) was set at 30 L·min^{-1}. The stability of all the collagen layers was enhanced by means of cross-linking with a 95% ethanol solution containing EDC and NHS at a weight ratio of 4:1 for 24 hours (37°C); the EDC and NHS (Sigma Aldrich, Germany) were used as received.

The mechanical properties were evaluated by means of the uniaxial tensile testing of rectangular strips of the layers. Tensile tests were conducted using a Zwick/Roell multipurpose testing machine equipped with a built-in video extensometer. By using contrasting marks on the surface of samples, the video extensometer automatically determined the reference length and elongation of the samples. Tensile experiments were conducted at a constant clamp velocity of 0.1 mm.s^{-1}. For a detailed description of the mechanical tests, please see *Appendix B.8*. In order to provide for a comparison with non-cross-linked samples, the mechanical properties were evaluated in the dry state.

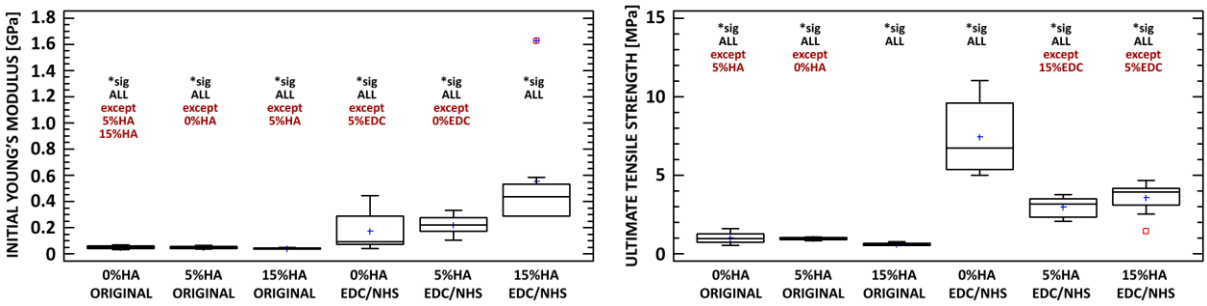

Fig. 60 Initial Young's modulus and ultimate tensile strength of the electrospun collagen layers with different amounts of hydroxyapatite (0, 5 and 15 wt%) prior to and after cross-linking with EDC/NHS. * denotes statistically significant differences (Kruskal-Wallis test, Bonferroni procedure, *0.05*, *n=10*).

The results of the mechanical tests verified the successful effect of cross-linking on the improvement of both the initial Young's modulus and the ultimate tensile strength (Fig. 60). The addition of hydroxyapatite does not affect the rate of the cross-linking reaction. The effect of hydroxyapatite was

also revealed. While the addition of 5 wt% HA exerted no effect on the Young's modulus, the addition of 15 wt% HA increased the modulus by 220%. Following the addition of ceramic nanoparticles, the collagen layers became brittle, as demonstrated partly by the increasing Young's modulus and partly by the decrease in the ultimate tensile stiffness (by 60%). A decrease in strength was also demonstrated following the addition of 5 wt% HA (by 50%). The mechanical properties were further evaluated following exposure to a simulated body environment.

The mechanical and structural stability were further analysed with respect to the intended application of selected antibiotics via impregnation. Hence, the collagen/hydroxyapatite electrospun layers were impregnated with an ethanol solution of vancomycin (vancomycin hydrochloride, Mylan S.A.S, France) in the amount of 10 wt% of the total weight of the collagen (EI0) and the collagen layers with 5 wt% HA (EI5) and 15 wt% HA (EI15). The testing of degradation was carried out by means of exposure to human blood plasma (16 donors with different blood groups, sex and age; supplemented with penicillin/streptomycin) under a temperature of 37°C, 5% CO_2 atmosphere, for 6 h and for 1, 3, 10, 15 and 30 days). The volume of the medium was maintained at a weight/volume ratio of 30 mg/15 mL.

Prior to the degradation test, FTIR spectroscopy was employed in order to characterise the composition of the samples and to verify the theoretical presence of vancomycin following impregnation. Vancomycin peaks following impregnation were easily identifiable (Fig. 61) principally in the 1585, 1420 to 1425, 1227 and 1060 cm^{-1} positions. The FTIR spectra also illustrated that the PEO was fully leached out following the cross-linking procedure.

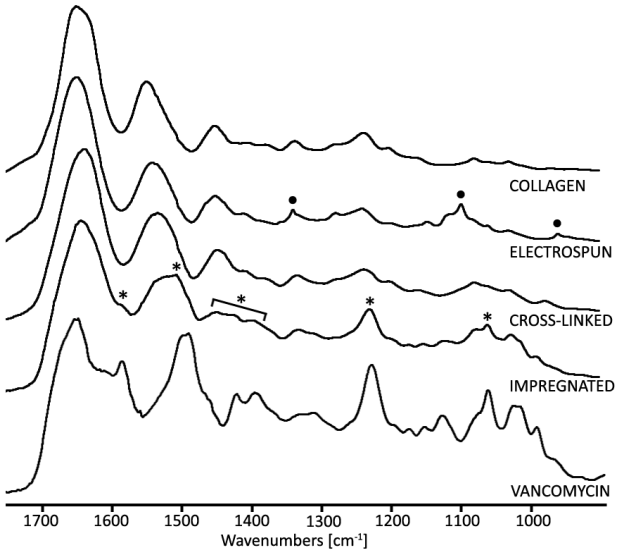

Fig. 61 Illustration of the composition of the collagen electrospun layers in each of the preparation stages from pure collagen, following electrospinning, following cross-linking and following impregnation. * denotes typical vancomycin bands, ● denotes the PEO bands. The FTIR spectra of pure vancomycin was added for comparative purposes.

The results obtained from the mechanical tests are shown in Figure 62. The electrospun collagen with all the HA concentrations exhibited an increase in tensile strength after 6 h of exposure to human blood plasma. From 6 to 360 h of exposure, the ultimate tensile stress stagnated and after 360 h a

slightly decreasing trend in the 0 and 5% of HA was observed, whereas the tensile strength of the 15% HA samples slightly increased. After 720 h, the ultimate tensile strength did not decrease to values less than the initial value in any of the cases. The elastic modulus of all the samples increased during 720 h of blood plasma exposure analogically compared to the samples in the dry state (0 h). The results of the mechanical tests revealed that the EI0, EI5 and EI15 layers remained stable following leaching in plasma.

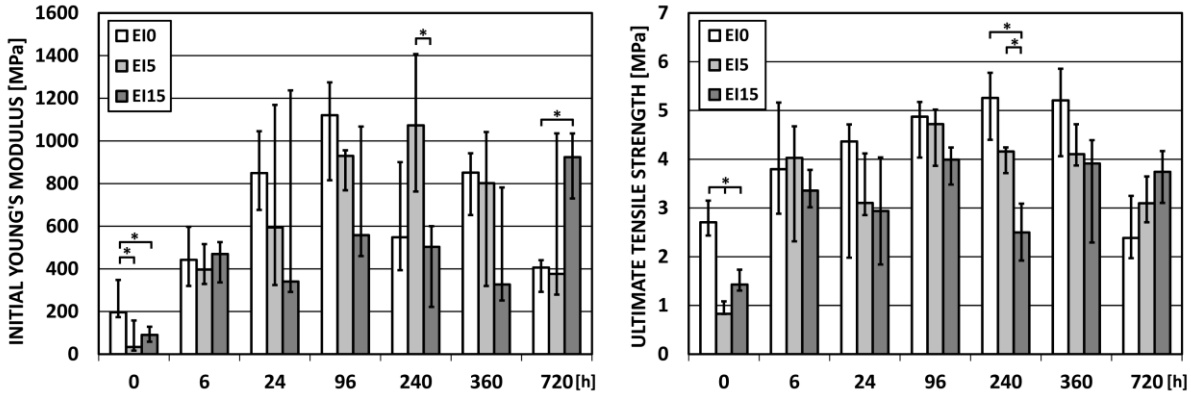

Fig. 62 Mechanical stability of the electrospun impregnated collagen layers without (EI0) and with 5 (EI5) and 15 (EI15) wt% of hydroxyapatite - initial Young's modulus and ultimate tensile strength during 720 hours of exposure in human blood plasma. * denotes statistically significant differences (media, IQR, Mann-Whitney, *0.05*, *n=6*).

With regard to the explanation for the increasing trend in the evaluated mechanical properties, other stability investigation methods were applied. The *in vitro* degradation behaviour of the collagen/HA samples in the blood plasma was also evaluated by means of calculating the mass loss and swelling ratio according to Eq. (6) and (7) (*Appendix B.3*). Moreover, the degradation tests under physiological conditions (PBS, 37°C) were used as an alternative approach by which to assess the stability of the collagenous layers; ultraviolet-visible spectrophotometry was employed for the quantification of the free amino groups released during the degradation of the samples (for details please see *Appendix B.6* and *B.9*).

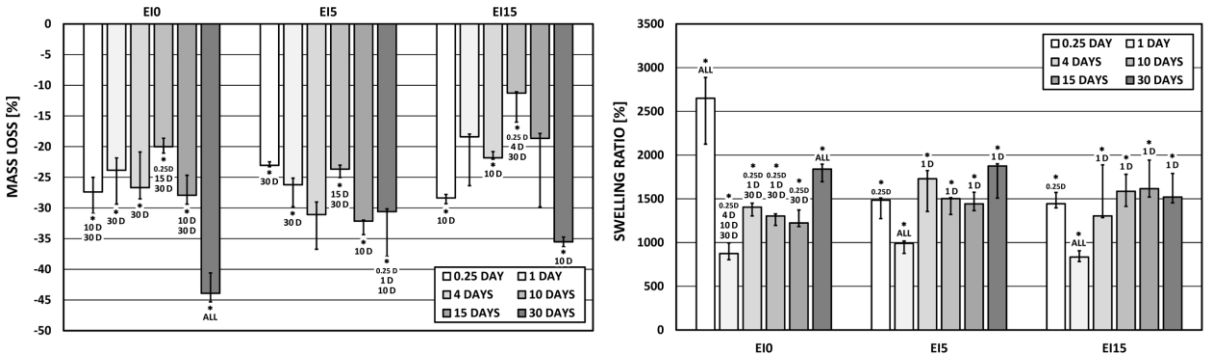

Fig. 63 Evaluation of the structural stability (mass loss, swelling ratio) of the electrospun impregnated collagen layers without (EI0) and with 5 (EI5) and 15 (EI15) wt% of hydroxyapatite in human blood plasma. * denotes statistically significant differences (median, IQR, Mann-Whitney, *0.05*, *n=6*).

The negative values of mass loss (Fig. 63) indicated a weight increase, which can be explained by the adsorption of the various components (proteins, saccharides and vitamins) of the blood plasma immediately following exposure (Fig. 64). This phenomenon was also apparent with respect to the swelling behaviour. No obvious dependence was detected of the increment size on the type of sample or time period. It can be concluded from the results of the study of behaviour in physiological environments and from a comparison with samples studied by Suchý et al. [37] that all the electrospun impregnated layers (EI0, EI5, and EI15) achieved the appropriate degree of cross-linking so as to create stable layers.

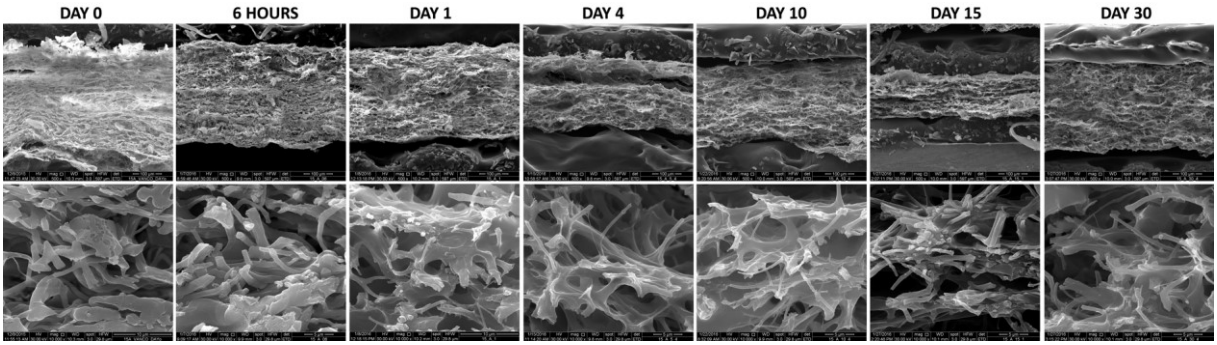

Fig. 64 Representative SEM images of the electrospun collagen layers with 15 wt% HA impregnated by vancomycin during exposure to blood plasma for 30 days (first line mag. 500x, second line 10,000x).

In addition, the collagen as such was found to remain stable within the electrospun impregnated samples during the whole immersion period (up to 100 days) as documented by the very low (approximately 0.014 mM) free amino acid concentration at the end of the experiment (Fig. 65).

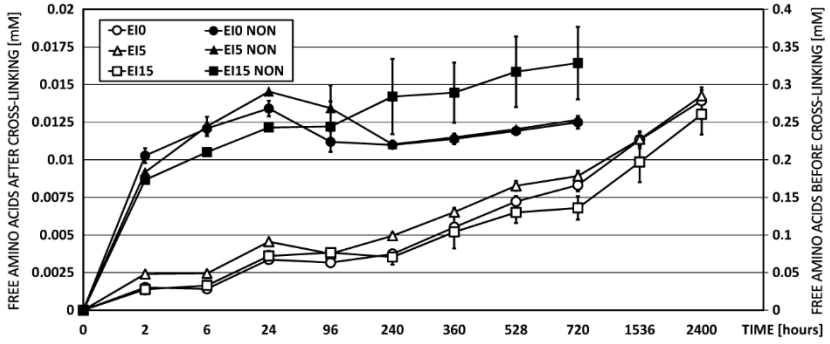

Fig. 65 The concentration of amino acids released from the electrospun impregnated collagen layers without (EI0) and with 5 (EI5) and 15 (EI15) wt% of hydroxyapatite and identical samples prior to cross-linking (NON); note that the opposite axis has a different scale (*n=3*).

The evaluations of structural and mechanical stability conducted in blood plasma for up to 30 days and in a simulated body environment for up to 100 days revealed that electrospun collagen modified by hydroxyapatite nanoparticles retains structural consistency, as proved by the very low free amino acid concentration at the end of the experiment (approximately 0.014 mM). Structural stability makes up a necessary precondition for providing a solid scaffold for cell migration and, hence, for the formation of new bone.

III.2.2 Adhesion between the electrospun collagen and titanium substrates

The aim of the intended usage consists of the direct application of collagen layers via electrospinning directly onto the surfaces of metal alloys. Since the performance of such surface layers is affected by the degree of adhesion between the coating and the substrate, it was necessary to assess the deposition process. For the purposes of the adhesion tests, titanium was selected as the model substrate based on the portfolio of implants produced by the company ProSpon which was involved in the project. The adhesion between the electrospun collagen layers and the titanium surfaces was determined by means of the adaptation of the shaft-loaded blister test [171] (Fig. 66). The adhesion was quantified based on calculating the maximum bond stress required for layer separation.

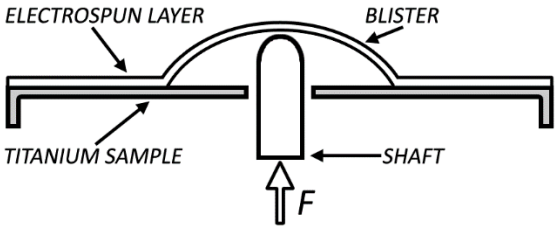

Fig. 66 Scheme of the shaft-loaded blister test, modified from B.M. Malyshev et al. 1965 [170].

Two kinds of surfaces currently applied to improve the osseointegration of orthopaedic implants were used as substrates for the deposition of collagen electrospun layers (Fig. 67), namely titanium plasma sprayed (*S*) and titanium 3D printed (*P*) commercial trabecular surfaces (ProSpon, Ltd., Czech Republic). Prior to electrospinning, the surfaces of the samples were chemically treated in order to evaluate the effect of four different methods on adhesion improvement.

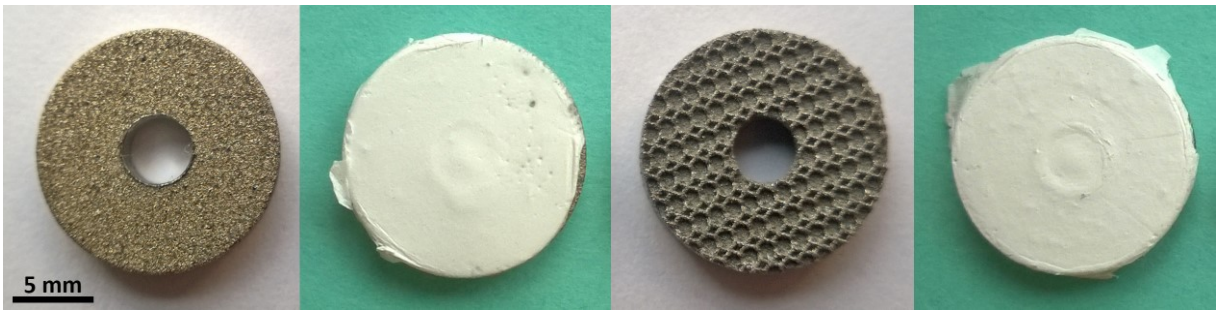

Fig. 67 Representative images of the plasma treated (left) and printed titanium (right) samples before and after the application of a collagen layer.

The first group of samples (*Ac*) was degreased by means of acetone in an ultrasound bath (UB) for 10min. The second group was (*Ac-PBS*) degreased (acetone, 10 min, UB), immediately followed by immersion in PBS (10 min), rinsed with deionized H_2O, dried in a hood. The samples from the third group (*Ac-HF-COL*) were degreased (acetone, 10 min, UB), etched for 2min in a solution of 5 g Na_3PO_4, 0.9 g NaF, 1.6 g (50wt% HF) supplemented with water up to 100 g, rinsed with H_2O (5 min) followed by fast drying (70°C) and immediately impregnated with a diluted collagen/water solution (1/10, w/w) containing EDC/NHS (4/1, w/w). Following cross-linking *in situ*, the samples were washed in 0.1 M Na_2HPO_4 (2 × 15 min), followed by rinsing using deionised water (5 min) and dried in a hood. Finally, the samples from the fourth group (*Ac-COL*) were degreased (acetone, 10 min, UB), dried, impregnated

with a diluted collagen/water solution (1/10, w/w) containing EDC/NHS (4/1, w/w) and washed following cross-linking as described above (*Ac-HF-COL*). Untreated samples served as the controls (*0*). Following these procedures, all the samples (each group *n=10*) were immediately coated with collagen by means of the electrospinning (1 hour) of the collagen solution, as described above.

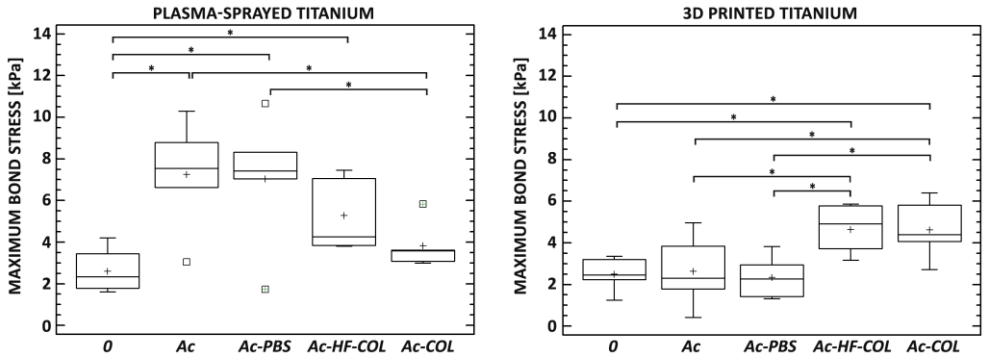

Fig. 68 Box-plots of the maximum bond stress required for the separation of the electrospun collagen layers from differently-prepared titanium surfaces. * denotes statistically significant differences (Fisher's LSD, *0.05*, *n=10*).

In terms of bond stress, no differences were determined between the chemically untreated plasma-sprayed and 3D printed surfaces (Fig. 68). The various chemical treatments exerted different effects on adhesion improvement. Very simple methods such as degreasing and degreasing/PBS immersion are able to significantly improve adhesion between collagen electrospun layers and plasma-sprayed substrates. The expected effect of etching was demonstrated in the case of both types of substrates. In the case of the 3D printed samples, only those treatments involving impregnation exerted a favourable effect on adhesion improvement, while impregnation had no effect in the case of the plasma-sprayed substrates. These results suggest that the degree of adhesion between collagen electrospun layers and titanium plasma-sprayed surfaces as well as titanium 3D printed surfaces can be improved via the chemical treatment of titanium surfaces.

Moreover, the adhesion of collagen layers was further analysed via the study of abrasion resistance. The ability of electrospun collagen to resist being worn away from the implant surface by friction during implantation was verified by means of an artificial bone model (polyurethane bars, 1522-05, Sawbones, USA). Ti6Al4V titanium alloy model samples (diameter of 5 mm, height of 8 mm) covered with electrospun collagen layers (thickness of 100 μm) were pushed through a drilled hole with a defined diameter thus simulating the application of a press-fit implant. The experiment was carried out on an unidirectional testing machine (MTS Mini Bionix, USA). The degree of adhesion was qualitatively evaluated via scanning electron microscopy accompanied by energy dispersive spectroscopy (EDS) (Quanta 450, FEI, USA; Apollo X, EDAX, USA). SEM images and EDS analysis (Figure 69) illustrated the ability of the collagen layers directly electrospun on titanium alloy surfaces to resist the friction that occurs during implantation. Unlike the partial damage suffered by the deposited collagen layers, the surface of the titanium samples were, with respect to the majority of the tested samples, covered with intact electrospun layers. The process of the direct deposition of collagen layers via electrospinning was further optimized aimed at the assessment of the homogeneous layers. Direct deposition on implants is documented in Figures 70 and 71.

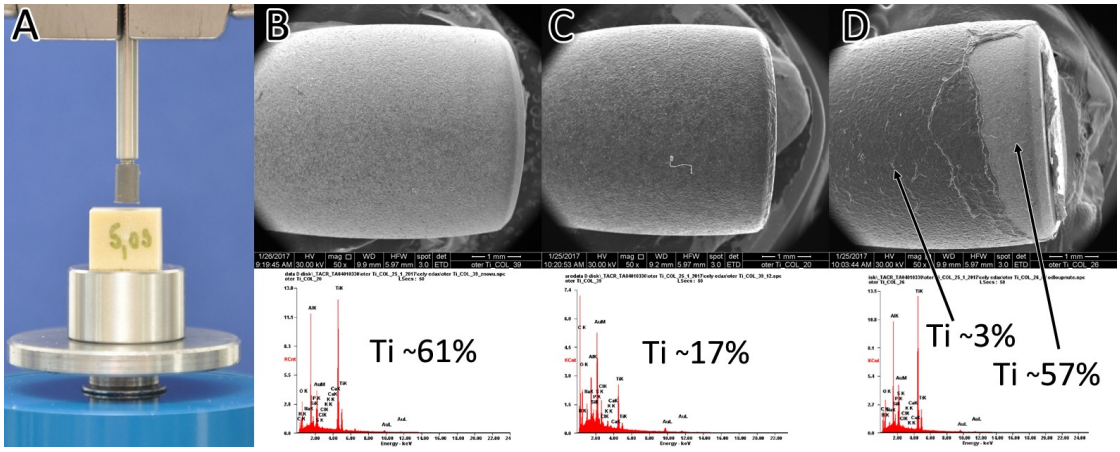

Fig. 69 The ability of collagen layers directly electrospun on titanium alloy surfaces to resist being worn away from the implant surface by friction that occurs during implantation was analysed by means of an abrasion experiment (A). The EDS analysis shows the approximate presence (wt%) of titanium on the surfaces before (B) and after (C) collagen deposition and after being pushed through the artificial bone (D).

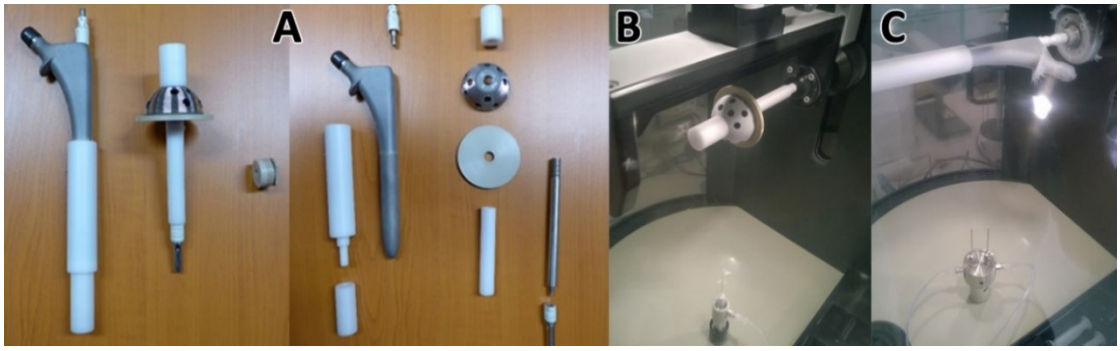

Fig. 70 Auxiliary jigs (A) for the direct deposition of collagen layers via electrospinning (4Spin, Contipro) on the surface of the acetabular (B) and femoral (C) components of a total hip replacement.

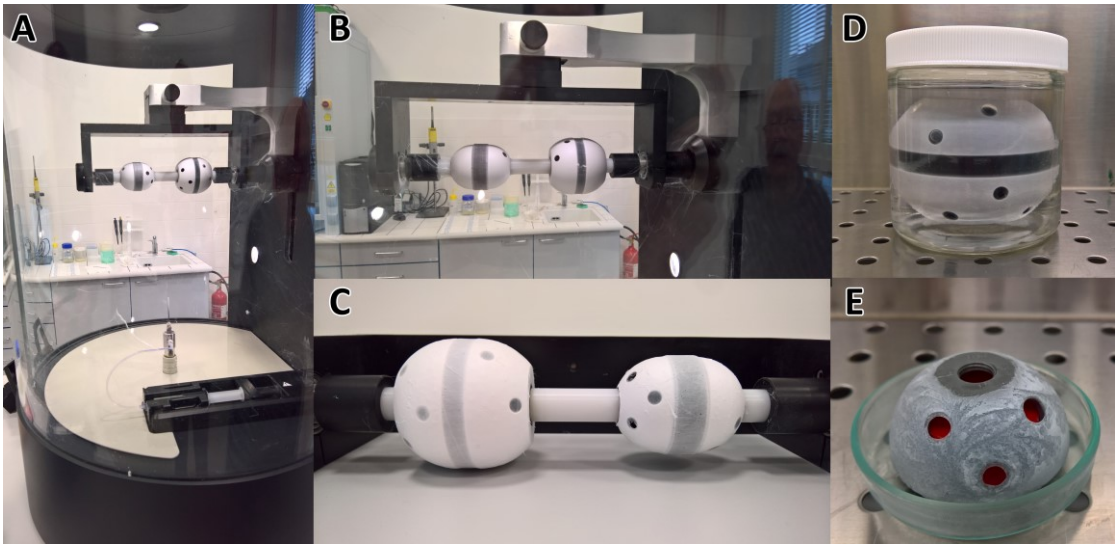

Fig. 71 Direct deposition of collagen layers via electrospinning (4Spin, Contipro) on the surface of the acetabular component of a total hip replacement (A-C) and the subsequent cross-linking of the deposited layer (D, E).

III.3 Evaluation of antimicrobial activity

III.3.1 Comparison of different deposition methods, microstructure vs. nanostructure

In the first stage of the evaluation of antimicrobial activity, collagen layers with various levels of porosity and structure were prepared aimed at the comparison of the micro- and nanostructures as well as the determination of efficient procedure for antibiotics loading. In this stage, vancomycin was selected as the model antibiotic agent. Collagen layers were prepared using three different methods. The microstructured were prepared by means of the lyophilisation of collagen dispersions with 0, 5 and 15 wt% of hydroxyapatite and 10 wt% of vancomycin. The nanostructured layers were prepared by electrospinning of the same dispersions containing 0, 5 and 15 wt% of hydroxyapatite and 10 wt% of vancomycin. After preparation, both kinds of layers were cross-linked by EDC/NHS. Finally, the last group of layers was prepared by means of the electrospinning of collagen dispersions with 0, 5 and 15 wt% of hydroxyapatite followed by EDC/NHS cross-linking and followed by impregnation with 10 wt% of vancomycin. Representative SEM images are given in Figure 72.

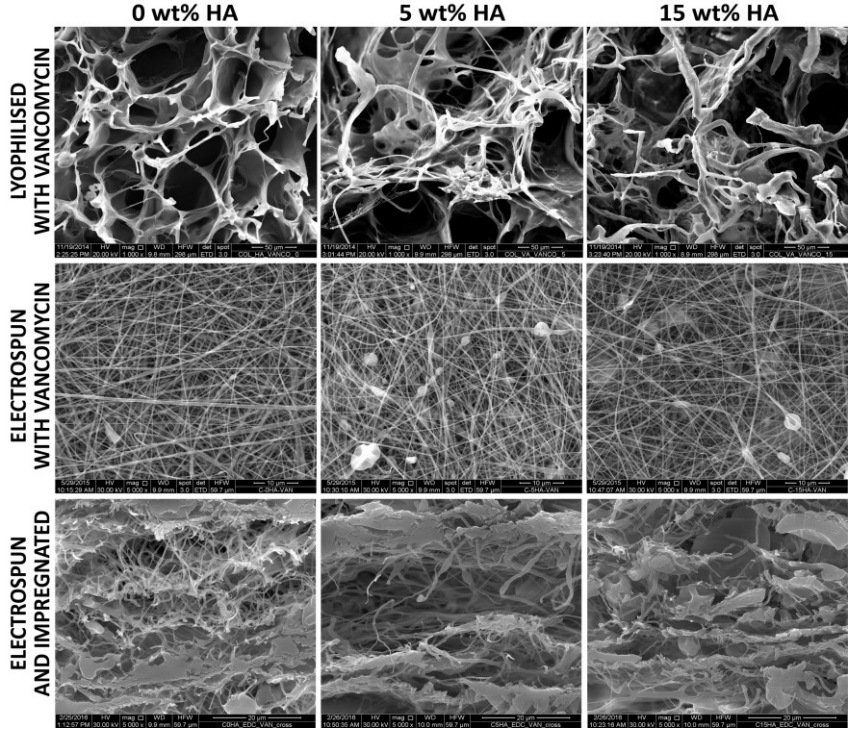

Fig. 72 Representative SEM images of cross-section of evaluated collagen/hydroxyapatite/vancomycin layers prepared by three different methods (first line mag. 1,000x, other images mag. 5,000x).

Firstly, an investigation was conducted of the *in vitro* release of vancomycin in PBS (pH 7.4, 37 °C). The solid phase extraction method and high performance liquid chromatography (HPLC) analysis were employed in order to characterise the *in vitro* release rates of the vancomycin and its crystalline degradation antibiotically inactive products over a 21-day period. Details of the HPLC analysis are described in *Appendix B.11*). Moreover, A methiciline-resistant *Staphylococcus aureus* (MRSA) isolate was used for the evaluation of antimicrobial activity. Model isolates were retrieved by means of the examination of hospital (General University Hospital, Prague, Czech Republic) patient specimens. The disc diffusion test was performed as described in *Appendix B.12*).

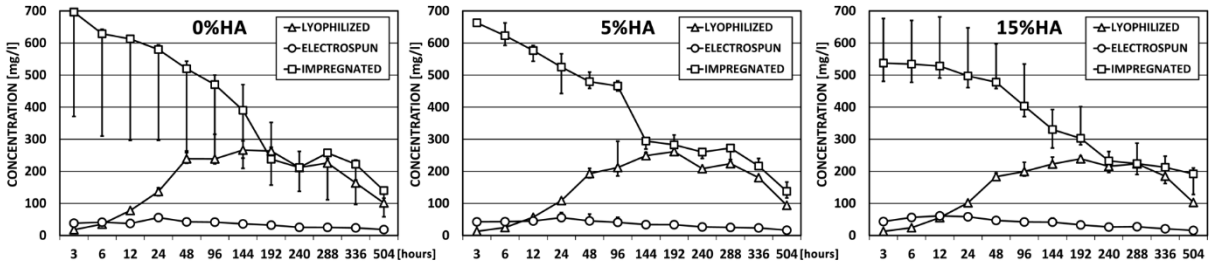

Fig. 73 The concentration of the released active form of vancomycin (median, IQR, *n=6*) with respect to samples with 0, 5 and 15 wt% of HA prepared using different methods.

All initial concentrations (3 hours) of active form of vancomycin were above minimum inhibitory concentration (MIC) for vancomycin resistant *Staphylococcus aureus* (VRSA), which is 16 mg/L (Fig. 73). The highest average concentration of vancomycin was achieved with respect to the lyophilised samples after 8 days (approximately 250 mg/L), the electrospun samples after 24 h (approximately 60 mg/L) and the electrospun impregnated samples after just 3 h (approximately 700 mg/L). Despite the considerable tendency of vancomycin degradation towards crystalline thermal degradation products, levels of the released active form of vancomycin remained above the MIC for VRSA >3 weeks, with the exception of the E15 samples (15.85 mg/l, 21st day). The maximum concentration of the released active form of vancomycin exceeded the MIC by up to 17 times (lyophilised samples), 4 times (electrospun samples) and up to 44 times (electrospun impregnated samples). By the end of the experiment, the MIC had been exceeded by up to 6 times (lyophilised), up to 12 times (electrospun impregnated) and was approximately equal in the case of the electrospun samples. The addition of hydroxyapatite exerted only a minor effect on vancomycin release.

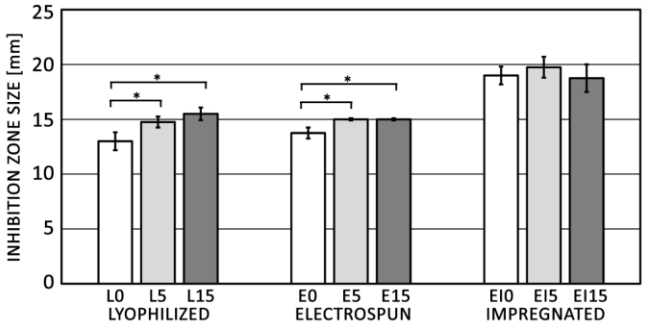

Fig. 74 Inhibition zone sizes of vancomycin loaded lyophilised, electrospun and electrospun impregnated samples with different amounts of hydroxyapatite in contact with MRSA isolates. * denotes statistically significant differences (mean, SD, Mann-Whitney, *0.05*, *n=7*).

The results of the evaluation of antimicrobial susceptibility (Fig. 74) are in agreement with the results of vancomycin release chromatography analysis (Fig. 73). The highest rates of antimicrobial activity were determined with respect to the electrospun impregnated samples (EI0, EI5, and EI15). Similar to previous results, no statistically significant differences were detected between the electrospun impregnated samples containing different amounts of hydroxyapatite.

Three preparation methods were investigated, two of which involved the direct addition of vancomycin to a collagen or collagen/hydroxyapatite dispersion from which micro-structured layers

were obtained by means of lyophilisation and nanostructured layers were obtained via electrospinning. The electrospinning method, which provides a high surface-to-volume ratio to the internal structure of the resulting material, was also utilised for the production of layers without the presence of vancomycin in the source dispersion, but with the addition of the antibiotic to the electrospun material via impregnation. This experiment demonstrated that the third method provides layers with the highest concentrations of released antibiotics over the longest time period. The addition of hydroxyapatite exerted only a minor effect on vancomycin release. The results of the evaluation of antimicrobial susceptibility were in agreement with the results of vancomycin release chromatography analysis. The highest rates of antimicrobial activity were determined with respect to the electrospun impregnated samples. This suggests that collagen/hydroxyapatite layers prepared by means of electrospinning with subsequent impregnation with vancomycin can be considered as the most suitable candidate for above all three methods studied here.

III.3.2 Comparison of different antibiotics

In the second stage of the evaluation of antimicrobial activity the collagen/hydroxyapatite electrospun layers were impregnated by vancomycin, gentamicin and their combination (Fig. 75). Collagen/hydroxyapatite layers containing different amounts of HA (0, 5 and 15 wt%) were tested for the *in vitro* release kinetics of antibiotics, antimicrobial activity against MRSA, gentamicin-resistant *Staphylococcus epidermidis* and *Enterococcus faecalis isolates*. In addition, the efficiency of gentamicin and its combination with vancomycin aimed at determining the potential synergistic effect of this combination compared with that of vancomycin alone was evaluated.

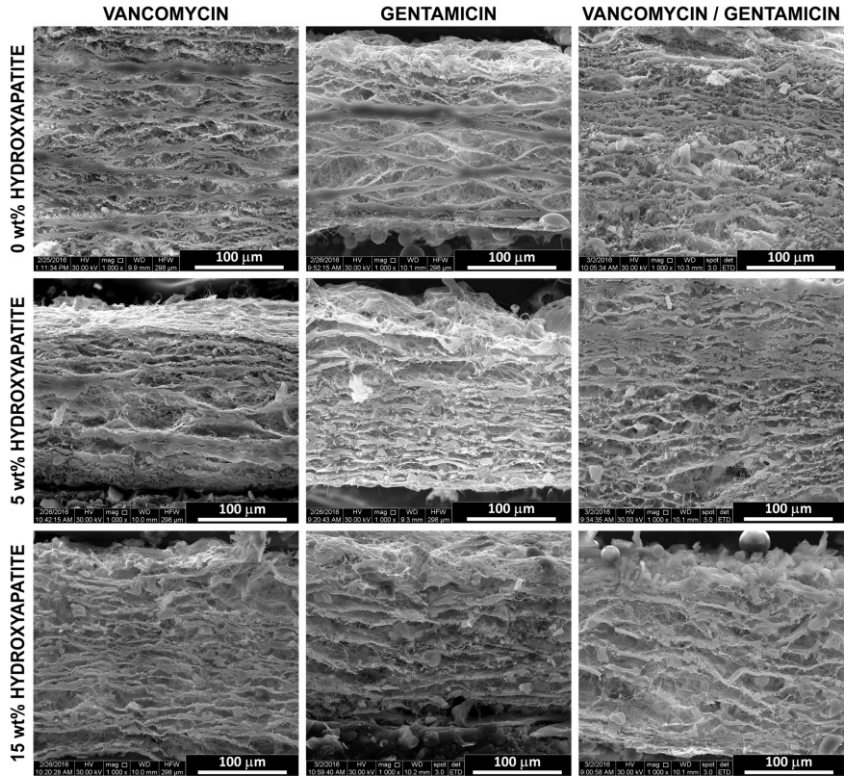

Fig. 75 Illustrative SEM images of cross-sections of the collagen/hydroxyapatite layers with differing amounts of hydroxyapatite impregnated with vancomycin, gentamicin or vancomycin/gentamicin (mag. 1,000x, bar 100 µm).

The *in vitro* release kinetics of the antibiotic components in PBS (37 °C) is assessed by means of the HPLC method (vancomycin) and ultra-high performance liquid chromatography with tandem mass spectrometry (gentamicin; for details please see *Appendix B.13*). The antimicrobial effects of the layers containing the various antibiotics are studied employing the agar diffusion testing technique against four different clinical bacterial isolates (for details please see *Appendix B.14*), an examination is conducted of the role of hydroxyapatite nanoparticles in antibiotic release.

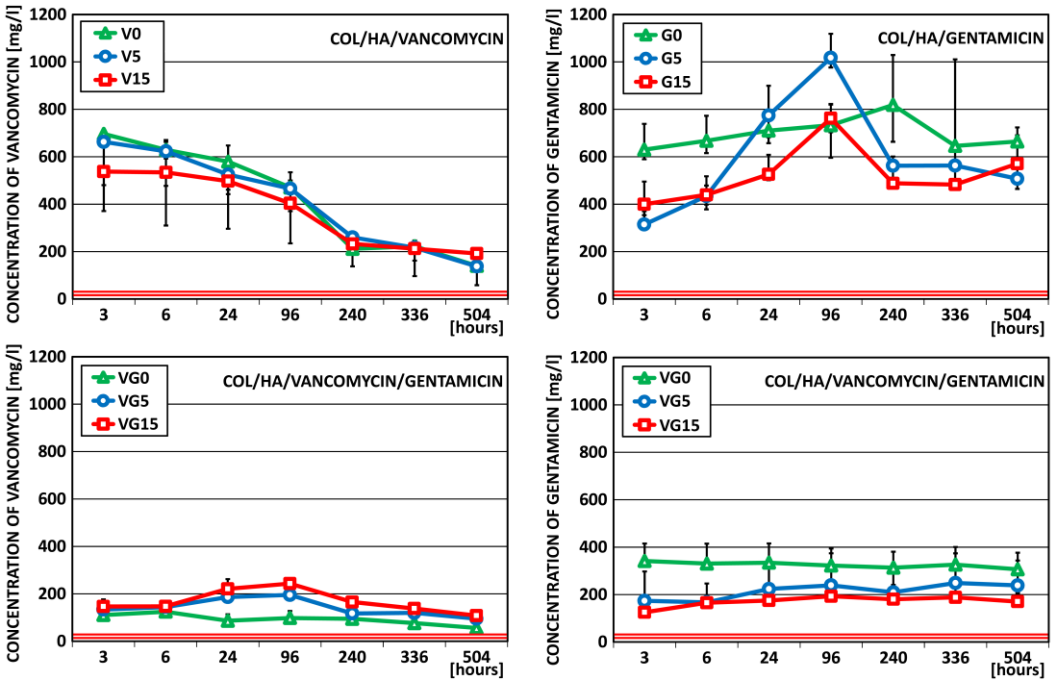

Fig. 76 Concentration of the released active forms of vancomycin and gentamicin (median, IQR, *n=6*) from the collagen/hydroxyapatite layers with differing amounts of hydroxyapatite and impregnated with vancomycin, gentamicin or vancomycin/gentamicin. V=vancomycin, G=gentamicin, VG=1/2 vancomycin+1/2 gentamicin; 0, 5, 15 = wt% of the HA in the COL/HA layers. The solid red lines denote the MIC for VRSA (16 mg/L) and *Enterococcus* spp. (32 mg/L).

The release kinetics profiles of vancomycin and gentamicin from the layers prepared in different ways are provided in Figure 76. The highest concentration of vancomycin was recorded with respect to vancomycin samples immediately after 3 h (0 wt% HA; approx. 700 mg/L) and the samples with vancomycin/gentamicin after 96 h (15 wt% HA; approx. 240 mg/L). The highest concentration of gentamicin was recorded with respect to the gentamicin samples after 96 h (5 wt%; approx. 1020 mg/L) and the vancomycin/gentamicin samples after 3 h (0 wt% HA; approx. 340 mg/L). The addition of hydroxyapatite exerted only a minor effect on vancomycin release in the case of both the vancomycin and vancomycin/gentamicin layers. Conversely, the release of gentamicin was significantly higher in the case of the layers containing no hydroxyapatite (samples with gentamicin and samples with combination of vancomycin/gentamicin), while the addition of HA decreased the rate of gentamicin elution from the 5 and 15 wt% layers within the first 6 h (gentamicin samples) and during the whole 21-day period (vancomycin/gentamicin samples). Levels of the released active form of vancomycin remained above the MIC for VRSA (16 mg/L) and *Enterococcus* spp. (32 mg/L) throughout the full 21

days of experimentation [51]. Similarly, levels of released gentamicin remained above the MIC for VRSA (16 mg/L) and *Enterococcus faecalis* (16 mg/L) [43].

The antimicrobial activity of all the collagen/hydroxyapatite samples against the four bacterial strains (Table 4.) assessed by means of the presence or absence of inhibition zones is provided in Figure 77. The layers prepared without antibiotics and used as negative controls did not present any inhibition to the growth of the bacteria (data not shown). The sizes of the inhibition zones surrounding the samples investigated were comparable or higher than those of standard antibiotic discs with vancomycin (CV) or gentamicin (CG), with the exception of the inhibition zone surrounding the samples with 5 wt% HA and gentamicin in the case of *E. faecalis* 2, with respect to which the inhibition zone diameter was slightly (but significantly) smaller. While no statistically significant differences between the CV and collagen/hydroxyapatite vancomycin layers were determined with respect to *S. aureus* and *S. epidermidis*, significantly higher inhibition zones were discovered in the case of both the enterococci. The complementary effect of the antibacterial activity was found to be present; this was visible particularly in the case of the gentamicin-resistant isolates, with respect to which vancomycin constituted the effective antimicrobial agent.

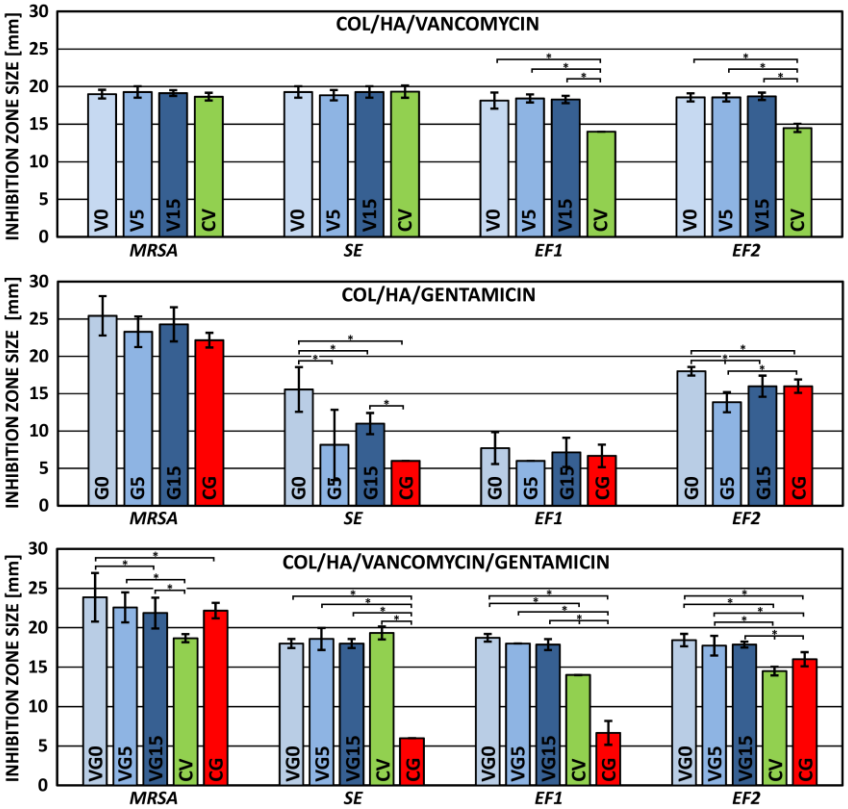

Fig. 77 Inhibition zone diameters (mean, SD) of the vancomycin, gentamicin and vancomycin/gentamicin loaded collagen layers with differing amounts of hydroxyapatite (0, 5, and 15 wt%) tested on clinically relevant bacterial isolates of methicillin-resistant *S. aureus* (MRSA), gentamicin-resistant *S. epidermidis* (SE) and two *E. faecalis* (EF1, EF2). * denotes statistically significant differences (Games-Howell, *0.05*, *n=7*). V=vancomycin, G=gentamicin, VG=1/2 vancomycin+1/2 gentamicin; 0, 5, 15 = wt% of the HA in the collagen layers. CV = control disc with vancomycin, CG = control disc with gentamicin.

Table 4. Susceptibility of the microorganisms used in this study. Susceptibility to vancomycin and gentamicin was estimated using standard antibiotic discs and the diffusion test.

microbial species	strain ID	vancomycin susceptibility	gentamicin susceptibility
S. aureus	MRSA	susceptible	susceptible
S. epidermidis	SE	susceptible	resistant
S. faecalis 1	EF1	susceptible	resistant
S. faecalis 2	EF2	susceptible	susceptible

The experimental results revealed that collagen/hydroxyapatite layers released high concentrations of vancomycin and gentamicin well above MIC for 21 days. The most rapid and highest rates of antibiotic release were determined for the layers containing vancomycin, in which case a burst release was followed by a gradual decrease in vancomycin concentration. Gentamicin, used as a single agent, was released at high concentration levels throughout the full 21 days of testing without the occurrence of a burst release. The presence of HA in the collagen layers was found not to affect the release kinetics of the vancomycin from the layers loaded only with vancomycin or its combination with gentamicin. Conversely, the presence of HA slowed down the release of gentamicin from the collagen/hydroxyapatite layers loaded with gentamicin and its combination with vancomycin. Generally, the modification of collagen by means of HA nanoparticles analogically to native bone tissue may have a positive effect on bioactivity, i.e. an increase in the rate of osseointegration. Such a modification altered the release of gentamicin without decreasing the antimicrobial activity. The combination of both antibiotics exerted a positive effect on the prolongation of the conversion of vancomycin to its major degradation product (data not shown). The antimicrobial effects of the layers with different antibiotics were compared via the application of the agar diffusion testing technique against four different clinical isolates. All the collagen/hydroxyapatite layers irrespective of the antibiotics employed exhibited potential antibacterial activity with respect to both the *Staphylococci* isolates and the gentamicin-resistant isolates. Complementarity was determined between vancomycin and gentamicin against gentamicin-resistant *Staphylococcus epidermidis* and both the *Enterococcus faecalis* isolates. This combination was also found to be more effective against methicillin-resistant *Staphylococcus aureus* than vancomycin as a single agent, despite the application of only half the concentrations of the two antibiotics. Since no major antagonistic effects between vancomycin and gentamicin were determined, it is assumed that the complementary or possibly synergistic effects of the antibiotics applied will broaden the antimicrobial spectrum of the proposed material against various multiple resistant strains in a similar way to that described previously [171,172]. From this point of view, the combination of vancomycin with gentamicin, moreover at only half concentration, appears to be more effective than monotherapy with vancomycin or gentamicin.

In summary, this experiment demonstrated the benefits and limitations of the single application and combination of vancomycin and gentamicin in collagen electrospun layers with differing amounts of hydroxyapatite. The application of vancomycin and its combination with gentamicin, unlike gentamicin as a single agent, were found to provide suitable candidates for the preparation of a powerful carrier for antibiotics.

III.4 Biological evaluation

Biological evaluation is an important part of the development of any medical implantable device. In the final stage of the development of a collagen coating for orthopaedic implants, a comprehensive biological evaluation was conducted. The evaluation of local carrier of antibiotics with osteoinductive properties represents two main aspects. In the first aspect, the effective concentration of antibiotics should not have cytotoxic effects. The second aspect represents the improvement in osseointegration with simultaneous preservation of antibacterial effect. Three different approaches were applied in order to address the cytotoxicity, infection prevention and osseointegration. Biological evaluation performed under *in vitro* and *in vivo* conditions is briefly described in next three chapters.

III.4.1 In vitro evaluation of cytotoxicity

Three different approaches were applied in order to address the cytotoxicity of the collagen/hydroxyapatite layers. Layer extracts as well as the layers themselves were tested for the metabolic activity of SAOS-2 bone-like cells and the morphology of the SAOS-2 cultured on the collagen/hydroxyapatite layers was analysed. In addition to the effect of antibiotics, the influence of the differing hydroxyapatite content in the layers (0, 5 or 15 wt%) on SAOS-2 metabolic activity and morphology was also evaluated. The experimental methods are in detail described in *Appendix B.15*.

As shown in Figure 78, the metabolic activity of SAOS-2 cultured in 1-day extracts of the layers containing antibiotics was comparable to the metabolic activity of SAOS-2 cultivated on the same layers with no antibiotics. Similarly, the metabolic activity of SAOS-2 cultured in 1-day layer extracts of all the tested layers was found to be comparable to the metabolic activity of SAOS-2 cultivated on the standard polystyrene surfaces (PS). A general cytocompatibility of the layer extracts was observed; this was further confirmed in this study by means of the investigation of the metabolic activity of SAOS-2 cultured directly on the surfaces of the layers.

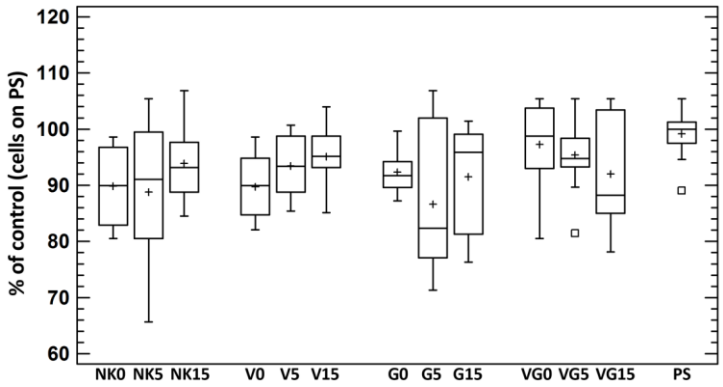

Fig. 78 Metabolic activity of SAOS-2 cultured for 24 h in 1-day collagen/hydroxyapatite layer extracts expressed as a percentage of the metabolic activity of SAOS-2 cultured on polystyrene surfaces in culture media (PS). No statistically significant differences between the antibiotic groups (V, G, VG) and the control group (NK) were observed nor were any statistically significant differences determined between any of the COL/HA layer groups and the PS group (Kruskal-Wallis, Bonferroni procedure, *0.05*, *n=4*). V = vancomycin, G = gentamicin, VG = 1/2 vancomycin+1/2 gentamicin; 0, 5, 15 = wt% of the HA in the collagen layers.

A decrease in the metabolic activity of SAOS-2 cultured on the collagen/hydroxyapatite layers with antibiotics compared to the relevant controls NK0, NK5 or NK15 was apparent with respect to almost all the samples, suggesting that at least a certain proportion of the cytotoxicity was induced by the antibiotics (Fig. 79). The results further revealed the effect of the HA in the layers on the metabolic activity of SAOS-2 which, surprisingly, is vancomycin specific. A comparison of SAOS-2 behaviour on days 2 and 8 revealed that all the layers impregnated only with vancomycin statistically significantly stimulated the metabolic activity of SAOS-2, indicating that such layers do not directly lead to cell death and detachment. Further, the significant positive effect of increasing the amount of HA in the layers with vancomycin on the metabolic activity of SAOS-2 was detected after both 2 and 8 days of culturing. This observation was confirmed by means of the fluorescent imaging (Fig. 80).

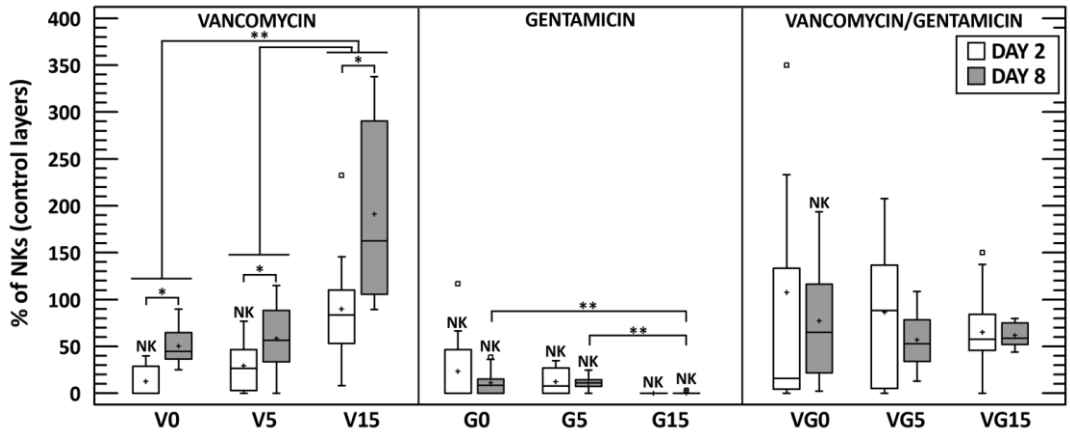

Fig. 79 Metabolic activity of SAOS-2 cultured on COL/HA layers with (V, G, VG) or without (NK) antibiotics for 2 days (white boxes) and 8 days (grey boxes). "NK" denotes statistically significant differences to the corresponding NK0, NK5 and NK15 controls (100% for each group) on the corresponding day (Kruskal-Wallis, Bonferroni procedure, *0.05*). * denotes statistically significant differences between the time points of each of the tested layers (Mann-Whitney, *0.05*, *n=4*). The sign ** denotes statistically significant differences within the groups with the same antibiotics separately on the second and eighth days (Kruskal-Wallis, Bonferroni procedure, *0.05*, *n=4*). V = vancomycin, G = gentamicin, VG = 1/2vancomycin+1/2gentamicin; 0, 5, 15 = wt% of hydroxyapatite.

Completely different results were obtained concerning the layers with gentamicin, with respect to which the metabolic activity of SAOS-2 decreased with increasing amounts of HA, especially after 8 days of culturing. Further, all the collagen/hydroxyapatite layers with gentamicin were found to be significantly cytotoxic when the metabolic activity of SAOS-2 was around 10–20% of the SAOS-2 cultured on the corresponding controls (NKs) (Fig. 79). This observation was proved by fluorescent microscopy (Fig. 80), i.e. the cells had not attached properly after 2 days of culture and had not proliferated after 8 days of culture and, moreover, their morphology exhibited a round-like shape indicating the cytotoxic effect of the gentamicin hindering the SAOS-2 attachment and proliferation processes.

Finally, with respect to the collagen/hydroxyapatite layers with combination of vancomycin and gentamicin, no significant effect of HA on the cytotoxicity of the antibiotics was determined. While the antibiotics mixture exerted a moderate cytotoxic effect on SAOS-2 with a metabolic activity of around

50–80% of that of the corresponding NKs, it was not deemed statistically significant except with concern to the layer without hydroxyapatite on day 8 (Fig. 79). Similar findings were obtained by means of fluorescent microscopy, according to which the cell count did not increase between the 2nd and 8th days of cultivation, and the SAOS-2 exhibited both round-like and cuboidal-like morphologies indicating a non-toxic and non-stimulating cell culture environment (Fig. 80).

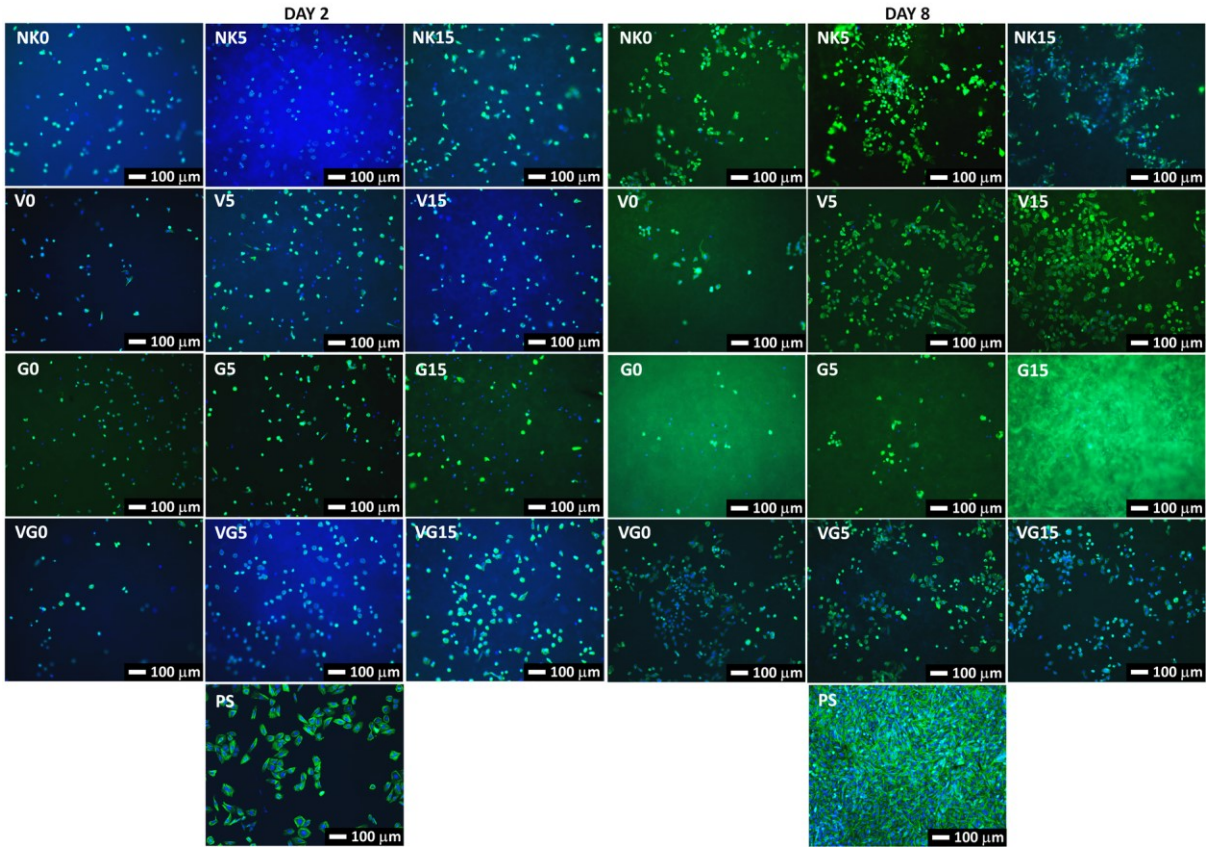

Fig. 80 Fluorescence images of SAOS-2 cultured for 2 and 8 days on collagen/hydroxyapatite layers with (V, G, VG) and without (NK) antibiotics (mag. 10x). The actin filaments representing cell morphology are stained in green and the cell nuclei are stained in blue. V = vancomycin, G = gentamicin, VG = 1/2vancomycin+1/2gentamicin; 0, 5, 15 = wt% of the hydroxyapatite in the collagen layers.

The limits of the positive effect of HA on SAOS-2 behaviour in relation to the type of antibiotic applied were both evident and surprising. It was supposed that this trend was closely connected to the differing release kinetics of vancomycin, gentamicin and their combination. The presence and amount of HA in the collagen layers did not affect the release of antibiotics from the layers (Fig. 76) and, moreover, the antibiotics released from the layers after 1 day of extraction were not found to exhibit cytotoxicity (Fig. 78). However, the release of antibiotics between 2 and 8 days decreased, increased and remained constant for vancomycin, gentamicin and their combination respectively (Fig. 76). This corresponds with the SAOS-2 metabolic activity trends which increased, decreased and remained constant for vancomycin, gentamicin and their combination respectively between 2 and 8 days of culturing. In addition, the detected low cytotoxicity of the layers with combination of vancomycin and gentamicin can be explained by the presence of half the amount of each type of antibiotic in the samples compared to the single antibiotic samples.

In summary, while the cytotoxicity of gentamicin at the applied concentration was determined to constitute an essential limiting factor, it was found that the cytotoxic effect can be reduced considerably via the lowering of the concentration of gentamicin and its combination with vancomycin, thus preserving the antimicrobial effect. In addition, the study revealed that collagen electrospun layers that exhibit sufficient antimicrobial activity are not directly toxic for human cells. With regard to both efficiency and safety, a combination of collagen with 15 wt% of hydroxyapatite and vancomycin or vancomycin plus gentamicin was found to present the most suitable material composition for the prevention of bone infection. For a subsequent *in vivo* biological evaluation, such layers with vancomycin were selected.

III.4.2 Evaluation of in vivo infection prevention

For the determination of the antimicrobial efficacy, 3D printed implants (Fig. 81 A, B) were prepared from standard implantable Concept Laser titanium alloy – CL 41 ELI (Ti6Al4V) with a trabecular structure (for details please see *Appendix A.4*). Titanium implants (an outer diameter of 2 mm, an inner diameter of 1.5 mm and a length of 5.5 mm) were covered by electrospun collagen layer with 15 wt% of hydroxyapatite (COLHA). A part of implants was subsequently impregnated by vancomycin in amount of 10 wt% to weight of electrospun layer (COLHA+V) and exposed to gamma sterilisation (25 kGy, BIOSTER, a.s., Czech Republic). In order to replicate a case of bone infection following primary implantation a clinical isolate of *S. epidermidis* from a rejected implant for the induction of infection in the femur of a rat model was applied. Thirty male Wistar rats aged 5 months (Masaryk University Brno, Czech Republic) were divided into 3 groups, i.e. a group with implanted COLHA+V layers without infection (*n=10*), a group with implanted COLHA layers with the *S. epidermidis* infection (*n=10*), and a group with implanted COLHA+V layers with the *S. epidermidis* infection (*n=10*). One implant was loosely inserted into a slightly larger prepared hole in the medullar cavity of the left femur of each animal. The hole was then sealed with PALACOS® (Heraeus Medical, USA) bone cement. During the operational procedure the COLHA and COLHA+V layers were impregnated with 2 µL of a clinical isolate *S. epidermidis* suspension (1.0 McFarland). The evaluation of *in vivo* infection prevention is in full details described in *Appendix B.16*.

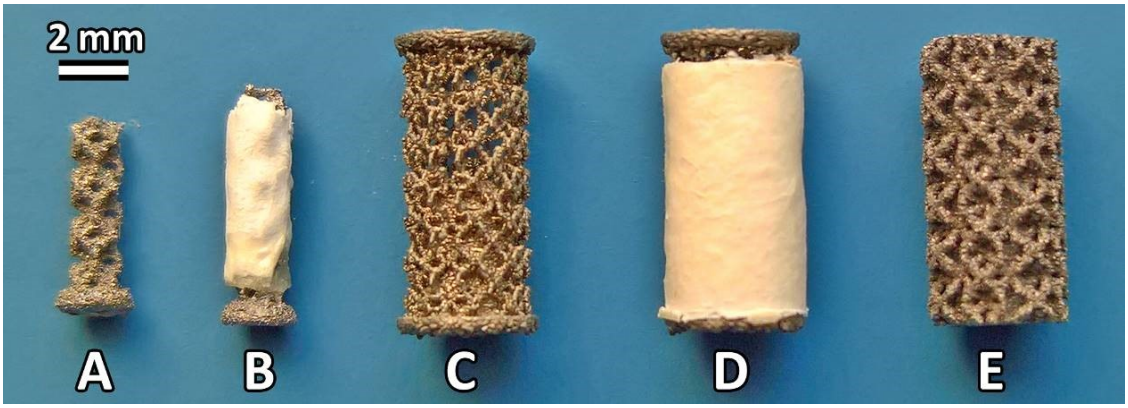

Fig. 81 Representative images of the titanium implants. Ti printed implant before (A) and after (B) the deposition of a COLHA+V layer intended for use in the antimicrobial activity experiment; Ti printed implant before (C) and after (D) the deposition of a COLHA+V layer intended for use in the osseointegration experiment; Ti printed control sample (E).

The morphology of the bone surrounding the implants 6 weeks following implantation is illustrated in Fig. 82. No signs of the infiltration of bacteria via persistent osteomyelitis were detected in any of the tested groups six weeks following the induction of infection and implantation. The consequences of resolved bone inflammation such as the porosity of the cortical bone were most obvious with respect to the COLHA+*S. epidermidis* group (the black arrows in Fig. 82 B), whereas the COLHA+V and COLHA+V+*S. epidermidis* groups exhibited only mild or no cortical bone porosity. The fibrous tissue detected in all the groups indicated resolved bone healing (the red stars in Fig. 82 B). The histological qualitative findings were subsequently quantified via micro-CT and EDS analysis.

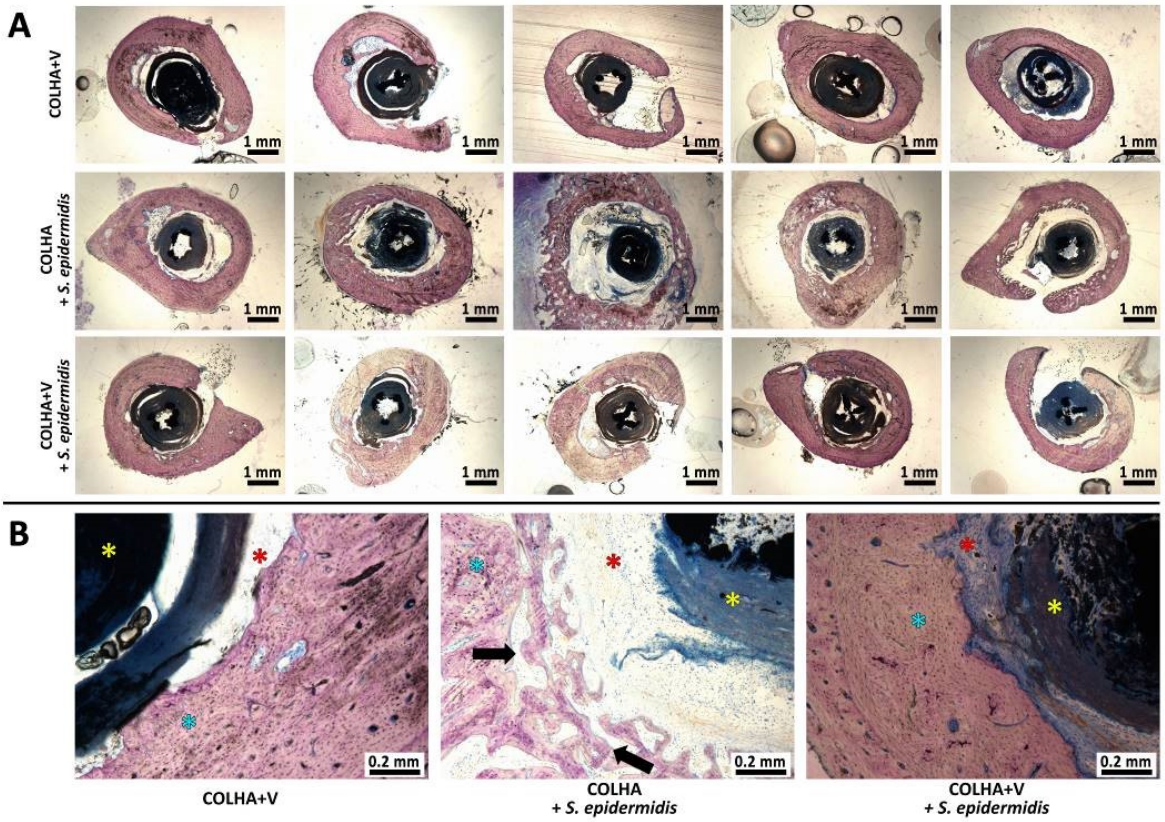

Fig. 82 Representative histological images of perpendicular sections of the femurs with Giemsa's azur eosin methylene blue staining (A) and details of the bone morphology (B) showing the bone tissue (blue stars), fibrous tissue (red stars), implants (yellow stars) and porous areas (black arrows).

The evaluation of antimicrobial activity was based on the hypothesis that inflammation at the site of implantation would lead to the alteration of the bone structure; hence, cortical bone porosity was selected as the corresponding parameter. The micro-CT visualisations (Fig. 83) revealed increases in cortical porosity in the following ascending order: 1) COLHA+V, 2) COLHA+V + *S. epidermidis*, 3) COLHA + *S. epidermidis*. The cortical bone of the specimens was then subjected to a 3D porosity analysis (Fig. 84) that revealed the following mean porosity values: COLHA+V=1.66%, COLHA+V + *S. epidermidis*=2.35% and COLHA + *S. epidermidis*=19.84%. The highest data variability was observed with concern to the COLHA+V + *S. epidermidis* experimental group. It is important to consider the limitations of this approach relating to the limited spatial resolution of micro-CT, i.e. the possible presence of non-detected and thus non-analysed pores. However, no other option is yet available for the non-

destructive whole-specimen 3D analysis of samples of such a size that provides for a considerably higher resolution than the method used in our study.

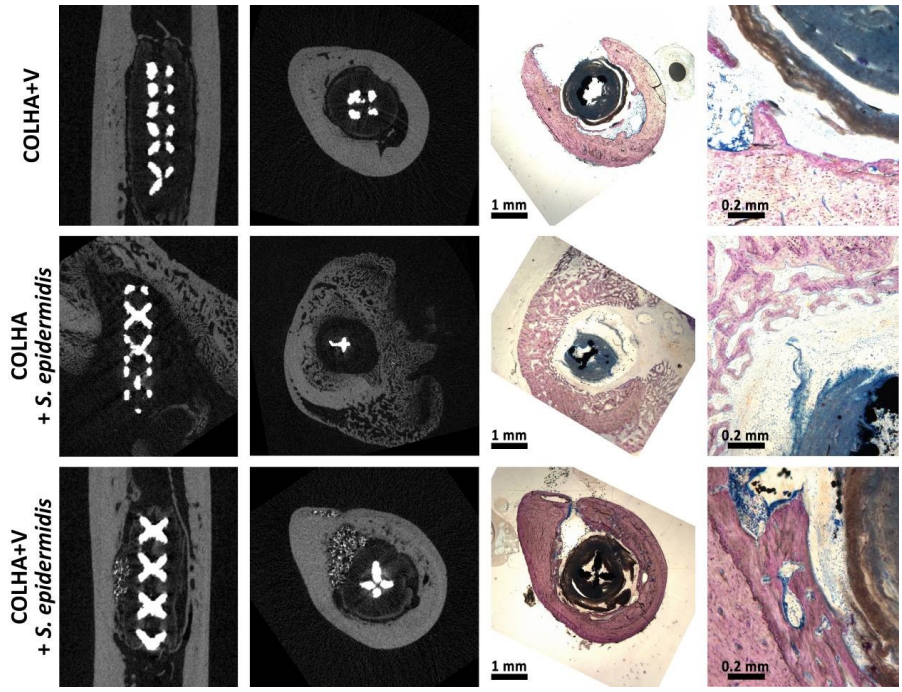

Fig. 83 Representative micro-CT and histological images of identical samples in the COLHA+V implants without the application of *S. epidermidis* (upper line), COLHA implants with *S. epidermidis* (middle line) and COLHA+V with *S. epidermidis* (bottom line) groups.

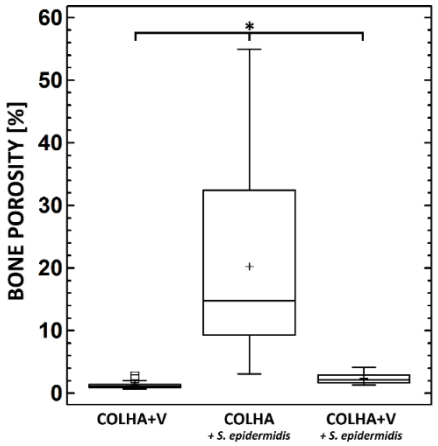

Fig. 84 Bone porosity of the rat femurs for the implants with a COLHA+V layer and for the implants with COLHA and COLHA+V layers with *S. epidermidis*. * denotes statistically significant differences (*0.05*, Kruskal-Wallis with the Bonferroni procedure, *n=5*).

Figure 85 provides a summary of the Ca/P weight ratio in the bone tissue of the explanted rat femurs. The average Ca/P ratio of bone mineral in the bone tissue of the explanted femurs with COLHA+V implants without the *S. epidermidis* was 1.90, i.e. the same as that of the COLHA+V implants with *S. epidermidis* (1.89), corresponding to molar ratios of 1.46 and 1.45 respectively. The determined molar ratios are in agreement with those in bioapatites which are considered to be Ca-deficient if they display

Ca/P molar ratios of less than 1.67, which is typical for stoichiometric HA. However, the Ca/P molar ratios determined in this study were less than those defined by Bigi et al. (1.5 – 1.63) [173] and by Termine et al. (1.63) [174] in rat bioapatites. A statistically significant decrease in the Ca/P weight ratio was determined with respect to the COLHA implants with *S. epidermidis* (see Fig. 85), i.e. in the case of untreated inflammation (1.85) corresponding to a Ca/P molar ratio of 1.42. The impregnation of the COLHA layer with vancomycin increased the Ca/P molar ratio to the level of that determined in the case of the COLHA+V implants without *S. epidermidis*.

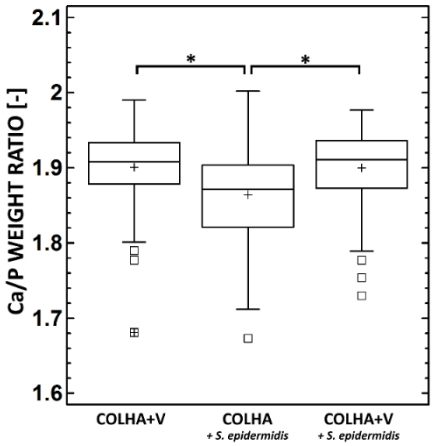

Fig. 85 Ca/P weight ratio in the bone tissue of the explanted rat femurs. * denotes statistically significant differences (*0.05*, Games-Howell, *n=5*).

The concentration of the active form of vancomycin released from the implants into the blood was determined 7 and 14 days following implantation. At day 7, the plasma of the animals without the *S. epidermidis* infection contained 1.42±0.87 mg/L and with the *S. epidermidis* infection 0.07±0.10 mg/L of vancomycin. At day 14, the plasma of the animals without the *S. epidermidis* infection contained 0.29±0.25 mg/L of vancomycin, while no concentration of vancomycin was detected in the plasma of the animals with the *S. epidermidis* infection (Fig. 86).

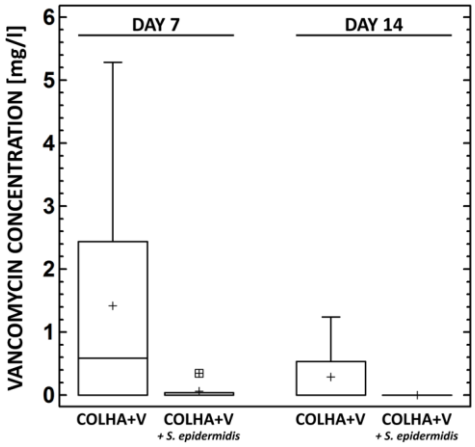

Fig. 86 Concentration of vancomycin in the rat blood plasma 7 and 14 days following implantation. Blood samples were taken from the animals with COLHA+V implants with (*+S. epidermidis*) and without *S. epidermidis*. No statistically significant differences were determined between the medians at the 95% confidence level (Mann-Whitney test, *n=5*).

III.4.3 Evaluation of osseointegration

For the determination of the osseoitegration, 3D printed implants (Fig. 81 C-D) were prepared from standard implantable Concept Laser titanium alloy – CL 41 ELI (Ti6Al4V) with a trabecular structure with an outer diameter of 4 mm, an inner diameter of 3.5 mm and a length of 8 mm (see Fig. 81 C). The deposited COLHA and COLHA+V electrospun layers finally filled the inner diameter of the implants up to 4 mm (Fig. 81 C). The Ti printed samples (CP) were prepared with the same structure and with a diameter of 4 mm and a length of 8 mm (Fig. 81 E). Following deposition and impregnation, all the samples were packed and sealed in indicator bags and exposed to gamma sterilisation (25 kGy, BIOSTER, a.s., Czech Republic). The study involved the use of three minipigs (females) aged 30-48 months and with body weights of 90 ± 20 kg. Six control (CP) and 6 experimental (COLHA, COLHA+V) samples were implanted in each of the three animals for 6 months. All the implants were press-fit inserted (i.e. without a gap between the bone and the implant). The evaluation of *in vivo* osseointegration is in full details described in *Appendix B.17*.

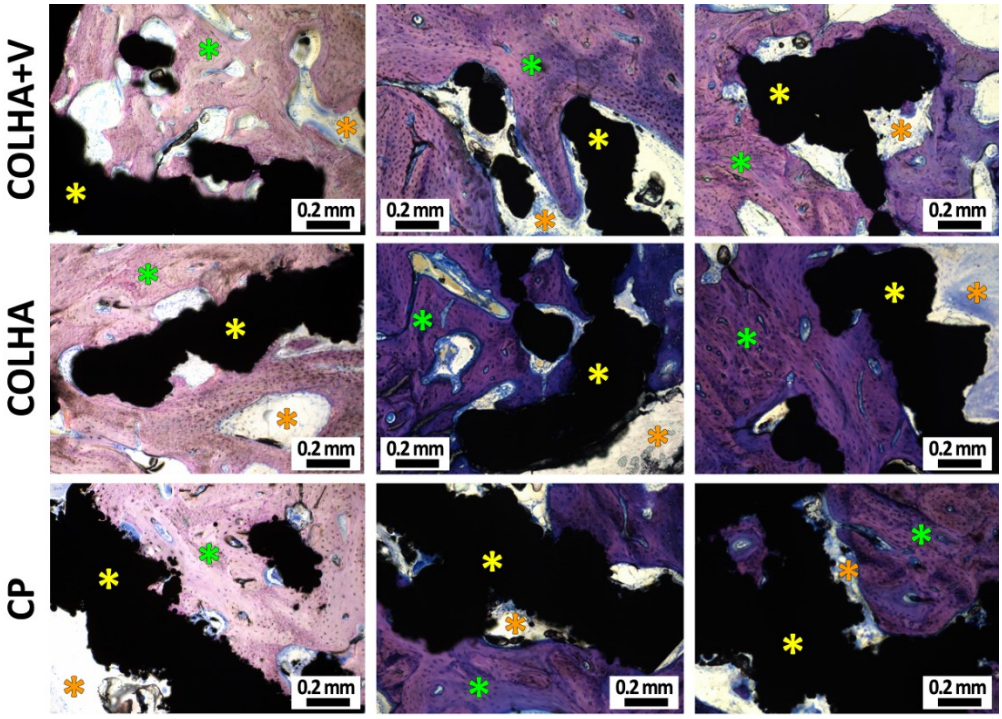

Fig. 87 Representative histological images (Giemsa's azur eosin methylene blue staining) of the printed titanium implants with collagen/hydroxyapatite layers without (COLHA) and loaded with vancomycin (COLHA+V) and the printed titanium control samples (CP). The green stars represent bone tissue outside of the implants, the orange stars represent connective tissue and the yellow stars the implants

New bone formation was observed with respect to all three groups of implants six months following implantation (Fig. 87). While new bone often formed within the trabecular structure of the implants, new bone formation was found to be more prevalent in the COLHA. Despite the fact that the inner surface of the implants (the hollow part of the thread) was found to be partially surrounded by connective tissue, both the base parts of the hollow cylindrical implants were also observed to be filled with bone tissue. In the case of the COLHA and COLHA+V samples, the porous structure of the implants allowed for bone tissue growth through the lower half of the implant. The qualitative histological

results were further quantified via the micro-CT analysis of new bone formation, while the inner part was excluded from the study.

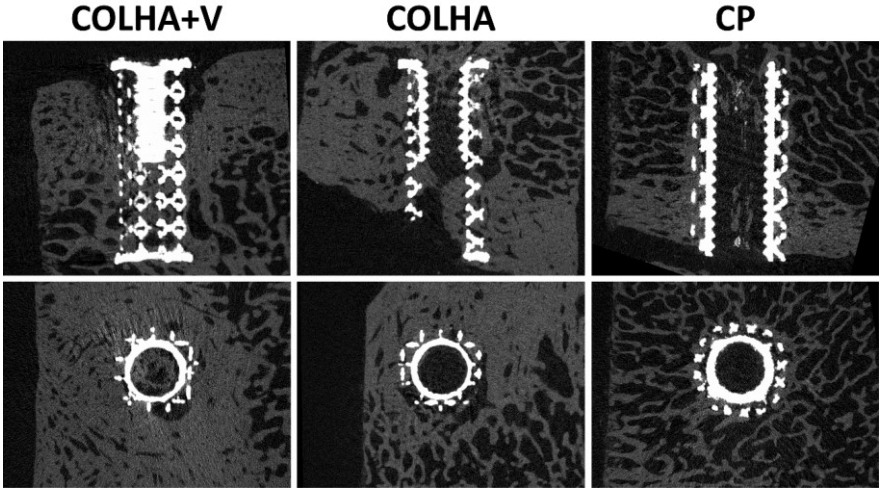

Fig. 88 Representative micro-CT images of the implanted titanium samples with collagen/hydroxyapatite electrospun layers with (COLHA+V) and without (COLHA) vancomycin and the control samples without an electrospun layer (CP).

The ratio of new bone (RNB) surrounding and penetrating the external surface of the implant was used in the quantitative comparison of the rate of osseointegration of the pure 3D printed samples (CP) and the 3D printed samples with a COLHA layer and COLHA layer with vancomycin (COLHA+V). Fig. 88 presents representative micro-CT images of the three types of titanium implants embedded partly in cortical bone and partly in trabecular bone.

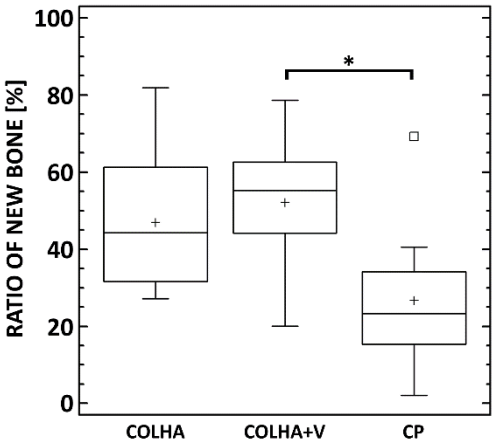

Fig. 89 Ratio of new bone integrated into the surface of the implanted titanium samples with collagen/hydroxyapatite electrospun layers with (COLHA+V) and without (COLHA) vancomycin and the control samples without an electrospun layer (CP). * denotes statistically significant differences (*0.05*, Kruskal-Wallis test with the Bonferroni procedure, *n=5*).

The micro-CT analysis confirmed that newly-formed bone had grown into the porous structure of all the implants. Moreover, the rate of ingrowth varied depending on the region of the cortical or trabecular bone subjected to assessment. The bone growth results are summarised in Fig. 89. The

average ratio of new bone increased in the order from the CP to the COLHA and to the COLHA+V samples. While statistically significant differences were observed between the CP and COLHA+V groups, no significant differences were determined between the COLHA and CP and COLHA and COLHA+V groups. The ratio of new bone indicated considerable bone ingrowth (mean, SD) on the COLHA (46.9±17.4%) and COLHA+V (52.2±16.9%) groups compared to the CP control group (26.7±18.4%).

III.4.4 Discussion

The most common microorganisms responsible for implant-associated infection consist of *S. aureus* and *S. epidermidis* [175]. In order to replicate the relevant clinical situation, biological evaluation involved the injection of a bacterial inoculum of *S. epidermidis* isolated from a rejected implant into the femoral medullary cavity of rats fitted with 3D printed titanium implants coated with collagen/hydroxyapatite with and without vancomycin. Six weeks following experimental infection and implantation, no significant signs of chronic infection were found in any of the experimental groups. However, the rats in the COLHA group without vancomycin with *S. epidermidis* displayed the obvious destruction of cortical bone as the result of infection. An alteration in the bone structure by means of increased bone porosity of up to 20% was evident in this group. In contrast, the rats in the infected group treated with COLHA with vancomycin exhibited a bone porosity occurrence of just 3% and those in the uninfected COLHA group of 2%. An increase in bone porosity constitutes one of the markers of bone inflammation and contributes significantly to poor implant osseointegration [176].

It is well known that the various tissues of the human body differ greatly in terms of the proportions of chemical elements. Thus, it can be expected that normal bone, inflamed bone and bone tumours, being of different tissues have specific and differing elemental compositions as, indeed, was proved by Zaichick and Zaichick [177]. According to the literature, this pathological process is associated with the alteration of the Ca/P ratio and a deficiency of microelements [178]. Several mechanisms of bone loss through osteomyelitis have been mentioned in the literature [179]. Even though bacterial biofilms are known to form via osteomyelitis, direct bacterial attack on bone is believed to make up a negligible mechanism [180]. Esmonde-White et al. [181] have hypothesised that bacterial biofilms are responsible for generating an acidic environment and, subsequently, that if the localised microenvironment cannot be adequately buffered, this environment leads to the dissolution of substituted carbonates and calcium ions. Consequently, a change may occur in the final Ca/P ratio in bone influenced by osteomyelitis. The value of the Ca/P ratio will probably depend (owing to the varying degree of substitution) on the part of the bone analysed. In this study, a statistically significant decrease in the Ca/P ratio was determined with respect to the COLHA implants with *S. epidermidis*, i.e. in the case of untreated inflammation. This decrease is in accordance with the conclusions formed by Esmonde-White et al. [181] who studied compositional changes in bone infected by the osteomyelitis of the diabetic foot and who proved the presence of pathological minerals such as brushite as well as uncarbonated apatite. They stated that the acidic environment caused by the osteomyelitis enabled the dissolution of carbonates in the bioapatite and the formation of brushite with a Ca/P molar ratio of 1. The findings of this study proved that the anti-microbial activity of COLHA+V layers is sufficient to prevent the development of bone infection in vivo.

In order to verify local antibiotic impact, the concentration of the active form of vancomycin released from the implants to the blood stream was determined 7 and 14 days following implantation. At day 7, the plasma of the animals without *S. epidermidis* infection contained up to 1.4 mg/L and those with *S. epidermidis* up to 0.1 mg/L of vancomycin. At day 14 the plasma of the animals without the *S. epidermidis* infection contained up to 0.3 mg/L of vancomycin, while no concentration of vancomycin was detected in the plasma of the animals with the *S. epidermidis* infection. In the case of the application of vancomycin in the form of continuous infusion, less than 10 mg/L of vancomycin in blood plasma is recommended in order to avoid renal failure or ototoxicity [182]. Results of presented study indicate that vancomycin applied via COLHA layers is capable of remaining locally within the bone with the minimal systemic loading of the organism [183].

Both a high degree of osseointegration and the prevention of infection are required for successful implantation [160]. In order to investigate the effect of collagen/hydroxyapatite layers and vancomycin on bone growth in a pig model, the control pure titanium printed implants were compared to the COLHA and COLHA+V implants. New bone formation was observed with concern to all three groups of implants six months following implantation. The micro-CT analysis quantitatively confirmed that newly-formed bone had grown into the porous structure of all the implants. The ratio of new bone indicated considerable bone ingrowth on the COLHA (~47%) and COLHA+V (~52%) compared to the CP control group (~27%). The application of collagen/hydroxyapatite layers improved the rate of osseointegration without the loading of vancomycin impairing *in vivo* bone growth into the implants.

Conclusion

Microstructured collagen materials for bone tissue regeneration. Optimal bone replacement materials imitate the real bone composition and structure so as to allow for the functioning of repair mechanisms by providing a temporary porous scaffold that, in turn, provides mechanical support for cells up to the time that the tissue has regenerated and remodelled itself naturally. The application of collagen is problematic due to its poor mechanical properties, high swelling rate in aqueous environments, low structural stability and low level of resistivity to the enzymatic degradation of its untreated form. The experiments presented herein demonstrated that the mechanical and structural properties of collagen can be improved via chemical cross-linking and via the creation of composite materials in which the collagen matrix is reinforced by fibres or particles. It was further demonstrated that the selection of the optimum cross-linking system constitutes a key factor. It has been shown that while the improvement of the stability of collagen scaffolds following cross-linking is demonstrated via an improvement in the mechanical properties, such changes cannot be evaluated separately without the evaluation of other effects principally on the secondary structure of the collagen and the overall structural properties of the collagen scaffolds. Only the combination of mechanical and structural analyses is able to provide reliable information on the success rate of such modifications. Moreover, it was shown that changes in the mechanical, chemical and structural properties should be evaluated in the hydrated rather than the dry state of the collagen. The hydrated state allows the collagen molecules to adopt conformations with maximal entropy, and the system exhibits a low level of dihedral energy. Such effects significantly influence the mechanical properties of the material in the environment for which it is designed. It was documented that with respect to the simulation of the body environment, the conditions must be considered very carefully. As with the evaluation of the structural parameters, it is crucial that the best method be selected for their characterisation.

Nanostructured collagen materials for bone tissue regeneration. The processing of collagen into submicron fibres or nanofibers represents a further promising approach to its application for bone tissue regeneration purposes. It is still unclear whether the electrospinning process as a whole influences the native structure of collagen. It has been demonstrated that the partial disturbance of its structure at some level following collagen dissolution and electrospinning can be improved via the creation of new additional chemical bonds between the collagen molecules. It has been shown that the suitable selection of the solution and the processing parameters as well as the suitable selection of the cross-linking system is able to preserve the native structure of collagen. The effects of cross-linking were demonstrated via an improvement in the mechanical properties and their stability under simulated body conditions accompanied by the simulation of cellular activity. Moreover, the variability of electrospun collagen was also demonstrated. It was shown that electrospun collagen evinces variability at some level in terms of its mechanical properties and secondary structure, and that the extent of the variability should be taken into account in the medical application design process.

Development of a soft on hard matter implant. One of the potential uses of the application of collagen-based materials concerns the development of a collagen coating for orthopaedic implants. It

is expected that such layers will be used particularly in the case of known prosthetic joint infections or as a preventative procedure for joint replacement at a potentially infected site. This study demonstrated the benefits and limitations of the single and combined application of antibiotics in collagen electrospun layers with differing amounts of hydroxyapatite. The study revealed that collagen electrospun layers that exhibit sufficient antimicrobial activity are not directly toxic for human cells. Moreover, it was demonstrated that collagen/hydroxyapatite layers directly electrospun on the surface of 3D printed titanium implants and impregnated with vancomycin have the potential to prevent infection while maintaining osseointegration. The antimicrobial activity of collagen/hydroxyapatite/vancomycin layers was found to be sufficient to prevent the development of bone infection *in vivo* as proved by a rat femur implant-related infection model with the inoculation of a clinically-relevant *Staphylococcus epidermidis* strain. *In vivo* tests employing a pig model concluded that a collagen/hydroxyapatite/vancomycin coating is capable of effectively improving the rate of osseointegration. Both the antimicrobial and osteoinductive functions of electrospun collagen/hydroxyapatite/vancomycin layers help to reduce the revision rate and enhance the long-term success of bone implants. The material composition as well as its preparation procedure have been submitted for the granting of a European patent by Suchý et al. (*A Nanocomposite Layer on the basis of Collagen Nanofibers and the Method for the Preparation thereof*, European Patent Office, application number EP17197245.8) and a Czech patent (*Nanokompozitní vrstva na bázi kolagenových nanovláken a způsob její přípravy*, Industrial Property Office of the Czech Republic, application number PV 2016-656).

Appendix A

Materials

A.1 Collagen scaffolds

In the first study described in *Chapter I.2*, collagen type I was isolated from freshwater fish skin (*Cyprinus Carpio*, *Třeboň carp*, Třeboň fishery, Czech Republic, controlled breeding). Collagen extraction was performed at a temperature of 20 °C. The skin was degreased for 48 h using diethylether and subsequently washed using distilled water. Preliminary extraction in a phosphate buffer (pH 7.4, 24 h, repeated three times) and a citrate buffer (pH 3.7, 24 h, repeated three times) was conducted so as to remove non-collagenous proteins and pigments. Collagen extraction was carried out by soaking the treated skin in 0.5 M acetic acid for 24 h followed by centrifugation (9 000 rpm). The liquid portion was dialysed against 0.1 M acetic acid in dialysis tubing (Spectra/Por, USA) for 2 × 24 h. The final solution was frozen at a temperature of −15 °C and lyophilised at −105 °C and at a pressure of approximately 1.3 Pa (BenchTop 4KZL, VirTis, USA).

In the second study described in this thesis (*Chapter I.3* The effects of different scaffold compositions in dry and hydrated states), commercial collagen type I was used (VUP Medical, Brno, Czech Republic).

Poly DL-lactide (PURASORB PDL05, Purac, Netherland) submicron fibre mats (diameter 275–300 nm, lower-upper quartile) were prepared by means of electrospinning from a 10 wt% chloroform solution (Nanospider NS LAB 500, Elmarco, Czech Republic). Prior to the preparation of the scaffolds, PDLLA fibres were homogenised using a disintegrator for 5 min at 14,000 rpm (DI 18, IKA, Germany) in distilled water, frozen at −15 °C for 24 h and subsequently lyophilised at −105 °C and at a pressure of ~1.3 Pa. Bioapatite (bCaP) was obtained from chemically and thermally treated bovine bone inspired by Murugan et al. [184]. The cortical bovine bone was sliced into pieces of the required size. Macroscopic soft tissue and marrow impurities were removed by means of boiling with a 2% NaCl solution at 150 °C and a pressure of 0.2 MPa in autoclave followed by degreasing in an acetone-ether mixture (ratio 3:2) for 24 h. The bone samples were then treated with 4% NaOH solution at 70 °C for 24 h. The product was washed with deionised water until a neutral reaction was obtained. The chemically treated bone samples were calcined overnight at 600 °C under atmospheric pressure and ambient humidity. The product was finally washed in deionised water and dried at 105 °C to constant weight. Sodium hyaluronate (HYA) powder (HySilk, Contipro, Czech Republic) was used as received.

Composite scaffolds based on a collagen matrix, PDLLA fibres, bCaP and HYA powder were prepared employing the following procedure: An aqueous collagen dispersion (5 wt%) was prepared by the swelling of collagen in deionised water, homogenised using a disintegrator (10 000 rpm, 10 min) and left for 60 min at a temperature of 20 °C. Collagen dispersion was further modified by means of PDLLA fibres, bCaP particles and HYA powder; final homogenisation was performed using the disintegrator (6 500 rpm, 10 min). The resulting dispersion was placed in separate cylindrical containers with an inner diameter of 10 mm, frozen at -70 °C for 3 h and then lyophilised. The final stage involved the cutting of the cylindrical specimens.

A.2 Comparison of different cross-linking conditions for collagen scaffolds

The collagen part of the scaffolds was cross-linked employing three different chemical treatments commonly published in literature as the PBS or ethanol solution of EDC/NHS (e.g. [59,84–86]) and a PBS solution of genipin (e.g. [85,86,88]). The first group of samples (EDC/NHS/EtOH) was cross-linked with an ethanol solution containing EDC and NHS at a weight ratio of 4:1 (EDC: 4.08 mg mL^{-1} and NHS: 1.02 mg mL^{-1}). EDC and NHS (Sigma Aldrich, Germany) were used as received. The second group (EDC/NHS/PBS) was cross-linked by means of a phosphate buffer saline solution (0.0027 M potassium chloride and 0.137 M sodium chloride, pH 7.4 at 25 °C) (PBS, Sigma Aldrich, Germany) containing EDC/NHS (weight ratio 4 : 1, EDC: 4.08 mg mL^{-1} and NHS: 1.02 mg mL^{-1}). The third group (GENIPIN) was cross-linked using a PBS containing genipin (Sigma Aldrich, Germany) at a concentration of 1.34 mg mL^{-1}. Following a reaction period of 24 h at room temperature (orbital shaker, 180 rpm), all the scaffolds were washed in the 0.1 M Na_2HPO_4 (2 × 45 min), followed by rinsing using deionised water (30 min), frozen at -15 °C for 5 h and lyophilised.

A.3 Final cross-linking conditions for collagen scaffolds

The collagen part of the scaffolds was cross-linked by EDC/NHS at a weight ratio of 4:1 (EDC: 4.08 mg mL^{-1} and NHS: 1.02 mg mL^{-1}) in ethanol solution (95 wt%). EDC and NHS (Sigma-Aldrich, Germany) were used as received. Following a reaction period of 24 h at 37 °C, all the scaffolds were washed in 0.1M Na_2HPO_4 (2 × 45 min), rinsed using deionised water (30 min), frozen at −30 °C for 5 h and lyophilised.

A.4 Preparation of the titanium implants

COLHA and COLHA+V layers were deposited upon two different printed titanium implants to be used for implantation in two subsequent *in vivo* experiments (*in vivo* infection prevention and osseointegration). 3D printed samples were prepared from standard implantable Concept Laser titanium alloy – CL 41 ELI (Ti6Al4V) powder (particle size 15-63 μm) with a trabecular structure designed using Magics computer-assisted design (CAD) software (Materialise, Belgium). The implants were fabricated by means of an SLM system (M2 Cusing Laser 1X200W, Concept Laser GmbH, Lichtenfels, Germany) based on the CAD (Magics, version 19.02, Belgium) data with a trabecular Dode-thick [MSG] shape and each with trabecula dimensions of 1.5 x 1.5 x 1.5 mm. The implants intended for the antimicrobial experiment in rats were of a nail-like shape (see Fig. 81 A, B) with an outer diameter of 2 mm, an inner diameter of 1.5 mm and a length of 5.5 mm. The nail-like shape ensured the protection of the electrospun layers when inserting the implant into the bone cavity. The implants intended for the osseointegration experiment in pigs were of a spool-like shape for the same reason. These samples had an outer diameter of 4 mm, an inner diameter of 3.5 mm and a length of 8 mm (see Fig. 81 C). The deposited COLHA and COLHA+V electrospun layers finally filled the inner diameter of the implants up to 4 mm (Fig. 81 C). The Ti printed samples (CP) were prepared with the same structure and with a diameter of 4 mm and a length of 8 mm (Fig. 81 E). All the titanium alloy samples intended for the osseointegration experiment (Fig. 81 C-E) were prepared with an M2.2 inner metric thread for the fixation of the insertion jig used in the implantation procedure. All the samples were ultrasonically washed with ethanol and distilled water and dried at 60°C overnight prior to the deposition of the electrospun layers. Following deposition and impregnation, all the samples were packed and sealed in indicator bags and exposed to sterilisation at a nominal dose of 25 kGy (BIOSTER, a.s., Veverská Bítýška, Czech Republic).

Appendix B

Methods

B.1 Characterisation of the mechanical properties of porous scaffolds

In order to describe the mechanical behaviour of the scaffolds, compression tests were performed by means of the adaptation of the ISO 13314 standard, which refers to the mechanical testing of porous and cellular metals. Cylindrical samples with a diameter of 10.2 mm and a length of 12 mm were tested (i.e. a sample length to diameter ratio of approximately 1.2). Plateau stress, elastic gradient, compressive proof stress and energy absorption were determined using an MTS Mini Bionix 858.02 system (MTS, USA) equipped with 100 N and 250 N load cells. The measurements were carried out at a constant crosshead speed of 2.0 mm min^{-1} (deformation rate approx. 0.003 s^{-1}, i.e. in the range of 10^{-3} and 10^{-2}).

B.2 Fourier transform infrared spectroscopy

The structure of the studied materials was evaluated by means of attenuated total reflection infrared spectrometry (FTIR) using a Protégé 460 E.S.P. infrared spectrometer (Thermo Nicolet Instruments, USA) equipped with an ATR device (GladiATR, PIKE Technologies, USA) with a diamond crystal. All the spectra were recorded in absorption mode at a resolution of 4 cm^{-1} and 128 scans. The areas of the bands (integral absorbencies) were determined using OMNIC 7 software.

Infrared spectroscopy can be used as analytical technique for interpretation of changes in collagen secondary structure after various processes (isolation, cross-linking, denaturation and sterilization). The FTIR spectra of collagen contain 5 amidic bands [138,139,143] typical for unique collagen structure: such as N–H stretching at ~3303 cm^{-1} for amide A and C–H stretching at ~3080 cm^{-1} for amide B. Generally, amide I bands (~1650 cm^{-1}) originate from C=O stretching vibrations coupled with N–H bending vibration. Amide II bands (~1550 cm^{-1}) arise from N–H bending vibrations coupled with C–N stretching vibrations. Other proofs for existence of triple helical structure are presence of a quartet of bands at ~1205, 1240, 1280 and 1340 cm^{-1} [185,186]. Another spectral region is so called carbohydrate region (960–1140 cm^{-1}) where subbands of non-collagenous proteins and carbohydrates are present [144].

The amide I region of the spectrum of collagen (~1650 cm^{-1}) can be deconvoluted into several distinct bands with maxima at ~1690, 1680, 1660, 1650, 1630-1635 and 1610-1615 cm^{-1} [143]. Band ~1660 cm^{-1} was assigned to the triple helix, with contribution from α-helix [143], while band ~1630-1635 cm^{-1} has been assigned to aggregate β-sheet structure and left-handed 3-10 helix in denatured state and imide residues [143]. Component at ~1610-1615 cm^{-1} are relating to aromatic amino acids which can be more spectroscopic active in case of denatured state of collagen, such as gelatine [139]. Band ~1650 cm^{-1} corresponds to random coils which are not usually presented in cross-linking collagen. Band at 1685-1690 cm^{-1} is attributed to β-turn and antiparallel β-sheet structure [143]. In some cases, it is not possible to resolve bands ~1680 and 1690 cm^{-1}, consequently they become evident such as one band at ~1685 cm^{-1}. Upon denaturation, the bands do not shift appreciably in position, but the

relative intensities of the 1660 and ~1635 cm^{-1} bands shift from > 1 to < 1, in other words, component found around ~1635 cm^{-1} increase and component found around 1660 cm^{-1} decrease in intensity.

B.3 Mass loss and swelling ratio

The *in vitro* degradation of the scaffolds was evaluated by means of the determination of mass loss and the swelling ratio after exposure to selected media. The extent of *in vitro* degradation was calculated according to the following equation:

$$D = \frac{W_0 - W_t}{W_0} 100\ [\%], \quad (6)$$

where D is mass loss, W_o is the initial dried weight of the sample and W_t is the dried weight of the sample after degradation.

The swelling ratio (E_{sw}) was calculated using the following equation:

$$E_{sw} = \frac{W_{sw} - W_0}{W_0} 100\ [\%], \quad (7)$$

where W_o is the initial dried weight of the sample and W_{sw} is the weight of the swollen sample. The weight of the swollen samples was measured following the removal of each sample from the medium and after a 1 minute delay and the removal of the excessive medium surrounding the sample. The dried weight of the samples was measured after lyophilisation.

B.4 Micro-CT analysis of dry and hydrated scaffolds

Micro-CT scans were acquired using SkyScan 1272 (Bruker, Belgium). All the specimens were scanned in air in the dry state. The hydrated specimens were scanned (immersed in deionised water in closed plastic tubes) at time intervals of 4, 8, 24 and 48 h following initial hydration. Prior to scanning in the hydrated state, the samples were X-ray contrasted using Lugol's solution (3.33 g/L iodine, 6.66 g/L potassium iodide). The samples were inserted into silicon tubes with an inner diameter of 6 mm, and 20 mL of Lugol's solution was applied using a linear pump in one direction (20 mL/h) and repeated in the reverse direction after a 30 min delay. Following contrasting, the samples were gently washed with deionised water and inserted into sample containers with deionised water. All the scans were conducted under the following scanning parameters: 4 µm pixel size, source voltage 60 kV, source current 166 µA, 0.25 mm Al filter, frame averaging (2), 180° rotation. The scanning time was ~1 h for each specimen. The flat-field correction was updated prior to each acquisition. Cross-section images were reconstructed from projection images taken with NRecon software (Bruker, Belgium) and using a modified Feldcamp algorithm with the adequate setting of the correction parameters (misalignment, ring artefact and beam hardening) so as to reduce the effect of computed tomography artefacts. Visualisations were acquired by means of DataViewer (2D cross-section images) and CTVox (3D images; Bruker, Belgium). Scaffold structure analysis, including porosity analysis, was performed by means of CTAn (Bruker) in 3D using a sphere fitting algorithm following image binarisation. The VOI (volume of interest) subjected to analysis was set within the scaffold structure and was cylindrical in shape (5 mm

in height and 5 mm in diameter) and excluded the superficial parts of the specimen which might have been altered as a consequence of the treatment of the specimen.

B.5 Hydraulic permeability measurement

Permeability at different time points was measured for each type of scaffold (at least 6 specimens per group), applying a constant flow rate (*Q*) and acquiring a pressure drop throughout the thickness of the scaffold *(ΔP*). Cylindrical specimens with a diameter of 5.5 mm and a thickness of 5 mm were used for testing purposes. The experimental layout consisted of: i) a perfusion chamber hosting a deformable silicone-made cartridge (Sylgard 184 Dow Corning Corporation) containing the scaffold and ensuring confined-flow perfusion; ii) a peristaltic pump (Ismatec IPC-N, Cole-Parmer GmbH) for ensuring fluid flow through the scaffold; and iii) an I/O acquisition system (NIDAQcard-6036E and LabViewTM, National Instruments) which was employed for the real-time monitoring and acquisition of pressure values. A Press-S-000 (PendoTECH, USA) pressure sensor provided inflow pressure values, while outflow pressure values were taken at atmospheric pressure in the adopted set-up (Figure 90).

Permeability measurements were performed in a water bath at a constant temperature (37°C), and deionised water was used as the working fluid. Several flow rate values were applied, increasing *Q* in the range 100-1000 µL/min (in steps of 100 µL/min). The *ΔP* measurements were repeated three times. The *ΔP-Q* data was registered after 5 minutes of hydration, allowing the estimation of the permeability at the starting point (K_0) following 4 (K_4), 8 (K_8) and 24 hours (K_{24}) from the starting point. A constant flow rate of 100 µl/min was maintained across the scaffold between the two subsequent measurement sessions. Permeability [m^2], based on Darcy's Law, was calculated using the following equation:

$$K = \frac{\vartheta\, t}{S\, m}, \tag{8}$$

where ϑ is the fluid viscosity, *t* is the mean scaffold thickness, *S* is the cross-sectional area and *m* is the slope of the linear interpolation of the *ΔP-Q* data acquired at different *Q* values for each specimen.

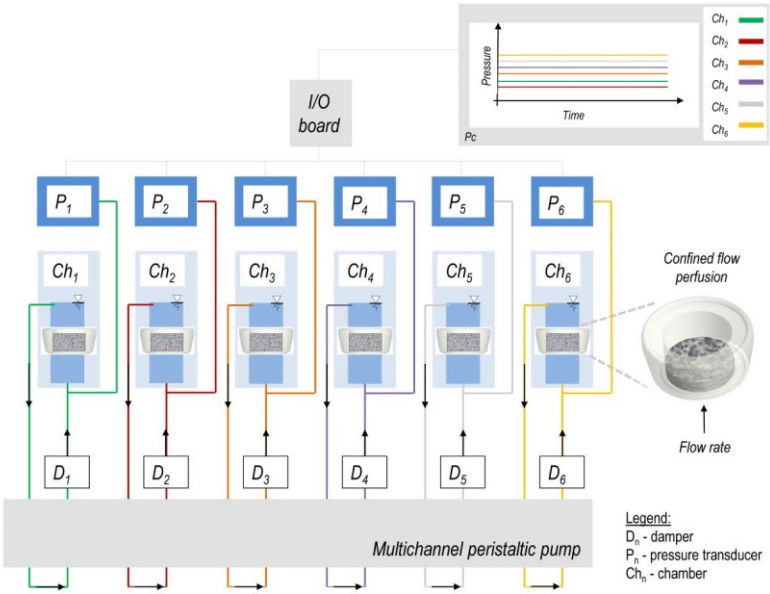

Fig. 90 Experimental set-up for permeability measurement [187].

B.6 Collagenase degradation

Collagenase degradation tests were performed according to [188]. Lyophilised scaffolds were immersed in 0.1M Tris-HCl containing 50mM $CaCl_2$ and incubated at 37 °C for 0.5 h. Subsequently, 0.1M Tris-HCl containing 50 units of collagenase from Clostridium histolyticum, Type I, (Sigma-Aldrich, Germany) was added to the solution and the scaffolds were immersed in the bath at 37 °C for 1 h. The reaction was terminated by means of the addition of 0.25M EDTA and cooling on ice. The samples were rinsed with deionised water three times and then immersed in ethanol for 3 h. They were then rinsed with deionised water, frozen at −30 ° C for 5 h and lyophilised. The mass loss was calculated from the dry weight prior to and following enzyme digestion.

B.7 Comprehensive micro-CT analysis for comparison of different approaches

The scaffold specimens were scanned using a micro-CT SkyScan 1272 (Bruker micro-CT, Kontich, Belgium) under the following parameters: pixel size 4.5 µm, source voltage 60 kV, source current 166 µA, Al filter 0.25 mm, rotation step = 0.1°, frame averaging (5), rotation 360°. The composite scaffolds were scanned in the dry state in air and mounted on specimen holders. The scanning time was approximately 4 h for each specimen. Flatfield correction was updated prior to each image acquisition. Projection images were reconstructed to form cross-section images via NRecon software (Bruker) using a modified Feldcamp algorithm. Software correction (misalignment, ring artifact and beam hardening) was performed in order to reduce the effect of computed tomography artifacts. Visualizations were acquired using a DataViewer (2D crosssection images; Bruker) and a CTVox (3D images; Bruker). Color-coded pore size values were based on 3D structure separation analysis. Prior to structure analysis, the datasets were binarized using an adaptive threshold and despeckle operations in 3D were applied to reduce image noise. These steps were optimized using TeiGen software [118]. The volume of interest (VOI) subjected to analysis was defined by the shrink-wrap procedure in 3D. Scaffold structure analysis, including porosity analysis, was performed by means of a CTAn (Bruker). The analysis of pore size in the whole specimen was performed in 3D using a sphere-fitting algorithm. 2D sections of the scaffolds (transverse plane perpendicular to the axis of the cylindrically-shaped specimens; 5 sections) were evaluated for pore size values employing the following parameters: major diameter (MD, major diameter of analysed pore), mean thickness (MT, based on circle-fitting algorithm similar to sphere-fitting procedure), biggest inner circle diameter (BICD, diameter of the biggest circle fitting analysed pore) and area-equivalent circle diameter (AECD, diameter of circle of area equivalent to area of analysed pore).

B.8 Characterisation of the mechanical properties of electrospun collagen

Mechanical properties were measured by a uniaxial tensile test in which the initial modulus of elasticity in the first or the last load cycle and the ultimate tensile strength of the collagen layer were evaluated. Measurements were carried out on a multi-axis test machine (Zwick/Roell, Germany) with force sensors U9B by HBM with a range of ±25N and ±250N equipped with a non-contact optical extensometer. This extensometer, using the contrast marks on the samples, records the course of deformation during loading. The data was recorded at a frequency of 20 Hz and stored on a computer. The position of the marks, the position of the clamping jaws and the force were measured. The mechanical properties of electrospun collagen in the dry state were evaluated after the first loading cycle. Because of viscoelastic behaviour of hydrated collagen, which also depends on the previous

deformation, it is necessary to load and relieve the sample several times before performing the inter-strength test. In the case of the experiment with cell cultivation, estimation of the initial modulus of elasticity occurred both for the first load cycle, thanks to which we can determine the effect of dermal fibroblasts and osteoblasts on the surface layers of the material, as well as the last load cycle from which the effect of cells on the inner structure of the material can be estimated. From the measured data, graphs of stress σ - strain ε relationships were plotted. The values for these charts were calculated from:

$$\sigma = \frac{F}{S} \ [MPa], \tag{9}$$

$$\varepsilon = \frac{\Delta l}{l_0} \ [-], \tag{10}$$

where *F* is the force measured by the force sensors [N], *S* is the cross sectional area of the unloaded sample [mm^2] (we consider the rectangular cross-section), Δl is the elongation of the sample determined by the change of the contrast marks on the samples [mm] and l_0 is the initial length of the sample [mm].

In the case of assessment of hydrated electrospun collagen variability, during the test procedure, 5 preloading cycles were carried out as preconditioning. The sixth loading sequence was used in the subsequent mathematical modelling. To this end, the engineering strain defined as the ratio of the elongation of the sample to its reference length, and nominal stress defined as the ratio of applied force to the reference cross-section of the sample were determined from experimental records.

B.9 Ultraviolet-visible spectrophotometry of free amino groups

Degradation tests under physiological conditions were used so as to assess the stability of the collagenous layers, and ultraviolet-visible spectrophotometry was used for the quantification of the free amino groups released during the degradation of the samples immersed in the PBS (37 °C, pH 7.4) and 2,4,6-trinitrobenzenesulphonic acid (TNBS, Sigma-Aldrich, Germany) solution. PBS was collected after selected time periods. The PBS collected (2.5 mL) was mixed with 2 mL of 0.1 M $NaHCO_3$ and 1 mL of 0.01% aqueous solution of 2,4,6-trinitrobenzenesulphonic acid (TNBS, Sigma-Aldrich, Germany). The mixture was incubated at 40 °C for 2 h. Subsequently, 1 mL of a 10% solution of sodiumdodecyl sulphate (Sigma-Aldrich, Germany) and 0.5 mL of 1 M HCl were added. Absorbance at 340 nm was measured using a Unicam UV 500 spectrophotometer and correlated to the concentration of free amino groups using a calibration curve obtained with L-lysine (Sigma-Aldrich, Germany) and L-α-amino-n-butyric acid (Lachema, Czech Republic).

B.10 Exposure in culture medium and in the presence of cells

For the exposure of electropsun collagen in simulated body conditions, dermal fibroblasts (iz_171017, Biomedical Centre, Medical Faculty in Pilsen, Charles University) and osteoblasts (human line SAOS-2) cultivated on the surface of the layers were used. Both cell types were first cultivated on 75 cm^2 polystyrene culture bottles (Techno Plastic Products, Switzerland) in culture medium. The culture medium contained Dulbecco's Modified Eagle Medium (DMEM, Thermo Fisher Scientific, USA), fetal

bovine serum (FBS, Thermo Fisher Scientific, USA), penicillin (100U/mL), streptomycin (0.1 mg/mL), L-glutamine, and 1% non-essential amino acid (Biosera, USA). Cultivation took place at 37 °C and 5% CO_2. On the day of the experiment, the dermal fibroblasts were sedimented with trypsin/EDTA and counted using a Bürker cell. For fluorescence microscopy and for measuring metabolic activity, collagen were prepared in the form of a 0.3 cm circle, rinsed for 20 min in 1% ethanol and 10 min in PBS. The samples were then placed in a 96 polystyrene panel (Techno Plastic Products, Switzerland) and immersed in 150 µm of culture medium until they were seeded with cells.

For mechanical tests, 9 × 50mm strips were rinsed for 20 minutes in 70% ethanol and 10 minutes in PBS. 20 × 50mm (SPL Life Sciences, Korea) culture chambers were each placed in two pieces and immersed in 4 mL of culture medium until they were fitted with cells. The dermal fibroblasts were diluted to a culture medium at a concentration of 30,000 cells/mL and loaded onto collagen samples at a deposition density of 15,000 cells/cm^2 and a volume of 150 µL. The osteoblasts were diluted to a culture medium at 30, 000 cells/mL and loaded onto collagen materials at a loading density of 15, 000 cells/cm^2 and a volume of 150 µL. Both cell types were cultured for 21 days, when the measurements ranged on days 1, 7, 14 and 21. The culture medium was changed three times a week.

Biological evaluation was carried out by means of fluorescence microscopy and determination of metabolic activity. Dermal fibroblasts and osteoblasts were dyed at 1, 7, 14 and 21 days after the start of the experiment. At each time, both cell types were cultured on COL and on polystyrene (PS) stained with a 1 µg/mL solution of calcein AM (Thermo Fisher Scientific, USA) in culture medium for 30 min at 37 °C and 5% CO_2. After the staining period, the samples were rinsed with PBS and transferred to the cover glass. Clear fluorescence images of both types of cells cultured on COL and PS were acquired using the Olympus IX83 (Olympus, Switzerland) microscope at 488nm excitation and 528nm emission. Images were processed using ImageJ (National Institute of Health, Bethesda, USA).

The metabolic activity of dermal fibroblasts and osteoblasts grown on COL and PS were measured at 1, 7, 14 and 21 days after the start of the experiment using the Alamar Blue assay method. From each sample, culture medium was aspirated and 150 µL of new culture medium containing 10× diluted Alamar Blue (ThermoFisher Scientific, USA) was added. Samples were incubated for 2 hours at 37 °C and 5% CO^2. Subsequently, 100 µL of culture medium was pipetted into a 96 plate (NUNC, Denmark) and the fluorescence of the solution at 530 nm excitation and 590 nm emission was measured using a Synergy HT (Biotek, USA) spectrophotometer. From the measured values, the fluorescence of the culture medium itself was read and the values were expressed as the fluorescence ratio at day 7, 14 and 21 on fluorescence. Values thus reflect the change in the metabolic activity of cultured cells on COL and on PS over time. The experiment was performed in 6 replicates.

B.11 Vancomycin release kinetics

An investigation was conducted of the *in vitro* release of vancomycin from COL/HA/VANCO layers prepared by means of three different methods. Six samples of each type of layer were placed on a sterile gauze pad and firmly caulked prior to being transferred to separate test tubes containing a weight/volume ratio of 200 mg/20 mL of PBS (pH 7.4) which were placed in an incubator at a temperature of 37 °C. The solid phase extraction method and HPLC analysis (HPLC on an Agilent 1200

series system equipped with a DAD diode array detector - Agilent Technologies) were then employed in order to characterise the in vitro release rates of the vancomycin and its crystalline degradation antibiotically inactive products over a 21-day period. Details of the HPLC analysis are described in an article written by Melicherčík et al. [189].

B.12 Antimicrobial activity (MRSA)

The evaluation of the antimicrobial susceptibility was conducted by means of the use of MRSA isolate retrieved from the hospital patient specimens (General University Hospital, Prague, Czech Republic). Inoculum was produced from an 18–24 h pure culture of the test isolates via a Mueller-Hinton agar medium. Suspensions were prepared from 1 to 4 colonies of the test isolates (only well-isolated, morphologically similar colonies grown on a non-selective medium) in 2 mL of sterile saline solution and the turbidity was adjusted (using a Densi 2, Erba Lachema densitometer, Brno, Czech Republic) to 0.5 of the McFarland turbidity standard (approximately 1–2 × 108 CFU/mL). Disc diffusion was performed using a Mueller-Hinton agar medium (Oxoid Ltd., Hampshire, UK; batch LOT1381672) with the test samples. Sterile cotton swabs were used to spread the inoculum evenly over the agar plates in three directions. Discs with a diameter of 6mm (*n=7*) were firmly applied to the dried surface of the inoculum agar plates using a sterile needle within a 15-minute time period and further incubated at 37 °C for 24 h. It was expected that the careful application of the inoculum and the streaking of the plates would result in even growth without the occurrence of separate colonies. The inhibition zones were read off using a ruler while holding each agar plate approximately 30 cm from the eye. Standard 6 mm antibiotic discs were used for positive control (PC) purposes, i.e. vancomycin 30 µg for *S. aureus*.

B.13 Gentamicin release kinetics

The UHPLC-tandem mass spectrometry method was used for the determination of gentamicin C components. Mass spectrometric detection was performed on a triple-quadrupole in the positive electrospray ionisation mode by means of multiple reaction monitoring (Agilent 1290 with Triple Quad 6470, Agilent Technologies, USA). Tobramycin (1 mg/L in 10% trichoroacetic acid) was taken as the internal standard. The developed method for the determination of gentamicin provides for the separation of the C1, C1a and C2 components. The selected reaction monitoring of the precursor-product ion transitions m/z of 478.5→ 322.1 (C1), 450.4→322.4 (C1a), 464.5→322.4 (C2+C2a+C2b) for gentamicin, and 468.3→163.2 for tobramycin were employed for quantification purposes. 25 µL of the sample was mixed with 50 µL of the internal standard for the precipitation of the proteins. The mixture was then centrifuged. Chromatographic separation was conducted using an InfinityLab Poroshell 120 PFP column (2.1×100 mm, 2.7 µm, Agilent Technologies) employing the binary gradient of the mobile phases (A – water with 1% heptafluorobutyric acid, B – 90% acetonitrile with 1% heptafluorobutyric acid) at a flow rate of 0.4 mL/min; separation was accomplished at 35 °C and the analysis time was 4 min. The LC-MS/MS method was successfully validated. The intra- and inter-day accuracy and precision were evaluated on two QC samples by means of multiple analysis, and the coefficients of variation were determined at 2.2–8.5% for the intra-assay, 3.2–9.3% for the inter-assay, and 6.6–9.8% for the precision.

B.14 Antimicrobial activity (4 isolates)

The antimicrobial activity was tested employing four different bacteria isolated from patients suffering from severe infections, i.e. *Staphylococcus aureus*, *S. epidermidis* and two *Enterococcus faecalis* isolates, and with differing susceptibility to the antibiotics used in this study. The disc diffusion test was performed using a Mueller-Hinton agar medium (Oxoid Ltd., Hampshire, UK) with the test bacteria according to the EUCAST recommendation [40]. Discs of 6mm in diameter (*n=7*) prepared from the tested COL/HA layers loaded with the appropriate antibiotics were firmly applied to the dried surface of the inoculum agar plates using a sterile needle and further incubated at 37 °C for 24 h. The diameters of the inhibition zones were subsequently measured. Standard 6mm antibiotic discs were used as standard controls, i.e. vancomycin 30 μg and/or gentamicin 10 μg for *S. aureus* and *S. epidermis*, and vancomycin 5 μg and/or gentamicin 30 μg for both *Enterococci*. Collagen/hydroxyapatite layers prepared without antibiotics were used as negative controls.

B.15 *In vitro* evaluation of cytotoxicity

SAOS-2 culture

Human osteoblast cells (SAOS-2 cell line derived from osteosarcoma, DSMZ, Germany) were cultured in McCoy's 5A medium without phenol red (PromoCell, Germany) supplemented with 15% heat inactivated foetal bovine serum (FBS) (PAA, Austria), penicillin (20 U/mL, Sigma-Aldrich, USA) and streptomycin (20 μg/mL Sigma-Aldrich, USA) at 37 °C in 5% CO_2.

Collagen/hydroxyapatite layer extracts test

The collagen/hydroxyapatite layers were fixed by means of CellCrown™ inserts (Sigma-Aldrich, USA) in 48-well plate (Thermo Scientific, USA), covered by 800 μl of fully supplemented McCoy's 5A medium and incubated at 37 °C and 5% CO_2 for 24 h. Subsequently, 400 μL of the extracts were transferred onto SAOS-2 pre-seeded on 48-well plate (20,000 cells/cm^2) 20 h prior to the treatment of the extracts. The metabolic activity of the SAOS-2 was measured 24 h following cultivation. SAOS-2 cultivated in a standard medium without layer extracts in 48-well plate were used as the control.

Direct collagen/hydroxyapatite layer test

The layers were fixed by means of CellCrown™ inserts (Sigma-Aldrich, USA) in 48-well plate (Thermo Scientific, USA) for the direct cultivation of SAOS-2 on the collagen/hydroxyapatite layers. 15 000 cells/cm^2 were seeded on the COL/HA layers and the metabolic activity was measured after 2 and 8 days of culturing. The medium was changed after 4 days of culturing. For control purposes, SAOS-2 were also cultivated on a 48- well plate standard tissue culture polystyrene surface (PS).

Metabolic activity measurement

The metabolic activity was measured (Cell Titer 96 AQueous One Solution Cell Proliferation Assay, MTS, Promega, USA) (i) 24 h following SAOS-2 cultivation in collagen/hydroxyapatite layer extracts, and (ii) 2 and 8 days following SAOS-2 cultivation directly on the COL/HA layers. The measurement of metabolic activity was performed according to the manufacturer's instructions. Absorbance (490 nm and 655 nm as the reference) was determined using a multi-detection micro-plate reader (SynergyTM 2, BioTek, USA). The results were normalised (in percentage) with respect to the controls.

Fluorescent microscopy of the SAOS-2 cultured on the collagen/hydroxyapatite layers

Following the measurement of metabolic activity, the SAOS-2 cultured directly on the layers for 2 and 8 days were fixed (4% paraformaldehyde in PBS, at room temperature (RT) for 15 min; Sigma-Aldrich, USA) and permeabilised (0.1% Triton X-100 in PBS at RT for 20 min; Sigma-Aldrich, USA). The cell nuclei were then stained with DAPI (dilution 1:1000, RT for 45 min; Sigma-Aldrich, USA) and the actin filaments with Phalloidin-Alexa Fluor 488 (dilution 1:500, RT for 45 min; Life Technologies, USA). Wide field images (10x and 40x lens) of the cells on the layers were acquired using an Eclipse Ti-S microscope and a DS-U2 digital camera (Nikon, Japan) and adjusted via the use of ImageJ software (Rasband, W.S., ImageJ, US National Institutes of Health, Bethesda, Maryland, USA, http://imagej.nih.gov/ij/, 1997–2015) and Cell Profiler (Broad Institute, USA) software.

B.16 Evaluation of *in vivo* infection prevention

The experimental infection rat model

In order to replicate a case of bone infection following primary implantation we applied a clinical isolate of *S. epidermidis* from a rejected implant for the induction of infection in the femur of a rat model followed by the determination of the antimicrobial efficacy of the implants with the COLHA + V and COLHA layers. The experiment was approved by the Animal Welfare Advisory Committee of the Ministry of Education, Youth and Sports of the Czech Republic (approval ID MSMT-249/2017-2). Thirty male Wistar rats aged 5 months (Masaryk University Brno, Czech Republic) were divided into 3 groups, i.e. a group with implanted COLHA+V layers without infection (*n=10*), a group with implanted COLHA layers with the *S. epidermidis* infection (*n=10*), and a group with implanted COLHA+V layers with the *S. epidermidis* infection (*n=10*). The experimental surgical procedure was performed under general anaesthesia. The animals were subjected to light inhalation anaesthesia induced by isoflurane in oxygen using an anaesthetic machine (Vetnar 1100, Grimed, Czech Republic) connected to an inhalation chamber. Following the elevation of the abdominal wall of the restrained animal, the anaesthetic mixture was carefully injected into the peritoneal cavity so as not to affect the intestine. The anaesthetic mixture was prepared prior to each experiment in a syringe via the mixing of propofol (100 mg/kg; Propofol 2%, Fresenius Kabi, Germany), medetomidine (0.1 mg/kg; NarcoStart®, Produlab Pharma B.V., Netherlands), and nalbuphine (0.1 mg/kg; Nalbuphin Orpha, Orpha-Devel Handels und Vertriebs GmbH, Austria). The anaesthetised animals were placed on a tempered operating table and continually supplied with oxygen via a face mask and monitored by means of pulse oximetry. During the operational procedure the COLHA and COLHA+V layers were impregnated with 2 µL of a clinical isolate *S. epidermidis* suspension (1.0 McFarland). One of the hind legs was shaved and disinfected, the animal was placed in the dorsal position and the pelvis positioned so as to provide comfortable lateral access to the femur. Following cutaneous incision, access was gently prepared between the hind leg *vastus fibularis* and *biceps femoris* muscles so as to expose the femur. A hole (2 x 5 mm) was then drilled into the femur and completed using a surgical milling cutter and Kirschner wire in order to enable the complete insertion of the implants into the medullary cavity. One of the implants was loosely inserted into a slightly larger prepared hole in the medullar cavity of the left femur of each animal. The hole was then sealed with PALACOS® (Heraeus Medical, U.S.A.) bone cement. The muscles and skin were treated separately with an absorbable suture and the surgical wound covered with Novikov solution. The general anaesthesia was then terminated by means of an IM injection of atipamezole (0.5 mg/kg; NarcoStop®, Produlab Pharma B.V., Netherlands). Following surgery, the

animals were provided with analgesia for 4 days using tramadol (12.5 mg/kg; Tramal®, STADA Arzneimittel AG, Bad Vilbel, Germany) and carprofen (5 mg/kg; Rimadyl®, Zoetis, Brazil) as recommended by Cannon et al. [190]. Subsequently, blood samples were collected from the tail vein at weekly intervals. Blood collection for the determination of the vancomycin concentration released from the implants was performed under light isoflurane anaesthesia (3% isoflurane in O_2) administered via a face mask. The animals were sacrificed after 6 weeks and femur samples were collected for histological and micro-CT analysis purposes. During the experiment the rats were kept under conventional conditions (12/12 dark/light cycle) according to EU directive 2010/63/EU in sterile polycarbonate microisolators (Bioscape, Germany) with bedding (Lignocel Select fine, JRS, Germany) and free access to water and pelletised feed (ST1, Velaz, Czech Republic).

Bone histology

The samples were processed into ground sections as described previously [119,191] for the purpose of the histological analysis. Briefly, the samples were fixed with a 10% formaldehyde solution (7 days), immersed in 70% ethanol and then micro-CT scanned. The samples were further dehydrated in ascending grades of ethanol and embedded for two days to methyl methacrylate (Merck Millipore, Darmstadt, Germany) without a polymerisation initiator. The samples were then emplaced in moulds with resin and polymerised. The polymerisation of the resin was initiated using benzoyl peroxide (Merck Millipore, Darmstadt, Germany). The blocks with the samples were then sectioned perpendicularly along the long axis of the implants. The samples were cut using a diamond disc, the cutting area of the blocks was ground using a sequence of abrasive papers and, finally, the samples were polished. A clean slide was then glued to the polished side and a second section was made approximately 300-500 µm from the slide and parallel to it. The slide with the section was ground once more to a final thickness of between 70-90 µm. The final polishing of the surface involved the use of paper coated with a fine textile cloth and 3 µm diamond paste. The papers used for grinding and polishing were positioned on a rotation desk with the samples pressed towards the desk (EcoMet™ 250, Struers, Ballerup, Hovedstaden, Denmark). Finally, the sections were stained with 20% Giemsa's azur eosin methylene blue solution (Merck Millipore, Darmstadt, Germany). The whole surface of the implant and the surrounding area was photographed using a bright field microscope with a 10x objective. We compared changes in the surrounding bone structure and the grade of infiltration by inflammatory cells by actively searching for signs of foreign-body cell reactions, insufficient osseointegration, osteolysis, periprosthetic infection and necrosis.

Micro-CT analysis

Micro-CT scans were acquired *ex-vivo* using a SkyScan 1272 (Bruker micro-CT, Kontich, Belgium) micro-CT device. Each of the femurs with inserted implants were mounted on a micro-stage and scanned immersed in 70% ethanol in a plastic tube. The long axes of the samples were oriented vertically. The scanning parameters were as follows: 10 µm pixel size, rotation step=0.2°, camera binning 2x2, source voltage 100 kV, source current 100 µA, 0.11mm Cu filter, frame averaging (2), 360° rotation; the scanning time was approximately 3 hours and 30 minutes for each specimen. The flat-field correction was updated prior to each acquisition. Cross-section images were reconstructed from the projection images using NRecon software (Bruker micro-CT, Kontich, Belgium) with a modified Feldkamp algorithm. Correction procedures were applied (misalignment, ring artefact and beam hardening

correction) so as to reduce the effect of computed tomography artefacts. Visualisations were acquired by means of DataViewer (2D cross-section images) and CTVox (3D images; Bruker, Kontich, Belgium).

The 3D analysis of the structure of the rat femurs with the implants (*n=10*) was conducted by means of CTAn (Bruker, Kontich, Belgium). In order to evaluate the changes in the bone structure, a region of interest was created in each specimen in the area surrounding the implant. The regions of interest were hand drawn in cross-sectional images and comprised cortical bone with the exclusion of the implant and cement material. The vertical dimension of the volume of interest (VOI) was defined via the length of the implant. The VOI was subjected to 3D analysis following the application of an image noise reduction procedure (based on image filtering in 3D) and binarisation. Image processing prior to the analysis was optimised using TeIGen software (Test Image Generator [118], https://mjirik.github.io/teigen). The results were presented in the form of cortical bone porosity:

$$P = \frac{Total\ porosity\ volume}{VOI\ volume}\ [\%]. \tag{11}$$

SEM and elemental analysis

The chemical composition of the bone mineral in the explanted rat femurs was verified by means of energy dispersive X-Ray spectroscopy (EDS) using an EDS SDD EDAX Apollo (EDAX Genesis system) detector on a scanning electron microscope (SEM; Quanta 450 Microscope, FEI, USA) in the high vacuum mode. The histological thin sections were carbon-coated on a K550X (Emitech, USA) sputter coater in an argon atmosphere prior to the analysis. The concentrations of elemental Ca and P and the Ca/P molar ratio were determined aimed at the assessment of changes in the bone mineral Ca/P weight ratio that reflected inflammatory processes. Kourkoumelis et al. [192] have used the EDS method for the evaluation of the Ca/P ratio at different sites in normal and osteoporotic rabbit bones. They proved that EDS provides a suitable analytical method for the *in vitro* quantification of the Ca/P ratio, that it demonstrates a high enough degree of precision for the taking of semiquantitative measurements and that it allows for a better statistical significance for the Ca/P ratio than does error-prone simple composition assessment. 10 measurements were carried out at different locations on the surface of the bone for each of the 8 histological thin sections and for each group of implants.

Vancomycin concentration in blood plasma

Blood samples were taken 7 and 14 days following surgery from the tail vein under light isoflurane anaesthesia (3% isoflurane in O_2) administered via a face mask. The blood samples were centrifuged (3000xg, 10 min) and the plasma samples stored at -80°C. Prior to the analysis, the samples were thawed and the vancomycin was quantified by means of high performance liquid chromatography (HPLC). The solid phase extraction method and HPLC analysis (HPLC on an Agilent 1260 series system equipped with a DAD diode array detector, Agilent Technologies) were employed for the characterisation of the *in vivo* release rates of the vancomycin and its crystalline degradation antibiotically-inactive products [189] from the implanted samples to the bloodstream in order to determine a possible systemic load. The HPLC method is described in an article written by Melichercik et al. [189].

B.17 Evaluation of osseointegration

Animals and operative procedure

All the experiments were carried out according to guidelines for the care and use of experimental animals as approved by the Resort Professional Commission of the CAS for the Approval of Projects with Experiments on Animals (Approved protocol No. 07/2017). The study involved the use of three minipigs (females) aged 30-48 months and with body weights of 90 ± 20 kg. The general anaesthesia of the miniature pigs was induced via the intramuscular injection of a TKX mixture (Tiletamin 2 mg/kg + Zolazepam 2 mg/kg + Ketamin 2 mg/kg + Xylazin 0.4 mg/kg). Six cylindrical samples of 4 mm in diameter and 8 mm in length were implanted under the proximal condyle of the right and left femurs under sterile conditions and guided by the general anaesthesia of the animals (Isoflurane, N_2O, Propofol, Fentanyl, Pancuronium bromide). Six control (CP) and 6 experimental (COLHA, COLHA+V) samples were implanted in each of the three animals for 6 months. All the implants were press-fit inserted (i.e. without a gap between the bone and the implant). The operational procedure was as follows: firstly, a longitudinal skin cut was made followed by a cut across the fascia in the proximal condyle area. The intramuscular septum was opened by means of the introduction of Hohmann bone elevators. The periosteum was removed using a Sauerbruch raspatory. Six holes with dimensions of 3.8 mm in diameter and a length of 10-12 mm were drilled using a surgical drill with continuous cooling via the application of a physiological solution. Once the holes had been prepared and rinsed with the physiological solution, the implants were inserted. The operation space was then cleaned using the physiological solution prior to hypodermis and skin suture, immediately following which X-ray images of the implant sites were taken using a C-arm ARCADIS Varic (Siemens). The animals were treated with ATB (Eficur, Betamox) and a non-steroidal anti-inflammatory drug (Flunixin) during the perioperative period and for the first four days after implantation. The animals were bred under standard conditions according to the rules applicable for the breeding of laboratory animals in the Czech Republic. Six months following implantation, the pigs were sacrificed via exsanguination under deep general anaesthesia conditions and the implants removed and fixed in a 10% formalin solution.

Bone histology

The samples were processed using the same procedure as that applied to the rat femurs (*Appendix B.16*). Sections of the pig femurs were stained using 20% Giemsa's azur eosin methylene blue solution (Merck Millipore, Darmstadt, Germany) and the whole surface of the implants photographed using a bright field microscope with a 10x objective. All the steps applied during the microscopic evaluation complied with ISO 10993-6.

Micro-CT analysis

The micro-CT scanning and image reconstruction procedures were conducted via the same procedure as that applied to the rat femurs. The 3D analysis of the implants was performed by means of CTAn (Bruker, Kontich, Belgium) with the aim of determining the ratio of new bone (RNB) surrounding and penetrating the external surface of the implants. The VOI was set as a hollow cylinder with a border defined by the implant base and the surface of the inner diameter (Fig. 91). The inner space of the samples (aperture for the inner thread) was excluded from the analysis. Image processing (i.e. noise reduction), binarisation and bit-wise operations (i.e. the subtraction of the implant structure from the

bone inside the VOI) were performed prior to the 3D analysis. The ratio of new bone volume was calculated as:

$$RNB = \frac{New\ bone\ volume\ (NB)}{VOI\ volume\ (V) - Implant\ volume\ in\ VOI\ (I)}\ [\%] \quad (12).$$

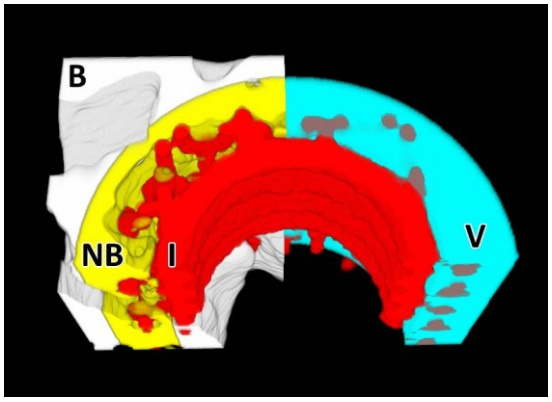

Fig. 91 Definition of the micro-CT regions. The VOI (V) consisted of a hollow cylinder with an outer diameter with the same dimensions as the drilled defect and an inner diameter of that of the implant (I) wall. The bone tissue is denoted as B (white) and the “new bone” inside the VOI as NB (yellow).

Appendix C

Statistical evaluation

The statistical analysis was performed using statistical software (STATGRAPHICS Centurion XVII, StatPoint, USA). The normally distributed numerical data were expressed as the arithmetical mean, SD (standard deviation). The normality of the data was confirmed using the Shapiro-Wilk and χ^2-tests. Outliers were identified via the Grubbs and Dixon tests. Non-normally distributed numerical data were expressed as the median, IQR (interquartile range). For comparative purposes, the data were also presented in the form of box-and-whiskers plots. A box was drawn extending from the lower quartile to the upper quartile of the sample (this interval covered the middle 50% of the values sorted from smallest to largest). A vertical line was drawn at the median and a plus sign was drawn at the sample mean. Whiskers were drawn from the edges of the box to the largest and smallest data values unless the values were situated unusually far from the box. Point symbols outside the whiskers indicated values which were >1.5 times the interquartile range (box width) above or below the box. All the points >3 times the interquartile range above or below the box were termed far outside points and are indicated by point symbols with plus signs superimposed above them. In the case of the presence of outside points, the whiskers were drawn to the largest and smallest data values which did not constitute outside points.

Statistically significant differences were checked for the normally distributed data by means of the parametric analysis of variance (F-test); Student–Newman–Keuls (SNK), and Fisher's least significant difference (LSD) multiple sample comparison tests were employed after confirming the following assumptions: (i) the distribution derived from each of the samples was normal and (ii) the variances of the population of the samples were equal to one another (assumption of homoscedasticity). Homoscedasticity was controlled by means of the Levene's, Bartlett's and Cochran's tests. Nonparametric analysis was conducted when either of the two above-mentioned assumptions were violated, followed by the performance of the Kruskal–Wallis test for multiple comparisons with the subsequent post-hoc test based on the Bonferroni procedure or the Mann–Whitney W-test with *p* value correction. Statistical significance was accepted at $p \leq 0.05$.

References

[1] S. Pina, V.P. Ribeiro, C.F. Marques, F.R. Maia, T.H. Silva, R.L. Reis, J.M. Oliveira, Scaffolding Strategies for Tissue Engineering and Regenerative Medicine Applications, Materials (Basel). 12 (2019) 1824. doi:10.3390/ma12111824.

[2] R. Murugan, S. Ramakrishna, Development of nanocomposites for bone grafting, Compos. Sci. Technol. 65 (2005) 2385–2406. doi:10.1016/J.COMPSCITECH.2005.07.022.

[3] T. Suchý, M. Šupová, P. Sauerová, M. Verdánová, Z.Z. Sucharda, Š. Rýglová, M. Žaloudková, R. Sedláček, M.H.M.H. Kalbáčová, T. Suchy, M. Supova, P. Sauerova, M. Verdanova, Z.Z. Sucharda, S. Ryglova, M. Zaloudkova, R. Sedlacek, M.H. Kalbacova, The effects of different cross-linking conditions on collagen-based nanocomposite scaffolds-an in vitro evaluation using mesenchymal stem cells, Biomed. Mater. 10 (2015) 65008. doi:10.1088/1748-6041/10/6/065008.

[4] J.M. Shapiro, M.L. Oyen, Hydrogel Composite Materials for Tissue Engineering Scaffolds, JOM. 65 (2013) 505–516. doi:10.1007/s11837-013-0575-6.

[5] P. Sauerova, T. Suchy, M. Supova, M. Bartos, J. Klima, J. Juhasova, S. Juhas, T. Kubikova, Z. Tonar, R. Sedlacek, M. Piola, G.B. Fiore, M. Soncini, M. Hubalek Kalbacova, Positive impact of dynamic seeding of mesenchymal stem cells on bone-like biodegradable scaffolds with increased content of calcium phosphate nanoparticles., Mol. Biol. Rep. 46 (2019) 4483–4500. doi:10.1007/s11033-019-04903-7.

[6] W.F. Liu, C.S. Chen, Engineering biomaterials to control cell function, Mater. Today. 8 (2005) 28–35. doi:10.1016/S1369-7021(05)71222-0.

[7] A.J. Wagoner Johnson, B.A. Herschler, A review of the mechanical behavior of CaP and CaP/polymer composites for applications in bone replacement and repair, Acta Biomater. 7 (2011) 16–30. doi:10.1016/J.ACTBIO.2010.07.012.

[8] J. Knychala, N. Bouropoulos, C.J. Catt, O.L. Katsamenis, C.P. Please, B.G. Sengers, Pore geometry regulates early stage human bone marrow cell tissue formation and organisation., Ann. Biomed. Eng. 41 (2013) 917–930. doi:10.1007/s10439-013-0748-z.

[9] J.M. Karp, P.D. Dalton, M.S. Shoichet, Scaffolds for Tissue Engineering, MRS Bull. 28 (2003) 301–306. doi:10.1557/mrs2003.85.

[10] J.M. Kemppainen, S.J. Hollister, Differential effects of designed scaffold permeability on chondrogenesis by chondrocytes and bone marrow stromal cells, Biomaterials. 31 (2010) 279–287. doi:10.1016/J.BIOMATERIALS.2009.09.041.

[11] W.-J. Li, C.T. Laurencin, E.J. Caterson, R.S. Tuan, F.K. Ko, Electrospun nanofibrous structure: A novel scaffold for tissue engineering, J. Biomed. Mater. Res. 60 (2002) 613–621. doi:10.1002/jbm.10167.

[12] W.K. Grier, E.M. Iyoha, B.A.C. Harley, The influence of pore size and stiffness on tenocyte bioactivity and transcriptomic stability in collagen-GAG scaffolds, J. Mech. Behav. Biomed. Mater. 65 (2017) 295–305. doi:10.1016/J.JMBBM.2016.08.034.

[13] A.J. Engler, S. Sen, H.L. Sweeney, D.E. Discher, Matrix Elasticity Directs Stem Cell Lineage Specification, Cell. 126 (2006) 677–689. doi:10.1016/J.CELL.2006.06.044.

[14] J. Glowacki, S. Mizuno, Collagen scaffolds for tissue engineering, Biopolymers. 89 (2008) 338–344. doi:10.1002/bip.20871.

[15] Y. Cheng, D. Ramos, P. Lee, D. Liang, X. Yu, S.G. Kumbar, Collagen functionalized bioactive nanofiber matrices for osteogenic differentiation of mesenchymal stem cells: bone tissue engineering., J. Biomed. Nanotechnol. 10 (2014) 287–298. doi:10.1166/jbn.2014.1753.

[16] P. Feng, P. Wu, C. Gao, Y. Yang, W. Guo, W. Yang, C. Shuai, A Multimaterial Scaffold With Tunable Properties: Toward Bone Tissue Repair, Adv. Sci. 5 (2018) 1700817. doi:10.1002/advs.201700817.

[17] U. Hempel, C. Preissler, S. Vogel, S. Möller, V. Hintze, J. Becher, M. Schnabelrauch, M. Rauner, L.C. Hofbauer, P. Dieter, Artificial extracellular matrices with oversulfated glycosaminoglycan

derivatives promote the differentiation of osteoblast-precursor cells and premature osteoblasts, Biomed Res. Int. 2014 (2014) 938368. doi:10.1155/2014/938368.
[18] C. Jungreuthmayer, S.W. Donahue, M.J. Jaasma, A.A. Al-Munajjed, J. Zanghellini, D.J. Kelly, F.J. O'Brien, A Comparative Study of Shear Stresses in Collagen-Glycosaminoglycan and Calcium Phosphate Scaffolds in Bone Tissue-Engineering Bioreactors, Tissue Eng. Part A. 15 (2008) 1141–1149. doi:10.1089/ten.tea.2008.0204.
[19] Y. Kuboki, H. Takita, D. Kobayashi, E. Tsuruga, M. Inoue, M. Murata, N. Nagai, Y. Dohi, H. Ohgushi, BMP-induced osteogenesis on the surface of hydroxyapatite with geometrically feasible and nonfeasible structures: topology of osteogenesis., J. Biomed. Mater. Res. 39 (1998) 190–199. doi:10.1002/(sici)1097-4636(199802)39:2<190::aid-jbm4>3.0.co;2-k.
[20] C. Shuai, Y. Li, G. Wang, W. Yang, S. Peng, P. Feng, Surface modification of nanodiamond: Toward the dispersion of reinforced phase in poly-l-lactic acid scaffolds, Int. J. Biol. Macromol. 126 (2019) 1116–1124. doi:10.1016/J.IJBIOMAC.2019.01.004.
[21] D. Gupta, J. Venugopal, S. Mitra, V.R. Giri Dev, S. Ramakrishna, Nanostructured biocomposite substrates by electrospinning and electrospraying for the mineralization of osteoblasts, Biomaterials. 30 (2009) 2085–2094. doi:10.1016/J.BIOMATERIALS.2008.12.079.
[22] F. Raiskup, E. Spoerl, Corneal Crosslinking with Riboflavin and Ultraviolet A. I. Principles, Ocul. Surf. 11 (2013) 65–74. doi:10.1016/J.JTOS.2013.01.002.
[23] B.P. Chan, K.-F. So, Photochemical crosslinking improves the physicochemical properties of collagen scaffolds, J. Biomed. Mater. Res. Part A. 75A (2005) 689–701. doi:10.1002/jbm.a.30469.
[24] A.I. Alford, K.M. Kozloff, K.D. Hankenson, Extracellular matrix networks in bone remodeling, Int. J. Biochem. Cell Biol. 65 (2015) 20–31. doi:10.1016/J.BIOCEL.2015.05.008.
[25] J.A. Matthews, G.E. Wnek, D.G. Simpson, G.L. Bowlin, Electrospinning of collagen nanofibers., Biomacromolecules. 3 (2002) 232–238. doi:10.1021/bm015533u.
[26] S. Liao, B. Li, Z. Ma, H. Wei, C. Chan, S. Ramakrishna, Biomimetic electrospun nanofibers for tissue regeneration, Biomed. Mater. 1 (2006) R45–R53. doi:10.1088/1748-6041/1/3/r01.
[27] C.P. Barnes, S.A. Sell, E.D. Boland, D.G. Simpson, G.L. Bowlin, Nanofiber technology: designing the next generation of tissue engineering scaffolds., Adv. Drug Deliv. Rev. 59 (2007) 1413–1433. doi:10.1016/j.addr.2007.04.022.
[28] B.W. Tillman, S.K. Yazdani, S.J. Lee, R.L. Geary, A. Atala, J.J. Yoo, The in vivo stability of electrospun polycaprolactone-collagen scaffolds in vascular reconstruction., Biomaterials. 30 (2009) 583–588. doi:10.1016/j.biomaterials.2008.10.006.
[29] M.J. McClure, S.A. Sell, D.G. Simpson, G.L. Bowlin, Electrospun Polydioxanone, Elastin, and Collagen Vascular Scaffolds: Uniaxial Cyclic Distension, J. Eng. Fiber. Fabr. 4 (2009) 155892500900400200. doi:10.1177/155892500900400204.
[30] W. He, T. Yong, W.E. Teo, Z. Ma, S. Ramakrishna, Fabrication and endothelialization of collagen-blended biodegradable polymer nanofibers: potential vascular graft for blood vessel tissue engineering., Tissue Eng. 11 (2005) 1574–1588. doi:10.1089/ten.2005.11.1574.
[31] S.A. Sell, M.J. McClure, K. Garg, P.S. Wolfe, G.L. Bowlin, Electrospinning of collagen/biopolymers for regenerative medicine and cardiovascular tissue engineering., Adv. Drug Deliv. Rev. 61 (2009) 1007–1019. doi:10.1016/j.addr.2009.07.012.
[32] J. Venugopal, L.L. Ma, T. Yong, S. Ramakrishna, In vitro study of smooth muscle cells on polycaprolactone and collagen nanofibrous matrices., Cell Biol. Int. 29 (2005) 861–867. doi:10.1016/j.cellbi.2005.03.026.
[33] Z.G. Chen, P.W. Wang, B. Wei, X.M. Mo, F.Z. Cui, Electrospun collagen-chitosan nanofiber: a biomimetic extracellular matrix for endothelial cell and smooth muscle cell., Acta Biomater. 6 (2010) 372–382. doi:10.1016/j.actbio.2009.07.024.
[34] K.S. Rho, L. Jeong, G. Lee, B.-M. Seo, Y.J. Park, S.-D. Hong, S. Roh, J.J. Cho, W.H. Park, B.-M. Min, Electrospinning of collagen nanofibers: effects on the behavior of normal human keratinocytes and early-stage wound healing., Biomaterials. 27 (2006) 1452–1461. doi:10.1016/j.biomaterials.2005.08.004.

[35] Š. Rýglová, M. Braun, T. Suchý, Collagen and Its Modifications-Crucial Aspects with Concern to Its Processing and Analysis, Macromol. Mater. Eng. 302 (2017) 1600460. doi:10.1002/mame.201600460.

[36] P. Lukáč, J.M. Hartinger, M. Mlček, M. Popková, T. Suchý, M. Šupová, J. Závora, V. Adámková, H. Benáková, O. Slanař, M. Bartoš, H. Chlup, L. Lambert, T. Grus, A novel gentamicin-releasing wound dressing prepared from freshwater fish Cyprinus carpio collagen cross-linked with carbodiimide, J. Bioact. Compat. Polym. 34 (2019) 246–262. doi:10.1177/0883911519835143.

[37] T. Suchý, M. Šupová, E. Klapková, L. Horný, Š. Rýglová, M. Žaloudková, M. Braun, Z. Sucharda, R. Ballay, J. Veselý, H. Chlup, F. Denk, The Sustainable Release of Vancomycin and Its Degradation Products from Nanostructured Collagen/Hydroxyapatite Composite Layers, J. Pharm. Sci. 105 (2016) 1288–1294. doi:10.1016/S0022-3549(15)00175-6.

[38] R. Krishnan, S. Sundarrajan, S. Ramakrishna, Green Processing of Nanofibers for Regenerative Medicine, Macromol. Mater. Eng. 298 (2013) 1034–1058. doi:10.1002/mame.201200323.

[39] S.J. Kew, J.H. Gwynne, D. Enea, M. Abu-Rub, A. Pandit, D. Zeugolis, R.A. Brooks, N. Rushton, S.M. Best, R.E. Cameron, Regeneration and repair of tendon and ligament tissue using collagen fibre biomaterials., Acta Biomater. 7 (2011) 3237–3247. doi:10.1016/j.actbio.2011.06.002.

[40] T.J. Koob, D.J. Hernandez, Material properties of polymerized NDGA-collagen composite fibers: development of biologically based tendon constructs., Biomaterials. 23 (2002) 203–212. doi:10.1016/s0142-9612(01)00096-5.

[41] K. Mao, J. Liu, X. Lian, Q. Wang, X. Wang, W. Mei, K. Mao, Controlled Release of rhBMP-2 and Vancomycin from nHAC/<I>α</I>-CSH Scaffold for Treatment of Chronic Osteomyelitis, J. Biomater. Tissue Eng. 5 (2015) 294–300. doi:10.1166/jbt.2015.1310.

[42] N. Fleiter, G. Walter, H. Bösebeck, S. Vogt, H. Büchner, W. Hirschberger, R. Hoffmann, Clinical use and safety of a novel gentamicin-releasing resorbable bone graft substitute in the treatment of osteomyelitis/osteitis, Bone Joint Res. 3 (2014) 223–229. doi:10.1302/2046-3758.37.2000301.

[43] T. Suchý, M. Šupová, P. Sauerová, M. Hubálek Kalbáčová, E. Klapková, M. Pokorný, L. Horný, J. Závora, R. Ballay, F. Denk, M. Sojka, L. Vištejnová, Evaluation of collagen/hydroxyapatite electrospun layers loaded with vancomycin, gentamicin and their combination: Comparison of release kinetics, antimicrobial activity and cytocompatibility., Eur. J. Pharm. Biopharm. (2019). doi:10.1016/j.ejpb.2019.04.021.

[44] A. Manchon, J. Prados-Frutos, C. Rueda-Rodriguez, C. Salinas-Goodier, M. Alkhraisat, R. Rojo, A. Rodriguez-Gonzalez, A. Berlanga, E. Lopez-Cabarcos, Antibiotic Release from Calcium Phosphate Materials in Oral and Maxillofacial Surgery. Molecular, Cellular and Pharmaceutical Aspects, Curr. Pharm. Biotechnol. 18 (2017) 52–63. doi:10.2174/1389201018666161114145827.

[45] M.P. Ginebra, T. Traykova, J.A. Planell, Calcium phosphate cements as bone drug delivery systems: A review, J. Control. Release. 113 (2006) 102–110. doi:10.1016/j.jconrel.2006.04.007.

[46] G. Schmidmaier, M. Lucke, B. Wildemann, N.P. Haas, M. Raschke, Prophylaxis and treatment of implant-related infections by antibiotic-coated implants: a review, Injury. 37 (2006) S105-12. doi:10.1016/j.injury.2006.04.016.

[47] S.W.N. Ueng, L.J. Yuan, N. Lee, S.S. Lin, S.J. Liu, E.C. Chan, J.H. Weng, In vivo study of hot compressing molded 50:50 poly (DL-lactide-co-glycolide) antibiotic beads in rabbits, J. Orthop. Res. 20 (2002) 654–661. doi:10.1016/S0736-0266(01)00174-7.

[48] Z. Ruszczak, W. Friess, Collagen as a carrier for on-site delivery of antibacterial drugs, Adv. Drug Deliv. Rev. 55 (2003) 1679–1698. doi:10.1016/j.addr.2003.08.007.

[49] D.J. Stinner, S.P. Noel, W.O. Haggard, J.T. Watson, J.C. Wenke, Local antibiotic delivery using tailorable chitosan sponges: The future of infection control?, J. Orthop. Trauma. 24 (2010) 592–597. doi:10.1097/BOT.0b013e3181ed296c.

[50] B.G. Yu, I.C. Kwon, Y.H. Kim, D.K. Han, K.D. Park, K. Han, S.Y. Jeong, Development of a local antibiotic delivery system using fibrin glue, J. Control. Release. 39 (1996) 65–70. doi:10.1016/0168-3659(95)00139-5.

[51] T. Suchý, M. Šupová, E. Klapková, V. Adamková, J. Závora, M. Žaloudková, Š. Rýglová, R. Ballay, F. Denk, M. Pokorný, P. Sauerová, M. Hubálek Kalbáčová, L. Horný, J. Veselý, T. Voňavková, R. Průša, The release kinetics, antimicrobial activity and cytocompatibility of differently prepared collagen/hydroxyapatite/vancomycin layers: Microstructure vs. nanostructure, Eur. J. Pharm. Sci. 100 (2017) 219–229. doi:10.1016/j.ejps.2017.01.032.

[52] M. Kazemzadeh-Narbat, S. Noordin, B.A. Masri, D.S. Garbuz, C.P. Duncan, R.E.W. Hancock, R. Wang, Drug release and bone growth studies of antimicrobial peptide-loaded calcium phosphate coating on titanium, J. Biomed. Mater. Res. Part B Appl. Biomater. 100B (2012) 1344–1352. doi:10.1002/jbm.b.32701.

[53] C.N. Manning, A.G. Schwartz, W. Liu, J. Xie, N. Havlioglu, S.E. Sakiyama-Elbert, M.J. Silva, Y. Xia, R.H. Gelberman, S. Thomopoulos, Controlled delivery of mesenchymal stem cells and growth factors using a nanofiber scaffold for tendon repair, Acta Biomater. 9 (2013) 6905–6914. doi:10.1016/J.ACTBIO.2013.02.008.

[54] J. Venugopal, S. Ramakrishna, Applications of polymer nanofibers in biomedicine and biotechnology, Appl. Biochem. Biotechnol. 125 (2005) 147–157. doi:10.1385/ABAB:125:3:147.

[55] M. Rampichová, J. Chvojka, M. Buzgo, E. Prosecká, P. Mikeš, L. Vysloužilová, D. Tvrdík, P. Kochová, T. Gregor, D. Lukáš, E. Amler, Elastic three-dimensional poly (ε-caprolactone) nanofibre scaffold enhances migration, proliferation and osteogenic differentiation of mesenchymal stem cells, Cell Prolif. 46 (2013) 23–37. doi:10.1111/cpr.12001.

[56] K. Novotna, M. Zajdlova, T. Suchy, D. Hadraba, F. Lopot, M. Zaloudkova, T.E.L. Douglas, M. Munzarova, M. Juklickova, D. Stranska, D. Kubies, D. Schaubroeck, S. Wille, L. Balcaen, M. Jarosova, H. Kozak, A. Kromka, Z. Svindrych, V. Lisa, K. Balik, L. Bacakova, Polylactide nanofibers with hydroxyapatite as growth substrates for osteoblast-like cells, J. Biomed. Mater. Res. - Part A. 102 (2014). doi:10.1002/jbm.a.35061.

[57] Y. Tokita, A. Okamoto, Hydrolytic degradation of hyaluronic acid, Polym. Degrad. Stab. 48 (1995) 269–273. doi:10.1016/0141-3910(95)00041-J.

[58] M. Yoshikawa, N. Tsuji, T. Toda, H. Ohgushi, Osteogenic effect of hyaluronic acid sodium salt in the pores of a hydroxyapatite scaffold, Mater. Sci. Eng. C. 27 (2007) 220–226. doi:10.1016/J.MSEC.2006.05.014.

[59] C.J. Doillon, C.F. Whyne, S. Brandwein, F.H. Silver, Collagen-based wound dressings: Control of the pore structure and morphology, J. Biomed. Mater. Res. 20 (1986) 1219–1228. doi:10.1002/jbm.820200811.

[60] F.J. O'Brien, B.A. Harley, I. V. Yannas, L. Gibson, Influence of freezing rate on pore structure in freeze-dried collagen-GAG scaffolds, Biomaterials. 25 (2004) 1077–1086. doi:10.1016/S0142-9612(03)00630-6.

[61] Y. Zhu, H. Wu, S. Sun, T. Zhou, J. Wu, Y. Wan, Designed composites for mimicking compressive mechanical properties of articular cartilage matrix, J. Mech. Behav. Biomed. Mater. 36 (2014) 32–46. doi:10.1016/J.JMBBM.2014.04.003.

[62] Y. Zhu, Y. Wan, J. Zhang, D. Yin, W. Cheng, Manufacture of layered collagen/chitosan-polycaprolactone scaffolds with biomimetic microarchitecture, Colloids Surfaces B Biointerfaces. 113 (2014) 352–360. doi:10.1016/J.COLSURFB.2013.09.028.

[63] G. Gorczyca, R. Tylingo, P. Szweda, E. Augustin, M. Sadowska, S. Milewski, Preparation and characterization of genipin cross-linked porous chitosan–collagen–gelatin scaffolds using chitosan–CO2 solution, Carbohydr. Polym. 102 (2014) 901–911. doi:10.1016/J.CARBPOL.2013.10.060.

[64] Y. Elsayed, C. Lekakou, F. Labeed, P. Tomlins, Fabrication and characterisation of biomimetic, electrospun gelatin fibre scaffolds for tunica media-equivalent, tissue engineered vascular grafts, Mater. Sci. Eng. C. 61 (2016) 473–483. doi:10.1016/J.MSEC.2015.12.081.

[65] N. Davidenko, J.J. Campbell, E.S. Thian, C.J. Watson, R.E. Cameron, Collagen–hyaluronic acid scaffolds for adipose tissue engineering, Acta Biomater. 6 (2010) 3957–3968. doi:10.1016/J.ACTBIO.2010.05.005.

[66] G.S. Offeddu, J.C. Ashworth, R.E. Cameron, M.L. Oyen, Structural determinants of hydration,

mechanics and fluid flow in freeze-dried collagen scaffolds, Acta Biomater. 41 (2016) 193–203. doi:10.1016/J.ACTBIO.2016.05.024.
[67] V. Beachley, X. Wen, Fabrication of nanofiber reinforced protein structures for tissue engineering, Mater. Sci. Eng. C. 29 (2009) 2448–2453. doi:10.1016/J.MSEC.2009.07.008.
[68] N. Davidenko, C.F. Schuster, D.V. Bax, N. Raynal, R.W. Farndale, S.M. Best, R.E. Cameron, Control of crosslinking for tailoring collagen-based scaffolds stability and mechanics, Acta Biomater. 25 (2015) 131–142. doi:10.1016/J.ACTBIO.2015.07.034.
[69] X. Wang, Q. Li, X. Hu, L. Ma, C. You, Y. Zheng, H. Sun, C. Han, C. Gao, Fabrication and characterization of poly(l-lactide-co-glycolide) knitted mesh-reinforced collagen–chitosan hybrid scaffolds for dermal tissue engineering, J. Mech. Behav. Biomed. Mater. 8 (2012) 204–215. doi:10.1016/J.JMBBM.2012.01.001.
[70] M.C. Varley, S. Neelakantan, T.W. Clyne, J. Dean, R.A. Brooks, A.E. Markaki, Cell structure, stiffness and permeability of freeze-dried collagen scaffolds in dry and hydrated states, Acta Biomater. 33 (2016) 166–175. doi:10.1016/J.ACTBIO.2016.01.041.
[71] R.J. Kane, H.E. Weiss-Bilka, M.J. Meagher, Y. Liu, J.A. Gargac, G.L. Niebur, D.R. Wagner, R.K. Roeder, Hydroxyapatite reinforced collagen scaffolds with improved architecture and mechanical properties, Acta Biomater. 17 (2015) 16–25. doi:10.1016/J.ACTBIO.2015.01.031.
[72] D. Yin, H. Wu, C. Liu, J. Zhang, T. Zhou, J. Wu, Y. Wan, Fabrication of composition-graded collagen/chitosan–polylactide scaffolds with gradient architecture and properties, React. Funct. Polym. 83 (2014) 98–106. doi:10.1016/J.REACTFUNCTPOLYM.2014.07.017.
[73] M. V. Jose, V. Thomas, D.R. Dean, E. Nyairo, Fabrication and characterization of aligned nanofibrous PLGA/Collagen blends as bone tissue scaffolds, Polymer (Guildf). 50 (2009) 3778–3785. doi:10.1016/J.POLYMER.2009.05.035.
[74] T. Arahira, M. Todo, Variation of mechanical behavior of β-TCP/collagen two phase composite scaffold with mesenchymal stem cell in vitro, J. Mech. Behav. Biomed. Mater. 61 (2016) 464–474. doi:10.1016/J.JMBBM.2016.04.019.
[75] J. Elango, J. Zhang, B. Bao, K. Palaniyandi, S. Wang, W. Wenhui, J.S. Robinson, Rheological, biocompatibility and osteogenesis assessment of fish collagen scaffold for bone tissue engineering, Int. J. Biol. Macromol. 91 (2016) 51–59. doi:10.1016/J.IJBIOMAC.2016.05.067.
[76] R. Tylingo, G. Gorczyca, S. Mania, P. Szweda, S. Milewski, Preparation and characterization of porous scaffolds from chitosan-collagen-gelatin composite, React. Funct. Polym. 103 (2016) 131–140. doi:10.1016/J.REACTFUNCTPOLYM.2016.04.008.
[77] R. Parenteau-Bareil, R. Gauvin, S. Cliche, C. Gariépy, L. Germain, F. Berthod, Comparative study of bovine, porcine and avian collagens for the production of a tissue engineered dermis, Acta Biomater. 7 (2011) 3757–3765. doi:10.1016/J.ACTBIO.2011.06.020.
[78] A. Arora, A. Kothari, D.S. Katti, Pore orientation mediated control of mechanical behavior of scaffolds and its application in cartilage-mimetic scaffold design, J. Mech. Behav. Biomed. Mater. 51 (2015) 169–183. doi:10.1016/J.JMBBM.2015.06.033.
[79] F. Ghorbani, H. Nojehdehian, A. Zamanian, Physicochemical and mechanical properties of freeze cast hydroxyapatite-gelatin scaffolds with dexamethasone loaded PLGA microspheres for hard tissue engineering applications, Mater. Sci. Eng. C. 69 (2016) 208–220. doi:10.1016/J.MSEC.2016.06.079.
[80] E. Jeevithan, R. Jeya Shakila, A. Varatharajakumar, G. Jeyasekaran, D. Sukumar, Physico-functional and mechanical properties of chitosan and calcium salts incorporated fish gelatin scaffolds, Int. J. Biol. Macromol. 60 (2013) 262–267. doi:10.1016/J.IJBIOMAC.2013.06.012.
[81] M. Kim, G.H. Kim, Electrohydrodynamic direct printing of PCL/collagen fibrous scaffolds with a core/shell structure for tissue engineering applications, Chem. Eng. J. 279 (2015) 317–326. doi:10.1016/J.CEJ.2015.05.047.
[82] T. Muthukumar, A. Aravinthan, J. Sharmila, N.S. Kim, J.-H. Kim, Collagen/chitosan porous bone tissue engineering composite scaffold incorporated with Ginseng compound K, Carbohydr. Polym. 152 (2016) 566–574. doi:10.1016/J.CARBPOL.2016.07.003.
[83] H. Cao, M.-M. Chen, Y. Liu, Y.-Y. Liu, Y.-Q. Huang, J.-H. Wang, J.-D. Chen, Q.-Q. Zhang, Fish

collagen-based scaffold containing PLGA microspheres for controlled growth factor delivery in skin tissue engineering, Colloids Surfaces B Biointerfaces. 136 (2015) 1098–1106. doi:10.1016/J.COLSURFB.2015.10.022.
[84] S.-N. Park, J.-C. Park, H.O. Kim, M.J. Song, H. Suh, Characterization of porous collagen/hyaluronic acid scaffold modified by 1-ethyl-3-(3-dimethylaminopropyl)carbodiimide cross-linking, Biomaterials. 23 (2002) 1205–1212. doi:10.1016/S0142-9612(01)00235-6.
[85] E. Prosecká, M. Rampichová, A. Litvinec, Z. Tonar, M. Králíčková, L. Vojtová, P. Kochová, M. Plencner, M. Buzgo, A. Míčková, J. Jančář, E. Amler, Collagen/hydroxyapatite scaffold enriched with polycaprolactone nanofibers, thrombocyte-rich solution and mesenchymal stem cells promotes regeneration in large bone defect in vivo, J. Biomed. Mater. Res. Part A. 103 (2015) 671–682. doi:10.1002/jbm.a.35216.
[86] C.-C. Tsai, R.-N. Huang, H.-W. Sung, H.C. Liang, In vitro evaluation of the genotoxicity of a naturally occurring crosslinking agent (genipin) for biologic tissue fixation, J. Biomed. Mater. Res. 52 (2000) 58–65. doi:10.1002/1097-4636(200010)52:1<58::AID-JBM8>3.0.CO;2-0.
[87] S. Gorgieva, Collagen- vs. Gelatine-Based Biomaterials and Their Biocompatibility: Review and Perspectives, in: V.K.E.-R. Pignatello (Ed.), IntechOpen, Rijeka, 2011: p. Ch. 2. doi:10.5772/24118.
[88] X. Zhang, X. Chen, T. Yang, N. Zhang, L. Dong, S. Ma, X. Liu, M. Zhou, B. Li, The effects of different crossing-linking conditions of genipin on type I collagen scaffolds: an in vitro evaluation, Cell Tissue Bank. 15 (2014) 531–541. doi:10.1007/s10561-014-9423-3.
[89] J.B. Rose, S. Pacelli, A.J. El Haj, H.S. Dua, A. Hopkinson, L.J. White, F.R.A.J. Rose, Gelatin-Based Materials in Ocular Tissue Engineering., Mater. (Basel, Switzerland). 7 (2014) 3106–3135. doi:10.3390/ma7043106.
[90] J.S. Yoo, Y.J. Kim, S.H. Kim, S.H. Choi, Study on genipin: a new alternative natural crosslinking agent for fixing heterograft tissue., Korean J. Thorac. Cardiovasc. Surg. 44 (2011) 197–207. doi:10.5090/kjtcs.2011.44.3.197.
[91] R. Touyama, K. Inoue, Y. Takeda, M. Yatsuzuka, T. Ikumoto, N. Moritome, T. Shingu, T. Yokoi, H. Inouye, Studies on the Blue Pigments Produced from Genipin and Methylamine. II .On the Formation Mechanisms of Brownish-Red Intermediates Leading to the Blue Pigment Formation, Chem. Pharm. Bull. (Tokyo). 42 (1994) 1571–1578. doi:10.1248/cpb.42.1571.
[92] S. Amin Yavari, R. Wauthle, J. van der Stok, A.C. Riemslag, M. Janssen, M. Mulier, J.P. Kruth, J. Schrooten, H. Weinans, A.A. Zadpoor, Fatigue behavior of porous biomaterials manufactured using selective laser melting, Mater. Sci. Eng. C. 33 (2013) 4849–4858. doi:10.1016/J.MSEC.2013.08.006.
[93] S.M. Ahmadi, G. Campoli, S. Amin Yavari, B. Sajadi, R. Wauthle, J. Schrooten, H. Weinans, A.A. Zadpoor, Mechanical behavior of regular open-cell porous biomaterials made of diamond lattice unit cells, J. Mech. Behav. Biomed. Mater. 34 (2014) 106–115. doi:10.1016/J.JMBBM.2014.02.003.
[94] K. Bobe, E. Willbold, I. Morgenthal, O. Andersen, T. Studnitzky, J. Nellesen, W. Tillmann, C. Vogt, K. Vano, F. Witte, In vitro and in vivo evaluation of biodegradable, open-porous scaffolds made of sintered magnesium W4 short fibres, Acta Biomater. 9 (2013) 8611–8623. doi:10.1016/J.ACTBIO.2013.03.035.
[95] A. Sionkowska, J. Skopinska-Wisniewska, M. Gawron, J. Kozlowska, A. Planecka, Chemical and thermal cross-linking of collagen and elastin hydrolysates, Int. J. Biol. Macromol. 47 (2010) 570–577. doi:10.1016/J.IJBIOMAC.2010.08.004.
[96] H. Staroszczyk, K. Sztuka, J. Wolska, A. Wojtasz-Pająk, I. Kołodziejska, Interactions of fish gelatin and chitosan in uncrosslinked and crosslinked with EDC films: FT-IR study, Spectrochim. Acta Part A Mol. Biomol. Spectrosc. 117 (2014) 707–712. doi:10.1016/J.SAA.2013.09.044.
[97] X.H. Wang, D.P. Li, W.J. Wang, Q.L. Feng, F.Z. Cui, Y.X. Xu, X.H. Song, M. van der Werf, Crosslinked collagen/chitosan matrix for artificial livers, Biomaterials. 24 (2003) 3213–3220. doi:10.1016/S0142-9612(03)00170-4.
[98] C. Chaubaroux, E. Vrana, C. Debry, P. Schaaf, B. Senger, J.-C. Voegel, Y. Haikel, C. Ringwald, J.

Hemmerlé, P. Lavalle, F. Boulmedais, Collagen-Based Fibrillar Multilayer Films Cross-Linked by a Natural Agent, Biomacromolecules. 13 (2012) 2128–2135. doi:10.1021/bm300529a.
[99] S.-S. Kim, K.-M. Ahn, M.S. Park, J.-H. Lee, C.Y. Choi, B.-S. Kim, A poly(lactide-co-glycolide)/hydroxyapatite composite scaffold with enhanced osteoconductivity, J. Biomed. Mater. Res. Part A. 80A (2007) 206–215. doi:10.1002/jbm.a.30836.
[100] Y. Wang, P.E. Tomlins, A.G.A. Coombes, M. Rides, On the Determination of Darcy Permeability Coefficients for a Microporous Tissue Scaffold, Tissue Eng. Part C Methods. 16 (2009) 281–289. doi:10.1089/ten.tec.2009.0116.
[101] M.M. Villa, L. Wang, J. Huang, D.W. Rowe, M. Wei, Bone tissue engineering with a collagen–hydroxyapatite scaffold and culture expanded bone marrow stromal cells, J. Biomed. Mater. Res. Part B Appl. Biomater. 103 (2015) 243–253. doi:10.1002/jbm.b.33225.
[102] M.J. Grimm, J.L. Williams, Measurements of permeability in human calcaneal trabecular bone, J. Biomech. 30 (1997) 743–745. doi:10.1016/S0021-9290(97)00016-X.
[103] D. Wen, C. Androjna, A. Vasanji, J. Belovich, R.J. Midura, Lipids and Collagen Matrix Restrict the Hydraulic Permeability Within the Porous Compartment of Adult Cortical Bone, Ann. Biomed. Eng. 38 (2010) 558–569. doi:10.1007/s10439-009-9858-z.
[104] A. Gautieri, S. Vesentini, A. Redaelli, M.J. Buehler, Hierarchical Structure and Nanomechanics of Collagen Microfibrils from the Atomistic Scale Up, Nano Lett. 11 (2011) 757–766. doi:10.1021/nl103943u.
[105] P. Fratzl, Collagen: Structure and Mechanics, an Introduction BT - Collagen: Structure and Mechanics, in: P. Fratzl (Ed.), Springer US, Boston, MA, 2008: pp. 1–13. doi:10.1007/978-0-387-73906-9_1.
[106] P. Kasten, I. Beyen, P. Niemeyer, R. Luginbühl, M. Bohner, W. Richter, Porosity and pore size of β-tricalcium phosphate scaffold can influence protein production and osteogenic differentiation of human mesenchymal stem cells: An in vitro and in vivo study, Acta Biomater. 4 (2008) 1904–1915. doi:10.1016/J.ACTBIO.2008.05.017.
[107] N.J. Walters, E. Gentleman, Evolving insights in cell–matrix interactions: Elucidating how non-soluble properties of the extracellular niche direct stem cell fate, Acta Biomater. 11 (2015) 3–16. doi:10.1016/J.ACTBIO.2014.09.038.
[108] K. Anselme, L. Ploux, A. Ponche, Cell/Material Interfaces: Influence of Surface Chemistry and Surface Topography on Cell Adhesion, J. Adhes. Sci. Technol. 24 (2010) 831–852. doi:10.1163/016942409X12598231568186.
[109] P. Dutta, S. Hajra, D.K. Chattoraj, Binding of water and solute to protein-mixture and protein-coated alumina., Indian J. Biochem. Biophys. 34 (1997) 449–460.
[110] B. Feng, J. Chen, X. Zhang, Interaction of calcium and phosphate in apatite coating on titanium with serum albumin, Biomaterials. 23 (2002) 2499–2507. doi:10.1016/S0142-9612(01)00384-2.
[111] T. Mygind, M. Stiehler, A. Baatrup, H. Li, X. Zou, A. Flyvbjerg, M. Kassem, C. Bünger, Mesenchymal stem cell ingrowth and differentiation on coralline hydroxyapatite scaffolds, Biomaterials. 28 (2007) 1036–1047. doi:10.1016/J.BIOMATERIALS.2006.10.003.
[112] F.A. Akin, H. Zreiqat, S. Jordan, M.B.J. Wijesundara, L. Hanley, Preparation and analysis of macroporous TiO2 films on Ti surfaces for bone–tissue implants, J. Biomed. Mater. Res. 57 (2001) 588–596. doi:10.1002/1097-4636(20011215)57:4<588::AID-JBM1206>3.0.CO;2-Y.
[113] D.M.L. Cooper, J.R. Matyas, M.A. Katzenberg, B. Hallgrimsson, Comparison of Microcomputed Tomographic and Microradiographic Measurements of Cortical Bone Porosity, Calcif. Tissue Int. 74 (2004) 437–447. doi:10.1007/s00223-003-0071-z.
[114] T.M. Keaveny, E.F. Morgan, G.L. Niebur, O.C. Yeh, Biomechanics of Trabecular Bone, Annu. Rev. Biomed. Eng. 3 (2001) 307–333. doi:10.1146/annurev.bioeng.3.1.307.
[115] T. Kokubo, H. Takadama, How useful is SBF in predicting in vivo bone bioactivity?, Biomaterials. 27 (2006) 2907–2915. doi:10.1016/J.BIOMATERIALS.2006.01.017.
[116] M. Bartoš, T. Suchý, R. Foltán, Note on the use of different approaches to determine the pore sizes of tissue engineering scaffolds: what do we measure?, Biomed. Eng. Online. 17 (2018) 110. doi:10.1186/s12938-018-0543-z.

[117] M. Bartos, T. Suchy, Z. Tonar, R. Foltan, M.H. Kalbacova, Micro-CT in tissue engineering scaffolds designed for bone regeneration: principles and applications, Ceramics-Silikáty. 62 (2018) 194–199. doi:10.13168/cs.2018.0012.
[118] M. Jiřík, M. Bartoš, P. Tomášek, A. Malečková, T.T. Kural, J. Horáková, D. Lukáš, T. Suchý, P. Kochová, M. Hubálek Kalbáčová, M. Králíčková, Z.Z. Tonar, M. Jirik, M. Bartos, P. Tomasek, A. Maleckova, T.T. Kural, J. Horakova, D. Lukas, T. Suchy, P. Kochova, M.H. Kalbacova, M. Kralickova, Z.Z. Tonar, Generating standardized image data for testing and calibrating quantification of volumes, surfaces, lengths, and object counts in fibrous and porous materials using X-ray microtomography, Microsc. Res. Tech. 81 (2018) 551–568. doi:10.1002/jemt.23011.
[119] T. Kubíková, M. Bartoš, Š. Juhas, T. Suchý, P. Sauerová, M. Hubálek-Kalbáčová, Z. Tonar, Comparison of ground sections, paraffin sections and micro-CT imaging of bone from the epiphysis of the porcine femur for morphometric evaluation, Ann. Anat. - Anat. Anzeiger. 220 (2018) 85–96. doi:10.1016/j.aanat.2018.07.004.
[120] R.A. Waeiss, T.C. Negrini, R.A. Arthur, M.C. Bottino, Antimicrobial effects of drug-containing electrospun matrices on osteomyelitis-associated pathogens, J. Oral Maxillofac. Surg. 72 (2014) 1310–1319. doi:10.1016/j.joms.2014.01.007.
[121] D.W.-C. Chen, J.-Y. Liao, S.-J. Liu, E.-C. Chan, Novel biodegradable sandwich-structured nanofibrous drug-eluting membranes for repair of infected wounds: An in vitro and in vivo study, Int. J. Nanomedicine. 7 (2012) 763–771. doi:10.2147/IJN.S29119.
[122] D.W. Chen, Y.-H. Hsu, J.-Y. Liao, S.-J. Liu, J.-K. Chen, S.W.-N. Ueng, Sustainable release of vancomycin, gentamicin and lidocaine from novel electrospun sandwich-structured PLGA/collagen nanofibrous membranes, Int. J. Pharm. 430 (2012) 335–341. doi:10.1016/j.ijpharm.2012.04.010.
[123] C.H. Jang, Y.B. Cho, Y.S. Jang, M.S. Kim, G.H. Kim, Antibacterial effect of electrospun polycaprolactone/polyethylene oxide/vancomycin nanofiber mat for prevention of periprosthetic infection and biofilm formation, Int. J. Pediatr. Otorhinolaryngol. 79 (2015) 1299–1305. doi:10.1016/j.ijporl.2015.05.037.
[124] L. Zhang, J. Yan, Z. Yin, C. Tang, Y. Guo, D. Li, B. Wei, Y. Xu, Q. Gu, L. Wang, Electrospun vancomycin-loaded coating on titanium implants for the prevention of implant-associated infections, Int. J. Nanomedicine. 9 (2014) 3027–3036. doi:10.2147/IJN.S63991.
[125] Y.-H. Hsu, D.W.-C. Chen, C.-D. Tai, Y.-C. Chou, S.-J. Liu, S.W.-N. Ueng, E.-C. Chan, Biodegradable drug-eluting nanofiber-enveloped implants for sustained release of high bactericidal concentrations of vancomycin and ceftazidime: in vitro and in vivo studies, Int. J. Nanomedicine. 9 (2014) 4347–4355. doi:10.2147/IJN.S66526.
[126] Y.-C. Chou, Y.-S. Cheng, Y.-H. Hsu, Y.-H. Yu, S.-J. Liu, A bio-artificial poly([D,L]-lactide-co-glycolide) drug-eluting nanofibrous periosteum for segmental long bone open fractures with significant periosteal stripping injuries, Int. J. Nanomedicine. 11 (2016) 941–953. doi:10.2147/IJN.S99791.
[127] F. Ordikhani, M. Dehghani, A. Simchi, Antibiotic-loaded chitosan--Laponite films for local drug delivery by titanium implants: cell proliferation and drug release studies, J. Mater. Sci. Mater. Med. 26 (2015) 269. doi:10.1007/s10856-015-5606-0.
[128] F. Ordikhani, E. Tamjid, A. Simchi, Characterization and antibacterial performance of electrodeposited chitosan–vancomycin composite coatings for prevention of implant-associated infections, Mater. Sci. Eng. C. 41 (2014) 240–248. doi:10.1016/j.msec.2014.04.036.
[129] C.-C. Yang, C.-C. Lin, J.-W. Liao, S.-K. Yen, Vancomycin-chitosan composite deposited on post porous hydroxyapatite coated Ti6Al4V implant for drug controlled release, Mater. Sci. Eng. C. 33 (2013) 2203–2212. doi:10.1016/J.MSEC.2013.01.038.
[130] J. Tu, M. Yu, Y. Lu, K. Cheng, W. Weng, J. Lin, H. Wang, P. Du, G. Han, Preparation and antibiotic drug release of mineralized collagen coatings on titanium, J. Mater. Sci. Mater. Med. 23 (2012) 2413–2423. doi:10.1007/s10856-012-4692-5.
[131] Z. Kong, M. Yu, K. Cheng, W. Weng, H. Wang, J. Lin, P. Du, G. Han, Incorporation of chitosan nanospheres into thin mineralized collagen coatings for improving the antibacterial effect,

Colloids Surfaces B Biointerfaces. 111 (2013) 536–541. https://www.sciencedirect.com/science/article/pii/S0927776513004426 (accessed January 8, 2020).
[132] A. Rogina, Electrospinning process: Versatile preparation method for biodegradable and natural polymers and biocomposite systems applied in tissue engineering and drug delivery, Appl. Surf. Sci. 296 (2014) 221–230. doi:10.1016/J.APSUSC.2014.01.098.
[133] K. Garg, G.L. Bowlin, Electrospinning jets and nanofibrous structures., Biomicrofluidics. 5 (2011) 13403. doi:10.1063/1.3567097.
[134] S.-H. Tan, R. Inai, M. Kotaki, S. Ramakrishna, Systematic parameter study for ultra-fine fiber fabrication via electrospinning process, Polymer (Guildf). 46 (2005) 6128–6134. doi:10.1016/J.POLYMER.2005.05.068.
[135] D.I. Zeugolis, S.T. Khew, E.S.Y. Yew, A.K. Ekaputra, Y.W. Tong, L.-Y.L. Yung, D.W. Hutmacher, C. Sheppard, M. Raghunath, Electro-spinning of pure collagen nano-fibres – Just an expensive way to make gelatin?, Biomaterials. 29 (2008) 2293–2305. doi:10.1016/J.BIOMATERIALS.2008.02.009.
[136] J. Bürck, S. Heissler, U. Geckle, M.F. Ardakani, R. Schneider, A.S. Ulrich, M. Kazanci, Resemblance of Electrospun Collagen Nanofibers to Their Native Structure, Langmuir. 29 (2013) 1562–1572. doi:10.1021/la3033258.
[137] S. Nalinanon, S. Benjakul, W. Visessanguan, H. Kishimura, Use of pepsin for collagen extraction from the skin of bigeye snapper (Priacanthus tayenus), Food Chem. 104 (2007) 593–601. doi:10.1016/J.FOODCHEM.2006.12.035.
[138] K.J. Payne, A. Veis, Fourier transform IR spectroscopy of collagen and gelatin solutions: deconvolution of the amide I band for conformational studies., Biopolymers. 27 (1988) 1749–1760. doi:10.1002/bip.360271105.
[139] D.A. Prystupa, A.M. Donald, Infrared study of gelatin conformations in the gel and sol states, Polym. Gels Networks. 4 (1996) 87–110. doi:10.1016/0966-7822(96)00003-2.
[140] L.H. Olde Damink, P.J. Dijkstra, M.J. van Luyn, P.B. van Wachem, P. Nieuwenhuis, J. Feijen, Cross-linking of dermal sheep collagen using a water-soluble carbodiimide., Biomaterials. 17 (1996) 765–773. doi:10.1016/0142-9612(96)81413-x.
[141] J. Kužma, L. Horný, T. Suchý, M. Šupová, Z. Sucharda, Electrospun Collagen Variability Characterized by Tensile Testing, in: J. Henriques, N. Neves, P. de Carvalho (Eds.), XV Mediterr. Conf. Med. Biol. Eng. Comput. -- MEDICON 2019, Springer International Publishing, Cham, 2020: pp. 1231–1238.
[142] H. Demiray, A note on the elasticity of soft biological tissues, J. Biomech. 5 (1972) 309–311. doi:10.1016/0021-9290(72)90047-4.
[143] O.S. Rabotyagova, P. Cebe, D.L. Kaplan, Collagen Structural Hierarchy and Susceptibility to Degradation by Ultraviolet Radiation, Mater. Sci. Eng. C. Mater. Biol. Appl. 28 (2008) 1420–1429. doi:10.1016/j.msec.2008.03.012.
[144] N.P. Camacho, P. West, P.A. Torzilli, R. Mendelsohn, FTIR microscopic imaging of collagen and proteoglycan in bovine cartilage., Biopolymers. 62 (2001) 1–8. doi:10.1002/1097-0282(2001)62:1<1::AID-BIP10>3.0.CO;2-O.
[145] L. Frommelt, Principles of systemic antimicrobial therapy in foreign material associated infection in bone tissue, with special focus on periprosthetic infection, Injury. 37 (2006) S87–S94. doi:10.1016/J.INJURY.2006.04.014.
[146] M.B. Nair, J.D. Kretlow, A.G. Mikos, F.K. Kasper, Infection and tissue engineering in segmental bone defects — a mini review, Curr. Opin. Biotechnol. 22 (2011) 721–725. doi:10.1016/J.COPBIO.2011.02.005.
[147] A. Simchi, E. Tamjid, F. Pishbin, A.R. Boccaccini, Recent progress in inorganic and composite coatings with bactericidal capability for orthopaedic applications, Nanomedicine Nanotechnology, Biol. Med. 7 (2011) 22–39. doi:10.1016/J.NANO.2010.10.005.
[148] M.N. Rahaman, B.S. Bal, W. Huang, Review: Emerging developments in the use of bioactive glasses for treating infected prosthetic joints, Mater. Sci. Eng. C. 41 (2014) 224–231.

doi:10.1016/J.MSEC.2014.04.055.
[149] H.W. Buchholz, H. Engelbrecht, Depot effects of various antibiotics mixed with Palacos resins | Uber die Depotwirkung einiger Antibiotica bei Vermischung mit dem Kunstharz Palacos., Chirurg. 41 (1970) 511–515.
[150] J.A. Inzana, E.M. Schwarz, S.L. Kates, H.A. Awad, Biomaterials approaches to treating implant-associated osteomyelitis, Elsevier, 2016. doi:10.1016/j.biomaterials.2015.12.012.
[151] K. Garvin, C. Feschuk, Polylactide-polyglycolide antibiotic implants., Clin. Orthop. Relat. Res. (2005) 105–110. doi:10.1097/01.blo.0000175720.99118.fe.
[152] B. Kankilic, E. Bayramli, E. Kilic, S. Dağdeviren, F. Korkusuz, Vancomycin containing PLLA/β-TCP controls MRSA in vitro, Clin. Orthop. Relat. Res. 469 (2011) 3222–3228. doi:10.1007/s11999-011-2082-9.
[153] İ. Gürsel, F. Korkusuz, F. Türesin, N. Gürdal Alaeddinoğlu, V. Hasırcı, I. Gursel, F. Korkusuz, F. Turesin, N.G. Alaeddinoglu, V. Hasirci, In vivo application of biodegradable controlled antibiotic release systems for the treatment of implant-related osteomyelitis., Biomaterials. 22 (2001) 73–80. doi:10.1016/s0142-9612(00)00170-8.
[154] S.-J. Liu, S.W.-N. Ueng, S.-S. Lin, E.-C. Chan, In vivo release of vancomycin from biodegradable beads, J. Biomed. Mater. Res. 63 (2002) 807–813. doi:10.1002/jbm.10406.
[155] K. Hirose, A. Marui, Y. Arai, T. Nomura, S. Inoue, K. Kaneda, T. Kamitani, M. Fujita, M. Mitsuyama, Y. Tabata, M. Komeda, Y. Tabata, M. Komeda, Sustained-release vancomycin sheet may help to prevent prosthetic graft methicillin-resistant Staphylococcus aureus infection, J. Vasc. Surg. 44 (2006) 377–382. https://www.sciencedirect.com/science/article/pii/S0741521406006331 (accessed January 8, 2020).
[156] U. Posadowska, M. Brzychczy-Wloch, E. Pamula, Injectable gellan gum-based nanoparticles-loaded system for the local delivery of vancomycin in osteomyelitis treatment, J. Mater. Sci. Mater. Med. 27 (2016) 1–9. doi:10.1007/s10856-015-5604-2.
[157] D.-W. Hong, P.-L. Lai, K.-L. Ku, Z.-T. Lai, I.-M. Chu, Biodegradable in situ gel-forming controlled vancomycin delivery system based on a thermosensitive mPEG-PLCPPA hydrogel, Polym. Degrad. Stab. 98 (2013) 1578–1585. doi:10.1016/j.polymdegradstab.2013.06.027.
[158] S.B. Adams Jr., M.F. Shamji, D.L. Nettles, P. Hwang, L.A. Setton, Sustained release of antibiotics from injectable and thermally responsive polypeptide depots, J. Biomed. Mater. Res. - Part B Appl. Biomater. 90 B (2009) 67–74. doi:10.1002/jbm.b.31254.
[159] F. Ordikhani, M. Dehghani, A. Simchi, Antibiotic-loaded chitosan–Laponite films for local drug delivery by titanium implants: cell proliferation and drug release studies, J. Mater. Sci. Mater. Med. 26 (2015). doi:10.1007/s10856-015-5606-0.
[160] J. Raphel, M. Holodniy, S.B.S.B. Goodman, S.C.S.C. Heilshorn, Multifunctional coatings to simultaneously promote osseointegration and prevent infection of orthopaedic implants, Biomaterials. 84 (2016) 301–314. doi:10.1016/j.biomaterials.2016.01.016.
[161] C. Makarov, I. Gotman, S. Radin, P. Ducheyne, E.Y. Gutmanas, Vancomycin release from bioresorbable calcium phosphate-polymer composites with high ceramic volume fractions, J. Mater. Sci. 45 (2010) 6320–6324. doi:10.1007/s10853-010-4444-1.
[162] T. Fang, J. Wen, J. Zhou, Z. Shao, J. Dong, Poly (ε-caprolactone) coating delays vancomycin delivery from porous chitosan/β-tricalcium phosphate composites, J. Biomed. Mater. Res. - Part B Appl. Biomater. 100 B (2012) 1803–1811. doi:10.1002/jbm.b.32747.
[163] O.S. Kluin, H.C. van der Mei, H.J. Busscher, D. Neut, A surface-eroding antibiotic delivery system based on poly-(trimethylene carbonate), Biomaterials. 30 (2009) 4738–4742. doi:10.1016/j.biomaterials.2009.05.012.
[164] K.C. Harth, M.J. Rosen, T.R. Thatiparti, M.R. Jacobs, I. Halaweish, S. Bajaksouzian, J. Furlan, H.A. Von Recum, Antibiotic-releasing mesh coating to reduce prosthetic sepsis: An in vivo study, J. Surg. Res. 163 (2010) 337–343. doi:10.1016/j.jss.2010.03.065.
[165] Q. Yao, P. Nooeaid, J.A. Roether, Y. Dong, Q. Zhang, A.R. Boccaccini, Bioglass®-based scaffolds incorporating polycaprolactone and chitosan coatings for controlled vancomycin delivery,

Ceram. Int. 39 (2013) 7517–7522. doi:10.1016/j.ceramint.2013.03.002.
[166] S.P. Noel, H.S. Courtney, J.D. Bumgardner, W.O. Haggard, Chitosan sponges to locally deliver amikacin and vancomycin: A pilot in vitro evaluation, Clin. Orthop. Relat. Res. 468 (2010) 2074–2080. doi:10.1007/s11999-010-1324-6.
[167] J.-C. Ruiz, C. Alvarez-Lorenzo, P. Taboada, G. Burillo, E. Bucio, K. De Prijck, H.J. Nelis, T. Coenye, A. Concheiro, Polypropylene grafted with smart polymers (PNIPAAm/PAAc) for loading and controlled release of vancomycin, Eur. J. Pharm. Biopharm. 70 (2008) 467–477. doi:10.1016/j.ejpb.2008.05.020.
[168] S. Leprêtre, F. Chai, J.-C. Hornez, G. Vermet, C. Neut, M. Descamps, H.F. Hildebrand, B. Martel, Prolonged local antibiotics delivery from hydroxyapatite functionalised with cyclodextrin polymers, Biomaterials. 30 (2009) 6086–6093. doi:10.1016/j.biomaterials.2009.07.045.
[169] E. Jean-Baptiste, N. Blanchemain, B. Martel, C. Neut, H.F. Hildebrand, S. Haulon, Safety, healing, and efficacy of vascular prostheses coated with hydroxypropyl-β-cyclodextrin polymer: Experimental in vitro and animal studies, Eur. J. Vasc. Endovasc. Surg. 43 (2012) 188–197. doi:10.1016/j.ejvs.2011.10.017.
[170] B.M. Malyshev, R.L. Salganik, The strength of adhesive joints using the theory of cracks, Int. J. Fract. 26 (1984) 261–275. doi:10.1007/BF00962959.
[171] J.W. Gigantelli, J. Torres Gomez, M.S. Osato, In vitro susceptibilities of ocular Bacillus cereus isolates to clindamycin, gentamicin, and vancomycin alone or in combination., Antimicrob. Agents Chemother. 35 (1991) 201 LP – 202. doi:10.1128/AAC.35.1.201.
[172] C. Watanakunakorn, J.C. Tisone, Synergism Between Vancomycin and Gentamicin or Tobramycin for Methicillin-Susceptible and Methicillin-Resistant Staphylococcus aureus Strains, Antimicrob. Agents Chemother. 22 (1982) 903 LP – 905. doi:10.1128/AAC.22.5.903.
[173] A. Bigi, G. Cojazzi, S. Panzavolta, A. Ripamonti, N. Roveri, M. Romanello, K.N. Suarez, L. Moro, Chemical and structural characterization of the mineral phase from cortical and trabecular bone, J. Inorg. Biochem. 68 (1997) 45–51. doi:10.1016/S0162-0134(97)00007-X.
[174] J.D. Termine, E.D. Eanes, D.J. Greenfield, M.U. Nylen, R.A. Harper, Hydrazine-deproteinated bone mineral, Calcif. Tissue Res. 12 (1973) 73–90. doi:10.1007/BF02013723.
[175] T. Tang, H. Ao, S. Yang, Y. Wang, W. Lin, Z. Yu, Y. Yang, In vivo evaluation of the anti-infection potential of gentamicin-loaded nanotubes on titania implants, Int. J. Nanomedicine. (2016) 2223. doi:10.2147/IJN.S102752.
[176] J. Zhou, X.G. Zhou, J.W. Wang, H. Zhou, J. Dong, Treatment of osteomyelitis defects by a vancomycin-loaded gelatin/β-tricalcium phosphate composite scaffold, Bone Joint Res. 7 (2018) 46–57. doi:10.1302/2046-3758.71.BJR-2017-0129.R2.
[177] S. Zaichick, V. Zaichick, Neutron activation analysis of Ca, Cl, Mg, Na, and P content in human bone affected by osteomyelitis or osteogenic sarcoma, J. Radioanal. Nucl. Chem. 293 (2012) 241–246. doi:10.1007/s10967-012-1645-x.
[178] E. Fiore, M. Levi, M. Gianesella, C. Benazzi, M. Morgante, A. Beltrame, C. Vaccaro, A. Gentile, Epiphysitis in fattening bulls: Radiological and pathologic findings, Large Anim. Rev. 22 (2016) 43–45.
[179] B. Henderson, S.P. Nair, Hard labour: bacterial infection of the skeleton., Trends Microbiol. 11 (2003) 570–577.
[180] R.A. Brady, J.G. Leid, J.H. Calhoun, J.W. Costerton, M.E. Shirtliff, Osteomyelitis and the role of biofilms in chronic infection, FEMS Immunol. Med. Microbiol. 52 (2008) 13–22. doi:10.1111/j.1574-695X.2007.00357.x.
[181] K.A. Esmonde-White, F.W.L. Esmonde-White, C.M. Holmes, M.D. Morris, B.J. Roessler, Alterations to Bone Mineral Composition as an Early Indication of Osteomyelitis in the Diabetic Foot, Diabetes Care. 36 (2013) 3652–3654. doi:10.2337/dc13-0510.
[182] X. Lian, H. Liu, X. Wang, S. Xu, F. Cui, X. Bai, Antibacterial and biocompatible properties of vancomycin-loaded nano-hydroxyapatite/collagen/poly (lactic acid) bone substitute, Prog. Nat. Sci. Mater. Int. 23 (2013) 549–556. doi:10.1016/j.pnsc.2013.11.003.

[183] C. Loc-Carrillo, C. Wang, A. Canden, M. Burr, J. Agarwal, Local Intramedullary Delivery of Vancomycin Can Prevent the Development of Long Bone Staphylococcus aureus Infection, PLoS One. 11 (2016) e0160187. doi:10.1371/journal.pone.0160187.
[184] R. Murugan, S. Ramakrishna, K. Panduranga Rao, Nanoporous hydroxy-carbonate apatite scaffold made of natural bone, Mater. Lett. 60 (2006) 2844–2847. doi:10.1016/J.MATLET.2006.01.104.
[185] M. Jackson, L.-P. Choo, P.H. Watson, W.C. Halliday, H.H. Mantsch, Beware of connective tissue proteins: Assignment and implications of collagen absorptions in infrared spectra of human tissues, Biochim. Biophys. Acta - Mol. Basis Dis. 1270 (1995) 1–6. doi:10.1016/0925-4439(94)00056-V.
[186] A. Pielesz, Temperature-dependent FTIR spectra of collagen and protective effect of partially hydrolysed fucoidan, Spectrochim. Acta Part A Mol. Biomol. Spectrosc. 118 (2014) 287–293. doi:10.1016/J.SAA.2013.08.056.
[187] T. Suchý, M. Šupová, M. Bartoš, R. Sedláček, M. Piola, M. Soncini, G.B. Fiore, P. Sauerová, M.H. Kalbáčová, Dry versus hydrated collagen scaffolds: are dry states representative of hydrated states?, J. Mater. Sci. Mater. Med. 29 (2018) 20. doi:10.1007/s10856-017-6024-2.
[188] J. Kozlowska, A. Sionkowska, Effects of different crosslinking methods on the properties of collagen-calcium phosphate composite materials., Int. J. Biol. Macromol. 74 (2015) 397–403. doi:10.1016/j.ijbiomac.2014.12.023.
[189] P. Melichercik, E. Klapkova, I. Landor, T. Judl, M. Sibek, D. Jahoda, The effect of Vancomycin degradation products in the topical treatment of osteomyelitis, Bratislava Med. J. 115 (2014) 796–799. doi:10.4149/BLL_2014_154.
[190] C.Z. Cannon, G.E. Kissling, D.R. Goulding, A.P. King-Herbert, T. Blankenship-Paris, Analgesic effects of tramadol, carprofen or multimodal analgesia in rats undergoing ventral laparotomy, Lab Anim. (NY). 40 (2011) 85–93. doi:10.1038/laban0311-85.
[191] V. Babuska, O. Moztarzadeh, T. Kubikova, A. Moztarzadeh, D. Hrusak, Z. Tonar, Evaluating the osseointegration of nanostructured titanium implants in animal models: Current experimental methods and perspectives (Review), Biointerphases. 11 (2016) 030801. doi:10.1116/1.4958793.
[192] N. Kourkoumelis, I. Balatsoukas, M. Tzaphlidou, Ca/P concentration ratio at different sites of normal and osteoporotic rabbit bones evaluated by Auger and energy dispersive X-ray spectroscopy, J. Biol. Phys. 38 (2012) 279–291. doi:10.1007/s10867-011-9247-3.

List of figures

Fig. 14 Energy absorption efficiency of the scaffolds in the dry and hydrated (24 and 48 h) states (median, IQR). * denotes statistically significant differences (Mann–Whitney, *0.05*, *n=6*) between different states (left) and different samples (right).

Fig. 12 Micro-CT visualisation of the 8 types of scaffolds in the dry state. Scale bar 1 mm.

Fig. 13 Pore size, closed porosity (CP) and open porosity (OP) of the composite scaffolds in the dry state measured employing micro-CT 3D analysis. All the values exhibited statistically significant differences except those values designated by the symbol "o" (Mann–Whitney, *0.05*, *n=3*).

Fig. 14 3D visualisations of sections of scaffold specimen in the same position (type 3) in the dry state and at different time intervals following initial hydration. The inner structures of the scaffolds are visible including the pore walls, pore spaces and bCaP particles (higher X-ray density). Increased scaffold structure thickness can be observed as a result of hydration with an X-ray contrast agent, probably due to collagen swelling. Scale bar 500 μm.

Fig. 15 The pore size, closed porosity (CP) and open porosity (OP) [%] of the composite scaffolds in the dry state and hydrated for 4, 8 and 24 h measured by means of micro-CT 3D analysis. All the values exhibit statistically significant differences except those values designated by the symbol "o" (Mann-Whitney, *0.05*, *n=3*).

Fig. 16 Permeability after 5 min hydration (0 h) and after 4, 8 and 24 h (arithmetical mean, standard deviation). * denotes statistically significant differences (Mann-Whitney, *0.05*, *n=6-11*) between different periods (left) and different samples (right).

Fig. 17 The mass loss of the scaffolds following 24, 48 and 576 (24 days) hours of immersion in α MEM. * denotes statistically significant differences (Mann-Whitney, *0.05*, *n=3*) between different states (left) and different samples (right).

Fig. 18 The swelling ratios of the scaffolds following 24, 48 and 576 (24 days) hours of immersion in α MEM. * denotes statistically significant differences (Mann–Whitney, *0.05*, *n=3*) between different states (left) and different samples (right).

Fig. 19 Left: the mass loss of the scaffolds after 1 hour of collagenase treatment and their comparison with non-cross-linked collagen (NC). * denotes statistically significant differences (Mann-Whitney, *0.05*) between the wt% collagen medians. Right: comparison of the ratio of integral absorbances PDLLA/COL and bCaP/COL of the original scaffolds and then following 1 h of collagenase treatment. * denotes statistically significant differences (Mann-Whitney, *0.05*, *n=4*) between the medians prior to and following collagenase degradation.

Fig. 20 SEM images of the original collagen scaffolds and those immersed in simulated body fluid (SBF) for 7 and 14 days.

Fig. 21 SEM images of the original collagen scaffolds and those immersed in human blood plasma for 7 and 14 days.

Fig. 22 SEM images of the original collagen scaffolds and those immersed in PBS for 7 and 14 days.

Fig. 23 Elastic gradient (elastic modulus) of the collagen scaffolds immersed in SBF, human blood plasma and PBS for 10 minutes, 7 and 14 days (*n=10*). The trend lines were added so as to highlight the evaluation of the elastic gradient.

Fig. 24 Plateau stress (compressive strength) of the collagen scaffolds immersed in SBF, human blood plasma and PBS for 10 minutes, 7 and 14 days (*n=10*). The trend lines were added to highlight the evaluation of the compressive strength.

Fig. 25 The mass loss of the scaffolds immersed in SBF, human blood plasma and PBS for 10 minutes, 7 and 14 days (*n=10*). The trend lines were added to highlight the evaluation of the mass loss.

Fig. 26 Representative SEM images (mag. 1,000x) of the inner structure of collagen scaffolds prior to experimentation (A) and exposed for 14 days in human blood plasma (B), SBF (C) and PBS (D). The detailed images reveal the adsorption of various components of the blood plasma (e.g. proteins, saccharides, vitamins, etc.) (B) and salt precipitates (C and D) after exposure in selected media.

Fig. 27 Photograph of the collagen composite scaffolds analysed in the study aimed at the evaluation of different approaches to determining the structural parameters.

Fig. 28 An example of the differences between the various approaches to determining porosity. The determined pore size values differ significantly with respect to the selected approaches. All the values exhibit statistically significant differences except those values designated by the symbol “o” (Kruskal-Wallis, Bonferroni procedure, *0.05*, *n=3*).

Fig. 29 An example of materials electrospun from collagen PBS/ethanol solutions with different collagen concentrations (3, 6, 9 and 16 wt%) and different concentrations of PBS. The SEM images illustrate the variability of the final product (mag. 20,000x, the bar represents 4 μm).

Fig. 30 Fibre diameters of electrospun layers prepared from different concentrations of PBS/ethanol solutions from a previous experiment (*n=250*). In the case of 1x PBS, no fibres were obtained.

Fig. 31 Fibres obtained via the electrospinning of a 16 wt% collagen 1xPBS/ethanol solution under different applied voltages (15-55 kV). Mag. 20,000x, the bar represents 4 μm.

Fig. 32 Mean diameter of fibres (*n=150*) electrospun from a 16 wt% collagen PBS/ethanol solution (calf skin) with different concentrations of PBS (1x, 10x and 20x). The electrical conductivity of the solutions differs in accordance with the PBS concentration; nevertheless, its influence on the fibre diameter is ambivalent.

Fig. 33 SEM images of layers electrospun from collagen (type I, calf skin) 8 wt% PBS/ethanol solution supplemented with different amounts of PEO (molecular weight 900,000) to collagen. Mag. 25,000x, the bar represents 4 μm.

Fig. 34 Representative SEM images of samples electrospun from collagen solutions (without PEO) with concentrations of (from left) 4, 8 and 16 wt% (mag. 20,000x, the bar represents 4 μm).

Fig. 35 Representative SEM images of samples electrospun from collagen solutions (with PEO) with concentrations of (from left) 4, 6 and 8 wt% (mag. 10,000x, the bar represents 5 μm).

Fig. 36 Representative SEM images of samples prepared employing the needleless (A, B) and needle (C, D) centrifugal force spinning of the collagen solutions (with PEO) with a concentration of 12 wt% and circumferential velocities of 15 $m.s^{-1}$ (A, C) and 35 $m.s^{-1}$ (B, D) (mag. 2,000x, the bar represents 20 μm).

Fig. 37 Comparison of the ratio of the integral absorbances of materials prepared using different spinning technologies. N15 and N35 – needle centrifugal spinning with a concentration of 12 wt% and circumferential velocities of 15 $m.s^{-1}$ and 35 $m.s^{-1}$; NL15 and NL35 – needleless centrifugal spinning with a concentration of 12 wt% and circumferential velocities of 15 $m.s^{-1}$ and 35 $m.s^{-1}$; ES+P and ES-P – electrospun from collagen solutions with a collagen concentration of 16 wt% (with and without PEO) and their comparison with lyophillized collagen (LYO), i.e. original collagen prior to its dissolution. * denotes statistically significant differences (Mann-Whitney, *0.05*, *n=10*).

Fig. 38 Comparison of the deconvoluted ATR-FTIR spectra of lyophilized collagen (LYO) and the NL35 material.

Fig. 39 SEM images of layers electrospun from an 8 wt% collagen (type I, fish skin) PBS/ethanol solution with 8 wt% PEO (to collagen) after exposure to a cross-linking ethanol (100%, 95% and 70%) solution with genipin (2.5/4 w/w to collagen). Mag. 5,000x, the bar represents 30 μm.

Fig. 40 SEM images of layers electrospun from an 8 wt% collagen (type I, fish skin) PBS/ethanol solution with 8 wt% PEO (to collagen) after exposure to cross-linking 70% and 100% ethanol solutions with EDC/NHS in three different concentrations. Mag. 10,000x, the bar represents 10 μm.

Fig. 41 Photographs and SEM images (mag. 5,000, bar 30 μm) of collagen layers (type I, fish skin) successfully cross-linked (except for genipin RT MIN) in a 70% ethanol solution with genipin or EDC/NHS in three different concentrations to collagen (w/w: MAX = 5/8, MID = 2.5/8, MIN = 1/8; EDC/NHS 4/1).

Fig. 42 Initial Young's modulus and ultimate tensile strength of the collagen electrospun layers before (ORIGINAL) and after cross-linking with EDC/NHS or genipin dissolved in 95 wt% or 70 wt% ethanol (EtOH) at 37°C. * denotes statistically significant differences (Mann-Whitney, *0.05*, *n=8*).

Fig. 43 SEM images of cross-linked collagen electrospun layers after cross-linking with EDC/NHS or genipin dissolved in 95 wt% or 70 wt% ethanol (37 °C). Mag. 25,000x, the bar represents 5 μm.

Fig. 44 SEM images of collagen electrospun layers after immersion in 100%, 95% and 70% ethanol with and without the EDC/NHS cross-linker at 37°C (mag. 5,000x).

Fig. 45 Initial Young's modulus and ultimate tensile strength of the collagen electrospun layers before (ORIGINAL) and after immersion in 100% and 95% ethanol and 95% ethanol with EDC/NHS at 37°C. "o" denotes values without statistically significant differences (Mann-Whitney, *0.05*, *n=8*).

Fig. 46 Initial Young's modulus and ultimate tensile strength of the collagen electrospun layers before (ORIG) and after cross-linking with EDC/NHS in three different concentrations and for three periods in 95 wt% ethanol at 37°C. * denotes statistically significant differences (Mann-Whitney, *0.05*, *n=6*).

Fig. 47 Initial Young's modulus and ultimate tensile strength of the collagen electrospun layers before (ORIG) and after cross-linking with EDC/NHS in three different concentrations and for three periods in 95 wt% ethanol at 37°C. * denotes statistically significant differences (Mann-Whitney, *0.05*, *n=6*).

Fig. 48 SEM images of collagen (type I, calf skin) electrospun layers cross-linked with theoretical, half and double theoretical concentrations of EDC/NHS for 24, 72 and 168 hours (mag. 10,000x).

Fig. 49 The concentration of amino acids released from the electrospun collagen prior to and after cross-linking with 1x, ½x and 2x theoretical concentrations of EDC/NHS for 24, 72 and 168 hours (*n=3*).

Fig. 50 Fluorescence images of dermal fibroblasts and osteoblasts cultivated on electrospun collagen and polystyrene (control) for 1, 7, 14 and 21 days. The cells were stained with calcein AM (bar 200 μm).

Fig. 51 Initial Young's modulus of the electrospun collagen layers exposed to DMEM without cells and with dermal fibroblasts or osteoblasts for 1, 7, 14 and 21 days. * denotes statistically significant differences (Kruskal-Wallis test, Bonferroni procedure, *0.05*, *n=8*).

Fig. 52 Ultimate tensile strength of the electrospun collagen layers exposed to DMEM without cells and with dermal fibroblasts or osteoblasts for 1, 7, 14 and 21 days. * denotes statistically significant differences (Kruskal-Wallis test, Bonferroni procedure, *0.05*, *n=8*).

Fig. 53 SEM images of the electrospun collagen layers illustrating the adsorption of medium components into the inner structure immediately 1 day after exposure to the medium with or without cells (mag. 50,000x).

Fig. 54 Initial Young's modulus (in the first loading cycle) of the electrospun collagen layers exposed to DMEM cell culture medium without cells and with dermal fibroblasts or osteoblasts for 1 and 21 days. * denotes statistically significant differences (Kruskal-Wallis test, Bonferroni procedure, *0.05*, *n=10*).

Fig. 55 Ratio of the helical and denatured collagen areas (1660/(1630+1615) of the electrospun collagen layers exposed to DMEM cell culture medium without cells and with dermal fibroblasts or osteoblasts for 1 and 21 days. * denotes statistically significant differences (Mann-Whitney, *0.05*, *n=10*).

Fig. 56 Representative SEM images of five collagen electrospun layers randomly selected for the evaluation of variability (first line: mag. 500x, bar 200 μm; second line: mag. 25,000x, bar 4 μm).

Fig. 57 2D cluster scatterplots showing clustering with respect to any of the variables of the stress-like material parameter μ and α. For comparative purposes, splines were used to connect the observations on the borders of each cluster, namely A: clusters represent the data sets of individual layers, B: the cluster represents the medians of each data set, the points represent particular determined parameters for each of the tested samples, C: the theoretical clustering assuming 5 clusters (i.e. 5 different layers), D: the clustering assuming 10 clusters as an optimum estimated by the elbow method.

Fig. 58 An example of the FTIR spectra and deconvoluted spectra of the amide I region of the electrospun collagen prior to and after cross-linking.

Fig. 59 Quantification of electrospun cross-linked collagen variability based on various FTIR parameters, namely the ratio of amide A and amide I areas, the ratio of the non-collagenous protein band and amide I areas, the areas of band 1615, 1630, 1660 and 1690. * denotes statistically significant differences (Kruskal-Wallis, Bonferroni procedure, *0.05*, *n=10*).

Fig. 60 Initial Young's modulus and ultimate tensile strength of the electrospun collagen layers with different amounts of hydroxyapatite (0, 5 and 15 wt%) prior to and after cross-linking with EDC/NHS. * denotes statistically significant differences (Kruskal-Wallis test, Bonferroni procedure, *0.05*, *n=10*).

Fig. 61 Illustration of the composition of the collagen electrospun layers in each of the preparation stages from pure collagen, following electrospinning, following cross-linking and following impregnation. * denotes typical vancomycin bands, ● denotes the PEO bands. The FTIR spectra of pure vancomycin was added for comparative purposes.

Fig. 62 Mechanical stability of the electrospun impregnated collagen layers without (EI0) and with 5 (EI5) and 15 (EI15) wt% of hydroxyapatite - initial Young's modulus and ultimate tensile strength during 720 hours of exposure in human blood plasma. * denotes statistically significant differences (media, IQR, Mann-Whitney, *0.05*, *n=6*).

Fig. 63 Evaluation of the structural stability (mass loss, swelling ratio) of the electrospun impregnated collagen layers without (EI0) and with 5 (EI5) and 15 (EI15) wt% of hydroxyapatite in human blood plasma. * denotes statistically significant differences (median, IQR, Mann-Whitney, *0.05*, *n=6*).

Fig. 64 Representative SEM images of the electrospun collagen layers with 15 wt% HA impregnated by vancomycin during exposure to blood plasma for 30 days (first line mag. 500x, second line 10,000x).

Fig. 65 The concentration of amino acids released from the electrospun impregnated collagen layers without (EI0) and with 5 (EI5) and 15 (EI15) wt% of hydroxyapatite and identical samples prior to cross-linking (NON); note that the opposite axis has a different scale (*n=3*).

Fig. 66 Scheme of the shaft-loaded blister test, modified from B.M. Malyshev et al. 1965 [170].

Fig. 67 Representative images of the plasma treated (left) and printed titanium (right) samples before and after the application of a collagen layer.

Fig. 68 Box-plots of the maximum bond stress required for the separation of the electrospun collagen layers from differently-prepared titanium surfaces. * denotes statistically significant differences (Fisher's LSD, *0.05*, *n=10*).

Fig. 69 The ability of collagen layers directly electrospun on titanium alloy surfaces to resist being worn away from the implant surface by friction that occurs during implantation was analysed by means of an abrasion experiment (A). The EDS analysis shows the approximate presence (wt%) of titanium on the surfaces before (B) and after (C) collagen deposition and after being pushed through the artificial bone (D).

Fig. 70 Auxiliary jigs (A) for the direct deposition of collagen layers via electrospinning (4Spin, Contipro) on the surface of the acetabular (B) and femoral (C) components of a total hip replacement.

Fig. 71 Direct deposition of collagen layers via electrospinning (4Spin, Contipro) on the surface of the acetabular component of a total hip replacement (A-C) and the subsequent cross-linking of the deposited layer (D, E).

Fig. 72 Representative SEM images of cross-section of evaluated collagen/hydroxyapatite/vancomycin layers prepared by three different methods (first line mag. 1,000x, other images mag. 5,000x).

Fig. 73 The concentration of the released active form of vancomycin (median, IQR, *n=6*) with respect to samples with 0, 5 and 15 wt% of HA prepared using different methods.

Fig. 74 Inhibition zone sizes of vancomycin loaded lyophilised, electrospun and electrospun impregnated samples with different amounts of hydroxyapatite in contact with MRSA isolates. * denotes statistically significant differences (mean, SD, Mann-Whitney, *0.05*, *n=7*).

Fig. 75 Illustrative SEM images of cross-sections of the collagen/hydroxyapatite layers with differing amounts of hydroxyapatite impregnated with vancomycin, gentamicin or vancomycin/gentamicin (mag. 1,000x, bar 100 μm).

Fig. 76 Concentration of the released active forms of vancomycin and gentamicin (median, IQR, *n=6*) from the collagen/hydroxyapatite layers with differing amounts of hydroxyapatite and impregnated with vancomycin, gentamicin or vancomycin/gentamicin. V=vancomycin, G=gentamicin, VG=1/2 vancomycin+1/2 gentamicin; 0, 5, 15 = wt% of the HA in the COL/HA layers. The solid red lines denote the MIC for VRSA (16 mg/L) and *Enterococcus* spp. (32 mg/L).

Fig. 77 Inhibition zone diameters (mean, SD) of the vancomycin, gentamicin and vancomycin/gentamicin loaded collagen layers with differing amounts of hydroxyapatite (0, 5, and 15 wt%) tested on clinically relevant bacterial isolates of methicillin-resistant *S. aureus* (MRSA), gentamicin-resistant *S. epidermidis* (SE) and two *E. faecalis* (EF1, EF2). * denotes statistically significant differences (Games-Howell, *0.05*, *n=7*). V=vancomycin, G=gentamicin, VG=1/2 vancomycin+1/2 gentamicin; 0, 5, 15 = wt% of the HA in the collagen layers. CV = control disc with vancomycin, CG = control disc with gentamicin.

Fig. 78 Metabolic activity of SAOS-2 cultured for 24 h in 1-day collagen/hydroxyapatite layer extracts expressed as a percentage of the metabolic activity of SAOS-2 cultured on polystyrene surfaces in culture media (PS). No statistically significant differences between the antibiotic groups (V, G, VG) and the control group (NK) were observed nor were any statistically significant differences determined between any of the COL/HA layer groups and the PS group (Kruskal-Wallis, Bonferroni procedure, *0.05*, *n=4*). V = vancomycin, G = gentamicin, VG = 1/2 vancomycin+1/2 gentamicin; 0, 5, 15 = wt% of the HA in the collagen layers.

Fig. 79 Metabolic activity of SAOS-2 cultured on COL/HA layers with (V, G, VG) or without (NK) antibiotics for 2 days (white boxes) and 8 days (grey boxes). "NK" denotes statistically significant differences to the corresponding NK0, NK5 and NK15 controls (100% for each group) on the corresponding day (Kruskal-Wallis, Bonferroni procedure, *0.05*). * denotes statistically significant differences between the time points of each of the tested layers (Mann-Whitney, *0.05*, *n=4*). The sign ** denotes statistically significant differences within the groups with the same antibiotics separately on the second and eighth days (Kruskal-Wallis, Bonferroni procedure, *0.05*, *n=4*). V = vancomycin, G = gentamicin, VG = 1/2vancomycin+1/2gentamicin; 0, 5, 15 = wt% of hydroxyapatite.

Fig. 80 Fluorescence images of SAOS-2 cultured for 2 and 8 days on collagen/hydroxyapatite layers with (V, G, VG) and without (NK) antibiotics (mag. 10x). The actin filaments representing cell morphology are stained in green and the cell nuclei are stained in blue. V = vancomycin, G = gentamicin, VG = 1/2vancomycin+1/2gentamicin; 0, 5, 15 = wt% of the hydroxyapatite in the collagen layers.

Fig. 81 Representative images of the titanium implants. Ti printed implant before (A) and after (B) the deposition of a COLHA+V layer intended for use in the antimicrobial activity experiment; Ti printed implant before (C) and after (D) the deposition of a COLHA+V layer intended for use in the osseointegration experiment; Ti printed control sample (E).

Fig. 82 Representative histological images of perpendicular sections of the femurs with Giemsa's azur eosin methylene blue staining (A) and details of the bone morphology (B) showing the bone tissue (blue stars), fibrous tissue (red stars), implants (yellow stars) and porous areas (black arrows).

Fig. 83 Representative micro-CT and histological images of identical samples in the COLHA+V implants without the application of *S. epidermidis* (upper line), COLHA implants with *S. epidermidis* (middle line) and COLHA+V with *S. epidermidis* (bottom line) groups.

Fig. 84 Bone porosity of the rat femurs for the implants with a COLHA+V layer and for the implants with COLHA and COLHA+V layers with *S. epidermidis*. * denotes statistically significant differences (*0.05*, Kruskal-Wallis with the Bonferroni procedure, *n=5*).

Fig. 85 Ca/P weight ratio in the bone tissue of the explanted rat femurs. * denotes statistically significant differences (*0.05*, Games-Howell, *n=5*).

Fig. 86 Concentration of vancomycin in the rat blood plasma 7 and 14 days following implantation. Blood samples were taken from the animals with COLHA+V implants with (*+S. epidermidis*) and without *S. epidermidis*. No statistically significant differences were determined between the medians at the 95% confidence level (Mann-Whitney test, *n=5*).

Fig. 87 Representative histological images (Giemsa's azur eosin methylene blue staining) of the printed titanium implants with collagen/hydroxyapatite layers without (COLHA) and loaded with vancomycin (COLHA+V) and the printed titanium control samples (CP). The green stars represent bone tissue outside of the implants, the orange stars represent connective tissue and the yellow stars the implants

Fig. 88 Representative micro-CT images of the implanted titanium samples with collagen/hydroxyapatite electrospun layers with (COLHA+V) and without (COLHA) vancomycin and the control samples without an electrospun layer (CP).

Fig. 89 Ratio of new bone integrated into the surface of the implanted titanium samples with collagen/hydroxyapatite electrospun layers with (COLHA+V) and without (COLHA) vancomycin and the control samples without an electrospun layer (CP). * denotes statistically significant differences (*0.05*, Kruskal-Wallis test with the Bonferroni procedure, *n=5*).

Fig. 90 Experimental set-up for permeability measurement [187].

Fig. 91 Definition of the micro-CT regions. The VOI (V) consisted of a hollow cylinder with an outer diameter with the same dimensions as the drilled defect and an inner diameter of that of the implant (I) wall. The bone tissue is denoted as B (white) and the "new bone" inside the VOI as NB (yellow).

List of tables

Brief biography of the author

Tomáš Suchý
Curriculum Vitae

Date and Place of Birth: November 22nd, 1977, Prague, Czech Republic
Nationality: Czech
Contact: Habartická 43/72, 190 00 Prague 9, tomas.suchy@fs.cvut.cz

EDUCATION

2003 - 2010 Czech Technical University in Prague, Faculty of Mechanical Engineering, Department of Mechanics, Biomechanics and Mechatronics
Ph.D. Program: Biomechanics
Optimizing and Evaluating the Biocompatibility of Fiber Composites with CaP Additives

1997 - 2003 Czech Technical University in Prague, Faculty of Mechanical Engineering, Department of Mechanics, Biomechanics and Mechatronics
MSc. (**Ing.**) Specialization: Biomedical and Rehabilitative Engineering

PROFESSIONAL PROFILE

Since 2012 **Head of the Composite and Carbon Materials Department**
Institute of Rock Structure and Mechanics, Academy of Sciences of the Czech Republic

Since 2005 **Assistant Professor**, Czech Technical University in Prague, Faculty of Mechanical Engineering, Department of Mechanics, Biomechanics and Mechatronics
Specialization: the analyses of the micro and macro mechanical properties of composite materials, statistical analysis.
Lectures on biomechanics, statistics and materials in medicine.

Since 2003 **Junior/Senior Researcher**, Department of Composite and Carbon Materials
Institute of Rock Structure and Mechanics, Academy of Sciences of the Czech Republic
Specialization: the R&D of advanced particulate, fiber reinforced and hybrid composites and composite structures for use in medicine, the optimization of preparation processes, the electrospinning of polymeric materials, structure-biocompatibility relations

2018 - 2019 **Researcher**, General University Hospital in Prague
Specialization: testing and programming of the porosity and degradation of collagen foams

2018 - 2020 **Researcher**, Faculty of Medicine in Plzeň, Charles University, EFRR project No. CZ.02.1.01/0.0/0.0/16_019/0000787 „Fighting INfectious Diseases“
Specialization: the testing of collagen carriers of antibiotics

Since 2016 Chair of the Czech Composite and Carbon Materials Society
Since 2015 Member of the committee of the Bioimplantology Association
Since 2004 Member of the Czech Society of Biomechanics

2010 Prof. Valenta and Prof. Čihák award for young scientists, Endowment Fund for Human Biomechanics

RESEARCH INTERESTS

The synthesis and mechanical and structural characterization of novel composite materials based on natural and synthetic polymers, the electrospinning of natural polymers, the isolation and characterization of collagen and the research and development of drug carriers and scaffolds for tissue engineering and regenerative medicine.

SELECTED GRANT PROJECTS

Mechanics of arterial delamination and crack propagation (GAČR, Czech Science Foundation, 20-11186S, principal investigator)

Bioartificial cardiovascular patches and vessels from porcine collagen reinforced with nano/microfibers using stem cells and dynamic culture (AZV Ministry of Health of the Czech Republic, NV19-02-00068, member of joint investigator team)

Development and comprehensive evaluation of a novel injectable, resorbable, porous bone substitute with the controlled release of antimicrobial agents (AZV Ministry of Health of the Czech Republic, 18-05-00379, member of joint investigator team).

Fighting INfectious Diseases (Ministry of Education, Youth and Sports of the Czech Republic, financed from the European Regional Development Fund, member of the team)

Comprehensive pre-clinical evaluation of lateral lumbar spine fusion with a hybrid biodegradable nanocomposite porous implant (AZV Ministry of Health of the Czech Republic, 17-31276A, member of the joint investigation team).

Development of a resorbable collagen-calcium phosphate nanolayer with the controlled elution of antibiotics for implant survival rate enhancement (Technology Agency of the Czech Republic, TA04010330, principal investigator).

Development and comprehensive pre-clinical testing of novel composite materials for bone surgery (AZV Ministry of Health of the Czech Republic, 15-25813A, member of joint investigator team)

Bioinspired Nanocomposite Structures for Bone Tissue Regeneration (GAČR, Czech Science Foundation, GA106/09/1000, member of the principal investigation team).

PROFILES

ORCID iD: http://orcid.org/0000-0002-2656-4280

INVITED LECTURES

"*If collagen is the answer, then what was the question?*", VII. International Conference Bioimplantology, 2015

"*Collagen - good, bad and ugly*", Czech-Slovak congress "Mezioborové přístupy v hojení ran", 2019

AD HOC REVIEWER

International Journal of Nanomedicine, International Journal of Polymeric Materials, Journal of Composite Materials, Acta Polytechnica, Engineering of Biomaterials

Czech Health Research Council, Ministry of Health of the Czech Republic

Bachelor and diploma theses reviewer (Technical University in Liberec, University of Chemistry and Technology in Prague, Czech Technical University in Prague)

ORGANIZING COMMITTEE

National conference "*Biomaterials and Their Surfaces*" (2008-2020)

International conference "*Bioimplantology*" (2017-2020)

NTHU Summer Course at the Czech Technical University in Prague, 2017

EXHIBITONS

Subject and realization of an exhibition entitled "T*o the BONE! Exhibition about bone structure, function and replacements*", Technical Museum in Brno, June 4th - September 29th 2019.

Guarantor of the materials section of the exhibition: "*MAN-MADE MAN - Technology and Medicine*" May 5th 2017 - May 27th 2018, National Technical Museum, Prague

PUBLICATIONS

Author and co-author of more than 80 papers (34 of them in peer-reviewed journals with impact factor), original works, lectures, 3 book chapters, 1 patent and 15 utility models, total number of citations 207, 159 without self-citations, *h*-index 9 (WOS, 02/08/2020).

List of selected publications

Leading author of articles in international peer-reviewed journals with impact factor received from the Journal of Citation Reports (IF)

T. Suchy, M. Supova, P. Sauerova, M. Hubalek-Kalbacova, E. Klapkova, M. Pokorny, L. Horny, J. Zavora, R. Ballay, F. Denk, M. Sojka, L. Vistejnova, Evaluation of collagen/hydroxyapatite electrospun layers loaded with vancomycin, gentamicin and their combination: Comparison of release kinetics, antimicrobial activity and cytocompatibility, Eur. J. Pharm. Biopharm. 140 (2019) 50–59. doi:10.1016/j.ejpb.2019.04.021. **IF 4,708, Q1 (28/267)**, JCR 2018

T. Suchy, M. Supova, M. Bartos, R. Sedlacek, M. Piola, M. Soncini, G.B. Fiore, P. Sauerova, M. Hubalek-Kalbacova, Dry versus hydrated collagen scaffolds: are dry states representative of hydrated states?, J. Mater. Sci. Mater. Med. 29 (2018). doi:10.1007/s10856-017-6024-2. **IF 2,448, Q2 (34/80)**, JCR 2017

T. Suchy, M. Supova, E. Klapkova, V. Adamkova, J. Zavora, M. Zaloudkova, S. Ryglova, R. Ballay, F. Denk, M. Pokorny, P. Sauerova, M. Hubalek-Kalbacova, L. Horny, J. Vesely, T. Vonavkova, R. Prusa, The release kinetics, antimicrobial activity and cytocompatibility of differently prepared collagen/hydroxyapatite/vancomycin layers: Microstructure vs. nanostructure., Eur. J. Pharm. Sci. 100 (2017) 219–229. doi:10.1016/j.ejps.2017.01.032. **IF 3,756, Q1 (54/257)**, JCR 2016

T. Suchy, M. Supova, E. Klapkova, L. Horny, S. Ryglova, M. Zaloudkova, M. Braun, Z. Sucharda, R. Ballay, J. Vesely, H. Chlup, F. Denk, The Sustainable Release of Vancomycin and Its Degradation Products From Nanostructured Collagen/Hydroxyapatite Composite Layers., J. Pharm. Sci. 105 (2016) 1288–1294. doi:10.1016/S0022-3549(15)00175-6. **IF 2,641, Q2 (59/163)**, JCR 2015

T. Suchy, M. Supova, P. Sauerova, M. Verdanova, Z. Sucharda, S. Ryglova, M. Zaloudkova, R. Sedlacek, M. Huubalek-Kalbacova, The effects of different cross-linking conditions on collagen-based nanocomposite scaffolds-an in vitro evaluation using mesenchymal stem cells., Biomed. Mater. 10 (2015) 65008. doi:10.1088/1748-6041/10/6/065008. **IF 3,697, Q1 (9/76)**, JCR 2014

T. Suchý, Š. Rýglová, K. Balík, K. Smetana, M. Šupová, Z. Sucharda, E. Filová, J. Havlíková, L. Bačáková, G.S. Martynková, Biological evaluation of polydimethylsiloxane modified by calcium phosphate nanoparticles for potential application in spine surgery, Sci. Adv. Mater. 5 (2013). doi:10.1166/sam.2013.1478. **IF 2,509, Q1 (45/241)**, JCR 2012

T. Suchý, K. Balík, R. Sedláček, Z. Sucharda, M. Sochor, J. Prokop, J. Beneš, J. Křena, Radiolucent composites providing high resistance against sterilization decomposition, Ceram. - Silikaty. 55 (2011). **IF 0,297, Q3 (16/25)**, JCR 2010

T. Suchý, K. Balík, M. Černý, M. Sochor, H. Hulejova, V. Pešáková, T. Fenolova, A composite based on glass fibers and siloxane matrix as a bone replacement, Ceram. - Silikaty. 52 (2008). **IF 0,488, Q2 (11/25)**, JCR 2007

Co-author of articles in international peer-reviewed journals with impact factor received from the Journal of Citation Reports (IF)

B. Svobodova, A. Kloudova, J. Ruzicka, L. Kajtmanova, L. Navratil, R. Sedlacek, **T. Suchy**, M. Jhanwar-Uniyal, P. Jendelova, L.M. Urdzikova, The effect of 808 nm and 905 nm wavelength light on recovery after spinal cord injury, Sci. Rep. 9 (2019). doi:10.1038/s41598-019-44141-2. **IF 4,011, Q1 (15/69)**, JCR 2018

P. Mitas, T. Grus, L. Lambert, M. Mlcek, H. Chlup, E. Honsova, M. Dohnalova, **T. Suchy**, A. Burgetova, J. Lindner, M. Spacek, The Influence of Purification of Carp Collagen Used in a Novel Composite Graft

with Sandwich Construction of the Wall on Its Biological Properties and Graft Patency Rates, Physiol. Res. 68 (2019) 603–610. doi:10.33549/physiolres.934117. **IF 1,701, Q4 (64/81)**, JCR 2018

P. Sauerova, **T. Suchy**, M. Supova, M. Bartos, J. Klima, J. Juhasova, S. Juhas, T. Kubikova, Z. Tonar, R. Sedlacek, M. Piola, G.B. Fiore, M. Soncini, M. Hubalek Kalbacova, Positive impact of dynamic seeding of mesenchymal stem cells on bone-like biodegradable scaffolds with increased content of calcium phosphate nanoparticles., Mol. Biol. Rep. 46 (2019) 4483–4500. doi:10.1007/s11033-019-04903-7. **IF 2,107, Q3 (217/299)**, JCR 2018

P. Stastny, R. Sedlacek, **T. Suchy**, V. Lukasova, M. Rampichova, M. Trunec, Structure degradation and strength changes of sintered calcium phosphate bone scaffolds with different phase structures during simulated biodegradation in vitro, Mater. Sci. Eng. C - Mater. Biol. Appl. 100 (2019) 544–553. doi:10.1016/j.msec.2019.03.027. **IF 4,959, Q1 (7/32)**, JCR 2018

M. Supova, **T. Suchy**, Z. Sucharda, E. Filova, J.N.L.M. der Kinderen, M. Steinerova, L. Bacakova, G.S. Martynkova, The comprehensive in vitro evaluation of eight different calcium phosphates: Significant parameters for cell behavior, J. Am. Ceram. Soc. 102 (2019) 2882–2904. doi:10.1111/jace.16110**. IF 3,094, Q1 (12/172)**, JCR 2018

P. Lukac, J.M. Hartinger, M. Mlcek, M. Popkova, **T. Suchy**, M. Supova, J. Zavora, V. Adamkova, H. Benakova, O. Slanar, M. Bartos, H. Chlup, L. Lambert, T. Grus, A novel gentamicin-releasing wound dressing prepared from freshwater fish Cyprinus carpio collagen cross-linked with carbodiimide, J. Bioact. Compat. Polym. 34 (2019) 246–262. doi:10.1177/0883911519835143. **IF 1,976, Q2 (38/87)**, JCR 2018

L. Vojtova, L. Michlovska, K. Valova, M. Zboncak, M. Trunec, K. Castkova, M. Krticka, V. Pavlinakova, P. Polacek, M. Dzurov, V. Lukasova, M. Rampichova, **T. Suchy**, R. Sedlacek, M.-P. Ginebra, E. Montufar, The Effect of the Thermosensitive Biodegradable PLGA–PEG–PLGA Copolymer on the Rheological, Structural and Mechanical Properties of Thixotropic Self-Hardening Tricalcium Phosphate Cement, Int. J. Mol. Sci. 20 (2019) 391. doi:10.3390/ijms20020391. **IF 4,183, Q2 (78/299)**, JCR 2018

L. Lambert, M. Novakova, P. Lukac, D. Cechova, L. Sukenikova, J. Hrdy, M. Mlcek, H. Chlup, **T. Suchy**, T. Grus, Evaluation of the Immunogenicity of a Vascular Graft Covered with Collagen Derived from the European Carp (Cyprinus carpio) and Bovine Collagen, Biomed Res. Int. (2019). doi:10.1155/2019/5301405. **IF 2,197, Q3 (94/162)**, JCR 2018

M. Jirik, M. Bartos, P. Tomasek, A. Maleckova, T. Kural, J. Horakova, D. Lukas, **T. Suchy**, P. Kochova, M. Hubalek-Kalbacova, M. Kralickova, Z. Tonar, Generating standardized image data for testing and calibrating quantification of volumes, surfaces, lengths, and object counts in fibrous and porous materials using X-ray microtomography, Microsc. Res. Tech. 81 (2018) 551–568. doi:10.1002/jemt.23011. **IF 1,087, Q3 (59/85)**, JCR 2017

J. Horakova, P. Mikes, A. Saman, V. Jencova, A. Klapstova, T. Svarcova, M. Ackermann, V. Novotny, **T. Suchy,** D. Lukas, The effect of ethylene oxide sterilization on electrospun vascular grafts made from biodegradable polyesters., Mater. Sci. Eng. C - Mater. Biol. Appl. 92 (2018) 132–142. doi:10.1016/j.msec.2018.06.041. **IF 5,080, Q1 (6/33)**, JCR 2017

J. Horakova, P. Mikes, A. Saman, T. Svarcova, V. Jencova, **T. Suchy**, B. Heczkova, S. Jakubkova, J. Jirousova, R. Prochazkova, Comprehensive assessment of electrospun scaffolds hemocompatibility, Mater. Sci. Eng. C - Mater. Biol. Appl. 82 (2018). doi:10.1016/j.msec.2017.05.011. **IF 5,080, Q1 (6/33)**, JCR 2017

G.T. Rocca, R. Daher, C.M. Saratti, R. Sedlacek, **T. Suchy**, A.J. Feilzer, I. Krejci, Restoration of severely damaged endodontically treated premolars: The influence of the endo-core length on marginal integrity and fatigue resistance of lithium disilicate CAD-CAM ceramic endocrowns, J. Dent. 68 (2018) 41–50. doi:10.1016/j.jdent.2017.10.011. **IF 3,770, Q1 (8/91)**, JCR 2017

M. Bartos, **T. Suchy**, Z. Tonar, R. Foltan, M. Hubalek-Kalbacova, Micro-CT in tissue engineering scaffolds designed for bone regeneration: principles and applications, Ceramics-Silikáty. 62 (2018) 194–199. doi:10.13168/cs.2018.0012. **IF 0,680, Q3 (19/27)**, JCR 2017

M. Bartos, **T. Suchy**, R. Foltan, Note on the use of different approaches to determine the pore sizes of tissue engineering scaffolds: what do we measure?, Biomed. Eng. Online. 17 (2018). doi:10.1186/s12938-018-0543-z. **IF 1,676, Q3 (51/78)**, JCR 2017

T. Kubikova, M. Bartos, S. Juhas, **T. Suchy**, P. Sauerova, M. Hubalek-Kalbacova, Z. Tonar, Comparison of ground sections, paraffin sections and micro-CT imaging of bone from the epiphysis of the porcine femur for morphometric evaluation, Ann. Anat. - Anat. Anzeiger. 220 (2018) 85–96. doi:10.1016/j.aanat.2018.07.004. **IF 1,852, Q2 (8/21)**, JCR 2017

S. Ryglova, M. Braun, **T. Suchy**, Collagen and Its Modifications-Crucial Aspects with Concern to Its Processing and Analysis, Macromol. Mater. Eng. 302 (2017). doi:10.1002/mame.201600460. **IF 2,863, Q2 (22/86)**, JCR 2017

M. Bacakova, F. Lopot, D. Hadraba, M. Varga, M. Zaloudkova, D. Stranska, **T. Suchy,** L. Bacakova, Effects of fiber density and plasma modification of nanofibrous membranes on the adhesion and growth of HaCaT keratinocytes, J. Biomater. Appl. 29 (2015). doi:10.1177/0885328214546647. **IF 2,197, Q2 (29/76)**, JCR 2014

K. Novotna, M. Zajdlova, **T. Suchy**, D. Hadraba, F. Lopot, M. Zaloudkova, T.E.L. Douglas, M. Munzarova, M. Juklickova, D. Stranska, D. Kubies, D. Schaubroeck, S. Wille, L. Balcaen, M. Jarosova, H. Kozak, A. Kromka, Z. Svindrych, V. Lisa, K. Balik, L. Bacakova, Polylactide nanofibers with hydroxyapatite as growth substrates for osteoblast-like cells, J. Biomed. Mater. Res. - Part A. 102 (2014). doi:10.1002/jbm.a.35061. **IF 2,841, Q1 (18/76)**, JCR 2013

E. Filová, **T. Suchý**, Z. Sucharda, M. Šupová, M. Žaloudková, K. Balík, V. Lisá, M. Šlouf, L. Bačáková, Support for the initial attachment, growth and differentiation of MG-63 cells: A comparison between nano-size hydroxyapatite and micro-size hydroxyapatite in composites, Int. J. Nanomedicine. 9 (2014). doi:10.2147/IJN.S56661. **IF 4,195, Q1 (32/256)**, JCR 2013

L. Machova Urdzikova, R. Sedlacek, **T. Suchy**, T. Amemori, J. Ruzicka, P. Lesny, V. Havlas, E. Sykova, P. Jendelova, Human multipotent mesenchymal stem cells improve healing after collagenase tendon injury in the rat, Biomed. Eng. Online. 13 (2014). doi:10.1186/1475-925X-13-42. **IF 1,746, Q2 (35/76)**, JCR 2013

M. Šupová, J. Svítilová, Z. Chlup, M. Černý, Z. Weishauptová, **T. Suchý**, V. Machovič, Z. Sucharda, M. Žaloudková, Relation between mechanical properties and pyrolysis temperature of phenol formaldehyde resin for gas separation membranes, Ceram. - Silikaty. 56 (2012). **IF 0,382, Q3 (17/25)**, JCR 2011

E. Filova, M. Parizek, J. Olsovska, Z. Kamenik, E. Brynda, T. Riedel, M. Vandrovcova, V. Lisa, L. MacHova, I. Skalsky, O. Szarszoi, **T. Suchy**, L. Bacakova, Perivascular sirolimus-delivery system, Int. J. Pharm. 404 (2011). doi:10.1016/j.ijpharm.2010.11.005. **IF 3,607, Q1 (57/252)**, JCR 2010

S. Rýglová, Z. Sucharda, M. Černý, **T. Suchý**, M. Šupová, M. Žaloudková, Particulate composite on the basis of ha and tcp microparticles and nanoparticles as a possible biomaterial for spine therapy, Ceram. - Silikaty. 54 (2010). **IF 0,649, Q2 (9/25)**, JCR 2009

K. Balík, **T. Suchý**, Z. Sucharda, Š. Rýglová, F. Denk, Design for a filler of an intervertebral cage for spine treatment on the basis of fibers and particulate composites, Ceram. - Silikaty. 53 (2009). **IF 0,644, Q2 (10/24)**, JCR 2008

K. Balík, **T. Suchý**, Z. Sucharda, M. Černý, L. Bačáková, M. Sochor, M. Šlouf, Effect of nano/micro particles of calcium phosphates on the mechanical properties of composites based on polysiloxane matrix reinforced by polyamide, Ceram. - Silikaty. 52 (2008). **IF 0,488, Q2 (11/25)**, JCR 2007

K. Balík, M. Sochor, H. Hulejová, **T. Suchý**, M. Černý, The influence of a short-term tissue culture medium storage on the mechanical properties of composites based on glass fibers and polysiloxane, Ceram. - Silikaty. 51 (2007). **IF 0,597, Q2 (11/26)**, JCR 2006

Co-author of articles in peer-reviewed journals without impact factor

P. Smatlikova, S. Juhas, J. Juhasova, **T. Suchy**, M. Hubalek Kalbacova, Z. Ellederova, J. Motlik, J. Klima, Adipogenic Differentiation of Bone Marrow-Derived Mesenchymal Stem Cells in Pig Transgenic Model Expressing Human Mutant Huntingtin, J. Huntingtons. Dis. 8 (2019) 33–51. doi:10.3233/JHD-180303.

P. Papoušek, Z. Král'ovská, **T. Suchý**, R. Procházková, Delayed donor reactions to blood donations - Anonymous electronic survey, Transfuze a Hematol. Dnes. 24 (2018).

T. Suchý, K. Balík, Z. Sucharda, M. Sochor, M. Lapčíková, R. Sedláček, Optimizing and evaluating the biocompatibility of fiber composites with calcium phosphate additives, Wiener Medizinische Wochenschrift. 161 (2011). doi:10.1007/s10354-011-0913-7.

I. Skalský, O. Szárszoi, E. Filová, M. Pařízek, A. Lytvynets, J. Malušková, A. Lodererová, J. Olšovská, Z. Kameník, E. Brynda, Z. Plichta, T. Riedel, V. Lisá, Z. Burdíková, M. Čapek, L. Grausová, **T. Suchý**, J. Pirk, L. Bačáková, A periadventitial sirolimus-eluting system in the prevention of neointimal hyperplasia in autologous venous grafts, Cor Vasa. 53 (2011).

Book chapters

M. Supova, **T. Suchy**, Chapter 2 - Bio-nanoceramics and Bio-nanocomposites, in: A.S.H. Makhlouf, and M. Scharnweber (Eds.), Handbook of nanoceramic and nanocomposite coatings and materials, Butterworth-Heinemann, Elsevier, 2015: pp. 29–58. doi:https://doi.org/10.1016/B978-0-12-799947-0.00002-X.

Balik K., **Suchy T.**, Cizmarova E., Spatenka P. Research and development of bio-composites for bone replacements during last 25 years. In: Desiderio V., Cizmarova E. (eds.), New Trends in Biomedical and Bio-Based Materials. Tri-State Bionanoechnology, Zittasu, 2018, ISBN 978-80-7609-017-1.

Balik K., **Suchy T.**, Sucharda Z., Cerny M., Supova M., Ryglova S., Bacakova L., Filova E., Sedlacek R., Sochor M. Výzkum kompozitních materiálů jako náhrad kostních štěpů pro aplikace ve formě jader meziobratlových rozpěrek. In: Interdisciplinární výzkum řešení problematiky páteřních náhrad. Praha: ČVUT FS, Ústav mechaniky, Laboratoř biomechaniky člověka, 2010. p. 106-115. Edice monografií České společnosti pro biomechaniku. Vol. 1. ISBN 978-80-01-04494-0.

Utility models

Suchy, T.; Supova, M.; Balik, K.; RyglovA, S.; Sucharda, Z.; Hubalek Kalbacova, M.; Sauerova, P.; Juhas, S.; Juhasova, J.; Klima, J.; Tonar, Z.; Kubikova, T.; Zaloudkova, M.; Braun, M.: Degradable composite bone tissue replacements with controlled degradation time based on bioapatite, collagen, poly(D.L-lactide) and sodium hyaluronate. Czech Republic. Utility model. CZ 31358. 2018-01-09.

Suchy, T.; Supova, M.; Balik, K.; RyglovA, S.; Sucharda, Z.; Hubalek Kalbacova, M.; Sauerova, P.; Juhas, S.; Juhasova, J.; Klima, J.; Tonar, Z.; Kubikova, T.; Zaloudkova, M.; Braun, M.: Degradable composite bone tissue composite replacements with controlled degradation time based on poly (DL-lactide), collagen, biaoapatite and sodium hyaluronate. Czech Republic. Utility model. CZ 31321. 2017-12-18.

Suchy, T.; Supova, M.; M.; Denk, F.; Ballay, R.; Sucharda, Z.; Horny, L.; Chlup, H.; Sedlacek, R.; Cejka, Z.; Cejka, Z.: A metal substrate with an electrostatically applied bioactive nanocomposite carrier of antibiotics based on collagen and calcium phosphate. Czech Republic. Utility model. CZ 31357. 2018-01-09.

Suchy, T.; Supova, M.; M.; Denk, F.; Ballay, R.; Sucharda, Z.; Horny, L.; Chlup, H.; Sedlacek, R.; Cejka, Z.; Cejka, Z.: A metallic substrate with an electrostatically applied bioactive nanocomposite layer based on collagen and calcium phosphate. Czech Republic. Utility model. CZ 31320. 2017-12-18.

Suchy, T.; Supova, M.; Denk, F.; Ryglova, S.; Sucharda, Z.; Zaloudkova, M.; Ballay, R.; Horny, L.; Vesely, J.; Chlup, H.: A bioactive nanocomposite carrier of antibiotics based on collagen, calcium phosphate, gentamicin and vancomycin. Czech Republic. Utility model. CZ 30259. 2017-01-17.

Suchy, T.; Supova, M.; Denk, F.; Ryglova, S.; Sucharda, Z.; Zaloudkova, M.; Ballay, R.; Horny, L.; Vesely, J.; Chlup, H.: Collagen-, calcium phosphate- and gentamicin-based biologically active nanocomposite carrier of antibiotics. Czech Republic. Utility model. CZ 30118. 2016-12-06.

Suchy, T.; Supova, M.; Ryglova, S.; Sedlacek, R.; Sucharda, Z.; Zaloudkova, M.; Balik, K.; Braun, M.; Horny, L.; Chlup, H.; Vesely, J.; Denk, F.: Biologically active nanocomposite layer based on collagen nanofibers with integrated calcium phosphate particles for applications in orthopedics. Czech Republic. Utility model. CZ 28981. 2015-12-14.

Balik K, **Suchy T**, Supova M, Sucharda Z, Ryglova S, Sedlacek R. Bone prostheses and fillers based on hybrid composite materials with nano-calcium deficient hydroxyapatite. Czech Republic. Utility model. CZ 26216. 2013-12-09.

Balik K, **Suchy T**, Supova M, Sucharda Z, Ryglova S, Sedlacek R. Bone prostheses and fillers based on particulate composite materials with nanocalcium defficient hydroxyapatite. Czech Republic. Utility model. CZ 26215. 2013-12-09.

Balik K, **Suchy T**, Supova M, Sucharda Z, Ryglova S, Sedlacek R. Bone prostheses and fillers based on particulate composite materials with sub-micron bioapatite. Czech Republic. Utility model. CZ 26214. 2013-12-09.

Balik K, **Suchy T**, Supova M, Sucharda Z, Ryglova S, Sedlacek R. Bone prostheses and fillers based on hybrid composite materials with sub-micron bioapatite. Czech Republic. Utility model. CZ 26213. 2013-12-09.

Balik K, **Suchy T**, Supova M, Sucharda Z, Ryglova S, Sedlacek R. Particulate composite replacements of bone tissue with nanosized calcium phosphate. Czech Republic. Utility model. CZ 22997. 2011-11-28.

Balik K, **Suchy T**, Supova M, Sucharda Z, Ryglova S, Sedlacek R. Hybrid composite substitutions of bone tissue with nano calcium phosphate. Czech Republic. Utility model. CZ 23060. 2011-12-12.

Balik K, **Suchy T**, Supova M, Sucharda Z, Ryglova S, Sedlacek R. Particulate composite replacements of bone tissue with nanosized hydoxyapatite. Czech Republic. Utility model. CZ 22996. 2011-11-28.

Balik K, **Suchy T**, Supova M, Sucharda Z, Ryglova S, Sedlacek R. Hybrid composite substitutions of bone tissue with nano hydroxyapatite. Czech Republic. Utility model. CZ 22946. 2011-11-14.